INFORMATION TO USERS

This manuscript has been reproduced from the microfilm master. UMI films the text directly from the original or copy submitted. Thus, some thesis and dissertation copies are in typewriter face, while others may be from any type of computer printer.

The quality of this reproduction is dependent upon the quality of the copy submitted. Broken or indistinct print, colored or poor quality illustrations and photographs, print bleedthrough, substandard margins, and improper alignment can adversely affect reproduction.

In the unlikely event that the author did not send UMI a complete manuscript and there are missing pages, these will be noted. Also, if unauthorized copyright material had to be removed, a note will indicate the deletion.

Oversize materials (e.g., maps, drawings, charts) are reproduced by sectioning the original, beginning at the upper left-hand corner and continuing from left to right in equal sections with small overlaps. Each original is also photographed in one exposure and is included in reduced form at the back of the book.

Photographs included in the original manuscript have been reproduced xerographically in this copy. Higher quality 6" x 9" black and white photographic prints are available for any photographs or illustrations appearing in this copy for an additional charge. Contact UMI directly to order.

UMI

A Bell & Howell Information Company
300 North Zeeb Road. Ann Arbor. MI 48106-1346 USA
313/761-4700 800/521-0600

Reproduced with permission of the copyright owner. Further reproduction prohibited without permission.

Reproduced with permission of the copyright owner. Further reproduction prohibited without permission.

DETACHMENT FOLDS OF THE NORTHEASTERN BROOKS RANGE, ALASKA - A BASIS FOR GEOMETRIC AND KINEMATIC MODELS OF DETACHMENT FOLDS

A

THESIS

Presented to the Faculty

of the University of Alaska Fairbanks

in Partial Fulfillment of the Requirements

for the Degree of

DOCTOR OF PHILOSOPHY

By

Thomas X. Homza, B.S., M.S.

Fairbanks, Alaska

August 1995

Reproduced with permission of the copyright owner. Further reproduction prohibited without permission.

UMI Number: 9608413

UMI Microform 9608413
Copyright 1995, by UMI Company. All rights reserved.

This microform edition is protected against unauthorized copying under Title 17, United States Code.

UMI

300 North Zeeb Road
Ann Arbor, MI 48103

Reproduced with permission of the copyright owner. Further reproduction prohibited without permission.

DETACHMENT FOLDS OF THE NORTHEASTERN BROOKS RANGE, ALASKA - A BASIS FOR GEOMETRIC AND KINEMATIC MODELS OF DETACHMENT FOLDS

By

Thomas X. Homza

RECOMMENDED:

Dr. C. L. Hanks

Dr. P. W. Layer

Dr. L. Shapiro

Dr. Wesley K. Wallace,
Advisory Committee Chair

Dr. Paul W. Layer
Head, Dept. of Geology & Geophysics

APPROVED:

Dean, College of Natural Sciences

Dean of the Graduate School

July 26, 1995

Date

Reproduced with permission of the copyright owner. Further reproduction prohibited without permission.

ABSTRACT

Detachment anticlines are defined by mechanically competent rock layers and form both by internal deformation of an adjacent weak layer and detachment above a lower competent unit. This study is important for:

1) Other fold-and-thrust belts. Detachment folds are probably very common in fold-and-thrust belts worldwide, but they are rarely recognized as such and are commonly mistaken for other fold-types. This is partly because a rigorous general model for detachment folds that allows for changes in detachment depth and for fixed-arc length kinematics is lacking in the geologic literature.

A general detachment fold model is presented here that:

a) is based on observations of natural folds in the northeastern Brooks Range of Alaska;

b) does not assume constant detachment depth or hinge-migration kinematics and;

c) allows quantification of non-plane strain.

The folds observed can be modeled kinematically as fixed-hinge buckle folds, whereas the fold geometry and distribution of strain indicators in each fold preclude the migrating-hinge kinematic interpretation that is common in published models. Layer-parallel shortening, initial fold asymmetry, initial stratigraphic thickness of the incompetent unit, and the nature of rheological gradations each predictably influence fold evolution.

This study suggests a general scenario for the evolution of a typical detachment fold. The area defined by a detachment anticline increases rapidly

Reproduced with permission of the copyright owner. Further reproduction prohibited without permission.

during early stages of folding and this is accompanied by a decrease in depth to detachment beneath synclines and the formation of fixed-hinge parasitic and disharmonic folds. This trend continues until the interlimb angle of the primary fold reaches 90°. Increased shortening requires volume-loss in the core and/or an increase in detachment depth beneath the fold. Finally, depending on the rheology of the system, the fold may lock and/or be truncated by a thrust fault.

2) Regional tectonics. The western part of the northeastern Brooks Range is mostly a passive-roof duplex, but this study shows that forward-propagating deformation occurred at various structural positions.

3) Economics. Detachment folds may form petroleum traps that require a treatment different than that for fault-bend or fault-propagation folds. Detachment fold traps may exist beneath the coastal plain of the Arctic National Wildlife Refuge.

Reproduced with permission of the copyright owner. Further reproduction prohibited without permission.

TABLE OF CONTENTS

Reproduced with permission of the copyright owner. Further reproduction prohibited without permission.

Reproduced with permission of the copyright owner. Further reproduction prohibited without permission.

Reproduced with permission of the copyright owner. Further reproduction prohibited without permission.

Reproduced with permission of the copyright owner. Further reproduction prohibited without permission.

Reproduced with permission of the copyright owner. Further reproduction prohibited without permission.

Reproduced with permission of the copyright owner. Further reproduction prohibited without permission.

Reproduced with permission of the copyright owner. Further reproduction prohibited without permission.

Reproduced with permission of the copyright owner. Further reproduction prohibited without permission.

Reproduced with permission of the copyright owner. Further reproduction prohibited without permission.

Reproduced with permission of the copyright owner. Further reproduction prohibited without permission.

Reproduced with permission of the copyright owner. Further reproduction prohibited without permission.

Reproduced with permission of the copyright owner. Further reproduction prohibited without permission.

Reproduced with permission of the copyright owner. Further reproduction prohibited without permission.

LIST OF FIGURES

Reproduced with permission of the copyright owner. Further reproduction prohibited without permission.

Reproduced with permission of the copyright owner. Further reproduction prohibited without permission.

Reproduced with permission of the copyright owner. Further reproduction prohibited without permission.

Reproduced with permission of the copyright owner. Further reproduction prohibited without permission.

Reproduced with permission of the copyright owner. Further reproduction prohibited without permission.

Reproduced with permission of the copyright owner. Further reproduction prohibited without permission.

Reproduced with permission of the copyright owner. Further reproduction prohibited without permission.

Reproduced with permission of the copyright owner. Further reproduction prohibited without permission.

Reproduced with permission of the copyright owner. Further reproduction prohibited without permission.

Reproduced with permission of the copyright owner. Further reproduction prohibited without permission.

Reproduced with permission of the copyright owner. Further reproduction prohibited without permission.

LIST OF TABLES

Reproduced with permission of the copyright owner. Further reproduction prohibited without permission.

LIST OF PLATES

Ten large-format plates, consisting of geologic maps and cross sections, are located in the back pocket of the dissertation. The plates are associated with Appendices 2 through 5 and are labeled accordingly (*e.g.* Plate A3.1 is associated with Appendix 3).

Plate A2.1	Geologic map of the headwaters area of Straight Creek
Plate A2.2	Balanced cross section across the Straight Creek detachment anticline
Plate A3.1	Geologic map of the Salisbury Creek area
Plate A3.2	Balanced cross section across the crest and backlimb of the western end of the northern Franklin Mountains anticlinorium
Plate A3.3	Geologic map of the western end of the southern Franklin Mountains anticlinorium
Plate A3.4	Geologic cross section of the western end of the southern Franklin Mountains anticlinorium
Plate A4.1	Geologic map of the Aichilik Forks area
Plate A4.2	Balanced cross section of the Aichilik Forks area
Plate A5.1	Geologic map of the Ellesmerian inlier on the Hulahula River
Plate A5.2	Geologic cross section of the Ellesmerian inlier on the Hulahula River

Reproduced with permission of the copyright owner. Further reproduction prohibited without permission.

ACKNOWLEDGMENTS

This work is dedicated to my parents, Ron and Mary Homza, who have always dedicated much of their work to me.

This study, begun in 1992, is a direct extension of my Master's thesis (Homza 1992a). Both studies were supervised by Dr. Wesley Wallace, the chairman of my graduate advisory committee. I appreciate Wes' dedication to me and my study. I sincerely thank him for his enthusiasm, technical assistance, and guidance throughout the years. He stuck with me through thick and thin and I continue to learn much from him. Without Wes' efforts, this project would not have been possible.

The remainder of my graduate advisory committee consisted of Drs. Catherine Hanks, Paul Layer, and Lewis Shapiro. Each made helpful suggestions for improving the dissertation and provided guidance in a variety of ways throughout the project. This is greatly appreciated. My friends, Stephen Crumley and Andrea Krumhardt helped with early-stage computer problems and late-stage rock-cutting chores, respectively. Thank you all.

My family provided moral support throughout my graduate years, even when it seemed as if the project would never end. I gratefully thank them for their patience and their confidence in me. I especially thank my wife, Julia, and brother, Mike, for their assistance in the field. They made for two adventurous and truly unforgettable summers in the Brooks Range. Julia had the particularly daunting task of living with someone who was working on a doctoral dissertation

Reproduced with permission of the copyright owner. Further reproduction prohibited without permission.

at home. She stood gracefully beside me on the emotional roller coaster that is graduate student life. Thanks, Jul.

The project was financially supported by a variety of sources. These are: the National Science Foundation (grant EAR-9304482); three grants from the University of Alaska Fairbanks: the Geist Fund, the Austin Cooley Award, and the Graduate Resource Fellowship; and a consortium of oil industry sponsors. The oil companies, all of which displayed their strong support for a healthy working relationship between industry and academia by funding the *Tectonics and Sedimentation Research Group* at the University of Alaska Fairbanks, include: Amoco, ARCO, BP Exploration (Alaska) Inc., Chevron, Conoco, Elf, Exxon, Japan National Oil Corporation, Mobil, Murphy, Phillips, Shell, Texaco, and Unocal. I extend my sincere thanks to each of these institutions for supporting academia, believing in this particular project, and helping to make this project a success.

Reproduced with permission of the copyright owner. Further reproduction prohibited without permission.

CHAPTER 1- INTRODUCTION*

STATEMENT OF THE PROBLEM

The recognition and understanding of detachment folds represent significant problems in the science of structural geology. Detachment folds are very common in fold-and-thrust belts and adjacent foreland petroleum provinces, but are rarely recognized as such and even when they are recognized, they are commonly misinterpreted. Consequently, current structural interpretations, including those relevant to petroleum exploration and production, may be inaccurate. This project addresses these problems and presents conclusions that 1) promote the recognition and understanding of detachment folds and 2) increase the accuracy of detachment fold analysis.

Detachment folds

A detachment fold is a fold in a mechanically competent rock layer that is cored by internally deformed less competent rock that is, in turn, adjacent to an unfolded competent unit (Fig. 1.1). This geometry, where an internally deformed unit is adjacent to an unfolded unit, requires that a detachment horizon, or décollement, exist between the two units. It has long been known that incompetent rock commonly accumulates in the cores of anticlines (Chamberlin 1910, Bucher 1933, Willis & Willis 1934, Goguel 1962, Laubscher 1962). Dahlstrom (1969) described the fundamental geometric characteristics of

---

* The last section of this chapter (page 43) explains the organization of the dissertation.

Reproduced with permission of the copyright owner. Further reproduction prohibited without permission.

detachment folds. Jamison (1987) and Mitra and Namson (1989) presented trigonometric models for detachment folds.

Detachment fold interpretation

Detachment folds are the only major fault-related fold type in fold-and-thrust belts that involves a substantial amount of incompetent (*i.e.* mechanically weak) rock, like salt or shale (Fig. 1.1). Although incompetent rock is common in most stratigraphic sequences, fault-related folds are most commonly interpreted using the fault-bend (Suppe 1983, Jamison 1987) or fault-propagation (Jamison 1987, Mitra 1990, Suppe & Medwedeff 1990) fold models (Fig. 1.2), which do not consider the mechanical influence of incompetent rock on fold geometry. Apparently, these geometric-kinematic interpretations of fault-bend or fault-propagation folding are used so often because of their familiarity and popularity. However, since the two models do not consider the implications for fold geometry of incompetent rock, they are inappropriate for analyzing folds involving significant amounts of incompetent rock (*e.g.* detachment folds).

Geometric-kinematic limitations of published models of detachment folds

Even when a fault-related fold is interpreted as a detachment fold and published geometric-kinematic models of detachment folds (*e.g.* Jamison 1987, Mitra & Namson 1989) are used in the analysis, the range of possible fold geometries is intrinsically limited (Fig. 1.3). This is because, while deforming, incompetent rock units tend to violate the basic assumptions used in cross section balancing and in published models of detachment folds. These assumptions are:

Reproduced with permission of the copyright owner. Further reproduction prohibited without permission.

1) deformation by plane strain where, in cross sectional view, no material moves into, or out of, the plane of section, and

2) deformation by constant incompetent unit thickness (detachment depth) where the bounding synclines of a detachment fold maintain a constant elevation above the detachment throughout fold-evolution (Fig. 1.4a).

This study presents evidence of non-plane strain and variable detachment depth for detachment folds in the northeastern Brooks Range, thus contradicting both basic assumptions.

Further, a *consequence* of the second assumption of published models, constant detachment depth, is the assumption that detachment folds form by "migrating-hinge" kinematics, where rocks in the competent layer move through the fold hinges during fold growth (Fig. 1.5). During hinge-migration, most parts of the competent layer experience both "hinge-type" deformation and "limb-type" deformation (Fig. 1.5). "Hinge-type" deformation in the competent unit of an anticline includes the development and preservation of contractional structures (*e.g.* minor folds and thrusts, cleavage, stylolites) (see Ramsay 1967, 1974). "Limb-type" deformation includes the development and preservation of bed-parallel shear associated with flexural-slip or flexural-flow folding (*e.g.* rotated pressure shadows, en-echelon tension fractures, bed-parallel slip surfaces) (see Ramsay 1967, 1974). Hinge-migration kinematics requires that limb-type structures re-deform, or structurally overprint, pre-existing hinge-type structures (Fig. 1.5). This migrating hinge kinematic mechanism is supported by *neither* mechanical theory nor recent geometric and detailed strain and growth history analyses of artificial or natural detachment folds (*e.g.* Biot 1961, Fischer *et al.*

Reproduced with permission of the copyright owner. Further reproduction prohibited without permission.

1992, Rowan & Kligfield 1992, Holl & Anastasio 1993, Hardy & Poblet 1994, Homza & Wallace 1995, Vergis *et al.* in review). These studies support a fixed-hinge, or fixed arc-length, kinematic mechanism (Fig. 1.5). Folds formed by fixed hinge kinematics buckle with a given arc-length, which involves limb-rotation rather than hinge-migration.

The documented evidence for fixed-hinge kinematics includes 1) a lack of hinge structures overprinted by limb structures on fold limbs (Homza & Wallace 1995) (Fig. 1.5), 2) syn-tectonic deposits showing evidence of limb-rotation (Holl & Anastasio 1993, Vergis *et al.* in review), and 3) the well-known fact that there is typically a greater abundance of contractional features in fold hinges than in the limbs (Ramsay 1974, Fischer *et al.* 1992, Homza & Wallace 1995). A fourth piece of evidence for fixed-hinge kinematics discussed in this study is the existence of parasitic folds near the base of the competent unit, which are difficult to form by a migrating hinge mechanism (L. Shapiro, oral comm. 1995).

Summary of the problem

Errors associated with either the use of published detachment fold models that incorporate invalid assumptions, or with incorrect interpretation of detachment folds as another fold-type, lead to inaccurate geometric and kinematic results. Such inaccurate results not only lead to the misrepresentation of fold-and-thrust structures, but they can be costly if they involve folds that are targeted in hydrocarbon exploration or production.

Reproduced with permission of the copyright owner. Further reproduction prohibited without permission.

OBJECTIVES OF THIS RESEARCH

This research has two objectives that are designed both to increase understanding of the geometry and kinematics of detachment folds in general and to refine the tectonic interpretation of the northeastern Brooks Range. The objectives are:

1) to describe the geometry and kinematic evolution of well-exposed detachment folds in the northeastern Brooks Range fold-and-thrust belt; and

2) to develop a more realistic and versatile model for the evolution of natural detachment folds.

The results are:

For objective 1: geologic maps, balanced cross sections, and structural interpretations of several natural detachment folds in the northeastern Brooks Range;

For objective 2: a general theoretical evolutionary model for detachment folds that a) does not assume constant detachment depth or migrating hinges and b) allows area changes due to the loss or gain of material within the fold to be recognized and quantified. The two elements of the research are strongly related since the model is based on the observed fold geometries and has also been used to analyze the geometric and kinematic evolution of the observed folds.

Two fundamental yet unresolved questions about detachment folds needed to be addressed in order to meet the objectives of the study. First, do detachment folds form by a fixed-hinge/rotating limb mechanism (*e.g.* Hardy & Poblet 1994), by a migrating-hinge/non-rotating limb mechanism (*e.g.* Mitra &

Reproduced with permission of the copyright owner. Further reproduction prohibited without permission.

Namson 1989), or by a combination of the two (Fig. 1.5)? Second, does the structural thickness of the detachment unit (depth-to-detachment) vary during folding and, if so, is it possible to predict the nature of such variation (Fig. 1.4)? The results of this study indicate that the detachment folds in the northeastern Brooks Range formed by a fixed-hinge/rotating limb mechanism and that the thickness of the detachment unit varied in a predictable way during folding.

LOCATION

Part of the project was a field-oriented study in the northeastern Brooks Range portion of the Arctic National Wildlife Refuge of northeastern Alaska. Access to this remote region was by helicopter, which allowed spike camps to be set up at each of 5 study areas (Fig. 1.6).

The study areas are each entirely north of the latitudinal tree line and this, together with high topographic relief, provided excellent exposures of folds clearly identifiable as detachment folds. Particular areas were chosen based on reconnaissance work by Wesley Wallace and by air-photo analysis by both Wesley Wallace and myself. Multiple small-scale detachment folds and at least one map-scale detachment fold were observed at each area. During the summer of 1992, I visited the study area at the headwaters of Straight Creek (Mt. Michelson B-3 Quad., T1S & T2S, R27E & R28E) and the study area at the West Fork of the Aichilik River (Demarcation Pt. Quad., T2S & T3S, R36E & R37E). Study areas I visited during the summer of 1993 included: The Salisbury Creek area (Mt. Michelson A-4 Quad., T3S & T4S, R24E & R25E); the Marsh Fork of the Canning River area (Mt. Michelson A-4 & Arctic D-4 Quads., T5S,

Reproduced with permission of the copyright owner. Further reproduction prohibited without permission.

R24E & R25E); and the Hulahula River area (Mt. Michelson A-1 & A-2 Quads., T3S & T4S, R31E & R32E).

METHODS

Geologic field mapping with an emphasis on structural geometry was carried out at the scale of 1:25,000 (Plates A3.1 - A5.2). Aerial photographs, topographic and regional geologic maps, a brunton compass, a jacob's staff, and various small-scale measuring devices were all used in mapping and data collection. Strike and dip data were collected from bedded units across folds and from fold axial surfaces, cleavage, faults, fractures, and shear zones where possible. Trend and plunge data were collected from fold hinges, bedding-cleavage intersections, and slickenlines. In order to constrain the kinematic mechanism of particular folds (Fig. 1.5), a counting technique for microscopic strain analysis was developed and carried out on oriented and unoriented samples. This method is similar to that of Fischer *et al.* (1992) and was designed to characterize the distribution of strain indicators with respect to limbs and hinge zones (*e.g.* Ramsay 1967, 1974) in order to constrain the kinematic mechanism of folding. Samples were collected from various positions across the folds in the Straight Creek, Salisbury Creek, and West Fork Aichilik River areas (see Appendix 1 for more on this method). Orientations and sample locations were projected down-plunge onto all sections using the method outlined by Ramsay and Huber (1987). For some sections, this method was incorporated into the computer program *PROject!*© (see Appendices 6 & 7 for more about projection techniques). The AutoCAD graphics package was used to compile

Reproduced with permission of the copyright owner. Further reproduction prohibited without permission.

the maps and construct both the cross sections and most of the figures used in this report.

TECTONIC SETTING

The northeastern Brooks Range fold-and-thrust belt is the northern continuation of the Rocky Mountain fold-and-thrust belt. Each study area is within the North Slope subterrane of the Arctic Alaska terrane (Moore *et al.* 1994) and includes both pre-Middle Devonian rocks, here loosely referred to as "basement", and younger cover rocks consisting mainly of the lower part of the Mississippian to Lower Cretaceous Ellesmerian sequence (Fig. 1.7).

The dominant structural style in the northeastern Brooks Range is a series of basement-cored east-west trending structural highs that are flanked by Ellesmerian sequence rocks (Fig. 1.6). These structures formed during growth of the north-directed, Cenozoic Romanzof uplift of Moore *et al.* (1994). This structural style and timing are different than those of the main axis of the Brooks Range where regional thrust sheets were transported northward in the Mesozoic.

Basement rocks in the study areas are relatively poorly understood and include Cambrian-Ordovician chert, phyllite, metasandstone and, locally, volcanic rocks. A regional angular unconformity separates basement rocks as young as Early Devonian from the overlying southward-facing (present coordinates) Ellesmerian passive margin sequence (Anderson *et al.* 1994) (Fig. 1.7). In the study areas, the passive margin sequence includes, in ascending stratigraphic order: the Mississippian Kekiktuk Conglomerate, the Mississippian

Reproduced with permission of the copyright owner. Further reproduction prohibited without permission.

Kayak Shale, the Mississippian-Pennsylvanian Lisburne Limestone, and, locally, the Permian-Triassic Sadlerochit Group (Fig. 1.7). The Sadlerochit Group in the study areas is represented by the Echooka Formation. Here, the Echooka is a succession of siltstone, shale, sandstone, and minor carbonate rocks. Rocks above the Sadlerochit were not observed in this study but include a series of alternating shale, sandstone, siltstone, and lesser carbonate rocks (Imm *et al.* 1993). These younger rocks record a transition from deposition on a south-facing passive margin to deposition in a north-directed foreland basin (*i.e.* a transition from pre- to syn-tectonic deposits). This transition is interrupted by several unconformities and depositional units that may record continental breakup (*e.g.* the Lower Cretaceous unconformity and Kemik Sandstone) (Mull 1987, Moore *et al.* 1994) (Fig. 1.7).

This study supports the conclusions of Wallace and Hanks (1990) that each of the several east-west trending, northward-convex structural highs, or anticlinoria, in the northeastern Brooks Range is composed of two elements (Fig. 1.8). These are:

1) a basement core, interpreted to consist of fault-bend folded horses in a regional-scale northward-directed duplex with a roof thrust in the Kayak Shale and a floor thrust at an unknown depth in the basement; and

2) a roof sequence deformed into kilometer-scale detachment folds defined by the competent Lisburne Limestone and formed above the incompetent and internally deformed Kayak Shale (Homza 1992a, Wallace 1993, Homza & Wallace 1995) (Fig 1.8).

Reproduced with permission of the copyright owner. Further reproduction prohibited without permission.

The Kekiktuk Conglomerate is beneath the roof thrust in the Kayak Shale and thus is not directly involved in the detachment folding but instead deformed with the basement as part of the horses in the duplex (Wallace & Hanks 1990). Thus, the basement and Kekiktuk Conglomerate together define the "sub-detachment competent unit" required for detachment folding.

ADVANTAGES OF THE NORTHEASTERN BROOKS RANGE AS A LOCATION FOR ANALYZING DETACHMENT FOLDS

The northeastern Brooks Range is an excellent place to study the process of detachment folding because:

1) Detachment folds are well-exposed there. The sub-detachment unit (Kekiktuk and basement), the incompetent unit (Kayak Shale), the competent folded unit (Lisburne Limestone), and the anticlinal and synclinal hinges of kilometer-scale folds are each exposed in many places. Excellent exposures and access allowed the lowest competent beds to be sampled and traversed from syncline to anticline to syncline for each fold, which enabled close observation of both mesoscopic structures and overprinting relationships. Thus, the exposure enables detailed analyses, which, in turn, allow constraints to be placed on the geometry and kinematics of detachment folding.

2) In the different study areas, folds that formed in the same stratigraphy can be observed in a variety of structural positions and stages of evolution. This allows the relationship between structural position, fold geometry, and shortening to be assessed, which, in turn, has implications for the regional tectonic interpretation of the northeastern Brooks Range. The specific structural

Reproduced with permission of the copyright owner. Further reproduction prohibited without permission.

position of each study area is discussed in context in Chapter 3, except for the Hulahula River area, which is discussed in Appendix 5.

3) The detachment folds are exposed in stratigraphy that is typical of fold-and-thrust belts (*i.e.* a sequence of alternating competent clastic and carbonate rocks and incompetent shales) and thus they can be used as analogs for structures in other stratigraphic successions elsewhere in the world.

4) Part of the Arctic coastal plain to the north of the northeastern Brooks Range is currently considered the most promising area in North America for large, undiscovered, on-shore hydrocarbon accumulations. The detachment folds discussed in this study may have analogs beneath the coastal plain in the same stratigraphy. If both the Lisburne Limestone and Kayak Shale are present beneath the coastal plain, they may contain hydrocarbon accumulations and/or their structural geometry may directly influence the geometry of potential reservoirs in the sandstones of the overlying Sadlerochit Group. The detachment folds described here may also be useful as analogs to folds that may exist elsewhere in the stratigraphy beneath the coastal plain. Such folds are likely to be smaller than those in the Lisburne because the competent unit intervals up-section are thinner than the Lisburne. The results of this study may be applied similarly to the subsurface of the North Slope west of the Arctic National Wildlife Refuge (see Chapter 4 for more about these implications).

ORGANIZATION OF THE DISSERTATION

This dissertation includes a collection of manuscripts that have been published, or are intended for publication, as scientific journal articles, state

Reproduced with permission of the copyright owner. Further reproduction prohibited without permission.

geological survey reports, or commercial products. Chapters 2 and 3 are manuscripts for scientific journals. These synthesize the major observations and interpretations and constitute the most significant contribution of the study.

Chapter 2 is an article that appeared, in modified format, in the April, 1995 issue of the *Journal of Structural Geology*. Co-authored by Wesley K. Wallace, this chapter presents our geometric and kinematic model for detachment folds and its application to a fold in the northeastern Brooks Range. The contributions of Dr. Wallace and myself for Chapter 2, are as follows: Dr. Wallace recognized that detachment folds are not widely recognized or well understood. He suggested a geometric framework for addressing the problem through geometric and kinematic modeling and advised in developing and presenting the model. He also established the conclusions about the differences among detachment folds, fault-bend folds, and fault-propagation folds (*i.e.* Table 2.1 and related text). I derived the geometry and equations and generated the graphs for the actual model, did the field work, interpreted the field observations in terms of the model, and wrote the initial draft of the chapter. Together, we developed the implications of the model and rewrote the text.

Several detachment folds in the northeastern Brooks Range are described in Chapter 3 and the detachment fold model is used to analyze their geometry and kinematics. Chapter 3 is also co-authored by Wesley K. Wallace and is to be submitted to the *Geological Society of America Bulletin* for publication. Dr Wallace advised in the selection of the areas in which to study natural detachment folds, in the approach toward analysis of their geometry and kinematics, and in the presentation of the research. I did the field work,

Reproduced with permission of the copyright owner. Further reproduction prohibited without permission.

constructed the balanced cross sections, applied the model presented in Chapter 2 to the natural folds, conceived of and generated the graphs and figures, and wrote the initial draft of the text. Together, we interpreted most of the observed folds and rewrote the text. Thus, Chapter 2 is a conceptual model for the geometry and kinematics of detachment folds, Chapter 3 documents natural detachment folds and how they relate to the model presented in Chapter 2, and both chapters are collaborative efforts.

Chapter 4 presents important implications of the research that are referred to, but are not discussed in detail, in Chapters 2 and 3. Neither Chapter 4 nor Chapter 5, which is a consise outline of the conclusions of this work, are intended for publication as such.

The nine appendices take the form of supplementary text including data and explanation of procedures. They provide detailed descriptions of:

- the strain-analysis technique used in Chapter 3 (Appendix 1);
- five study areas in the northeastern Brooks Range and their detachment folds, including geologic maps and balanced cross sections (located in the back pocket of the dissertation) (Appendices 2, 3, 4, & 5);
- a method, developed during this study, for projecting data onto a geologic cross section (Appendix 6). This section is also intended for publication in a scientific journal. It is to be co-authored by Wesley K. Wallace. Our recognition of the need for a refined projection technique arose from a conversation between us in 1992. I designed the method and wrote the report. Together, Wes and I rewrote the report.

Reproduced with permission of the copyright owner. Further reproduction prohibited without permission.

- the use of a computer program, developed during this study, which automates the process of projecting data onto a geologic cross section (Appendix 7). The program is an AutoLISP function (≅ 50 pages of code, ≅ 40 kilobytes) to be used with the AutoCAD design program.
- the use of a second computer program that was also developed during this study and is written in AutoLISP for AutoCAD. This program automates the process of constructing balanced detachment fold geometries according to the models presented in Chapter 2 (Appendix 8).

Although Appendices 6 and 7 do not address detachment folds specifically, they are included because they describe tools developed during this study for accurately depicting fold geometries in cross section. Appendices 2 and 3 have been released and appendices 4 and 5 are to be released as Public Data Files by the Alaska Division of Geological and Geophysical Surveys. Appendix 7 is part of a copyrighted commercial software product, *PROject!*©. Although only the users' guide is given here, the program can be purchased from *RockWare, Inc.*, a scientific software distribution company. The computer program described in Appendix 8, *Detfold*, is considered "shareware" and is included in this dissertation in two formats, 1) the AutoLISP code is printed in Appendix 9 and 2) the program is loaded on the 3.5" disk at the end of the manuscript.

Reproduced with permission of the copyright owner. Further reproduction prohibited without permission.

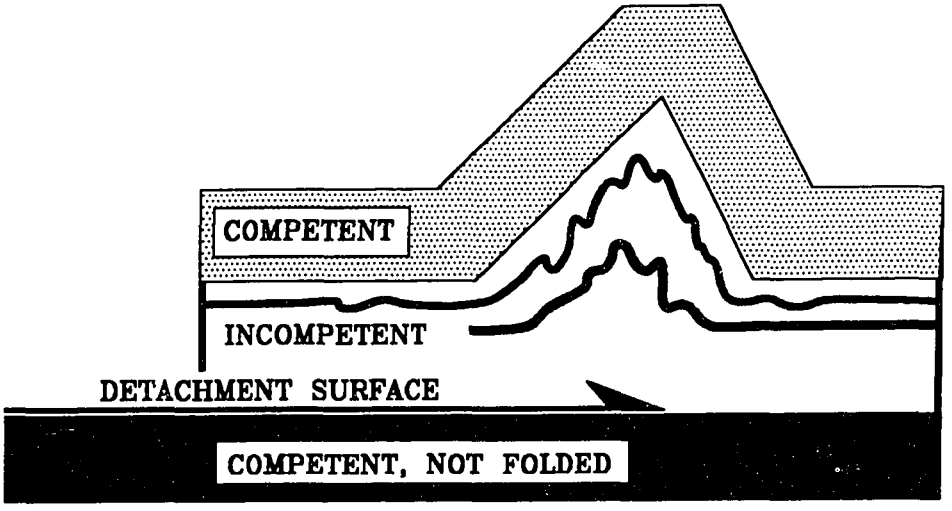

Figure 1.1. A diagram of an idealized detachment fold showing the position of the essential incompetent rock unit.

Reproduced with permission of the copyright owner. Further reproduction prohibited without permission.

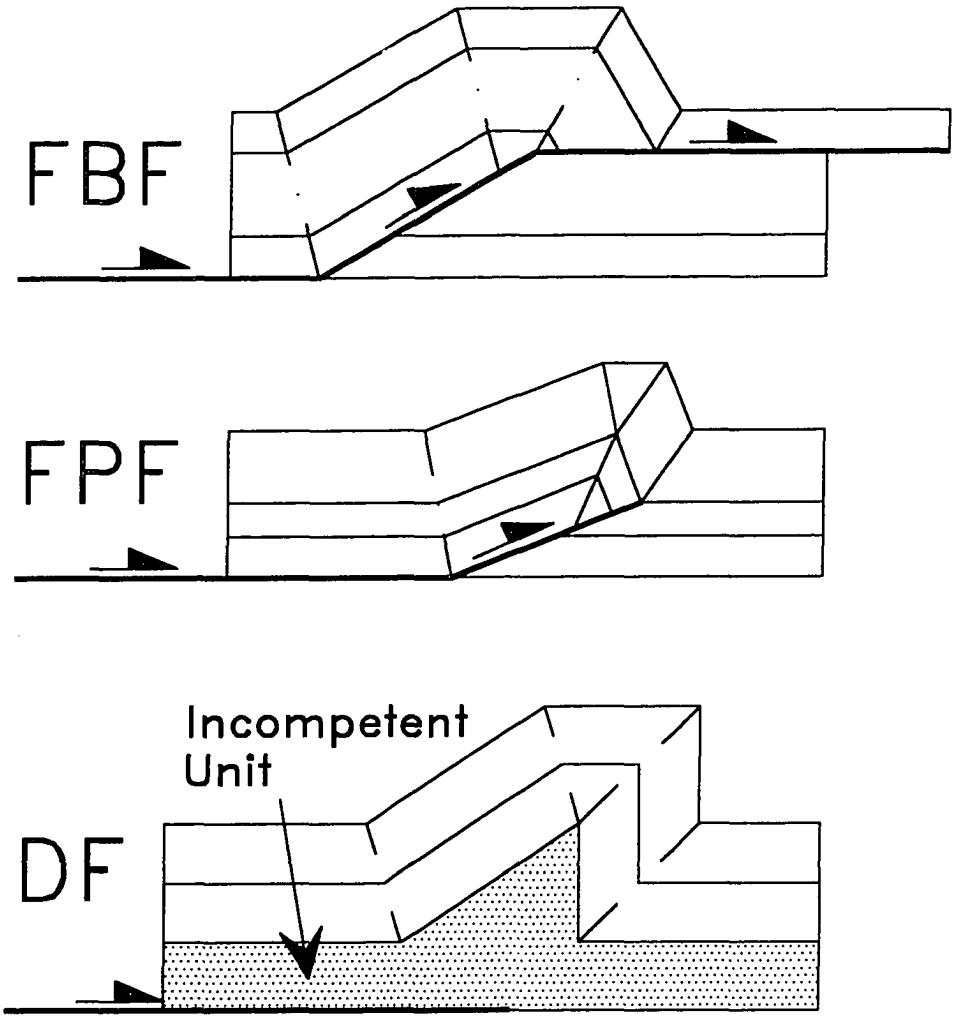

Figure 1.2. The three models of thrust-related folds in fold-and-thrust belts. The fault-bend fold (FBF), fault-propagation fold (FPF), and detachment fold (DF).

Reproduced with permission of the copyright owner. Further reproduction prohibited without permission.

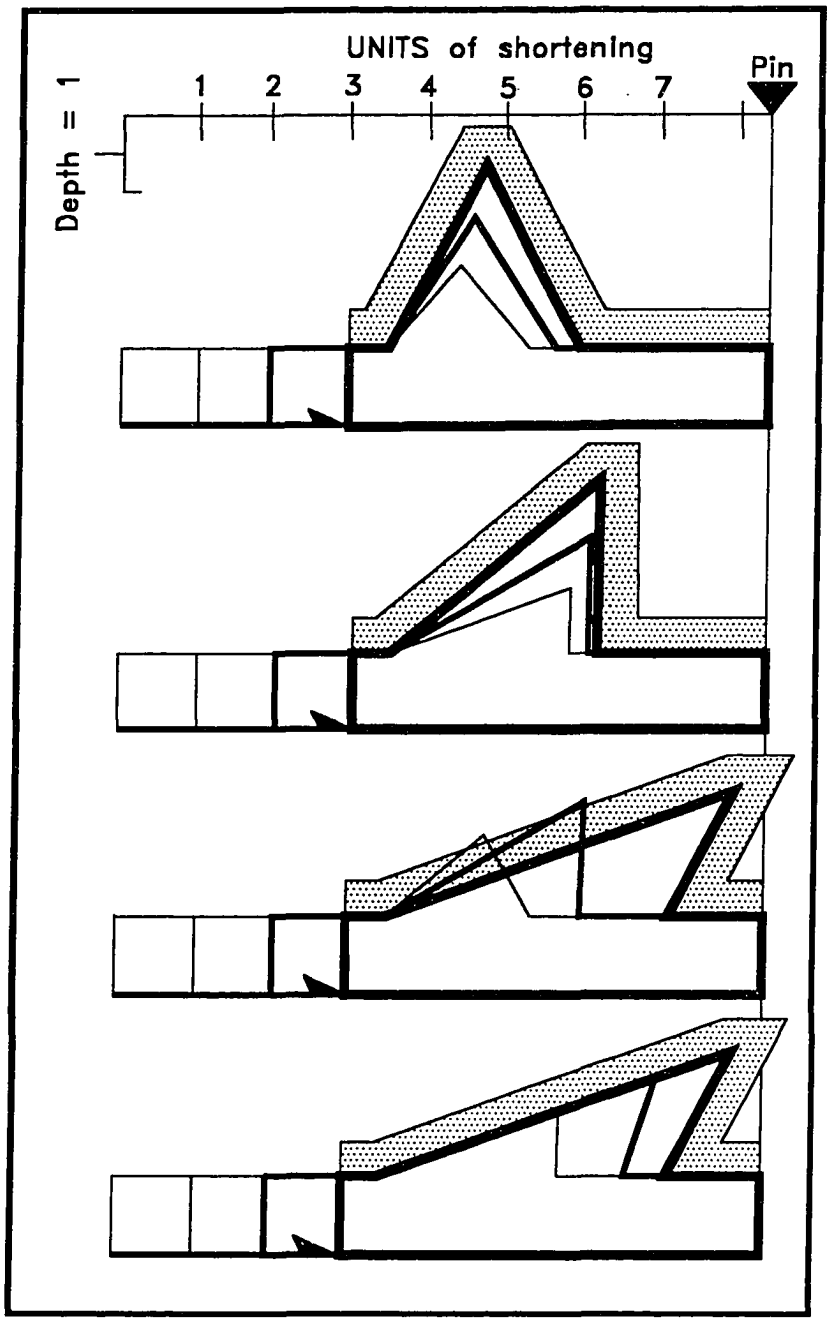

Figure 1.3. Diagram showing geometric-kinematic paths possible using published geometric models (*e.g.* Jamison 1987, Mitra & Namson 1989). Progressively thicker lines indicate successive steps in fold evolution with increasing shortening above a constant detachment depth. For clarity, the competent unit is shown as shaded only in its final geometry.

Reproduced with permission of the copyright owner. Further reproduction prohibited without permission.

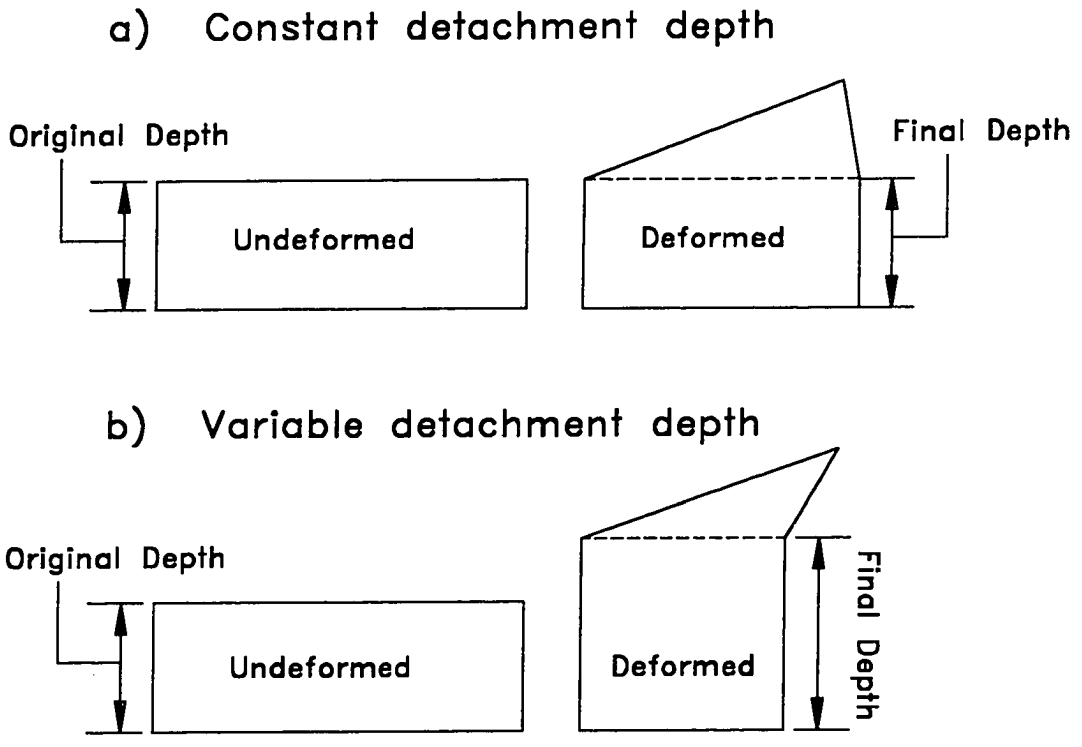

Figure 1.4. Diagram illustrating the concept of detachment depth variation as measured at the hinges of the synclines bounding the detachment anticline. a) The thickness of the detachment unit remains constant during folding - constant detachment depth. b) The thickness of the detachment unit changes during folding (increases in this case) - variable detachment depth.

Reproduced with permission of the copyright owner. Further reproduction prohibited without permission.

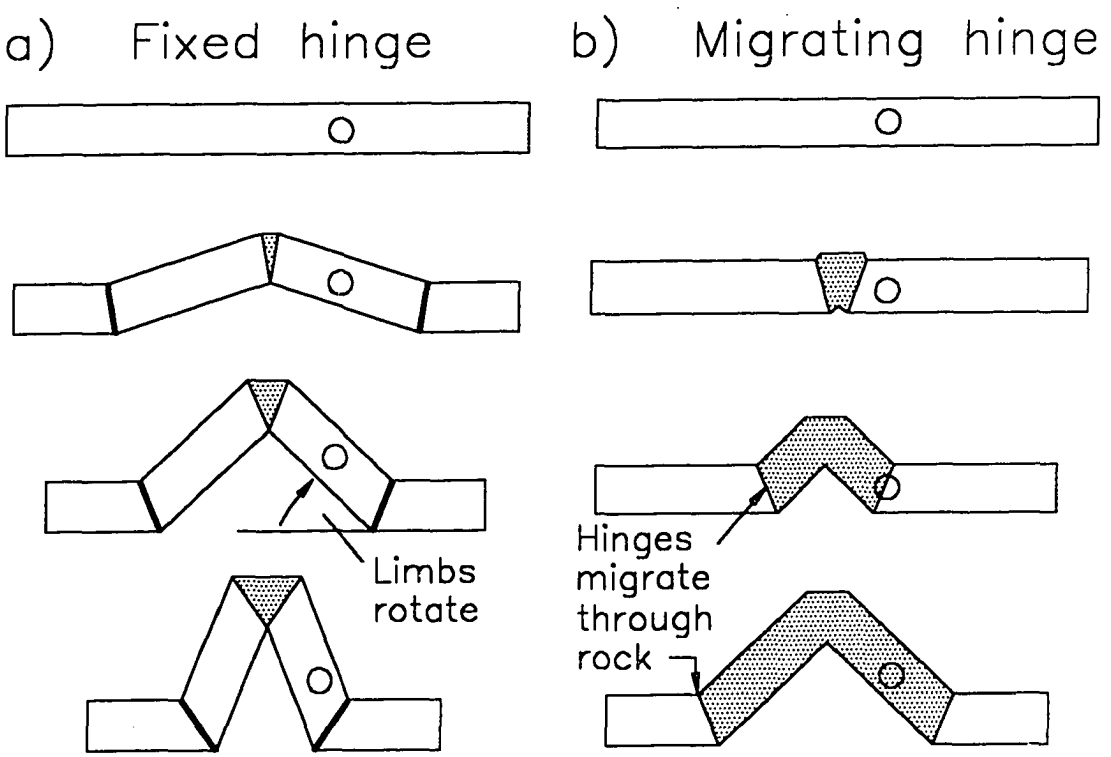

Figure 1.5. Diagram showing the fundamental difference in kinematics between fixed- and migrating hinge folding. The circle represents a particle path and the shaded area represents rock that has experienced hinge-type deformation. (a) The arc-length remains constant and hinges are fixed throughout the evolution of the fold, the particle experiences only limb-type deformation. (b) The arc-length increases and the particle is rolled through a hinge and experiences hinge-type deformation followed by limb-type deformation.

Reproduced with permission of the copyright owner. Further reproduction prohibited without permission.

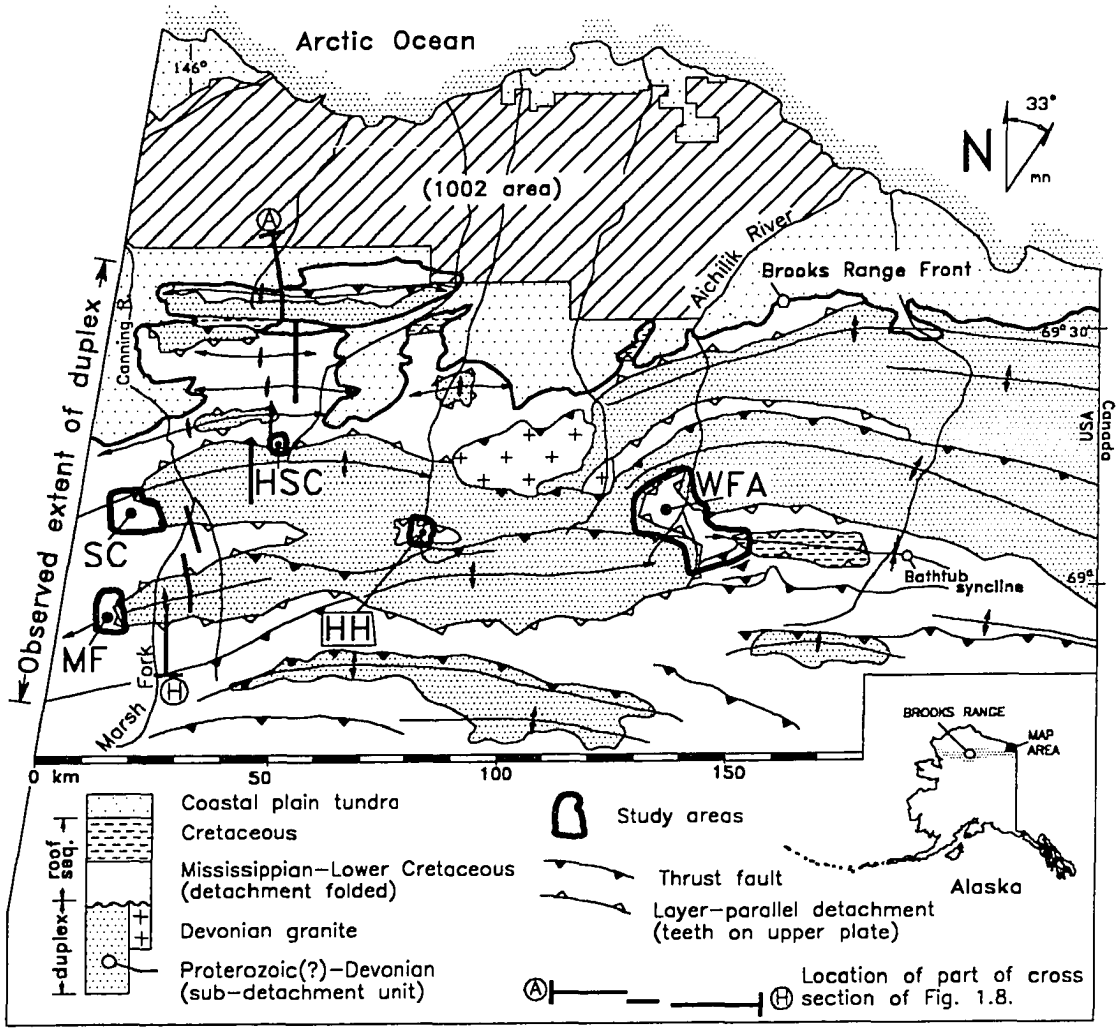

Figure 1.6. Simplified structural map of the northeastern Brooks Range and coastal plain of the Arctic National Wildlife Refuge (including the "1002" area) showing the study areas, the regional anticlinoria, and the location of the cross section of figure 1.8. HSC = Headwaters of Straight Creek area (Appendix 2, Plates A2.1 & A2.2), SC = Salisbury Creek area (Appendix 3, Plates A3.1 & A3.2), MF = Marsh Fork area (Appendix 3, Plates A3.3 & A3.4), WFA = West Fork Aichilik River area (Plates A4.1 & A4.2), HH = Hulahula River area (Appendix 5, Plates A5.1 & A5.2).

Reproduced with permission of the copyright owner. Further reproduction prohibited without permission.

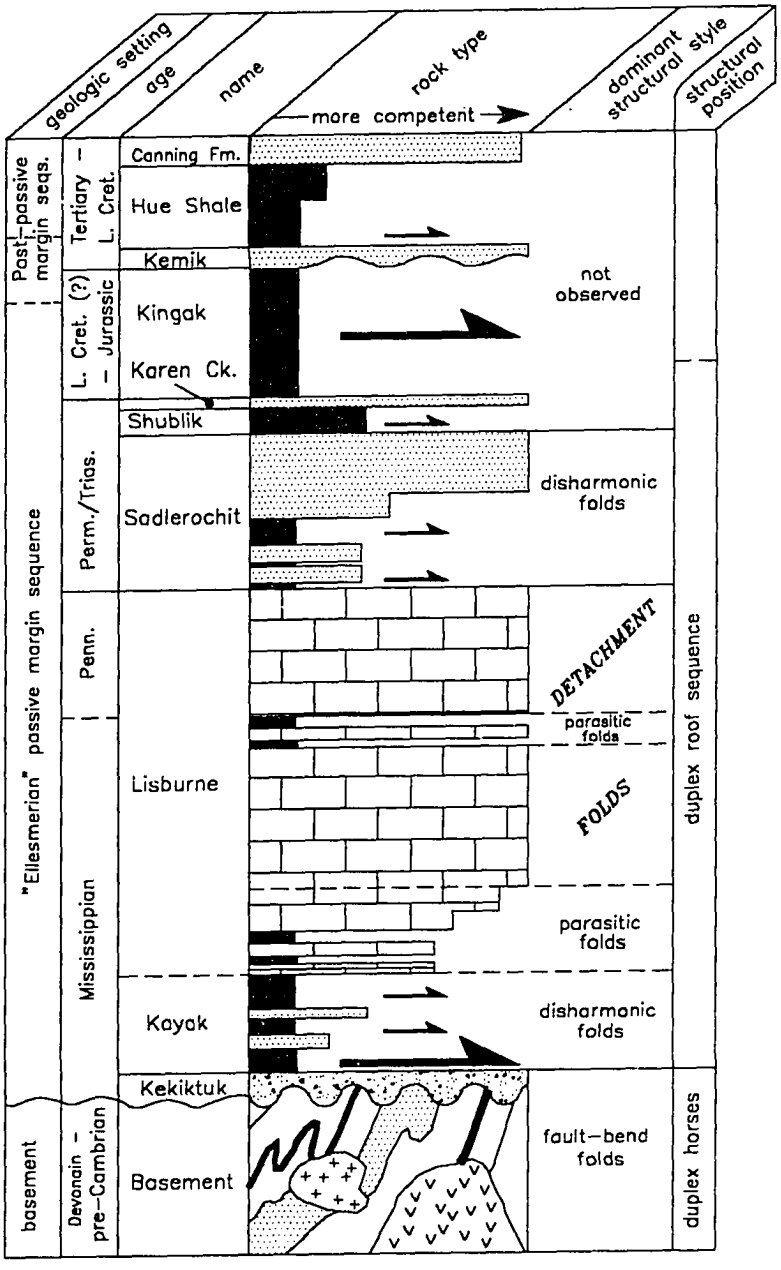

Figure 1.7. Generalized stratigraphic column of rocks involved in the detachment folding in the northeastern Brooks Range. Scale is approximate.

Reproduced with permission of the copyright owner. Further reproduction prohibited without permission.

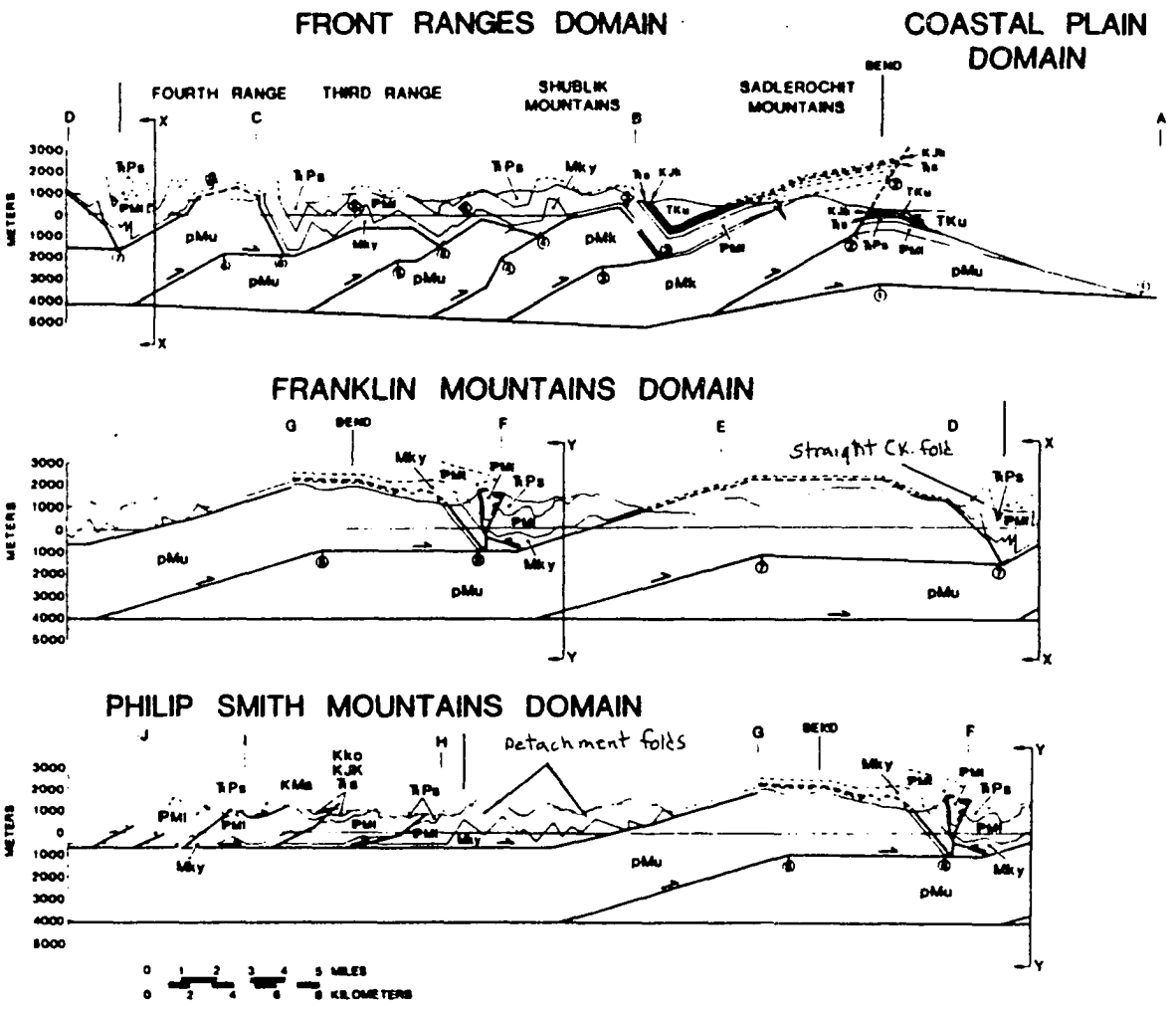

Figure 1.8. Balanced Cross section across the northeastern Brooks Range near the Canning River showing both the interpreted fault-bend folded horses in the regional duplex and the relative structural position of the detachment folds in the roof sequence (from Wallace 1993).

Reproduced with permission of the copyright owner. Further reproduction prohibited without permission.

CHAPTER 2*- THE GEOMETRIC AND KINEMATIC MODELING OF DETACHMENT FOLDS

Three major types of thrust-related folds have been recognized in fold-and-thrust belts (Jamison 1987) (Fig. 2.1): fault-bend folds (Suppe 1983, Jamison 1987), fault-propagation folds (Jamison 1987, Mitra 1990, Suppe & Medwedeff 1990), and detachment (or décollement) folds (Dahlstrom 1969, 1970, 1990, Jamison 1987, Mitra & Namson 1989, Mitra 1992). Detailed descriptions have been given of the geometry and kinematics of fault-bend folds (Suppe 1983) and fault-propagation folds (Suppe & Medwedeff 1990, Mitra 1990). However, a comparable treatment of the geometry and kinematics of detachment folds is lacking in the literature to date. Here we present two geometric models for detachment folds that provide a framework for describing and constraining their kinematic evolution.

Alternating mechanically competent and incompetent rock units constitute the stratigraphy in most fold-and-thrust belts, and folds in relatively competent units with internally deformed weaker rock in their cores are common. We consider a detachment fold to be a fold in a relatively competent rock unit that is cored by internally deformed less competent rock that is separated from another competent unit by a detachment horizon or décollement. Detachment folds may be bounded by detachment horizons above, below, or both. Many detachment

---

* Published as: Homza, T. X. & Wallace, W. K. 1995. Geometric and kinematic models for detachment folds with fixed and variable detachment depths. *J. Struct. Geol.* **17**, 575-588.

Reproduced with permission of the copyright owner. Further reproduction prohibited without permission.

folds may be buckle folds, but many buckle folds are not detachment folds because they are not bounded by a detachment horizon.

Geometries that we consider characteristic of detachment folds are widespread in nature and have been recognized since the 19th century (see Willis & Willis (1934) for a review). However, because of the lack of a clear and widely used definition of the term "detachment fold," many folds with appropriate geometries have not been explicitly identified as detachment folds. Consequently, it is difficult to use published information to assess the full range of detachment fold geometries that exist in nature. Another difficulty in documenting the geometry and kinematics of detachment folds is that few geometric constraints can be imposed upon deforming incompetent rocks, thus requiring the use of simplifying assumptions about fold geometry and kinematics.

Here, we describe quantitatively the implications of one fundamental assumption that is commonly made about detachment folds: that detachment depth remains constant during folding. We have chosen to focus on this assumption because its validity and quantitative implications haven't been as thoroughly explored as others and because variability of detachment depth due to thinning or thickening of the incompetent unit is quite plausible in detachment folds (Wiltschko & Chapple 1977, Davis & Engelder 1985).

We have developed two simple, theoretical, quantitative models for the geometry of detachment folds based on the law of conservation of volume (Goguel 1962, Dahlstrom 1969, 1990, Mitra & Namson 1989). The first model is for detachment folds formed above a detachment unit of constant thickness (constant detachment depth model) and the second is for detachment folds

Reproduced with permission of the copyright owner. Further reproduction prohibited without permission.

formed above a detachment unit that changes thickness during folding (variable detachment depth model).

We do not assume that these models directly represent natural folds. Rather, they provide idealized standards against which natural folds can easily be compared. Such comparisons can be made using easily obtained geometric measurements, rather than values related to fold mechanics or dynamics that are far more difficult to constrain. The explicit assumptions incorporated in the models serve to isolate the variables that may influence fold geometry and kinematics.

CONSERVATION OF LINE-LENGTH AND AREA IN DETACHMENT FOLDS

The concepts of conservation of bed length and cross-sectional area (*e.g.* Goguel 1962, Hossack 1979, Geiser 1988) are widely known and applied to the balancing of structural cross sections in foreland fold-and-thrust belts that have been deformed in plane-strain at relatively low temperatures and pressures (Woodward *et al.* 1985, 1989). Our detachment fold models, as well as those of Dahlstrom (1969, 1990), Jamison (1987), and Mitra & Namson (1989) rely fundamentally on these two concepts. The first concept is that competent units form parallel folds by flexural slip, with cross-sectional bed length being conserved during deformation. The second is that cross-sectional area is conserved during deformation.

Conservation of bed length can be expressed as the "line-length constraint":

$$S = L_f - L_1 \qquad (2.1),$$

Reproduced with permission of the copyright owner. Further reproduction prohibited without permission.

where S is shortening, L_f is the arc-length of a reference bed after folding and L_1 is the horizontal component of the folded length of the reference bed (Fig. 2.2).

Conservation of cross-sectional area can be expressed as "the area constraint":

$$SD_C = A_f \qquad (2.2),$$

where D_C is constant detachment depth and A_f is the area of the incompetent unit uplifted above its undeformed regional base level as a result of shortening (Fig. 2.2).

In an ideal detachment fold, bed length is conserved in the parallel-folded competent unit that defines the fold but not in the detached, incompetent unit that cores the fold. An incompetent unit, such as salt or shale, does not form parallel folds at the scale of the entire unit, but rather deforms internally by some combination of folding, faulting, and penetrative strain. Thus, these units tend to thicken during deformation so that unit length apparently decreases. Although line-length balancing is invalid for incompetent rocks, conservation of cross-sectional area is still assumed to apply. The contact between the competent unit and the adjacent incompetent unit defines the original length of that incompetent unit. Thus, equations (2.1) and (2.2) can be combined as "the equal area equation":

$$D_C = A_f / (L_f - L_1) \qquad (2.3).$$

This relationship has been accepted and widely used in various forms with differing degrees of success since Chamberlin (1910) first used it to estimate detachment depths beneath Appalachian folds (Bucher 1933, Goguel 1962, Laubscher 1962, Dahlstrom 1969, Jamison 1987, Mitra & Namson 1989,

Reproduced with permission of the copyright owner. Further reproduction prohibited without permission.

Thompson 1989, Mitra 1992, Epard & Groshong 1993). Recent applications of the "equal-area method" to the geometry and kinematics of detachment folds have assumed unchanging detachment depth during deformation (Jamison 1987, Mitra & Namson 1989, Epard & Groshong 1993). The models presented below explore the implications of this assumption and the consequences of relaxing it.

THE MODELS

We present two simple, idealized geometric models for detachment folds that are based on relating the line-length and area constraints. The only assumptions about mechanical behavior are that an upper competent unit deforms by parallel folding and a lower incompetent unit deforms internally. These mechanical concepts of competent vs. incompetent, which are difficult to quantify practically, are represented in the models by their geometric equivalents, fixed vs. variable thickness and length, which are easy to observe and measure. The models assume a simple triangular fold form common among natural detachment folds (*e.g.* Jamison 1987, Wallace & Hanks 1990, Homza 1992a, Wallace 1993), but the equations presented below can be modified to accommodate more complicated geometries. An ideal parallel kink-fold geometry is used for the competent unit, with no thinning or thickening of limbs, and plane strain is assumed, so there is no change in cross-sectional area during shortening. The models consider only single folds and so apply only to those multi-fold systems in which adjacent detachment folds do not overlap. Bed-parallel shear is assumed to be absent outside of the detachment fold in

Reproduced with permission of the copyright owner. Further reproduction prohibited without permission.

both the competent and incompetent units and the detachment surface is assumed to parallel the regional datum defined by the fold (Fig. 2.2). Thus, the major geometric constraints for both models are simply that the competent unit must conserve line-length and the incompetent unit must conserve area. The sole difference between the two models is the assumption of constant depth in the first model, but not in the second.

Constant detachment depth model

The first model represents detachment folds formed above a detachment horizon that maintains a constant depth (thickness) during folding (Fig. 2.2). The power of this model lies in the fact that both detachment depth and shortening can be determined independently given only the geometry of the detachment fold. This geometry can be expressed uniquely in terms of any three of the following variables, including at least one linear dimension: interlimb angle (γ), backlimb dip (α), forelimb dip (ω), wavelength (W), and height (H) (where γ and $\omega < 180^\circ$ and $\alpha < 90^\circ$). The equations derived here are expressed in terms of γ, α, and H, and all angles are expressed in degrees.

Using the appropriate variables above, the area constraint (equation 2.2) can be expressed as:

$$D_C = WH/2S \qquad (2.4).$$

Similarly, the line-length constraint (equation 2.1) can be expressed as:

$$S = \sqrt{(H^2 + X^2)} + \sqrt{(H^2 + Y^2)} - W \qquad (2.5),$$

where X and Y are the bases of two separate right triangles that, together, describe the form of the fold. The following relationships are also implicit from Figure 2.2:

Reproduced with permission of the copyright owner. Further reproduction prohibited without permission.

$$W = X + Y \quad (2.6),$$

$$\alpha + \gamma + w = 180^{o} \quad (2.7),$$

$$Y = H \cot \omega \quad (2.8),$$

$$X = H \cot \alpha \quad (2.9).$$

Substituting equations (2.8) and (2.9) into equation (2.6), and expressing w as $(180 - \gamma - \alpha)$ yields:

$$W = H \{\cot (180 - \gamma - \alpha) + \cot \alpha\} \quad (2.10).$$

To solve for the shortening that is geometrically required to uplift the area bounded by the triangular fold, substitute equations (2.8), (2.9), and (2.10) into equation (2.5) , again expressing ω as $(180 - \gamma - \alpha)$, and rearrange such that:

$$S = \sqrt{\{H^2 + (H\cot\alpha)^2\}} + \sqrt{[H^2 + \{H\cot(180 - \gamma - \alpha)\}^2]} - H\{\cot(180 - \gamma - \alpha) + \cot\alpha\} \quad (2.11).$$

To solve for the fixed detachment depth (D_C) that is geometrically required to uplift the area bounded by the triangular fold, substitute equations (2.10) and (2.11) into equation (2.4) and rearrange such that:

$$D_C = H^2\{\cot(180 - \gamma - \alpha) + \cot\alpha\} / 2(\sqrt{\{H^2 + (H\cot\alpha)^2\}} + \sqrt{[H^2 + \{H\cot(180 - \gamma - \alpha)\}^2]} - H\{\cot(180 - \gamma - \alpha) + \cot\alpha\} \quad (2.12).$$

Notice that the detachment depth calculation is based on the area constraint (equation 2.2), whereas the shortening calculation is based on the line-length constraint (equation 2.1), and that each is expressed entirely in terms of fold geometry (*i.e.* γ, α, and H). Equations (2.10), (2.11) and (2.12) can be solved in terms of the forelimb dip, ω, simply by substituting ω for α (also note that the expression $(180 - \gamma - \alpha)$ is left in expanded form so it can easily be

Reproduced with permission of the copyright owner. Further reproduction prohibited without permission.

replaced by ω, since $\omega = (180 - \gamma - \alpha)$). Solving equations (2.11) or (2.12) in terms of W rather than H, or in terms of α and ω rather than γ, requires different sequences of substitution that are not presented here. Equation (2.12) is analogous to equation (21) of Jamison (1987).

In conclusion, if any three of the variables γ, α, ω, H, W, S, or D_C are known, including at least one linear dimension, the others can be determined, specifying a unique fold geometry and size.

The constant-depth diagram

The relationship between shortening and fold geometry must be considered in order to determine possible kinematic paths for detachment folds. This relationship was considered qualitatively by Dahlstrom (1990), but was not directly addressed by either Jamison (1987) or Mitra & Namson (1989). The fold geometries predicted by our model can be plotted as a function of shortening/constant detachment depth (S/D_C) vs. wavelength/height (W/H), with interlimb angle (γ) and backlimb dip (α) varying according to equations (2.11) and (2.12) (Fig. 2.3). Every point on this "constant-depth diagram" describes one and only one fold form, although the size of each form varies as a function of shortening and detachment depth. Length ratios are used on this plot instead of absolute lengths in order to represent the large number of variables on a single plot for fold geometry, which can be used to trace kinematic paths.

Since the kinematic evolution of a fold is controlled by increasing shortening, this plot constrains the possible kinematic paths that an ideal detachment fold may follow. The kinematic path must be continuous from the inception to the final form of the fold. Since the detachment depth is held

Reproduced with permission of the copyright owner. Further reproduction prohibited without permission.

constant, any fold must follow a path with an increasing value of S/D_C as shortening increases.

Implications of the constant-depth diagram for the kinematic evolution of ideal detachment folds

The lower boundary of the field of possible fold geometries in figure 2.3 is the "line of symmetrical folds", which is asymptotic to $S/D_C = 0$. In order for the graphical plot of successive geometries of an evolving fold to proceed from the $S/D_C = 0$ line to the line of symmetrical folds, the fold must either: 1) nucleate at $W/H = \infty$; or 2) nucleate with a geometry corresponding to the upper boundary of a finite field for which our equations have no solutions (shaded area on Fig. 2.3). Thus, natural detachment folds could: 1) nucleate with a very high W/H and initially symmetrical geometries; or 2) nucleate after a finite amount of shortening was accommodated by mechanisms other than folding (see Biot 1961, Dixon & Tirrul 1991, and Abbassi & Mancktelow 1992 for additional discussion and references about fold nucleation). In either case, the relative position of the line of symmetrical folds at the base of the range of permissible shapes implies that the initial form of an *ideal* detachment fold is symmetrical.

Folds may become asymmetrical with increasing shortening depending on whether or not the kinematic path follows the line of symmetrical folds. If detachment depth is fixed, equations (2.11) and (2.12) require that at least two limb angles change with increasing shortening (Figs. 2.3 & 2.4). Thus, growth of a self-similar, fixed limb-dip geometry is not possible with a fixed detachment depth (Figs. 2.3 & 2.5a). If detachment depth is fixed, the equations also require

Reproduced with permission of the copyright owner. Further reproduction prohibited without permission.

an increase in total limb length as shortening increases so that fixed arc-length buckle folds are not possible (Fig. 2.5b) (Dahlstrom 1990).

Variable detachment depth model

The variable detachment depth model (Fig. 2.6) permits a wider range of geometries and kinematic paths than does the constant depth model. In this model, the fold area depends simply on fold geometry and is independent of detachment depth. We define D_o as the undeformed thickness of the incompetent unit (original depth), D_f as the final thickness of the incompetent unit beneath the fold (final depth), and ΔD as the variation in incompetent unit thickness during deformation (Fig. 2.6) such that:

$$\Delta D = D_f - D_o \quad (2.13),$$

$$A_o + A_{Do} = A_f + A_{Do} + A_{\Delta D} \quad (2.14),$$

$$A_o = SD_o \quad (2.15),$$

$$A_{Do} = W(D_o) \quad (2.16),$$

$$A_f = WH/2 \quad (2.17),$$

and the "area differential"

$$A_{\Delta D} = W(\Delta D) \quad (2.18).$$

These equations can be combined to yield:

$$D_f = D_o S/W + D_o - H/2 \quad (2.19),$$

or:

$$D_f/D_o = S/W + 1 - H/2D_o \quad (2.20).$$

Given a specific fold geometry, either the final detachment depth beneath the fold (D_f) or the original detachment depth (D_o) can be determined if the other is known. D_o is invariant, since it represents the undeformed thickness of the

Reproduced with permission of the copyright owner. Further reproduction prohibited without permission.

incompetent unit. We assume D_o is known, as would be the common case where the undeformed stratigraphic thickness of the incompetent unit can be determined outside the fold. However, we stress that if D_f is known, D_o can be determined by modifying the equations.

The area differential

The area differential ($A_{\Delta D}$ in Fig. 2.6) represents the difference between the displaced area ($A_o = SD_o$) and the cross-sectional area of the fold (A_f). The area differential can be either positive or negative depending on whether the fold area is smaller or larger, respectively, than the displaced area. A positive area differential indicates a final detachment depth that is greater than the original detachment depth, perhaps due to layer-parallel thickening in the incompetent unit (*e.g.* Fig. 2.6). Such structural thickening beneath folds is a common feature in physical models of folds (*e.g.* Dixon & Tirrul 1991) and in natural detachment folds (*e.g.* Wallace 1993, Homza 1992a, 1993). A negative area differential indicates an original depth that is greater than the final depth, perhaps due to vertical transport of excess material from directly beneath the fold into the fold. Such thinning during folding is also a common feature both in physical models of folds and in natural folds, especially in the early stages of fixed arc-length folding when W/H is large (Wiltschko & Chapple 1977, Dixon & Tirrul 1991, Dixon & Liu 1992). In order to establish a quantitative relationship between the undeformed and shortened states, it is necessary to define boundaries on the area within which the incompetent unit may move during deformation. In this model, material is arbitrarily assumed not to be transported through the lines perpendicular to the detachment surface and connected to the

Reproduced with permission of the copyright owner. Further reproduction prohibited without permission.

synformal hinges bounding the fold, although the thickness of the incompetent unit directly beneath the synformal hinges may vary. In other words, all of the material in and beneath the antiform is assumed to have originated in the area bounded by the synformal hinges and the geometry outside of the synforms is not considered. The regional datum as defined by the synformal hinges at the base of the competent unit is also assumed to remain parallel to the detachment surface.

The variable-depth diagram

Detachment folds formed above an incompetent layer that changed thickness during deformation, such that $D_f \neq D_o$, can be plotted on a variable-depth diagram (Fig. 2.7). The diagram consists of two linked graphs: the upper graph is analogous to the constant-depth diagram since it is used to plot fold geometries and every point on the graph represents one and only one fold form; the lower graph has the same X-axis as the upper graph and is used to determine the variation in detachment depth. As with the constant-depth plot, length ratios are used on the upper graph in order to allow the large number of variables to be shown on a single plot for fold geometry. For any fold geometry, only one linear dimension is needed to calculate the others using the equations above. The lower graph is required to accommodate the additional variable, detachment depth. It is the plot of a straight line, the "depth line", for which the slope is one and $(1 - H/2D_o)$ is the Y-intercept (equation 2.20). The position of this line on the Y-axis is determined, therefore, by H and D_o. However, since D_o remains constant, any shift of the depth line on the Y-axis along a kinematic path is a function only of variation in H (Figs. 2.8 & 2.9).

Reproduced with permission of the copyright owner. Further reproduction prohibited without permission.

Determining the detachment depth for a given detachment fold with a known D_O requires several steps (Figs. 2.8 & 2.9). First, the fold geometry must be plotted as a point on the upper graph. Second, a depth line with the appropriate Y-intercept is constructed on the lower graph. Finally, a vertical line, representing S/W of the fold, is drawn to link the point defining the geometry with the depth line. The S/W line and the depth line intersect on the lower graph at a point which defines the D_f/D_O value (Y-value) for the given geometry and given D_O. Thus, D_f can easily be calculated since D_O and D_f/D_O are now both known. It is important to note that multiple depth lines may be needed in order to trace the geometric evolution of a fold along a particular kinematic path since the evolution may involve changes in the value of H (*e.g.* Fig. 2.9).

Implications of the variable-depth diagram for the kinematic evolution of ideal detachment folds

A fold evolves incrementally as shortening increases. Its kinematic path must be a continuous curve for which values of either S/H or S/W increase. Either ratio may decrease. If both ratios decrease together, however, then shortening decreases, which is not a viable kinematic path. All other paths are considered geometrically viable, although some may be geologically implausible. The line of symmetrical folds on this diagram is asymptotic to S/H = 0, suggesting identical geometric implications to those described above for fold nucleation with a fixed detachment depth. An infinite array of geometrically possible kinematic paths can be plotted on the variable-depth diagram. Examples of kinematic paths for fixed arc-length (Figs. 2.8 & 2.9), constant-depth (Figs. 2.10a & 2.11), and self-similar (Figs. 2.10b & 2.11) folds are shown

Reproduced with permission of the copyright owner. Further reproduction prohibited without permission.

here to illustrate specific implications of variable detachment depth for fold evolution.

Fixed arc-length growth requires a path of first increasing, then decreasing depth, as has been noted by Wiltschko & Chappie (1977) and Dahlstrom (1990) (Figs. 2.8 & 2.9). On the variable-depth diagram, a kinematic path for geometries with a constant detachment depth requires that the S/W line and the depth lines intersect at $D_f/D_o = 1$ for every increment of growth (Figs. 2.10a & 2.11). Self-similar geometric growth requires a decrease in detachment depth as shortening increases in order for the geometry to balance (Figs. 2.10b & 2.11).

THE KINEMATICS OF DETACHMENT FOLDS: FIXED OR MIGRATING HINGES?

Empirical observations and mechanical considerations suggest that buckle folds in a competent layer bounded by incompetent material nucleate with an arc length that is a function of rheology and competent layer thickness, and retain a constant arc length, and hence fixed hinges, as shortening increases and the fold grows (de Sitter 1956, Biot 1961, Currie *et al.* 1962, Ramberg 1964, Ramsay 1967, 1974, Johnson 1977, Abassi & Mancktelow 1992, Fischer *et al.* 1992, Mancktelow & Abassi 1992) (Fig. 2.12a). Mitchell & Woodward (1988) assumed that detachment folds form by this fixed arc-length buckling mechanism, and Thompson (1989), Fischer *et al.* (1992), Rowan & Kligfield (1992), and Holl & Anastasio (1993) provide evidence for fixing-hinge growth of folds that could be interpreted as detachment folds. We have observed multiple

Reproduced with permission of the copyright owner. Further reproduction prohibited without permission.

detachment folds whose distribution of strain indicates that hinges were fixed during most or all of folding (*e.g.* Homza 1993). An important implication of fixed-hinge fold growth is that fold limbs rotate during fold growth, as observed in many natural folds (*e.g.* Hardy & Poblet 1994), in contrast with the fixed limb orientations of ideal fault-bend or fault-propagation folds (Suppe 1983, Suppe & Medwedeff 1990, Mitra 1990).

Dahlstrom (1990) pointed out that fixed arc-length folding is incompatible with conservation of cross-sectional area for a constant detachment depth, which requires a linear relationship between shortening and uplifted cross-sectional area (equation 2.2) (Fig. 2.13). In contrast, Wiltschko & Chapple (1977) documented a non-linear relationship between uplifted area and shortening for symmetrical fixed arc-length folds (Figs. 2.8a, 2.9, & 2.13). The incompatibility between constant detachment depth and fixed arc-length folding is particularly obvious for fixed arc-length folds with interlimb angles less than a critical value, below which uplifted area decreases with increasing shortening (Fig. 2.13) (Wiltschko & Chapple 1977). Wiltschko & Chapple (1977) resolved this problem by assuming that incompetent material moves from synforms to antiforms as uplifted area initially increases, then flows out of the antiforms as area decreases with increasing shortening, resulting in a change in detachment depth with fold evolution. The present models quantitatively illustrate the fundamental incompatibility of the assumption of constant detachment depth with the growth of fixed arc-length folds. They show that detachment depth must change as a fixed arc-length fold evolves (Figs. 2.5b & 2.8), and allow the

Reproduced with permission of the copyright owner. Further reproduction prohibited without permission.

required changes in detachment depth to be determined (equation 2.19 & Figs. 2.8 & 2.9).

In order for a detachment fold to grow with a constant detachment depth, the uplifted area in its core must increase linearly as shortening increases (Fig. 2.13). This requires an increase in length of one or more fold limbs, which in turn requires hinge migration (Fig. 2.12b). Growth of folds by hinge migration has been documented for kink bands (Weiss 1968, Stewart & Alvarez 1991), and has been used to model fault-bend folds (Suppe 1983) and fault-propagation folds (Suppe & Medwedeff 1990). Dahlstrom (1990) and Butler (1992) concluded that hinge migration is likely during growth of detachment folds and some Alpine fold nappes, respectively. The geometric models of detachment folds of Jamison (1987) and Mitra & Namson (1989) both assume a fixed detachment depth and fold growth by hinge migration.

Thus, some evidence argues for fixed-hinge growth of detachment folds whereas geometric models assuming constant detachment depth require the growth of detachment folds by hinge migration. Whether any or all natural detachment folds grow with fixed hinges remains an important but unresolved question. Since our first model is based on the assumption of constant detachment depth, it requires hinge migration for the growth of detachment folds. However, the variable detachment depth model shows that fixed arc-length folds, as well as other folds with geologically reasonable kinematic paths that are incompatible with fixed-depth models, may evolve above a detachment unit that varies in thickness during deformation (Figs. 2.8 & 2.10b). The observation that detachment depth does in fact commonly vary in natural detachment folds (*e.g.*

Reproduced with permission of the copyright owner. Further reproduction prohibited without permission.

Wiltschko & Chappie 1977, Davis & Engelder 1985, Wallace 1993, Homza & Wallace, unpublished field observations) suggests that the variable-depth model may have useful application to natural detachment folds.

APPLICATION OF THE VARIABLE DETACHMENT DEPTH METHOD TO A NATURAL DETACHMENT FOLD

The Salisbury Creek anticline in the northeastern Brooks Range of Alaska is defined by several hundred meters of the competent Mississippian to Pennsylvanian Lisburne Limestone and is cored by the internally deformed, incompetent Mississippian Kayak Shale (Fig. 2.14). Stratigraphically beneath the Kayak Shale, the Mississippian Kekiktuk Conglomerate is deformed in folds with much longer wavelength and larger interlimb angle, requiring a detachment to exist in the Kayak Shale (Namson & Wallace 1986, Wallace & Hanks 1990, Homza 1993, Wallace 1993).

If constant line-length, plane strain, and chevron geometry (shown as an enveloping surface on figure 2.14) are assumed, then the geometry of the Salisbury Creek anticline requires 62 m of shortening (the fold is plotted on figure 2.7). If constant detachment depth is also assumed, then equations (2.3) and (2.12) require a detachment depth (D_C) of 75 m (Fig. 2.14). If constant depth in not assumed and the undeformed thickness (D_O) of the Kayak Shale is used in equation (2.19), then the final thickness (D_f) that is required for the fold to be balanced can be determined to be 121 m. The observed detachment surface projects into the plane of section at 115 m (D_D) beneath the southern

Reproduced with permission of the copyright owner. Further reproduction prohibited without permission.

syncline, and thus agrees well with the depth calculated if constant detachment depth is not assumed.

Since the variable detachment depth method incorporates an additional observational constraint, the undeformed thickness (D_o), it is less sensitive to observational uncertainties than is the constant depth method. For example, if the detailed geometry of the Salisbury Creek anticline, where S = 65 m and A_f = 3809 m^2, is used in the calculations instead of the triangular enveloping surface, then D_c = 59 m and D_f = 128 m. Thus, using the enveloping surface as an approximation creates an error of 16 m in the constant-depth calculation, but it creates an error of only 7 m in the variable-depth calculation. This difference in sensitivity holds true for other variables as well.

Since the variable-depth solution incorporates the additional data (D_o) and more closely matches the projected depth, it is considered more reasonable than the constant-depth solution. Hence, the kinematic path followed by the Salisbury Creek anticline is not restricted by the requirement of constant detachment depth and could have evolved geometrically by either fixed- or migrating-hinge kinematics. The area observed beneath the fold (W * D_p = 147 m * 115 m = 16,905 m^2) is less than the area calculated using the variable-depth model (W * D_f = 147 m * 128 m = 18, 816 m^2) by ~ 1911 m^2. This discrepancy suggests that a significant amount of incompetent rock could have been removed from the fold. Strong solution cleavage and stylolitization in the Kayak Shale in the core of the anticline support this suggestion.

Shortening (thickening) of the incompetent unit outside of the fold presumably is accommodated in the competent unit by folding, which would also

Reproduced with permission of the copyright owner. Further reproduction prohibited without permission.

result in an overestimate of thickening below the fold using the variable-depth model. However, thickening in the incompetent unit outside of the fold is not accounted for by the variable-depth model, since an assumption of the model is that no incompetent material flows through the synclinal hinges bounding the detachment fold. The difficulty in determining the distance over which fold shortening has influenced incompetent unit thickness and how changes in incompetent unit thickness are partitioned between adjacent folds is a fundamental problem with this or any geometric model for detachment folds.

Qualitative analysis of the distribution of strain in the Salisbury Creek anticline provides constraints on its kinematic evolution. The anticlinal hinge is extremely strained and includes many minor contractional faults with a variety of orientations and offsets, abundant centimeter-scale folds, well-developed calcite-filled veins that parallel and cross-cut bedding, tectonic brecciation, solution cleavage, and stylolitization. The synclines bounding the forelimb and the backlimb are similarly very strained. Little solution cleavage and only very minor stylolitization are apparent in the backlimb. Centimeter-thick chert beds at the base of the Lisburne Limestone record only a few poorly developed veins and no tectonic brecciation in the backlimb. The only significant deformation in the backlimb is recorded by bed-parallel slickensides indicating flexural slip and a late-stage thrust fault with about 10 m of displacement. Forelimb deformation includes tectonically brecciated and boundinaged chert beds, minor cleavage, bed-parallel veins of stretched calcite fibers, and stretched bed-parallel slickenfibers indicating north-over-south flexural slip.

Reproduced with permission of the copyright owner. Further reproduction prohibited without permission.

There is no indication of structures reflecting hinge migration through the backlimb, nor is there any definitive indication of such structures in the forelimb. The intensity of tectonic brecciation and interbed shear in the forelimb permits the possibility that either adjacent hinge migrated through the forelimb during the early stages of fold growth. However, we prefer a fixed-hinge interpretation because the contractional faults, cross-cutting veins, minor folds, and intense solution cleavage that characterize the adjacent fold hinges are lacking in the forelimb. Consequently, we suggest that the Salisbury Creek anticline formed by fixed-hinge buckling, with structural thickening of the Kayak Shale, volume loss in the Kayak Shale due to fluid migration out of the core of the fold, and late-stage thrust faulting in the backlimb.

DISCUSSION

Incorporation of different assumptions into the variable-depth model

The example illustrates that the variable-depth model can be applied with some success to a natural detachment fold and, at least for that fold, yields a better approximation than the constant-depth model. A variety of modifications can be made to the variable-depth model to accommodate departures of natural folds from the basic assumptions incorporated in the model. For instance, the example illustrates a problem with the assumption of constant cross-sectional area of the incompetent unit within the synforms bounding the fold. In its present form, the model does not account for changes in cross-sectional area of the incompetent unit due to flow through synformal hinges, loss or gain of rock

Reproduced with permission of the copyright owner. Further reproduction prohibited without permission.

volume, and/or transport of rock into or out of the plane of section. The effect of observed area changes can easily be accommodated in the model by making appropriate corrections to the area differential ($A_{\Delta D}$), provided that the area changes affect only the incompetent unit and do so uniformly. Applying such corrections will yield a corrected value of the change in thickness (ΔD), although determining accurate values of corrections for natural folds may be difficult in practice. The need for determining the values of corrections is eliminated if both original (D_o) and final (D_f) detachment depth are known, allowing the change in thickness (ΔD), and consequent loss or gain of area, to be determined directly. Non-uniform changes in the area of the incompetent unit and uniform or non-uniform changes in the length of the competent unit would necessitate more complicated corrections, requiring a detailed knowledge of the amount, distribution, and timing (relative to folding) of any area or length changes.

Although only simple triangular fold geometries are considered in the model, the same approach could be applied to other fold geometries, although the complexity of the problem will increase as the number of possible hinges is increased and if non-linear limbs are considered. The model could be modified to accommodate vertical differences in layer-parallel shear in the incompetent unit by using the shear profile to define the trailing surface of the deformed area of the incompetent unit. This would enable a correct change in thickness (ΔD) to be determined, rather than the incorrect value that would be determined if the value of shortening indicated by the fold shape was used assuming no vertical differences in layer parallel shear in the incompetent unit. The model is not affected by vertical variations in layer-parallel shear in the competent unit since

Reproduced with permission of the copyright owner. Further reproduction prohibited without permission.

it addresses only the geometry of the interface between the competent and incompetent units.

Comparison of ideal detachment folds with ideal fault-bend and fault-propagation folds

The present models provide a quantitative basis for the conclusion that ideal detachment folds are intrinsically less constrained, and hence less predictable, than ideal fault-bend or fault-propagation folds (Fig. 2.1). Similar relationships among fold geometry (width, height, backlimb dip, forelimb dip), shortening, and detachment depth can be established for all three fold types. However, a greater range of geometries for detachment folds is possible within the common assumptions of plane strain and constant cross-sectional area, detachment depth, and competent bed length and thickness (Jamison 1987) (Table 2.1). This reflects the fact that both backlimb and forelimb dip are dependent on ramp angle in ideal fault-bend and fault-propagation folds (Suppe 1983, Suppe & Medwedeff 1990, Mitra 1990, Jamison 1987), whereas the mobility of the incompetent unit in detachment folds requires no such linkage between backlimb and forelimb dip. If the assumption of constant detachment depth is relaxed for detachment folds, as in our variable-depth model, an even wider range of values of original and final detachment depth are possible for each fold geometry.

The contrast is even more apparent in the kinematic evolution of ideal fault-bend and fault-propagation folds versus that of ideal detachment folds (Table 2.1). Detachment depth and interlimb angle are fixed during growth of ideal fault-bend and fault-propagation folds as long as it is assumed that bed

Reproduced with permission of the copyright owner. Further reproduction prohibited without permission.

thickness remains constant and no vertical gradient exists in layer-parallel shear (Suppe 1983, Suppe & Medwedeff 1990, Mitra 1990, 1992, Jamison 1987). These constraints exist because the ideal fold geometry is controlled by fixed, competent footwall ramps. The mobility of the incompetent unit in an ideal detachment fold allows a fundamentally different kinematic evolution from these "rigid-ramp" folds. Variation of backlimb and/or forelimb dip are geometrically possible with the constant-depth model (Fig. 2.4), allowing a wider variety of kinematic paths, yet self-similar (fixed backlimb and forelimb dip) fold growth is not (Fig. 2.5a). If the assumption of constant detachment depth is relaxed for detachment folds, as in our variable-depth model, an even wider array of kinematic paths is possible, including fixed-hinge (Fig. 2.8) and self-similar (Fig. 2.10b) fold growth, as well as a variety of paths that are geometrically possible, but not kinematically or mechanically plausible.

Fixed, competent footwall ramps account for migrating hinges in the hangingwalls of ideal fault-bend and fault-propagation folds (Table 2.1). However, there is no rigid "footwall" topography in a detachment fold, thereby precluding the geometric requirement of migrating hinges. In fact, the inherent mobility of the incompetent unit in detachment folds suggests that a focus on the geometry of the competent unit may be the best approach to constraining the possible geometries and kinematic paths of detachment folds. Given the observational and theoretical evidence in support of fixed-hinge growth of buckle folds, it may well be that fixed hinges in the competent unit are the dominant control on the geometry and kinematic evolution of detachment folds. Under the

Reproduced with permission of the copyright owner. Further reproduction prohibited without permission.

assumptions of our models, such growth is possible only if incompetent unit thickness, and hence detachment depth, varies.

Applicability of our models to natural detachment folds

Our geometric models, in and of themselves, don't indicate the behavior of natural detachment folds. However, they do provide a simple, mathematically constrained basis to explore what is geometrically and kinematically possible given a well-defined set of starting assumptions. These conceptual models can be tested against natural detachment folds with well-constrained geometry and/or kinematic evolution in order to determine which of the assumptions are valid for those folds, hopefully leading to some general insights into the geometry and kinematics of natural detachment folds. However, the wide range of variability that the models demonstrate to be possible, coupled with the likelihood that some of the assumptions are not appropriate for natural detachment folds, indicates that caution should be used in applying these --or any other-- simple, geometric models to the reconstruction of natural detachment folds whose geometry is not fully constrained by data. Specifically, a unique solution for detachment depth from fold geometry alone is possible only if constant detachment depth is assumed, and this assumption has been shown to be invalid for at least some natural detachment folds. While the variable-depth model allows determination of either original or final detachment depth if the other is known, it is only an approximation because it requires the geologically unreasonable assumption that no incompetent material is transported through the bounding synformal hinges of a detachment fold.

Reproduced with permission of the copyright owner. Further reproduction prohibited without permission.

The same basic technique upon which our models are based, line-length balancing of the competent unit and area balancing of the incompetent unit, can overcome some of the limitations of the geometric models if it is applied over a large enough area to account for complex flow of the incompetent unit. Specifically, balancing along a long enough line of section may account for flow through synclinal hinges and balancing of multiple sections along strike may account for flow transverse to the line of section. Careful observations of mesoscopic and microscopic structures and strain measurements may be needed to validate model assumptions and to correct for departures from those assumptions. These certainly are not new insights, and are routinely addressed in discussions of cross-section balancing (*e.g.* Woodward *et al.* 1985, 1989). However, by demonstrating the sheer variability in possible detachment folds, our models illustrate the limits of simple geometric models in reconstructing detachment folds whose geometry and detachment depth are not fully constrained, particularly if it is not assumed that detachment depth remains constant. These points emphasize the importance of using additional approaches in reconstructing detachment fold geometry, rather than relying on simple geometric models as heavily as may be possible with geometrically more constrained folds, such as fault-bend or fault-propagation folds.

CONCLUSIONS

We have presented two conceptual geometric models for idealized detachment folds that provide strict quantitative constraints on the fold geometry and kinematics possible given an explicit set of starting assumptions. The

Reproduced with permission of the copyright owner. Further reproduction prohibited without permission.

constant detachment depth model shows that growth of a detachment fold with constant detachment depth requires a linear increase in area with increasing shortening. This, in turn, precludes fixed-hinge (fixed arc-length) and self-similar (fixed limb-dip) fold growth, both of which require non-linear changes of area with increasing shortening. Fold growth along these kinematic paths, as well as others that are precluded by the constant detachment depth model, is possible if the assumption of constant detachment depth is relaxed, as in the variable detachment depth model. Both models require detachment folds to nucleate with symmetrical geometries or very high ratios of wavelength to height.

Variable detachment depth, as determined by incompetent unit thickness in synforms, has been observed in natural detachment folds, and fixed-hinge growth of buckle folds is supported by observational and theoretical evidence. Together, these suggest that the variable-depth model is a better approximation for many natural detachment folds than any constant-depth model.

The mobility of the incompetent unit in detachment folds makes these folds intrinsically less constrained than ideal fault-bend and fault-propagation folds, which have rigid footwall ramps. This intrinsic variability limits the usefulness of simple geometric models for reconstructing the geometry of natural detachment folds. This reinforces the importance of balancing over a sufficiently large area, across and along structural strike, to account for variations in detachment depth and of evaluating strain to correct model assumptions. However, as has been shown here, geometric models are very useful to assess the geometric and kinematic implications of specific assumptions, and can serve

Reproduced with permission of the copyright owner. Further reproduction prohibited without permission.

as a basis for testing the validity of those assumptions for natural detachment folds whose geometry is well constrained.

Reproduced with permission of the copyright owner. Further reproduction prohibited without permission.

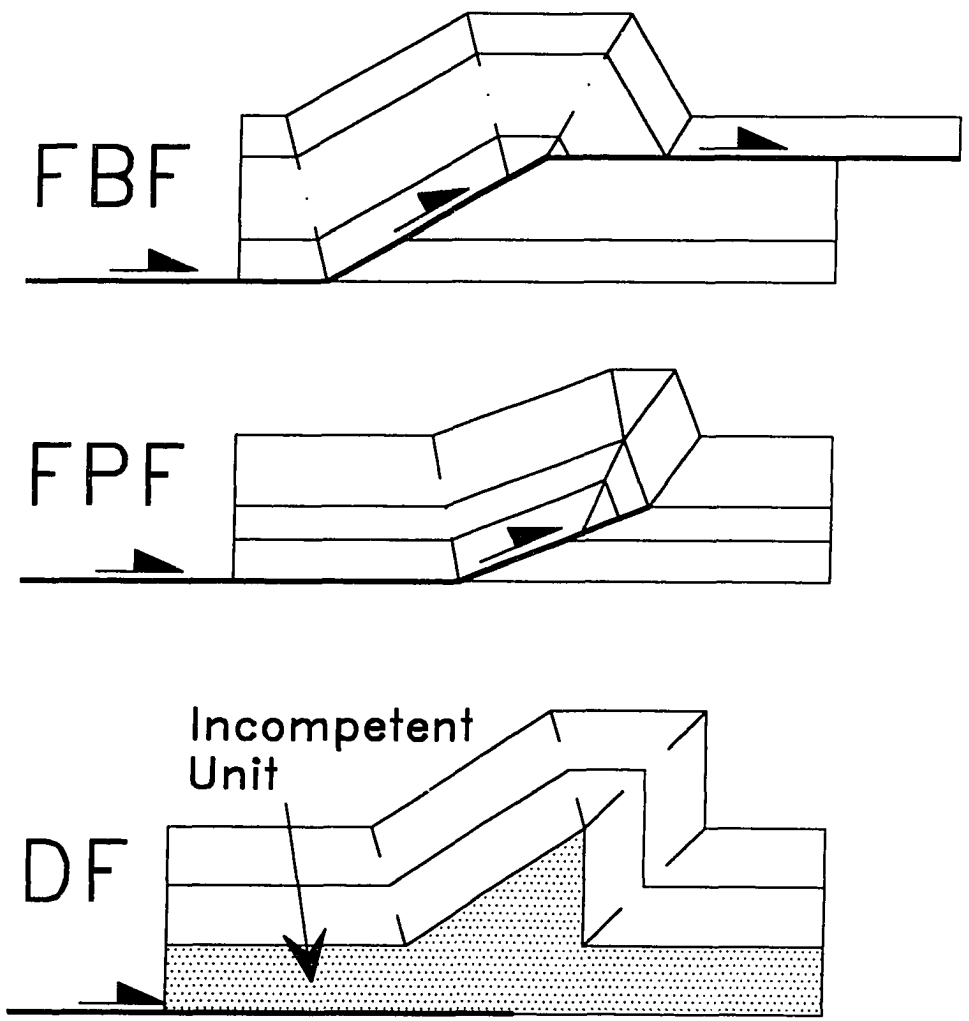

Figure 2.1. Three major types of thrust-related folds in fold-and-thrust belts: Fault-bend fold (FBF), fault-propagation fold (FPF), and detachment fold (DF).

Reproduced with permission of the copyright owner. Further reproduction prohibited without permission.

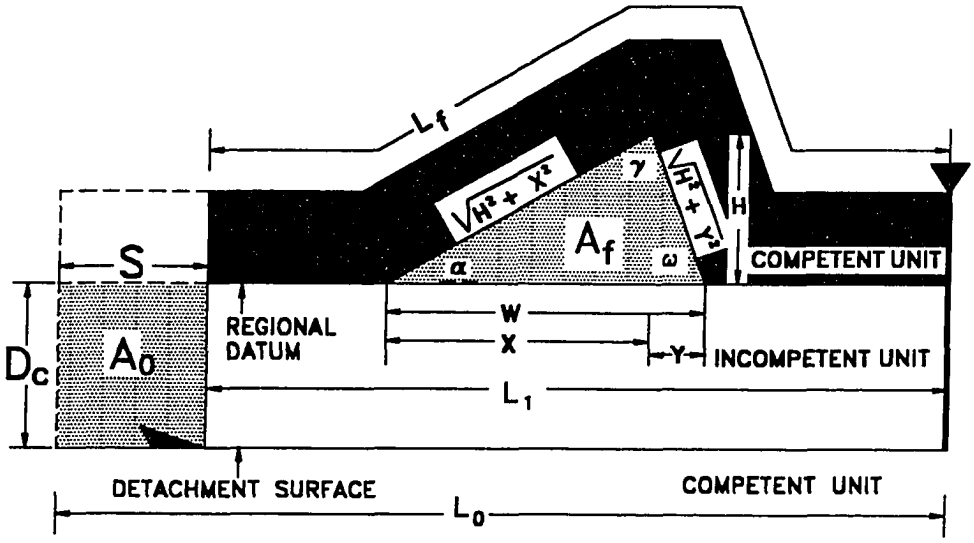

Figure 2.2. Geometric basis for the fixed detachment depth model. As the incompetent unit is displaced and shortened, conservation of cross-sectional area requires that the displaced area (A_0) equal the uplifted area (A_f). Conservation of line-length requires the contact between competent and incompetent units to retain its original length ($L_0 = L_f$). See text for explanation of other variables.

Reproduced with permission of the copyright owner. Further reproduction prohibited without permission.

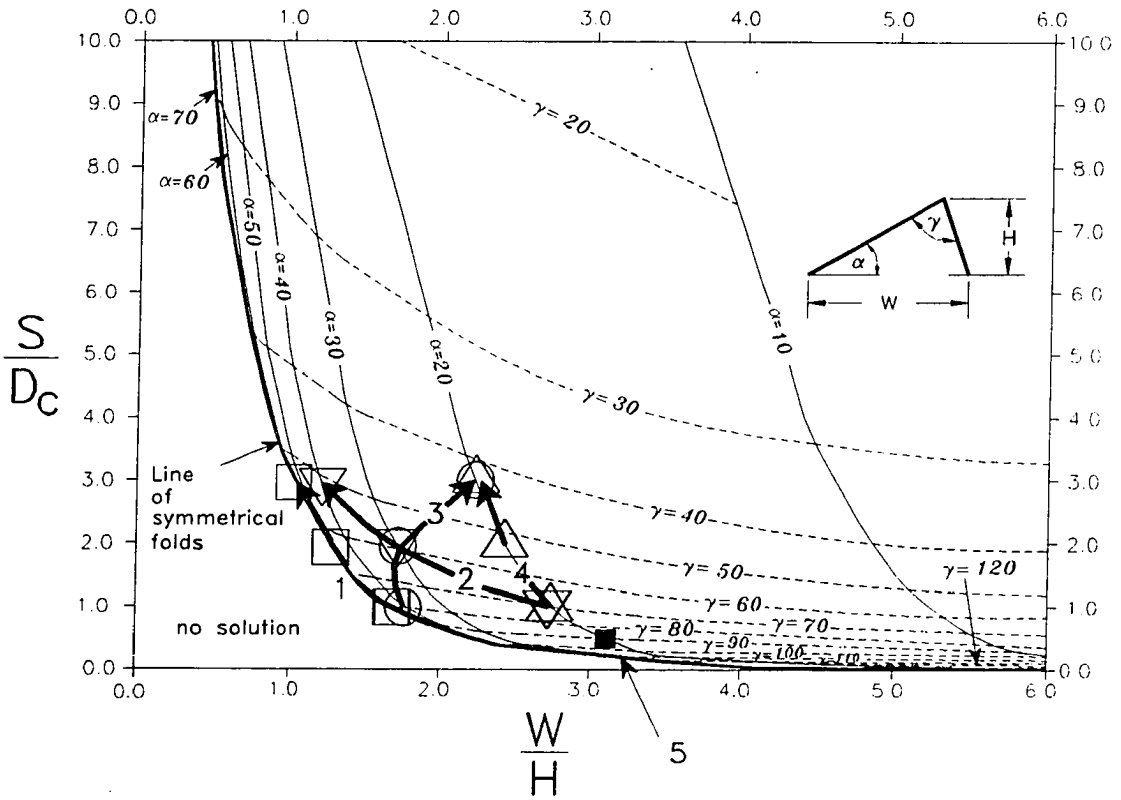

Figure 2.3. The constant detachment depth diagram. See text for discussion. Any point on the graph outside of the "no solution" area defines one and only one triangular fold geometry. No trigonometric solutions exist for the shaded region. See Figs. 2.4 & 2.5 for explanation of symbols and numbered kinematic paths.

Reproduced with permission of the copyright owner. Further reproduction prohibited without permission.

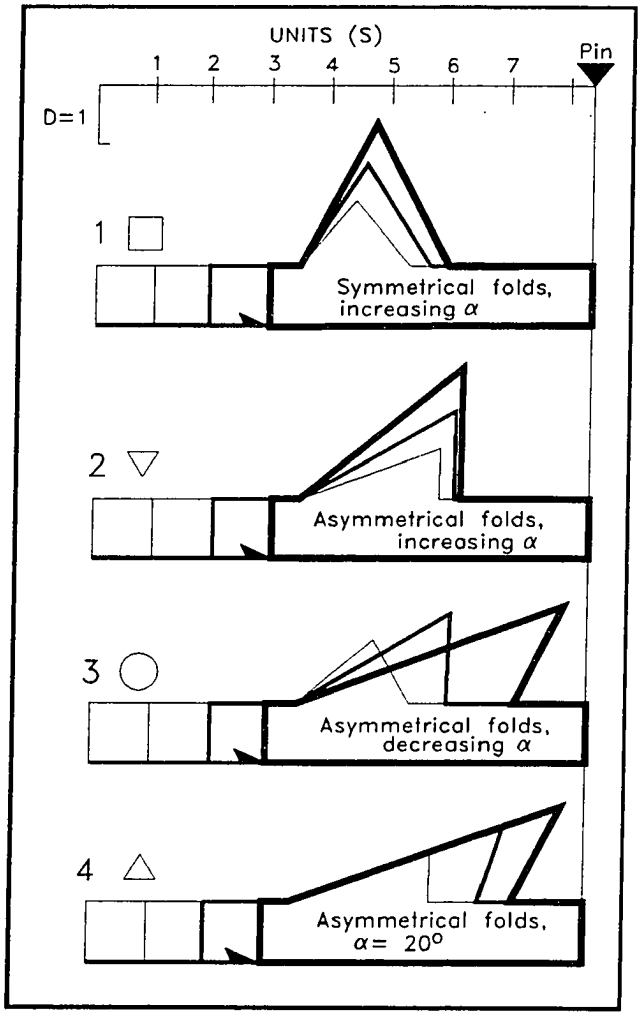

Figure 2.4. Kinematic evolutions of fold geometries compatible with the constant detachment depth model. Progressively thicker lines indicate successive steps in fold evolution with increasing shortening above a constant detachment depth. Numbered lines on Fig. 2.3 represent the kinematic paths for each fold sequence, and symbols mark points describing the geometry of the successive steps in the evolution of each fold.

Reproduced with permission of the copyright owner. Further reproduction prohibited without permission.

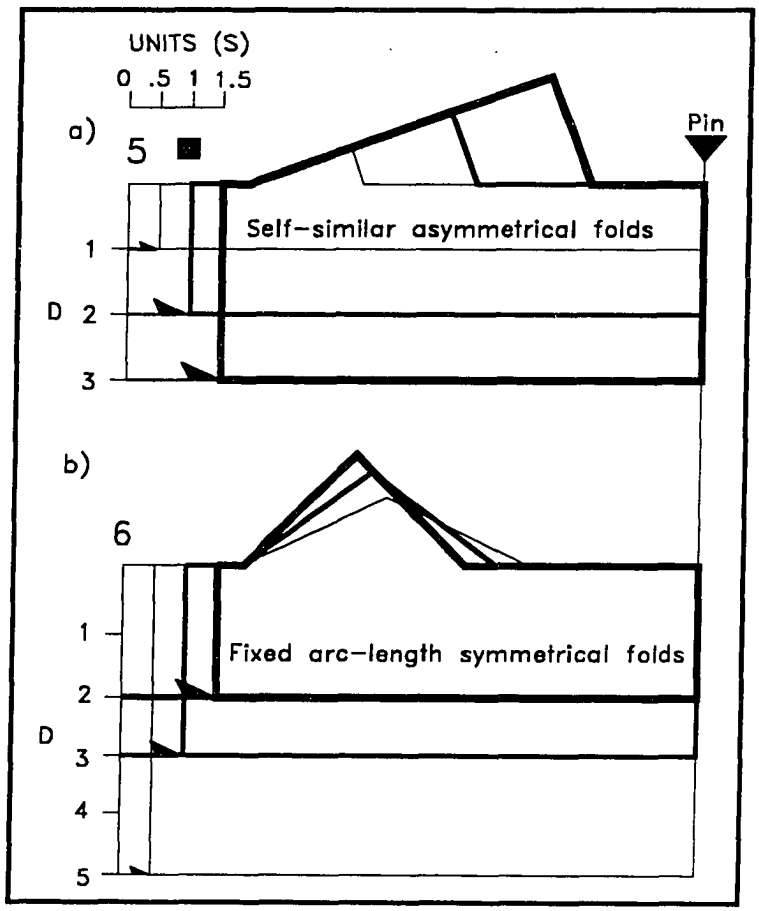

Figure 2.5. Successive fold geometries in sequences 5 and 6 are systematically related, but are kinematically impossible within the bounds of the constant detachment depth model because they require variation in detachment depth. Progressively thicker lines indicate successive steps in fold evolution with increasing shortening. Sequence 5 plots as a point on Fig. 2.3, whereas sequence 6 is omitted for clarity.

Reproduced with permission of the copyright owner. Further reproduction prohibited without permission.

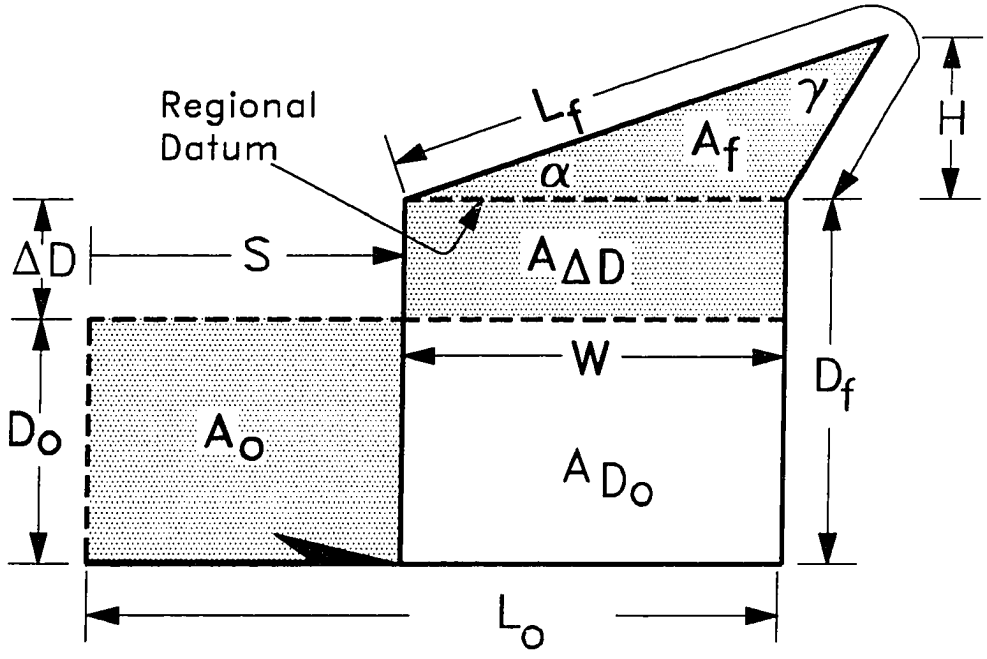

Figure 2.6. Geometric basis for the variable detachment depth model. As the incompetent unit is displaced and shortened, conservation of cross-sectional area requires that the displaced area (A_o) equal the uplifted area (A_f) plus the area differential ($A_{\Delta D}$), Conservation of line-length requires the contact between competent and incompetent units to retain its original length (L_o = L_f). See text for explanation of other variables.

Reproduced with permission of the copyright owner. Further reproduction prohibited without permission.

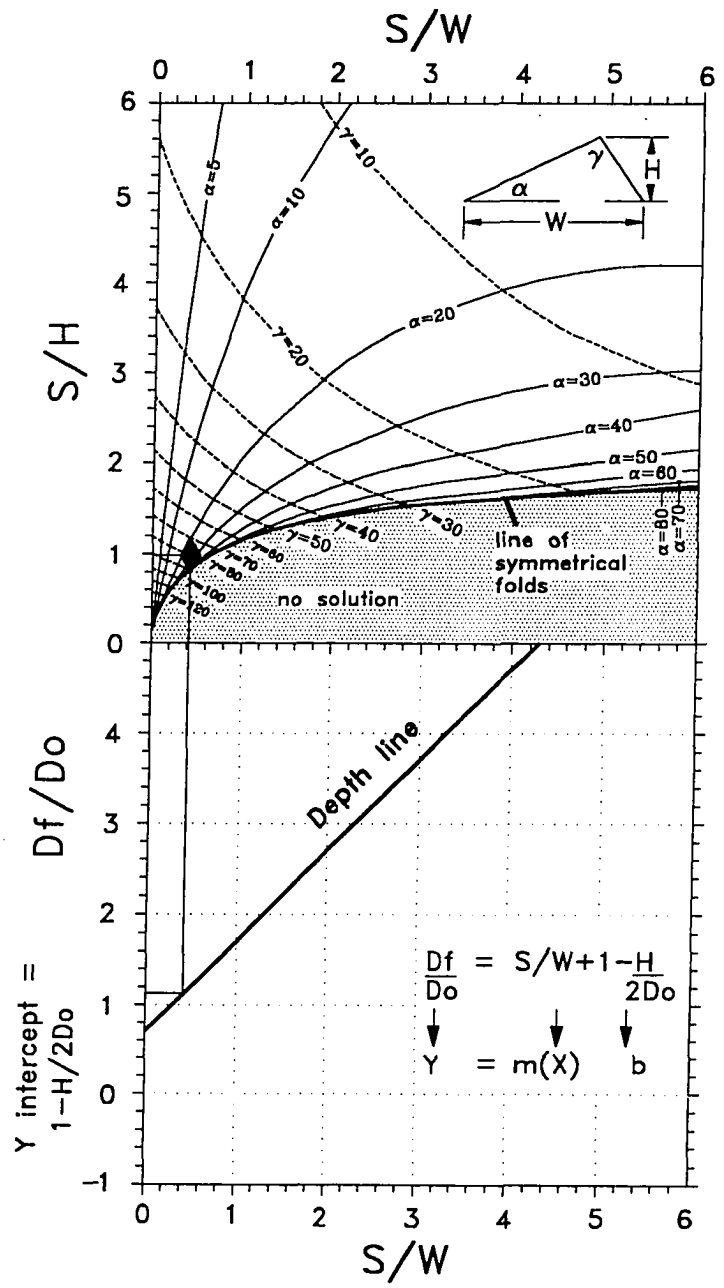

Figure 2.7. The variable detachment depth diagram. See text for discussion. D_f/D_0 = depth ratio. Any point on the upper graph outside of the "no solution" area defines one and only one triangular fold geometry. Detachment depth is determined using D_f/D_0, which is the Y-value of the point of intersection of S/W and the appropriate depth line. The fold in figure 2.14 is plotted on this diagram.

Reproduced with permission of the copyright owner. Further reproduction prohibited without permission.

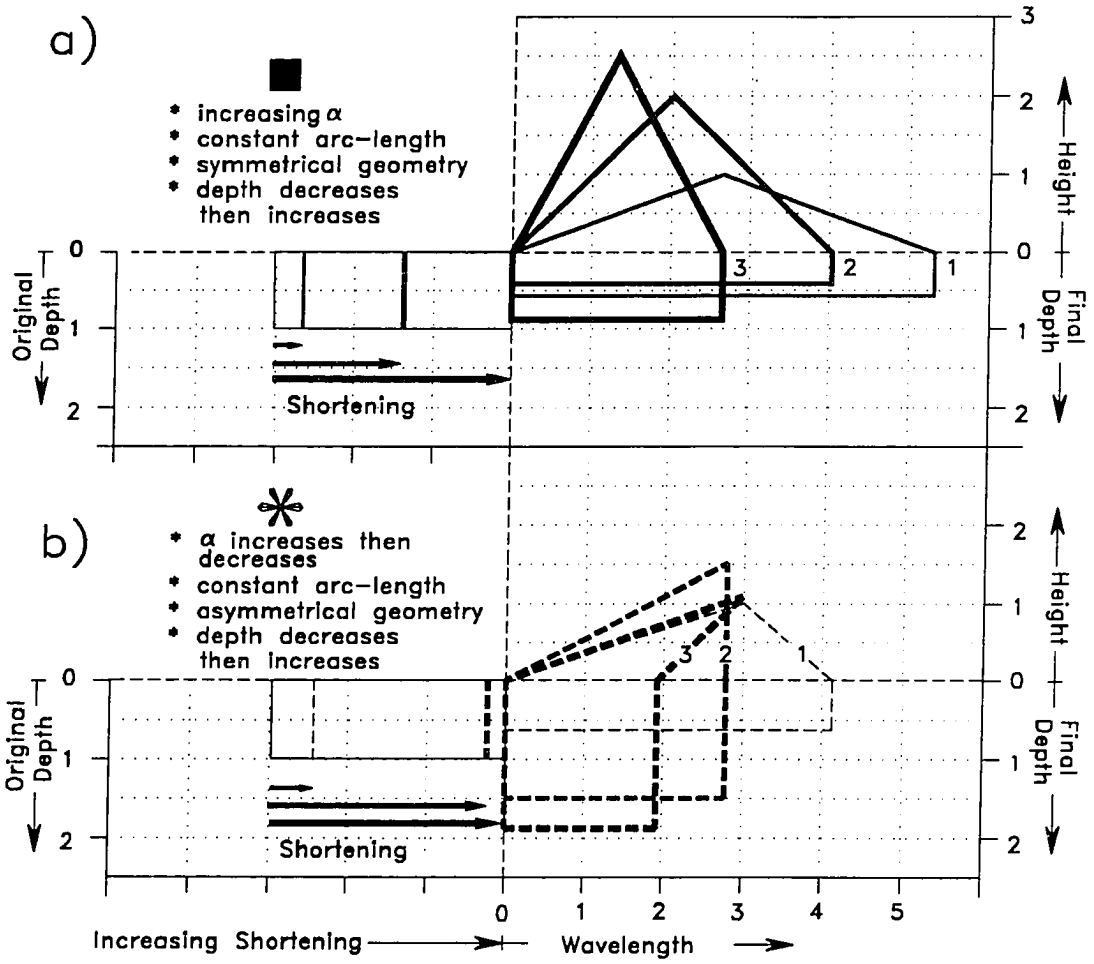

Figure 2.8. Kinematic evolution of a) symmetrical and b) asymmetrical fixed-hinge (fixed arc-length) folds. The line weight and shortening increase for folds 1 through 3. The original depth is fixed for each sequence, but depth, height, and wavelength vary with increasing shortening. The symbols and line-type (*i.e.* solid vs. dashed) correspond to the graphical plot of these sequences on figure 2.9. The stratigraphic position of the detachment surface remains constant whereas the thickness of the incompetent unit (and hence detachment depth) varies. To simplify geometric comparison in these figures, the regional datum is used as a fixed reference frame although in natural folds it is more likely that the detachment surface would remain fixed and the elevation of the regional datum would change with incompetent unit thickness.

Reproduced with permission of the copyright owner. Further reproduction prohibited without permission.

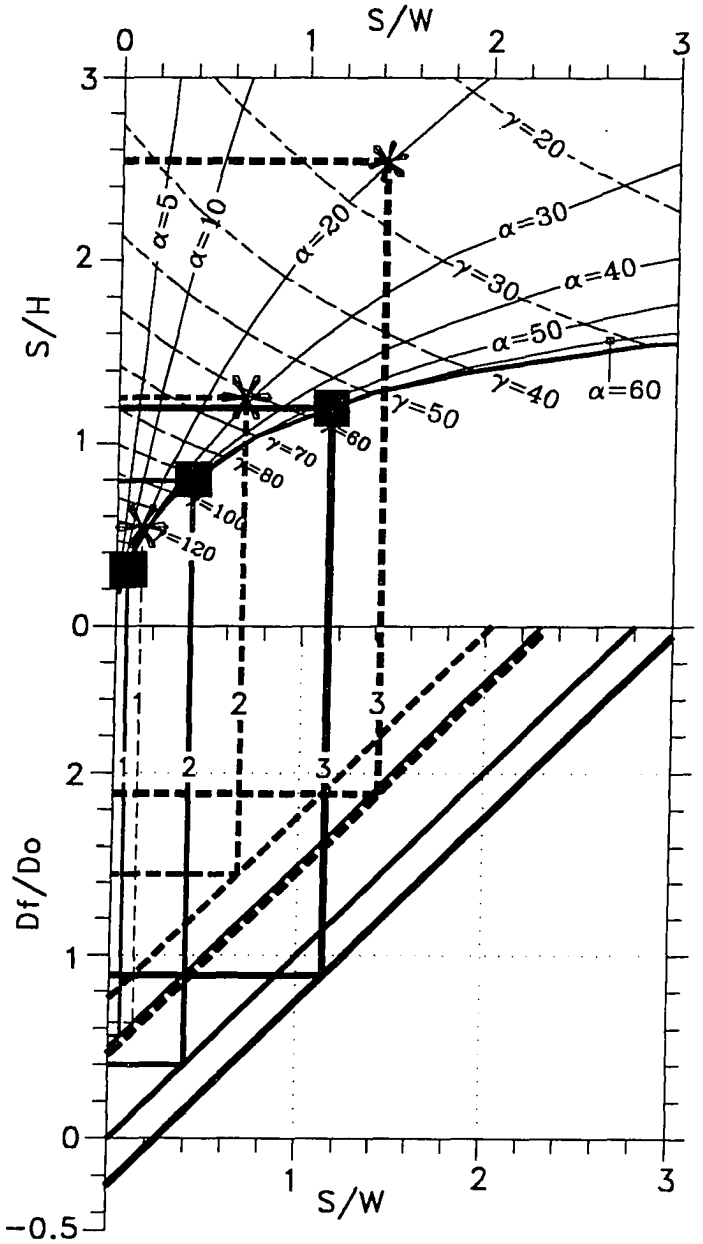

Figure 2.9. Graphical plot of the two fold sequences in figure 2.8 on the variable-depth diagram. The line thicknesses and line-types correspond to the folds in figure 2.8. The plot of fold sequence 8a (■) moves up the line of symmetrical folds and the correlative D_f/D_0 values show a decrease, then an increase, although D_f is less than D_0 for the geometries shown. D_f/D_0 decreases then increases for fold sequence 8b (*) with the depth for the first fold being less than D_0, and greater than D_0 for the later folds shown.

Reproduced with permission of the copyright owner. Further reproduction prohibited without permission.

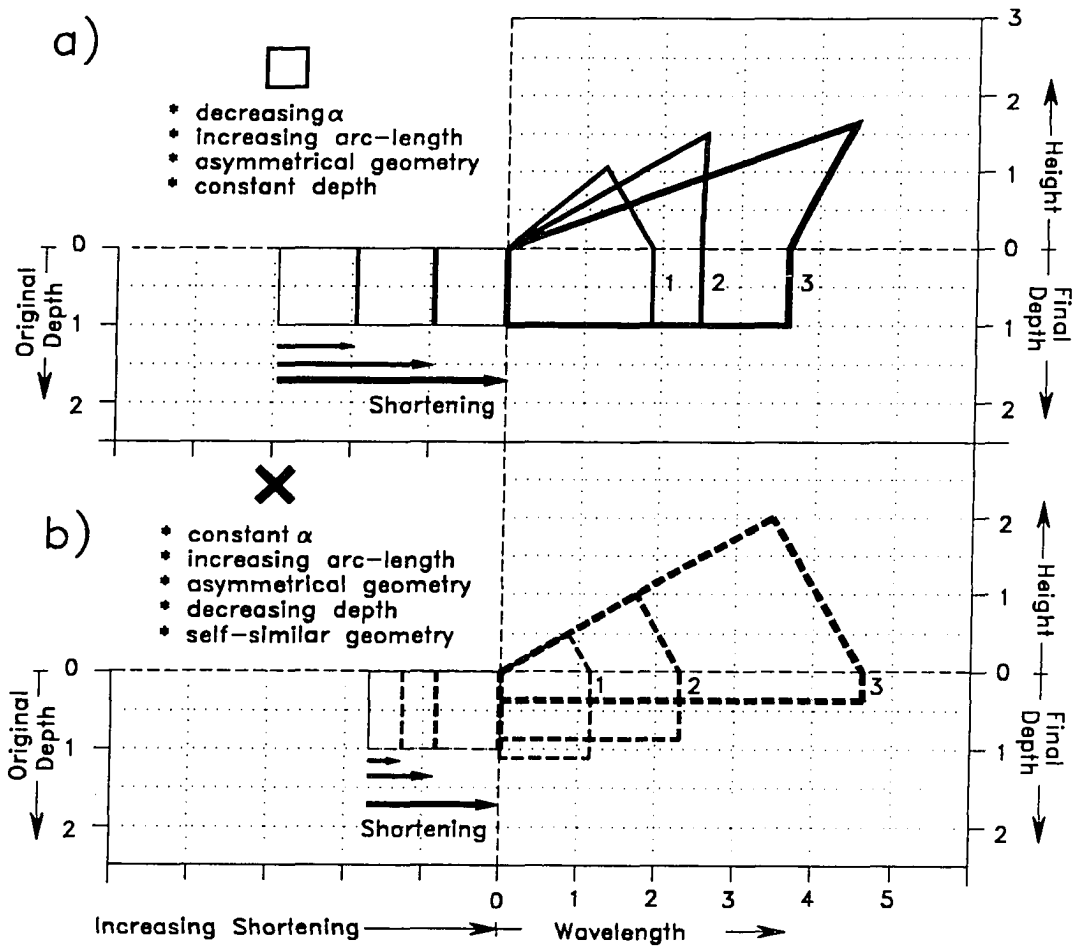

Figure 2.10. Kinematic evolution of a) a constant-depth fold sequence and b) a fold sequence of self-similar geometries. See figure 2.8 for explanation. The symbols and line-type (*i.e.* solid vs. dashed) correspond to the graphical plot of these sequences on figure 2.11.

Reproduced with permission of the copyright owner. Further reproduction prohibited without permission.

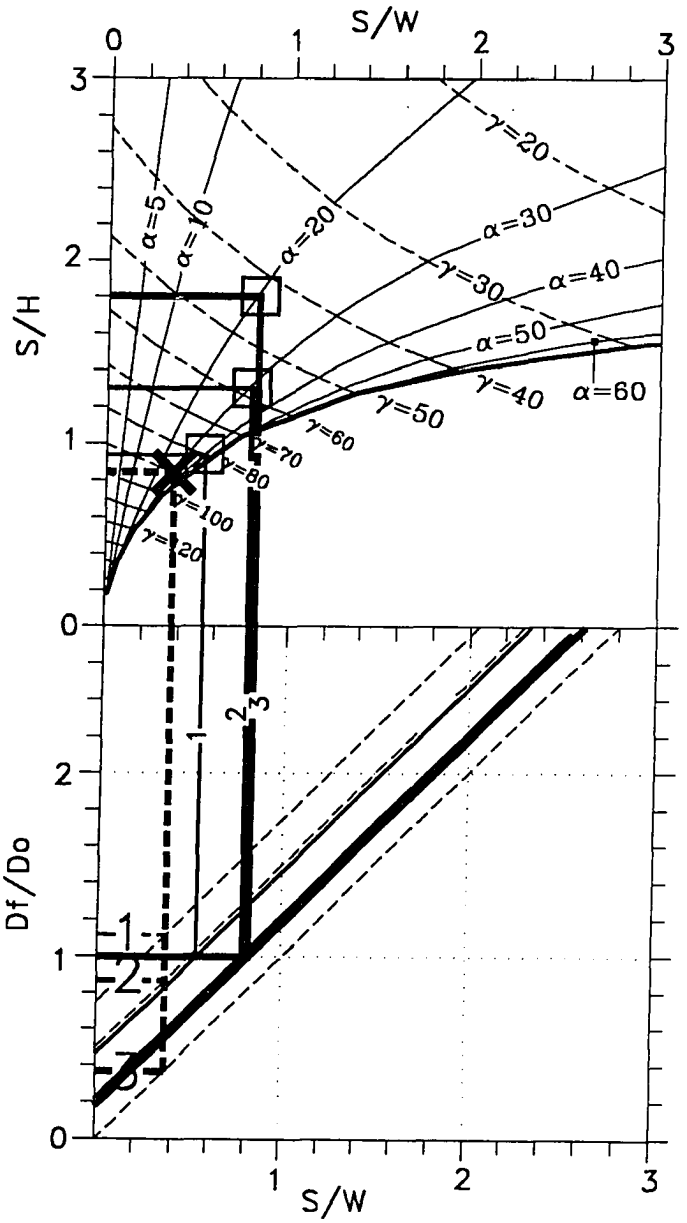

Figure 2.11. Graphical plot of the two fold sequences in figure 2.10 on the variable-depth diagram. The line thicknesses and line-types correspond to the folds in figure 2.10. The plot of fold sequence 10a (□) shows a and g decreasing while both S/H and S/W increase. The detachment depth is constant, so $D_f/D_0 = 1$. The plot of fold sequence 8b (X) is a single point since the geometry is self-similar; detachment depth progressively increases.

Reproduced with permission of the copyright owner. Further reproduction prohibited without permission.

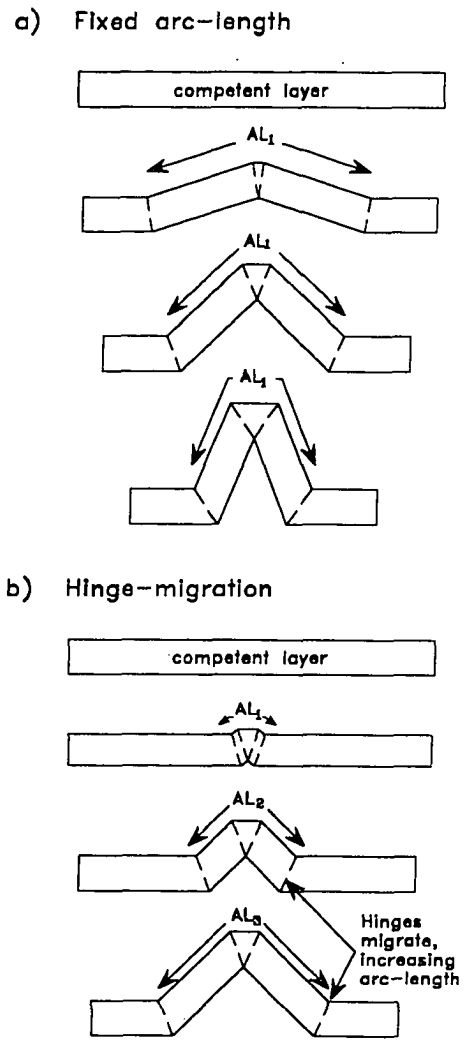

Figure 2.12. Diagram showing the fundamental difference in kinematics between fixed arc-length folding (a), in which the arc-length remains constant and hinges are fixed throughout the evolution of the fold, and folding by hinge-migration (b), in which arc-length increases. AL = arc length.

Reproduced with permission of the copyright owner. Further reproduction prohibited without permission.

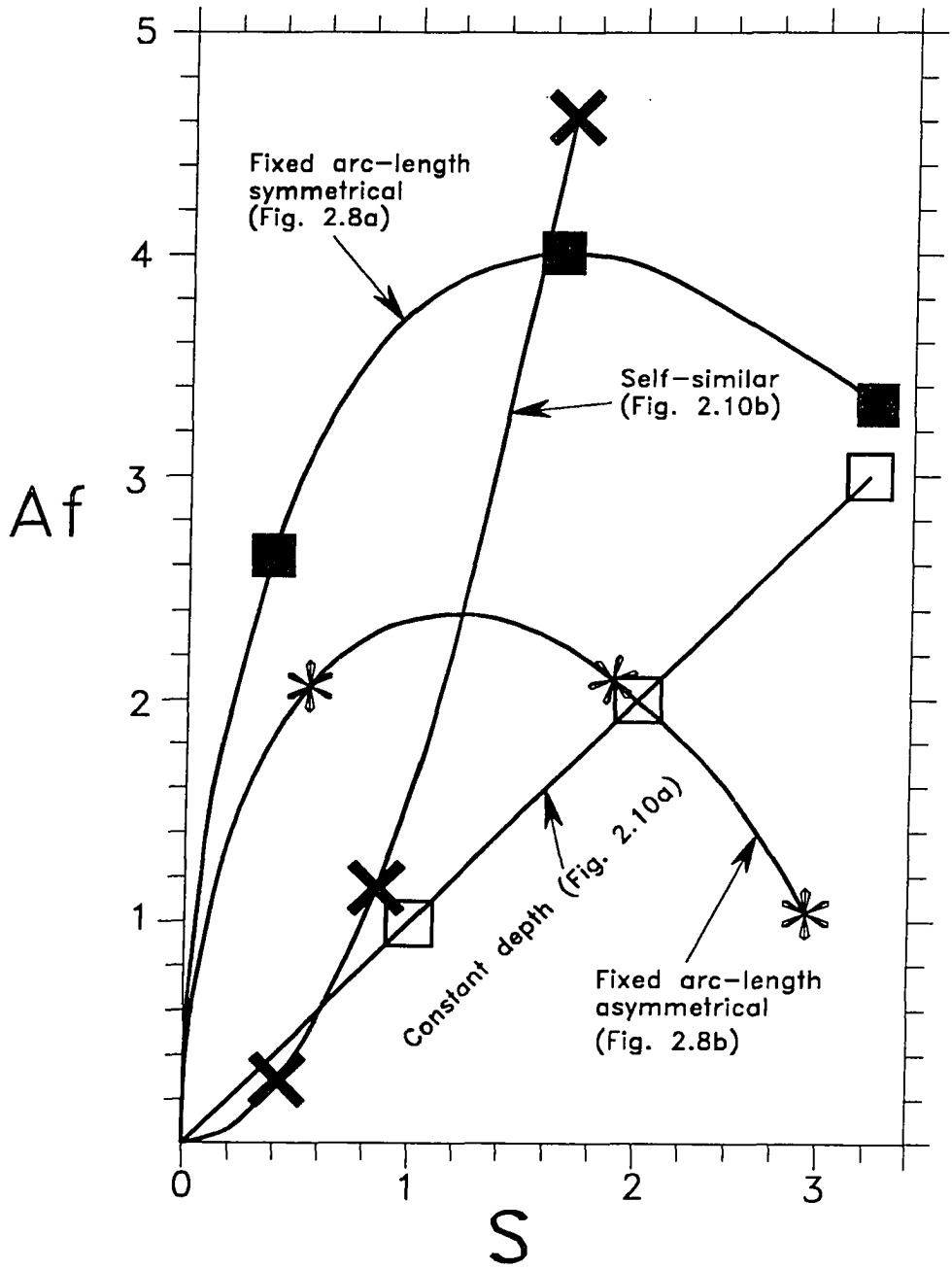

Figure 2.13. Plot of shortening (S) vs. uplifted cross-sectional area (A_f) for fold sequences in figures 2.8 and 2.10. Any fold sequence with a constant detachment depth D_C follows a straight line with slope D_C. Other fold sequences follow non-linear curves.

Reproduced with permission of the copyright owner. Further reproduction prohibited without permission.

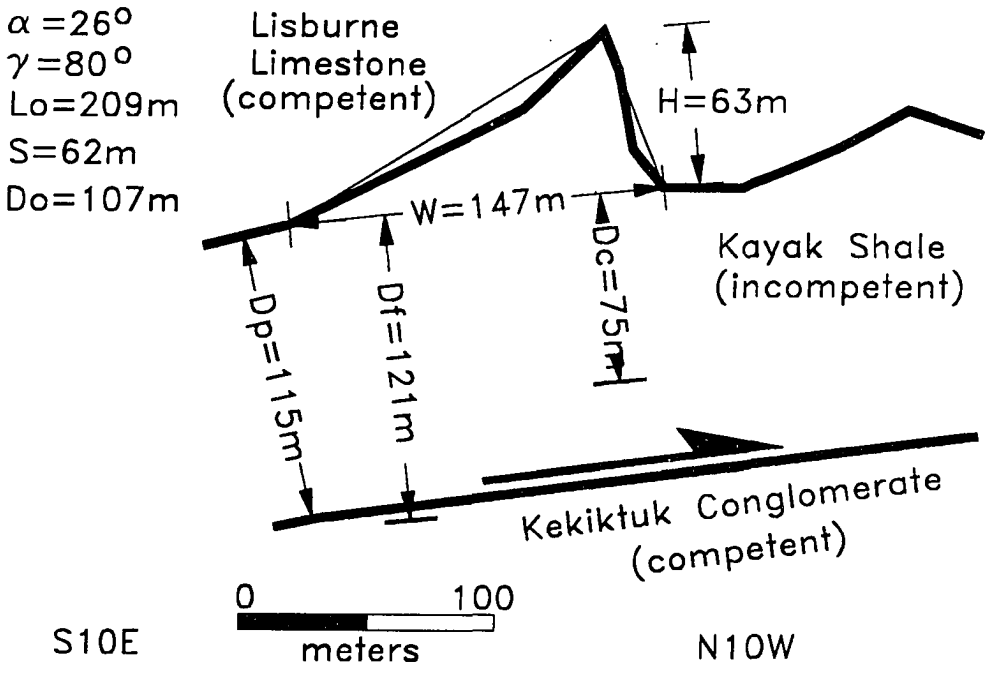

Figure 2.14. Simplified cross section of the Salisbury Creek anticline showing detachment depth solutions calculated using both the conventional equal-area technique (equation 2.2) and the variable-depth technique (equation 2.19). The fold axis is horizontal and the plane of section is vertical. Calculations use the enveloping surface shown. D_c = detachment depth calculated from equations (2.2) or (2.12), D_f = detachment depth calculated from equation (2.19), D_0 = undeformed thickness of Kayak Shale determined from a panel of Lisburne Limestone that parallels the detachment surface. D_p = depth to detachment projected into the line of section. Other variables as illustrated in figures 2.2 and 2.6. The fold geometry is plotted on figure 2.7.

Reproduced with permission of the copyright owner. Further reproduction prohibited without permission.

Reproduced with permission of the copyright owner. Further reproduction prohibited without permission.

Table 2.1. Table comparing the geometric and kinematic characteristics of ideal fault-bend folds, fault-propagation folds, and detachment folds with fixed or migrating hinges. References: (1) Jamison (1987), (2) Suppe (1983), (3) Suppe & Medwedeff (1990), (4) this paper. Notes: Constant bed thickness (parallel folding) assumed in competent units. Ramp assumed to step from bed-parallel detachment (décollement) for FBF and FPF. *(I) mode I FBFs, (II) mode II FBFs. Ψ Geometrically unconstrained; the most geologically plausible paths are noted.

	Fault-bend fold (1,2)	Fault-propagation fold (1,3)	Detachment fold (migrating hinges) (1,4)	Detachment fold (fixed hinges) (4)
Mechanical stratigraphy	Competent	Competent	Competent over incompetent	Competent over incompetent
Rigid footwall ramp	Yes	Yes	No	No
Detachment depth	Constant	Constant	Constant *or* variable (Incompetent unit thickness)	Variable (Incompetent unit thickness)
Fixed vs. migrating hinges	Fixed in HW ramp Migrating over FW ramp	Migrating except in anticlinal core	Migrating	Fixed
Fixed vs. rotating limbs	Fixed	Fixed	Fixed *or* rotating	Rotating
Forelimb dip	0-60° (I), 60-180° (II)*	0-180°	0-180°	0-180°
Backlimb dip	0-30°	0-60°	0-180°	0-180°
Kinematic paths				
Arc length	Increasing	Increasing	Increasing Ψ	Fixed
Wavelength	Increasing	Increasing	Incr. *or* decreasing Ψ	Decreasing
Height	Increasing to maximum	Increasing	Increasing *or* increasing *then* decreasing Ψ	Increasing *then decreasing*

CHAPTER 3*- NATURAL DETACHMENT FOLDS IN THE NORTHEASTERN BROOKS RANGE

A detachment fold (Jamison 1987, Mitra & Namson 1989, Dahlstrom 1990, Groshong & Epard 1994, Homza & Wallace 1995) is a fold in a relatively competent rock layer that is cored by internally deformed less competent rock that is separated from another competent unit by a detachment surface (Fig. 3.1). Mechanically layered stratigraphy characterized by distinct competent and incompetent units is very common in fold-and-thrust belts and lends itself to the formation of detachment folds. Thus, it is likely that detachment folds are at least as common in fold-and-thrust belts as "rigid-ramp" folds such as fault-bend (Suppe 1983, Jamison 1987) or fault-propagation folds (Jamison 1987, Mitra 1990, Suppe & Medwedeff 1990). However, due to the relatively unconstrained behavior of incompetent rock, the geometry and kinematics of detachment folds are relatively complex and less well understood than for fault-bend or fault-propagation folds. Definitions and models for detachment folds are less widely known and recognized than those for fault-bend and fault-propagation folds. Many detachment folds probably have been described in the scientific literature, but are not explicitly identified as such. Thus, we believe detachment folds commonly are misinterpreted as fault-bend and fault-propagation folds.

This report focuses on three fundamental yet unresolved questions about detachment folds that, we feel, must be addressed in order to enable both the

---

* In preparation for publication in Geological Society of America Bulletin as "Analysis of detachment folds in the Arctic National Wildlife Refuge (ANWR), northeastern Brooks Range fold-and-thrust belt, Alaska", by Thomas X. Homza and Wesley K. Wallace

Reproduced with permission of the copyright owner. Further reproduction prohibited without permission.

recognition and the reliable geometric interpretation of detachment folds, especially in the subsurface. First, do detachment folds form by a fixed-hinge/rotating limb mechanism (*e.g.* Hardy & Poblet 1994), by a migrating-hinge/non-rotating limb mechanism (*e.g.* Mitra & Namson 1989), or by a combination of the two? Second, does the thickness of the detachment unit (depth-to-detachment) vary structurally during folding and, if so, is it possible to predict the nature of such variation? Third, what role is played in detachment folding by gradations in competency resulting from variations in rock type, bed thickness, and interbedding? To assess these questions, we have analyzed well-exposed natural detachment folds using the "variable detachment-depth model" (VDDM) (Homza & Wallace 1995). The VDDM is a geometric and kinematic model for detachment folds that does not depend on the assumption of migrating hinges and constant detachment depth, as is the case in previously published models (Jamison 1987, Mitra & Namson 1989).

All of the folds we observed can best be described kinematically as fixed arc-length (fixed-hinge) buckle folds because the geometry and distribution of strain-indicators in each fold precludes a migrating-hinge mechanism. Structures in both the competent and incompetent units provide evidence for structural changes in both detachment unit thickness (depth-to-detachment) and cross-sectional area, both of which are required by the observed fold geometries. We suspect that gradations in competency within the folds have led to complex parasitic and disharmonic secondary folds that cause significant departures from the predictions of published models, including the VDDM.

Reproduced with permission of the copyright owner. Further reproduction prohibited without permission.

The study area is in the Arctic National Wildlife Refuge of Alaska, south of the controversial "1002 area", which is the most promising onshore region in North America for large undiscovered oil fields (Fig. 3.2). The northeastern Brooks Range is well suited for the study of detachment folds because they are clearly identifiable as such and, in different areas, they involve the same general stratigraphy in a variety of structural positions and stages of evolution. For this study, folds were analyzed from four different parts of the northeastern Brooks Range fold-and-thrust belt.

GEOLOGIC SETTING

The northeastern Brooks Range is the northern extension of the Rocky Mountain system and its stratigraphy is equivalent to that in the sub-surface of the Alaskan North Slope petroleum province (Moore *et al.* 1994, Anderson *et al.* 1994). In the northeastern Brooks Range, Paleozoic rocks are divided into two groups that are separated by a sub-Middle Devonian angular unconformity (Fig. 3.3) (Moore *et al.* 1994). The pre-Middle Devonian rocks, referred to here as "basement", are a heterogeneous group of multiply deformed and slightly metamorphosed sedimentary and volcanic rocks (Table 3.1). Paleozoic rocks above the unconformity are part of a mixed carbonate and clastic sequence formed on a southward-facing passive margin. In the study area, this sequence includes, in ascending order, the Mississippian Kekiktuk Conglomerate, the Mississippian Kayak Shale, the Mississippian-Pennsylvanian Lisburne Limestone, and the Permian-Triassic clastic Sadlerochit Group (Table 3.1).

Reproduced with permission of the copyright owner. Further reproduction prohibited without permission.

The dominant structure of the northeastern Brooks Range fold-and-thrust belt is a passive-roof duplex (Banks & Warburton 1986) that consists of two distinct structural units: 1) a series of northward-displaced fault-bend folded horses marked by regional anticlinoria and 2) an overlying roof sequence that is deformed into kilometer-scale detachment folds (Namson & Wallace 1986; Wallace & Hanks 1990; Wallace 1993). The unseen floor thrust of the duplex is interpreted to lie within the basement and the roof thrust is within the Kayak Shale. The Kekiktuk Conglomerate has deformed with the basement as part of the horses (Wallace & Hanks 1990). All of the folds described in this article are part of the roof sequence of the duplex and are classified as detachment folds because 1) they are defined by a competent unit (Lisburne Limestone), 2) they are cored by an internally deformed incompetent unit (Kayak Shale), and 3) the incompetent unit is detached from and displaced relative to an underlying competent unit (Kekiktuk Conglomerate and basement) (Homza & Wallace 1995) (Figs. 3.1 & 3.3). The detachment surface above which the folds have formed has been folded by the regional anticlinoria, which has affected the orientation and, perhaps, evolution of the detachment folds. The Kayak Shale grades lithologically upward in most locations into a transitional "lowest Lisburne" (Table 3.1) unit that is treated as part of the competent unit in the model presented here. The Kekiktuk Conglomerate and the basement are referred to collectively here as the "sub-detachment unit".

Reproduced with permission of the copyright owner. Further reproduction prohibited without permission.

METHODS

Geologic mapping (scale 1:25,000) (Homza 1993, 1994) has been used to constrain the cross-sectional (normal to plunge) geometry of each fold, whereas observations of meso- and microscopic strain indicators have provided evidence to distinguish between fixed- and migrating-hinge mechanisms (*e.g.* Fischer *et al.* 1992, Rowan & Kligfield 1992). For each fold, we have used the cross-sectional geometry and the strain information, together with the variable detachment depth model, to estimate variations in detachment depth and fold area in order to constrain the evolution of each fold.

Strain indicators and kinematics

Migrating-hinge fold kinematics requires that either the synclinal and/or anticlinal hinge move through the competent unit during folding. This suggests that strain indicators that are typical of hinges should be preserved in the fold limbs. For example, if structures typically found in the limbs of flexural slip folds (*e.g.* en-echelon tension fractures, orthogonal bedding-normal fractures, and indicators of top-toward the anticline interbed shear (Ramsay & Huber 1983, 1987, Marshak & Mitra 1988)) are observed in the limb position and they overprint structures typically found in hinges (*e.g.* intense axial planar cleavage, small-scale contractional folds and faults (Ramsay & Huber 1983, 1987)), then the relationship supports migrating-hinge kinematics. If, however, no such overprinting relationships are observed and no "hinge structures" are in the limbs, then no evidence for hinge-migration kinematics exists. The character, scarcity, and distribution of micro-strain indicators in the Lisburne Limestone

Reproduced with permission of the copyright owner. Further reproduction prohibited without permission.

precludes detailed micro-strain analyses (*e.g.* Ramsay & Huber 1983). So this study utilizes a semi-quantitative strain analysis similar to that used by Fischer *et al.* (1992) to distinguish between fixed- and migrating-hinge kinematics. Our analysis consisted of comparing the number of common micro-structures in the hinges to those in the limbs of folds and noting overprinting relationships. These structures include evidence of crystal-plastic deformation (calcite twins, deformation bands), flattened grains, rotated grains, cleavage (spaced and penetrative), stylolites, intra-grain microfractures, and veins. The method is described in Appendix 1. Excellent exposures and access allowed the lowest competent beds to be sampled and traversed from syncline to anticline to syncline for each fold, which enabled close observation of both mesoscopic structures and overprinting relationships.

The variable detachment depth model (VDDM)

The VDDM focuses on the geometry of the incompetent unit and is briefly described here (see Homza & Wallace 1995 for a detailed explanation). Consider an anticline that formed by plane strain and with constant area and bed-length above an incompetent unit of rock with a given *un*deformed stratigraphic thickness (original detachment depth D_o) (Fig. 3.4). If the final deformed thickness of that unit (D_f), as measured beneath the adjacent synclines, equals D_o, then the depth to detachment has remained constant during folding and the area of incompetent rock displaced to form the fold (A_o) equals the area uplifted within the fold (A_f). It follows that the shortening (S) required to form the fold times the original depth (D_o) equals the area uplifted within the fold. This is the basis of the widely accepted "depth-to-detachment

Reproduced with permission of the copyright owner. Further reproduction prohibited without permission.

calculation" ($SD_O = A_f$) (Fig. 3.4b) (Chamberlin 1910). Most fault-related fold models assume a constant detachment depth (*e.g.* Suppe 1983, Jamison 1987, Mitra & Namson 1989), which requires a migration of hinges during fold growth (Homza & Wallace 1995). Although the assumption that $SD_O = A_f$ may be valid for rigid-ramp folds, it is not necessarily true for detachment folds. Instead, if it is assumed that $D_O \neq D_f$, as in figures 3.4a & 3.4c, then $A_O \neq A_f$, $SD_O \neq A_f$, hinge-migration is not required, and the conventional depth to detachment calculation is invalid, even if total area is conserved (Figs. 3.4a & 3.4c).

The VDDM can be used either in the conventional sense, where $D_O = D_f$, or where $D_O \neq D_f$. Thus, it enables evaluation of both fixed- and migrating-hinge folds formed above a detachment unit that may or may not have changed thickness during folding (Fig. 3.4). The model requires a knowledge of D_O and/or D_f (Fig. 3.4). If either depth is known, then the other can be calculated for any triangular fold geometry using:

$$D_f = D_O S/W + D_O - H/2 \qquad (3.1)$$

where W = wavelength and H = height, measured relative to the competent-incompetent contact (Fig. 3.4) (see Homza & Wallace (1995) for derivations and the use of limb-dip instead of W or H). To simplify discussion, the model incorporates an "area differential" variable ($A_{\Delta D}$), defined as the difference between the area displaced (A_O) and the area uplifted within the fold (A_f), or alternatively, in terms of depth:

$$A_{\Delta D} = W (D_f - D_O). \qquad (3.2)$$

Reproduced with permission of the copyright owner. Further reproduction prohibited without permission.

A positive area differential indicates a final depth that is greater than the original depth (Fig. 3.4c) and a negative area differential indicates a final depth that is less than the original depth (Fig. 3.4a).

The area beneath a symmetrical or asymmetrical triangular fixed-hinge fold initially increases rapidly, then decreases as the fold tightens beyond an interlimb angle (γ) of 90° (Fig. 3.5a) (*e.g.* Wiltschko & Chapple 1977). According to our model, this initial increase in fold area is accommodated by material moving from beneath synclines into the triangular fold, thereby decreasing both the elevation of the synclines and the $A_{\Delta D}$ value (*i.e.* $D_f < D_o$). As the fold passes through $\gamma = 90°$, area is squeezed out of the triangle and moves beneath synclines, which requires either increasing both the synclinal elevation and $A_{\Delta D}$ (*i.e.* $D_f > D_o$) and/or volume loss in the incompetent unit. Layer-parallel shortening before folding serves to decrease the amount of required variation in $A_{\Delta D}$ (*e.g.* Groshong & Epard 1994) (Fig. 3.5b). If $A_{\Delta D} = 0$ (*i.e.* $D_f = D_o$) throughout folding, then the relationship between shortening and uplifted area is linear and a hinge-migration mechanism is required (Dahlstrom 1990, Homza & Wallace 1995).

Thus, by comparing natural fold geometries and associated detachment depths to predictions of the VDDM, and taking into account the distribution of strain indicators in both the competent (*e.g.* Fischer *et al.* 1992, Groshong & Epard 1994) and incompetent units, it is possible to constrain the kinematic path of the fold and estimate area loss or gain. Although the distribution of strain in the competent unit provides powerful evidence for differentiating between fixed- vs. migrating-hinge kinematics (Fischer *et al.* 1992, Rowan & Kligfield 1992),

Reproduced with permission of the copyright owner. Further reproduction prohibited without permission.

comparison of natural fold geometries with the geometric predictions of the VDDM provides an independent basis for distinguishing between fixed- and migrating-hinge kinematics. The primary limitation of the VDDM is that it is based on the unlikely assumption that no material moves laterally *through* the synclines in the plane of section (Fig. 3.4). The limits imposed by this assumption suggest that the detachment depth variations predicted by the model are maximum variations.

THE DETACHMENT FOLDS

The study areas include four cross-sectional transects of varying length from different structural positions with respect to the underlying horses. The transects are discussed in order of decreasing interlimb angle, γ (γ is measured as an enveloping surface covering the competent-incompetent contact for the purpose of order, however, γ varies up structural section in most folds).

The Straight Creek fold (SCF)

The Straight Creek anticline (Homza 1993) lies above the north-dipping leading edge of a horse in the central part of the duplex (Figs. 3.2 & 3.6). Both the sub-detachment unit (basement and Kekiktuk Conglomerate) and the competent-incompetent couplet (Lisburne Limestone and Kayak Shale) that define the detachment fold are well exposed for several kilometers down plunge. However, the anticlinal hinge of the fold is eroded in the upper part of the competent unit, forming a topographic low along the entire trace of the fold (Fig. 3.7).

Reproduced with permission of the copyright owner. Further reproduction prohibited without permission.

Geometry of the Straight Creek fold

The SCF is an open (γ = 78°), inclined, symmetrical, angular, disharmonic, parallel detachment anticline with a wavelength of 839 m and a height of about 398 m. The fold plunges 15° toward N77°E (Fig. 3.6; Table 3.2). The thickness of the Kayak Shale varies from about 270 m beneath the synclines to about 650 m in the core. Although the axial surface dips almost 60° SE, the SCF is relatively symmetrical and its axial surface is nearly perpendicular to the underlying detachment surface. Parasitic folds in the lowest Lisburne Limestone and disharmonic folds within the Kayak Shale are exposed across the SCF, are most abundant along the axial trace of the SCF, and have an asymmetry that consistently indicates top-toward-the-anticline shear (Figs. 3.6 & 3.7).

Strain indicators in the competent folded unit

The abundance of strain indicators is much greater in both primary and parasitic hinge zones than in planar limbs (Fig. 3.8a). In hinge zones in the Lisburne Limestone, penetrative solution cleavage is the most significant deformation mechanism in the finer-grained rocks, whereas intra-grain fracture, calcite twinning, stylolitization, and grain rotation are most important in the coarser-grained rocks (Appendix 1). In the limbs, most strain indicators are notably less abundant and penetrative deformation is essentially absent (Fig. 3.8a, Appendix 1), except where thin, fine-grained horizons contain minor fault gouge and/or shear-zone fabric that resulted from bed-parallel shear associated with flexural-slip folding. The most abundant features in the limbs are grains rotated toward bedding-perpendicular, flattened grains with long axes

Reproduced with permission of the copyright owner. Further reproduction prohibited without permission.

perpendicular to bedding, and calcite twins. The bedding-perpendicular orientation of grains around the fold suggest that they were aligned before folding and represent bedding-parallel shortening. Limb structures are not anywhere observed to overprint hinge structures. Although parasitic folds are common in the lowest Lisburne Limestone in the primary anticlinal hinge zone, the limbs of these folds contain no penetrative fabrics and many fewer strain indicators than do their hinges. Hinge deformation is observed in the upper, more competent part of the Lisburne Limestone only in the northern syncline in the form of the penetrative cleavage. We hypothesize that a similar high-strain zone in the Lisburne in at least the lower part of the anticlinal hinge was preferentially eroded.

Strain indicators in the detachment unit

Two 10 m thick competent quartz sandstone units within the Kayak Shale lie between thicker, less competent shales and define complex folds in the lower part of the core of the SCF that are disharmonic with respect to the SCF (Figs. 3.6 & 3.7). Some of these folds are associated with "into-the-plane" thrust faults (*i.e.* with displacements sub-parallel to the fold trend) and they are tightest (in some cases isoclinal) along the lower boundary of the sandstones. Intra-grain microfractures, quartz veins, deformation lamellae, flattened grains, and spaced cleavage are abundant in the hinges of these folds. In contrast, in the limbs, beds contain many fewer veins, no visible cleavage, and rounder, less fractured grains with more uniform extinction.

Shales in the Kayak in the cores of both the SCF and the tight intra-formational disharmonic folds display a penetrative solution cleavage that has

Reproduced with permission of the copyright owner. Further reproduction prohibited without permission.

transposed bedding. In the cores of some tight folds, the shale is either completely removed and the fold is truly isoclinal (Fig. 3.7) or it is reduced to a siliceous gouge, whereas pencil cleavage is common in more open cores. Beneath the planar limbs of both the SCF and the disharmonic folds, the Kayak Shale is fissile with a spaced cleavage sub-parallel to bedding.

Kinematic interpretation of the Straight Creek fold

Qualitative indications of layer-parallel shortening before folding suggest that regardless of how the incipient Straight Creek fold formed, beds were first shortened and thickened to some degree. The distribution of penetrative deformation in the hinges of the primary anticline, the parasitic folds in the lowest Lisburne, and the disharmonic folds in the Kayak, together with the lack of hinge structures overprinted by limb structures, is compatible with fixed-hinge/rotating limb folding. Conversely, this distribution of strain indicators is incompatible with migrating-hinge kinematics (Butler 1992, Fischer *et al.* 1992).

Fixed-hinge kinematics are further supported by the geometry of the fold when analyzed with both the standard constant depth-to-detachment method (*e.g.* Chamberlin 1910, Jamison 1987, Mitra & Namson 1989) and the VDDM. First, we consider the standard calculation where D_C^C is the calculated constant detachment depth, A_f^m is the measured fold area, and the displaced area (A_O) is assumed to equal A_f^m (Fig. 3.9a):

$$D_C^C = A_f^m/S. \qquad (3.3)$$

$$D_C^C = 179{,}967\ m^2/621\ m = 290\ m.$$

Reproduced with permission of the copyright owner. Further reproduction prohibited without permission.

When this solution is compared with the measured depth to detachment beneath the fold (D_f^m = 260 m), a discrepancy of about 30 m results between calculated and measured detachment depth. Further, if we multiply this number by the fold wavelength (839 m), the calculation suggests that about 25,000 m² more incompetent material should be present beneath the fold than can be accounted for (Fig. 3.9a, Table 3.2).

The variable detachment depth method does not assume that $A_o = A_f^m$. To use the VDDM, we first take the measured undeformed stratigraphic thickness of the Kayak Shale as the measured original detachment depth (D_o^m) to calculate the area differential:

$$A_{\Delta D} = SD_o^m - A_f^m. \quad (3.4)$$

$$A_{\Delta D} = 167{,}049\ m^2 - 179{,}967\ m^2 = -12{,}918\ m^2.$$

Then, we solve for the calculated final detachment depth beneath the fold (D_f^c) using equation (3.2):

$$D_f^c = A_{\Delta D}/W + D_o \quad (3.5)$$

$$D_f^c = (-12918\ m^2/839\ m) + 269\ m = 254\ m.$$

When this solution is compared with the measured depth to detachment, a discrepancy of about -6 m results between calculated and measured detachment depth. If we multiply this number by the fold wavelength (839 m), the calculation suggests that about 5000 m² less incompetent material should be present than is

Reproduced with permission of the copyright owner. Further reproduction prohibited without permission.

accounted for beneath the fold (Fig. 3.9, Table 3.2). This number is a minimum because the calculations do not account for loss of area by solution cleavage, as is observed in the core. This area discrepancy could represent errors resulting from imprecise measurements. However, thrust faults in the core that indicate material transport into the plane of section suggest that the area disparity may reflect and quantify such non-plane strain.

In any case, for the Straight Creek fold, the VDDM provides a better fit to the observations than does the conventional depth-to-detachment calculation. The geometric solution suggests that the detachment depth effectively decreased during folding from 269 m to 260 m as material moved from the synclines into the anticlinal core, as in fixed-hinge folding (*e.g.* Wiltschko & Chapple 1977). The asymmetry of disharmonic folds in the Kayak is consistent with such motion. The general location of the SCF on figures 3.5a & 3.5b ($\cong$ 35% shortening) suggests that, when fold growth ceased, the area differential, although still negative, was approaching zero (*i.e.* detachment depth was increasing, and thus, was once less than the current depth). Since solution cleavage indicates area loss in the core, the detachment depth would likely increase at a slower rate than indicated on the idealized constant-area graphs of figure 3.5.

Thus, considering both the geometric modeling of the SCF and the distribution of strain indicators within it, we hypothesize that 1) early layer-parallel shortening is recorded in the limbs, 2) the uplifted area initially increased rapidly (Fig. 3.5) as fold limbs rotated about both the primary and parasitic hinges, which were fixed with respect to the rock, 3) the distance between the

Reproduced with permission of the copyright owner. Further reproduction prohibited without permission.

synclines and the detachment (detachment depth) decreased by at least 9 meters (from D_o to D_f) as the limbs rotated and material moved into the anticlinal core, and 4) further limb-rotation resulted in a decrease in uplifted area which promoted area loss by penetrative solution cleavage in the core, perhaps coupled with a minor increase in detachment depth (from Fig. 3.5). Even with area loss due to solution cleavage, a net area gain is still apparent in the core of the SCF, suggesting non-plane strain, which is supported by into-the-plane thrust faults in the lower anticlinal core.

The Salisbury Creek anticline (SCA)

The Salisbury Creek transect lies above the same fault-bend folded horse as the Straight Creek fold but is about 35 km southwest of the SCF and structurally overlies the gently dipping backlimb of the horse (Figs. 3.2 & 3.10). The form surfaces of the sub-detachment unit, the detachment horizon, and the competent unit together describe a series of north-vergent to upright and symmetrical detachment folds. One particularly well-exposed north-vergent anticline, the Salisbury Creek anticline (SCA) (Homza & Wallace 1995, Homza 1994), is discussed in detail below.

Geometry of the Salisbury Creek anticline

At the Lisburne-Kayak contact, the Salisbury Creek anticline is an open to tight, inclined, northward asymmetric, angular, disharmonic, parallel detachment fold with a wavelength of 147 m, a height of 63 m, and a slight westward plunge. The fold can be traced for 20 km down plunge where, up structural section, it increases in height, wavelength, and interlimb angle. At the hinge on the Kayak-

Reproduced with permission of the copyright owner. Further reproduction prohibited without permission.

Lisburne contact, the fold interlimb angle is about 40°, but this angle increases to about 80° both up and down structural section. The change in dip of the contact down section defines secondary synforms on the limbs of the anticline (Figs. 3.10 & 3.11). A train of smaller detachment folds lies immediately hindward of the SCA at the Kayak-Lisburne contact.

Strain indicators in the competent folded unit

Five parasitic folds that are out of phase with the fold train at the Kayak-Lisburne contact are exposed higher in the upper Lisburne where it contains alternating competent-incompetent layers (Figs. 3.3 & 3.12). These upper parasitic folds are about five kilometers off the section line and hence cannot be projected accurately onto the section. However, beds in the Lisburne above and below these folds are relatively straight, indicating that these parasitic folds are detached from adjacent layers. In the synclinal and anticlinal hinges at the Kayak-Lisburne contact, many minor thrust faults and folds are exposed, and well-developed calcite-filled veins, solution cleavage, and stylolites are associated with them (Fig. 3.8b). Although the forelimb is more deformed than the backlimb (Homza & Wallace 1995), no evidence was observed that limb structures overprinted hinge structures in either limb. A single thrust fault with less than 10 m of displacement duplicates part of the lowest Lisburne in the backlimb (Fig. 3.11).

Strain indicators in the detachment unit

Asymmetric disharmonic folds in several meter-thick competent sandstone units within the Kayak indicate top-toward-the-anticline shear. Strain

Reproduced with permission of the copyright owner. Further reproduction prohibited without permission.

in the detachment unit increases toward the hinge of the anticline, where the tightest disharmonic folds are developed in the sandstones between shale layers that display both crenulation cleavage, and solution cleavage. A siliceous gouge-like cataclasite is exposed in the uppermost Kayak, in the core of the SCA, where the fold is tightest.

Kinematic interpretation of the Salisbury Creek anticline

For the SCA, the variable depth equations (equations 3.4 & 3.5) result in closer matches between observed and calculated depths and uplifted areas than did the constant depth equation (equation 3.3) (Table 3.2). The geometry of the SCA and the VDDM suggest that the synclines were elevated by about 8 m (positive $A_{\Delta D}$). An apparent net area loss of 1911 m^2 in the incompetent core of the fold (Table 3.2) suggests non-plane strain, which is supported by strong solution cleavage and cataclasite development exposed in the core near the Kayak-Lisburne contact, where the fold is tightest. The strong hinge deformation, lack of overprinted hinge structures on the limbs, top-toward the anticline shear in the Kayak, and the better geometric fit of the SCA to the VDDM than to the constant-depth, migrating-hinge model, suggest fixed-hinge kinematics for the SCA. Thus, the SCA is interpreted as a fixed-hinge detachment fold formed with limb rotation, area loss, an increase in detachment depth, and minor thrust faulting in the backlimb.

The West Fork anticline (WFA)

The West Fork transect crosses the central part of the fold-and-thrust belt along the west fork of the Aichilik River (Fig. 3.2). The transect includes multiple

Reproduced with permission of the copyright owner. Further reproduction prohibited without permission.

detachment folds above at least three horses (Fig. 3.13). In this region, the lowest Lisburne is very rich in chert and has nearly no fine-grained carbonate component. Thus, the competent-incompetent contact is sharp here, rather than gradational as it is at other locations.

Linking thrusts in the regional duplex apparently are more closely spaced here than in the other study areas. Just to the south of and to the west of the West Fork transect, thrusts are observed to cut up section from the basement and through the forelimbs of detachment folds in the roof sequence (Homza 1992a). Thus, there is a close association between folds in the roof sequence and thrust faults in the basement along this transect. However, the folds in the roof sequence clearly are detachment folds since the Kayak Shale is thickened in each fold core (Figs. 3.13 & 3.14), whereas fault-bend and fault-propagation folds involving both the Kayak and the Lisburne are apparently absent. Here, most detachment folds are open to tight, angular, and north-vergent. We focus our analysis on the West Fork anticline (WFA) (Fig. 3.14), a large anticline exposed along strike for over 10 km in the central part of the transect and that is truncated up plunge by a linking fault in the duplex.

Geometry of the West Fork anticline (WFA)

The WFA and its adjacent forward syncline (Figs. 3.13 & 3.14) are close ($\gamma \cong 60°$), inclined, northward asymmetric, angular, parallel folds that plunge 10° toward S81°E. The WFA contains only a few small parasitic folds, hence its geometry is nearly triangular. As with anticlines in each study area, the hinge of the WFA is preferentially eroded in many areas. The fold is tightest in the hinge at the Kayak-Lisburne contact and this local increase in tightness introduces

Reproduced with permission of the copyright owner. Further reproduction prohibited without permission.

open, secondary synforms up structural section in the limbs of the anticline. However, down-plunge exposures of the WFA show that, like the SCA, its interlimb angle increases up section and parasitic folds that cannot be accurately projected up plunge onto the section are present within the upper Lisburne.

The base of the Kayak is not exposed beneath the WFA and its position is interpreted based on observations on the section line immediately north and south of the fold (Fig. 3.13). The Kayak Shale is interpreted to be 725 m thick in the core of the anticline and is observed to be 184 m thick where it is relatively undeformed beneath straight panels of Lisburne two kilometers to the north.

Strain indicators in the competent folded unit

Mesoscopic contractional faults and tight folds are abundant along the Kayak-Lisburne contact in the hinge of the WFA but are absent in the limbs. Mesoscopic and limited microscopic samples show that strain-indicators are concentrated in fold hinges along the West Fork transect and that grain rotation and cleavage are the most abundant observed deformation mechanisms (Fig. 3.8c). Again, the most common features in the limbs are stylolites, flattened grains, and rotated grains, all of which may be associated with layer-parallel strain prior to folding since they are bedding-perpendicular all around the fold. Interbed slip surfaces are apparent in the limbs in the Lisburne. As with all the other areas, penetrative cleavage is much more common in hinges than in limbs and represents the most significant microscopic form of shortening in the lowest Lisburne.

Reproduced with permission of the copyright owner. Further reproduction prohibited without permission.

Strain indicators in the detachment unit

Several meter-thick competent limestone beds lie within the Kayak Shale along this transect. In the anticlinal core of the WFA, these beds are tightly folded and offset along south-dipping thrust faults with meter-scale displacements. Strain in the shale component of the Kayak in the core of the WFA is dominated by penetrative solution cleavage that has transposed bedding.

Kinematic interpretation of the West Fork anticline

The West Fork anticline has a relatively simple geometry, but one that requires complex kinematics to account for its excess area. The linking fault that defines the leading edge of a horse in the underlying duplex truncates the forelimb up plunge, but it is interpreted to lie directly beneath the fold at the section line (Fig. 3.13). This strongly suggests that folding was a response, at least in part, to thrusting, so the conventional assumption of detachment fold formation above a simple straight detachment is not applicable. Since the base of the Kayak, which is observed to be the detachment in the other areas, is not observed here, we must estimate its position and geometry. The variable depth model may be applied in order to determine the area that must be accounted for and to constrain a kinematic model that incorporates this area and the role of thrusting.

Again we will contrast results of the constant-depth, migrating-hinge model and the VDDM. Using the conventional constant-depth assumption and the known area (equation 3.3), the WFA either requires a detachment depth of 375 m or it includes about 203,794 m^2 of excess uplifted area. When the known

Reproduced with permission of the copyright owner. Further reproduction prohibited without permission.

D_o value (184 m) and the area differential are used with the VDDM (equations 3.4 & 3.5), then the final detachment depth beneath the fold is calculated to be -4 m. Exposures projected about two kilometers in the plane of section suggest a projected depth to detachment of at least 184 m, as is shown in the cross section.

With this depth, the WFA presents a problem because about one half of the area uplifted within the fold cannot be accounted for given the observed fold shortening. However, this extra area can be accounted for by one of several alternative models: The first involves "bulldozing" the Kayak Shale in front of the basement horse along the sub-fold thrust. Excess area beneath the fold would be pushed into place by excess shortening in the basement and Kayak Shale relative to the Lisburne, as is apparent on the reconstruction. This excess shortening could have been taken up in the Lisburne north and/or south of the line of section by forward and/or hindward displacement, respectively, of the Lisburne relative to the Kayak Shale.

The second model invokes inversion tectonics. According to this model, an anomalously thick sequence of Kayak Shale was deposited in a local extensional basin produced during pre-Middle Devonian rifting (Anderson *et al.* 1994). This basin would be preferentially inverted along the observed thrust fault during Cenozoic orogenesis and the excess basinal thickness would become excess uplifted area in the WFA. In effect, this model suggests that the original detachment depth of 184 m is too shallow and an inclined detachment is required at a depth of at least 374 m beneath the synclines.

Reproduced with permission of the copyright owner. Further reproduction prohibited without permission.

The third alternative model suggests that the excess incompetent rock was pushed along plunge into the plane of section. This model is consistent with the relatively steep plunge of the WFA. For each model, the VDDM allows the excess area to be calculated, depending upon which original depth is selected. The cross section, as drawn, permits any of the alternative models.

The Marsh Fork transect (MFT)

The Marsh Fork transect includes impressive exposures above the crest and gently dipping forelimb of the southernmost horse in the duplex (Figs. 3.2 & 3.15). The form surface of the sub-detachment unit, the entire Kayak Shale, the Kayak-Lisburne contact, and the lowest Lisburne Limestone are each very well exposed in the area.

Geometry of the Marsh Fork transect

Two primary anticlines that are separated by a straight panel parallel to the detachment unit are observed along this transect. At the Kayak-Lisburne contact, each anticline is composed of a train of smaller detachment folds with hinges that coalesce up section in the upper Lisburne Limestone into a large fold (Fig. 3.15 Plate A3.3). The thickness of the Kayak Shale varies greatly from about 290 m beneath the straight panel to upwards of 700 m in some anticlinal cores. The detachment fold trains include open to isoclinal (tightest at the Kayak-Lisburne contact in anticlinal hinges), upright to inclined, disharmonic, parallel, and mostly angular folds (Fig. 3.16). The hinges of the tightest anticlines consistently form topographic lows due to preferential erosion where strain is greatest.

Reproduced with permission of the copyright owner. Further reproduction prohibited without permission.

Strain indicators along the Marsh Fork transect

In the lowest Lisburne Limestone, mesoscopic strain indicators are concentrated in the hinges of all observed folds. The most common strain indicators are penetrative cleavage, tectonic breccia, veins, and minor folds and faults. Strain indicators are more common in limbs of tighter folds than in more open folds. Minor thrust faults (≤ 5 m displacement) were seen exclusively in hinge zones.

Strain indicators in the Kayak Shale are also concentrated in the hinge zones and the intensity of strain corresponds roughly with the tightness of the overlying fold in the Lisburne Limestone. Kayak in the hinges of more open detachment folds typically contains open-to-close disharmonic folds and relatively less penetrative axial planar cleavage than Kayak beneath isoclines. Beneath isoclinal anticlines, the uppermost Kayak is typically a mixed carbonaceous-siliceous, gouge-like cataclasite. These cataclasties are associated with both shale that displays transposed laminations parallel to penetrative cleavage and various forms of silica and carbonate mineralization. All of these features beneath isoclinal anticlines suggest fluid migration in the Kayak.

The asymmetry of fold trains defined by competent horizons within the Kayak suggests top-toward-the-anticline shear in the Kayak. The undeformed thickness of the Kayak is typically less than 250 m in the northeastern Brooks Range (Imm *et al.* 1993, our unpublished observations), about 40 m less than the thinnest Kayak exposed along the transect. Since even the thinnest section of Kayak in this area displays structural thickening by folding, thrusting, and

Reproduced with permission of the copyright owner. Further reproduction prohibited without permission.

internal deformation, we conclude that the Kayak Shale has been thickened everywhere along this transect.

Kinematic interpretation of the Marsh Fork transect

The complex geometry and abundance of parasitic folds along the Marsh Fork transect preclude simple geometric modeling. However, the geometric and mesoscopic strain observations along the transect indicate that the detachment horizon did not maintain constant thickness during deformation. Rather it was significantly thickened beneath anticlines, synclines, and straight panels, which indicates that a constant-depth model does not apply to these folds. The distribution of mesoscopic structures suggests that hinges were fixed during folding and that incompetent rock flowed toward anticlinal cores. Thus, we suggest that the major detachment folds in the competent unit formed as culminations of chevron-like parasitic folds that describe larger anticlines (Plate A3.4). These folds were accommodated in the incompetent unit by thickening and minor area-loss manifested by solution cleavage and recrystallization in tight fold cores. Since the lowest Kayak is dramatically shortened directly above generally flat and undeformed beds of Kekiktuk , we suggest that the stratigraphic position of the detachment remained near the base of the Kayak Shale throughout deformation. However, we stress that the thickness of the detachment unit increased everywhere along this transect.

Reproduced with permission of the copyright owner. Further reproduction prohibited without permission.

THE WAVELENGTH-TO-THICKNESS RATIO

A strong correlation between fold wavelength and competent unit thickness has been recognized for fixed-hinge folds in a competent unit lying stratigraphically between two very thick incompetent units (Currie *et al.* 1962, and many others). The average wavelength-to-thickness ratio (W/T) for the folds in these studies is about 27 (Fig. 3.17). In the northeastern Brooks Range, the Lisburne Limestone is about one kilometer thick and it forms fixed-hinge folds with wavelengths on the order of one kilometer. Thus, the wavelength-to-thickness ratio observed here is about 1. The question of why, mechanically, the Lisburne folds have such a small ratio is beyond the scope of the present study, but could be approached by considering the mechanical stratigraphy.

Although the rock sequence that overlies the Lisburne contains competent sandstone units up to 100 meters thick, as a whole it is less dominant than the Lisburne because individual units are thinner and contain more shale than the Lisburne. The Lisburne is underlain by the relatively thin Kayak Shale. Thus, the Lisburne Limestone clearly represents the dominant member of Currie *et al.* (1962) and probably controls the primary and parasitic fold geometry. However, there is no related "continuous infinite medium" (Fig 3.3) that is required for the models of Currie *et al.* (1962). Currie *et al.* (1962) explicitly emphasize both the importance of variation in mechanical stratigraphy on fold geometry and the difficulty in applying their model to regional-scale folds.

Thus, the prediction of $W/T \cong 27$ is not expected for Lisburne folds due to the non-ideal mechanical stratigraphy (*i.e.* the Currie *et al.* (1962) model is not applicable to the detachment folds in the Lisburne). However, our observations

Reproduced with permission of the copyright owner. Further reproduction prohibited without permission.

suggest that a dominant member will form folds having small W/T ratios when it both: 1) overlies a thin detachment above a unit that is not folded and 2) underlies a thick sequence of units with significant competency contrasts. Further, we stress that kilometer-scale fixed-hinge buckle folds can and do form even where great thicknesses of incompetent rock are lacking and the W/T is very small.

INFLUENCE OF MECHANICAL STRATIGRAPHY AT THE COMPETENT-INCOMPETENT CONTACT

In the northeastern Brooks Range, the contact between the detachment unit (Kayak Shale) and the competent unit (Lisburne Limestone) is commonly sedimentologically (LePain 1993) and mechanically gradational (Fig. 3.3). The top of the Kayak is typically defined by the uppermost meter-thick, fissile, black shale interval. However, structurally weak shales persist into the lowest Lisburne, which is primarily composed of decimeter-thick carbonate beds. Higher in the Lisburne, the shales are effectively absent and the carbonate beds of the upper Lisburne are meters thick and very strong. This stratigraphy results in an upward gradation in structural style from penetrative fabrics and small-scale faults and folds in the lowest, finest-grained rocks, to parasitic flexural-slip folds in the transitional strata, to primary flexural-slip folds in the upper part of the competent unit.

Such stratigraphic variations are common in the rocks of fold-and-thrust belts and probably result in structural gradations in detachment folds. Increasing competent bed thickness and abundance in a multilayer stratigraphy

Reproduced with permission of the copyright owner. Further reproduction prohibited without permission.

leads to folds with greater wavelength and interlimb angle (Currie *et al.* 1962, Ramsay 1974, Ramsay & Huber 1987). Geometric models are of limited use in describing folds involving stratigraphically controlled gradations in geometry and kinematics since models assume sharp boundaries in competency and simple geometries.

GENERALIZED DETACHMENT FOLD EVOLUTION

The folds observed in the northeastern Brooks Range define a range in geometry and complexity of anticlines, with their form and distribution of strain indicators suggesting fixed-hinge and variable detachment depth kinematics. Consequently, we can use these examples, together with the variable detachment depth model, as a guide to describe the evolution of a generalized, fixed-hinge detachment fold. Figure 3.18 shows the evolution of such a fold, including layer-parallel shortening, parasitic and disharmonic folding, and variations in detachment depth. This figure is not a balanced model, but rather it is a schematic diagram that illustrates the geometric variation we think is typical in the evolution of detachment folds in the northeastern Brooks Range.

Initial shortening is taken up in each unit by layer-parallel shortening (stage b). In early, open geometries (stage c), fold area is greater than displaced area (negative area differential) and increases with increasing shortening. This requires transport of incompetent material into the anticlinal core, which results in a decrease in detachment depth and synclinal elevation. In such cases, constant depth models would overestimate the depth to detachment beneath the fold, as with the Straight Creek fold. As the fold

Reproduced with permission of the copyright owner. Further reproduction prohibited without permission.

evolves, parasitic and disharmonic folds develop, with their size and abundance depending on the percentage of incompetent rock and the average bed thickness (Ramsay & Huber 1987).

As shortening increases, a point is reached beyond which fold area begins to decrease, resulting in transport of incompetent material out of the anticlinal core and a consequent increase in detachment depth and synclinal elevation (the final geometry of the Straight Creek fold suggests it is at this stage). Fold area eventually equals displaced area (area differential is zero, just beyond stage d), so that the predicted final thickness equals original depth. Only at this stage of development can a fixed-hinge, variable-depth fold, for a "geologic instant", successfully be described using a geometric model that assumes fixed depth and migrating hinges.

As the fold tightens further and its area continues to decrease, displaced area exceeds fold area (positive area differential, stage e) and the difference between the two increases with increased shortening. Thus, the final depth beneath the fold exceeds the original depth and constant-depth models would underestimate the depth to detachment beneath the fold, as with the Salisbury Creek anticline. In addition to thickening of the detachment unit, the Salisbury Creek anticline responded to decreasing fold area by penetrative deformation in its core that caused area to be lost in solution. Figure 3.19 is a schematic diagram of a typical detachment fold in the northeastern Brooks Range at approximately stage e of this fold evolution. The diagram graphically shows a distribution of meso- and microscopic strain indicators similar both to those we observed and to those noted by Ramsay (1974) and Fischer *et al.* (1992).

Reproduced with permission of the copyright owner. Further reproduction prohibited without permission.

With increased shortening, hinge zones of folds in the anticlines along the Marsh Fork transect were penetratively deformed as interlimb angles decreased to tight-to-isoclinal geometry (stage e to f). Very tight geometries in the SCA, MFT, and WFA occur only in the anticlinal hinge at the competent-incompetent contact and may represent the onset of isoclinal "lift-off" folding (Mitra & Namson 1989) (stage f). The area differential of these folds quickly increased as they were elevated above the original elevation of the competent-incompetent contact (stage f). Thrust faults (*e.g.* stage f) may cut through the fold at any stage of its history, depending on the structural behavior of the sub-detachment unit and/or the locking angle of the dominant member (*e.g.* Ramsay 1974). For example, part of the West Fork anticline was truncated at least by stage e by a thrust cutting up from the sub-detachment unit.

CONCLUSIONS

Detachment folds in the northeastern Brooks display a range of geometries and constraints on kinematic evolution. This principal conclusions of this study are:

- The distribution of and intensity of strain indicators and minor structures indicate that the folds formed by fixed-hinge kinematics in the competent unit (Fig. 3.19).
- Direct observations and analysis using the variable detachment depth model indicate that the structural thickness of the incompetent unit (detachment depth) varied during fold evolution (Table 3.3).

Reproduced with permission of the copyright owner. Further reproduction prohibited without permission.

- All of the observed folds displayed a discrepancy between the actual area observed (or inferred, as with the WFA) within the anticline and the displaced area (calculated as the product of shortening and the original thickness of the incompetent unit). This discrepancy could reflect some combination of :
  - Depositional variability in the original thickness of the incompetent unit at each fold.
  - Non-plane strain by structural transport and/or solution.
  - Transport of material through synclines (*i.e.* a local discrepancy between shortening in the competent and incompetent units).
- Observations indicate that the fold geometry is controlled in detail by competency contrasts (bed thickness, rheology, and percent strong beds in a stratigraphic sequence), with the size and spacing of folds reflecting influences from each structural member.
- Constant-depth, migrating-hinge models do not work for the folds observed in the northeastern Brooks Range.
- The variable detachment depth model is more useful for fold analysis than for the reconstruction of geometry because of the mobility of incompetent material (into/out of the confines of the fold in the plane of section or into/out of the plane of section).
- The observed fold geometries and analysis using models suggest general characteristics of detachment folds that include:
  - fixed-hinge kinematics
  - variation in detachment depth
  - complex and non-uniform structural stratigraphy that promotes parasitic folding and other secondary structures

Reproduced with permission of the copyright owner. Further reproduction prohibited without permission.

- deformation of the incompetent unit by mechanisms other than parallel folding
- layer-parallel shortening
- area-loss during folding

These characteristics are difficult to model quantitatively using geometric models (contrast figures 3.1 & 3.18).

- This study suggests that typical detachment folds evolve according to the following scenario: Folds initially buckle with the hinges fixed with respect to the rock. A rapid increase in anticline area is accommodated by material transport into the core and a decrease in incompetent unit thickness beneath synclines. Anticlines reach a maximum area at an interlimb angle of about 90°. Factors that offset this rapid area increase include layer-parallel shortening, fold asymmetry, and a relatively thick incompetent unit. Normal stratigraphic variations and gradations result in thinner beds and competent-incompetent interbedding within and between the primary competent and incompetent units. This may lead to the formation of fixed-hinge parasitic folds, especially near the competent-incompetent unit contact, and disharmonic folds in the incompetent unit. As an anticline tightens, the fold area decreases, at least in part by formation of solution cleavage in fold cores. Local conditions may cause the fold to respond to continued tightening in any or all of the following ways: incompetent unit flow and solution may result in isoclinal geometries and lift-off folding involving hinge-migration; it may lose additional area by non-plane strain; and/or it may become elevated above the original position of the syncines (*i.e.* elevated

Reproduced with permission of the copyright owner. Further reproduction prohibited without permission.

above regional). The fold may be truncated by a thrust fault at any time, depending on the local structure. Since this evolutionary scenario is intrinsically variable, it is not viewed as "ideal", but rather "typical" of detachment folds developed in fold-and-thrust belts.

Reproduced with permission of the copyright owner. Further reproduction prohibited without permission.

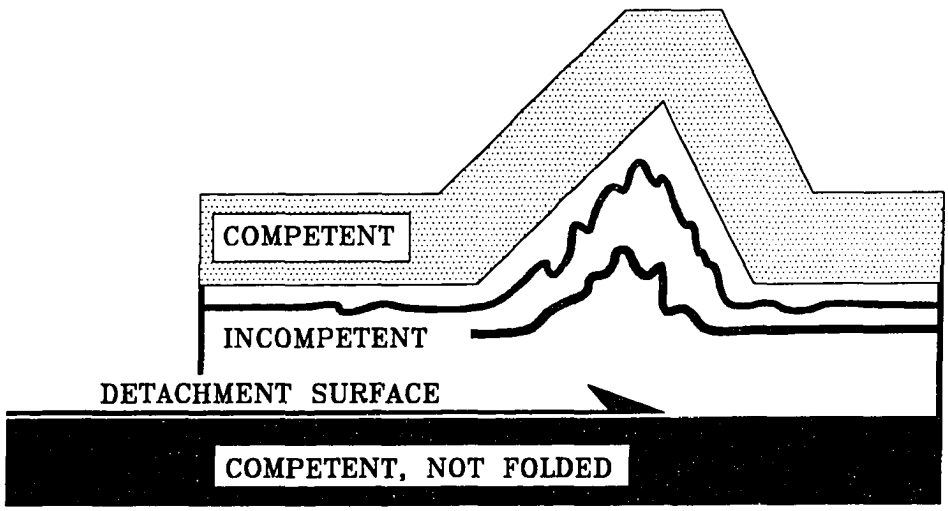

Figure 3.1. An idealized model of a detachment fold showing the essential mechanical layering of competent-incompetent-competent stratigraphic units.

Reproduced with permission of the copyright owner. Further reproduction prohibited without permission.

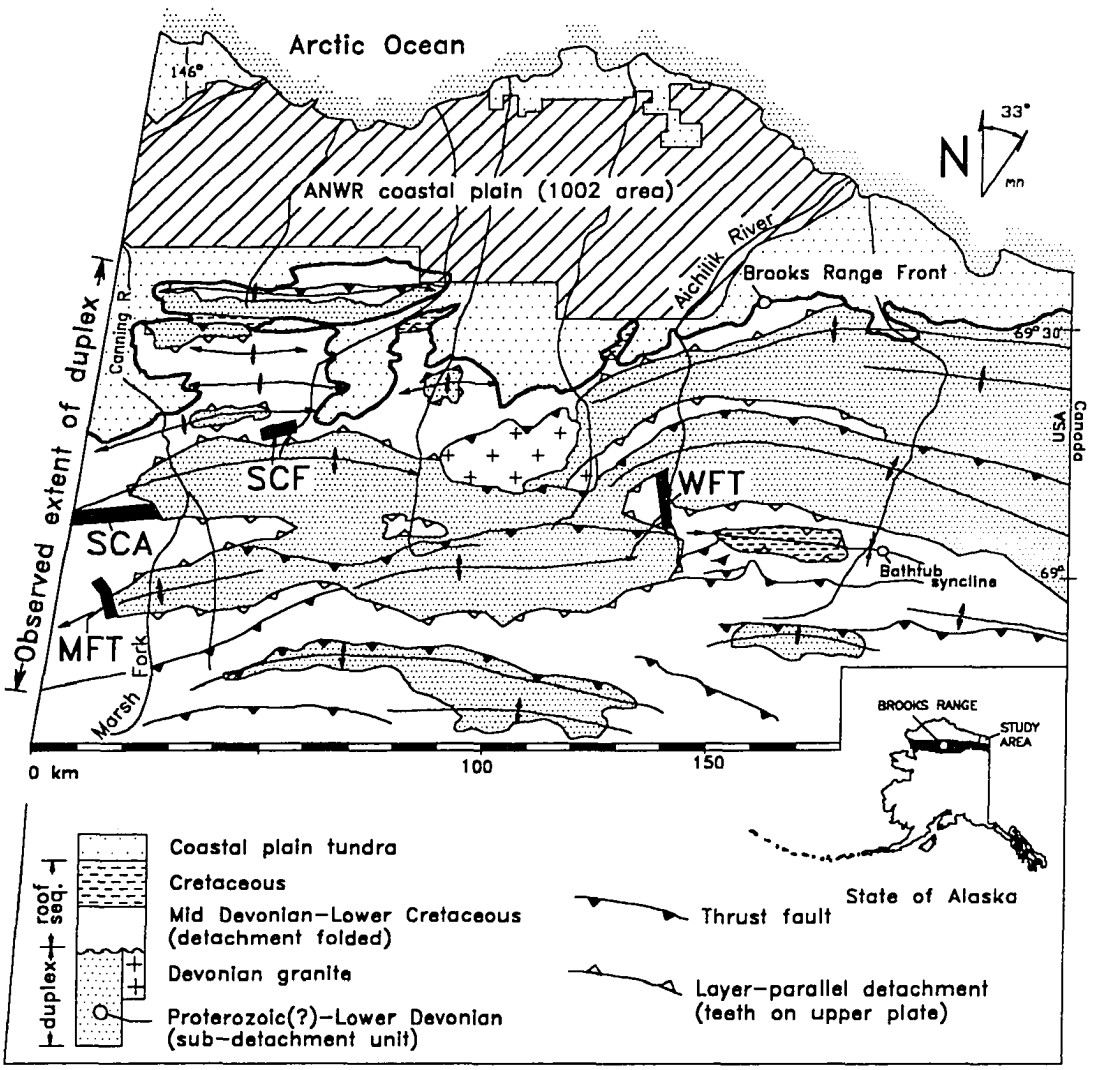

Figure 3.2. Simplified structural map of the northeastern Brooks Range and coastal plain of the Arctic National Wildlife Refuge showing the study areas and the regional anticlinoria that define fault-bend folded horses. SCF = Straight Creek fold, SCA = Salisbury Creek anticline, MFT = Marsh Fork transect, WFT = West Fork transect.

Reproduced with permission of the copyright owner. Further reproduction prohibited without permission.

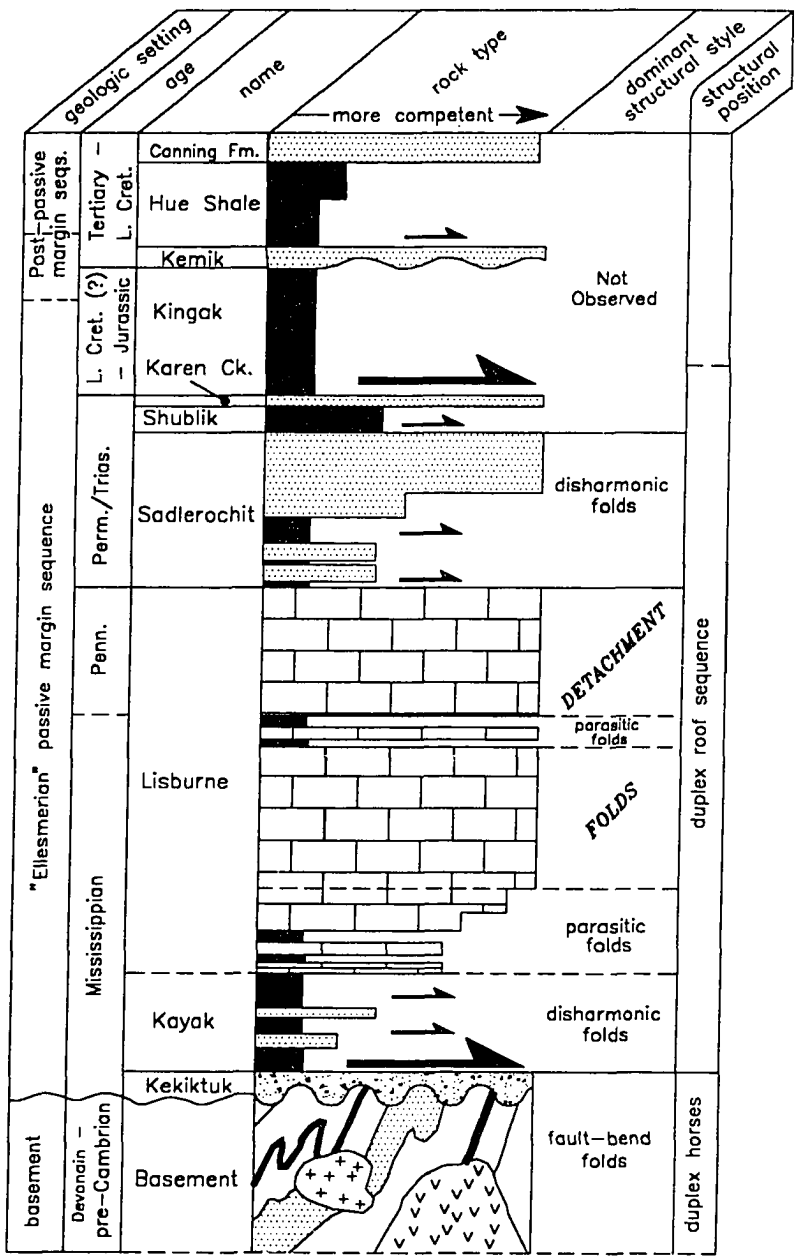

Figure 3.3. Generalized column of the part of the stratigraphy in the northeastern Brooks Range that is referred to in this article. The lower large arrow indicates the location of the duplex roof thrust and the detachment beneath the detachment folds.

Reproduced with permission of the copyright owner. Further reproduction prohibited without permission.

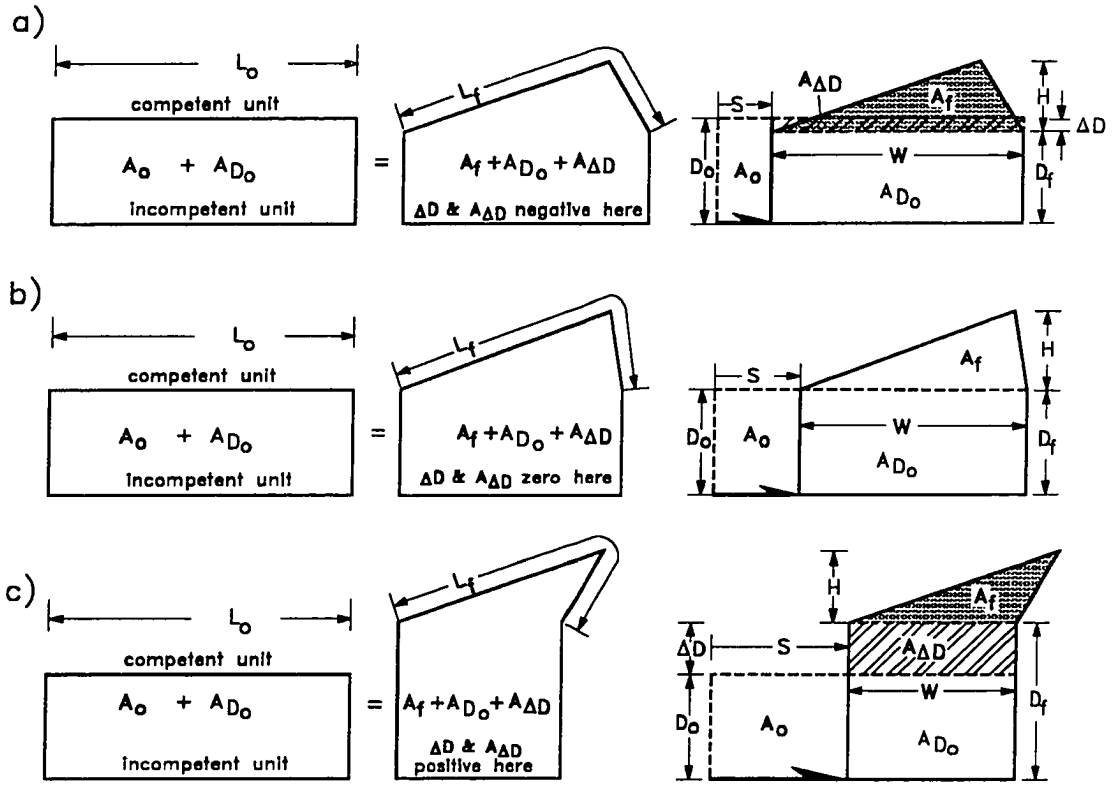

Figure 3.4. The variable detachment depth model for detachment folds showing folds formed in an incompetent unit of original thickness (D_0). a) balanced model of an early-stage fold with small shortening and negative $A_{\Delta D}$. b) balanced model of an intermediate-stage fold with $A_{\Delta D}$ = 0. c) balanced model of a late-stage fold with large shortening and positive $A_{\Delta D}$. The original (L_0) and final (L_f) lengths of the competent-incompetent contact are equal. A_{D0} = the total area of incompetent rock minus the displaced area (A_0). $\Delta D = (D_f - D_0)$. Other variables explained in text.

Reproduced with permission of the copyright owner. Further reproduction prohibited without permission.

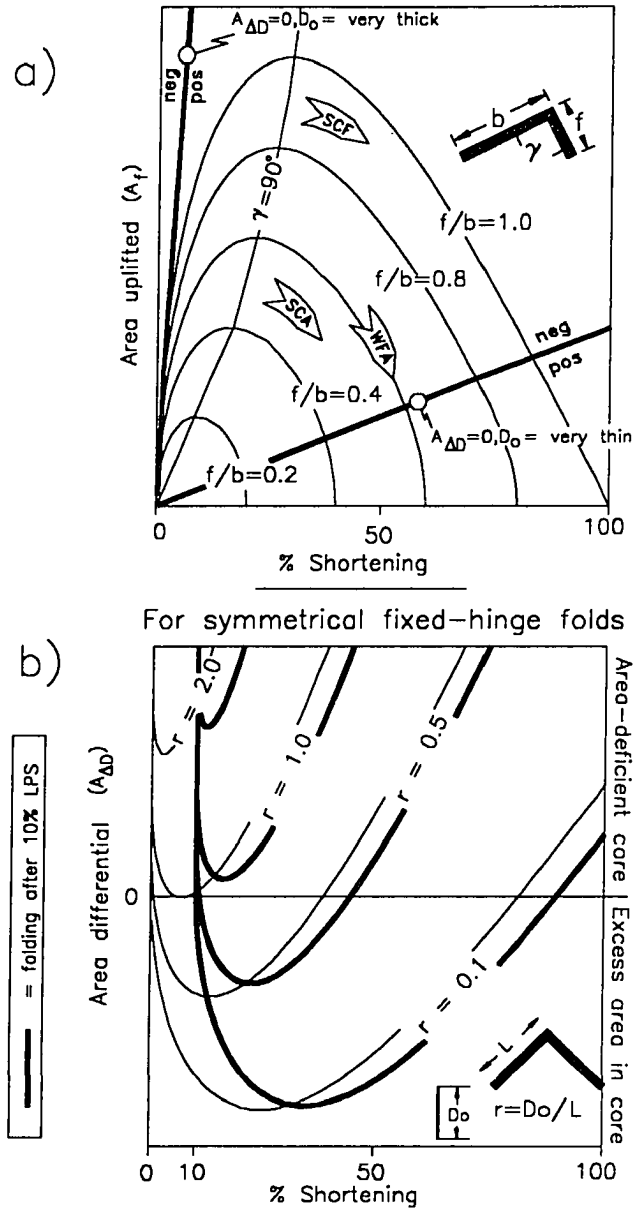

Figure 3.5. a) Graph of uplifted area (A_f) vs. percent shortening for folds with varying symmetry and constant total limb length. For a given asymmetry, maximum A_f occurs at γ = 90°, which is reached at low shortening for asymmetrical folds. The two thick lines are examples of paths required for constant-depth folds above either a thick or thin detachment. Three folds from this study are plotted on the graph. b) Graph of $A_{\Delta D}$ vs. shortening for symmetrical fixed-hinge folds of varying original depth : limb length ratios. A positive shift in $A_{\Delta D}$ values results in folds formed after 10% layer-parallel shortening. The folds plotted on graph (a) may be roughly compared to positions on graph (b) since the X-axes are the same, however, separate versions of graph (b) are required to accurately plot each fold. This is because graph (b) is only for a specific fold symmetry.

Reproduced with permission of the copyright owner. Further reproduction prohibited without permission.

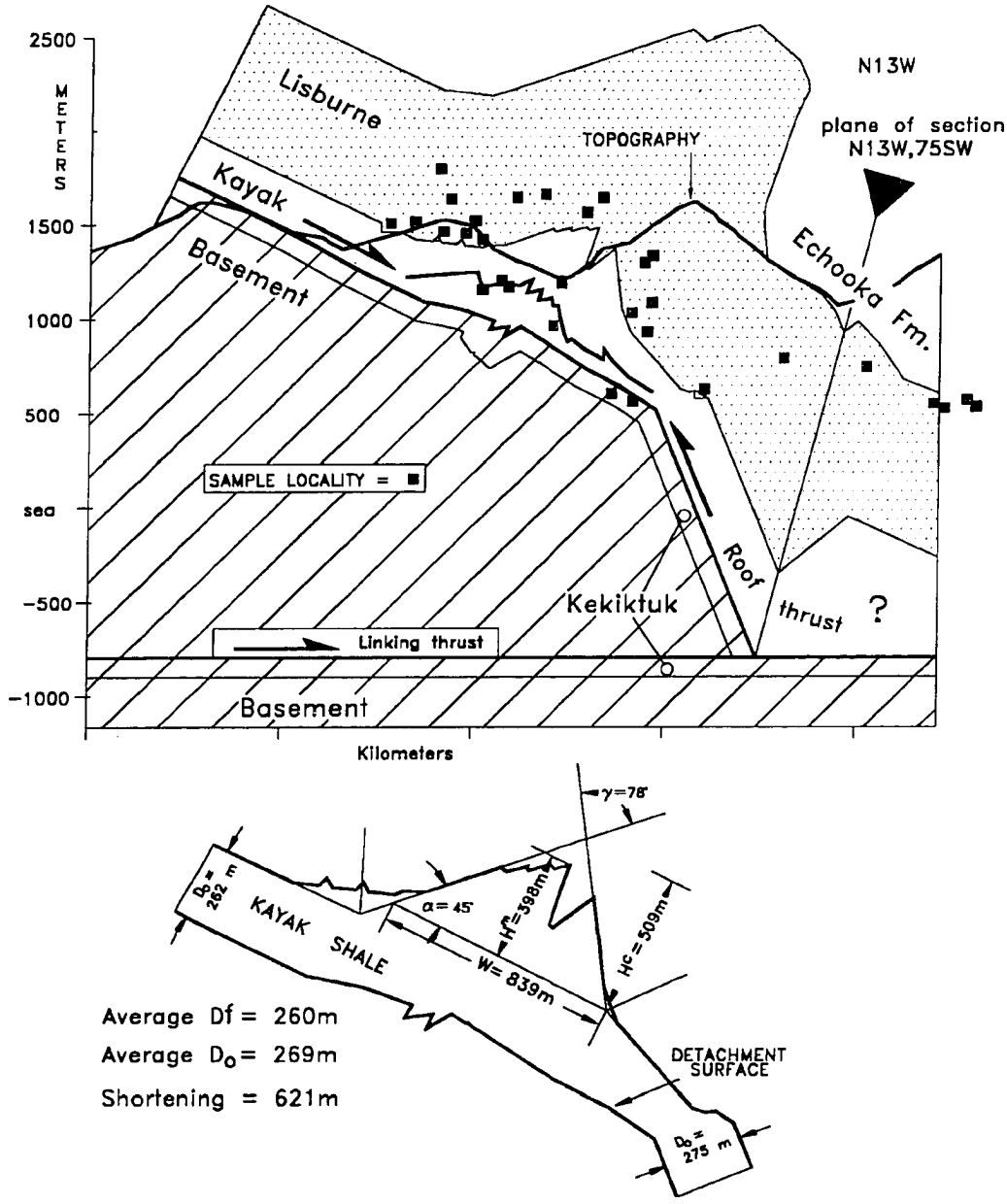

Figure 3.6. Balanced cross section through the Straight Creek fold showing strain sample localities and the geometry used to calculate the values in table 3.2.

Reproduced with permission of the copyright owner. Further reproduction prohibited without permission.

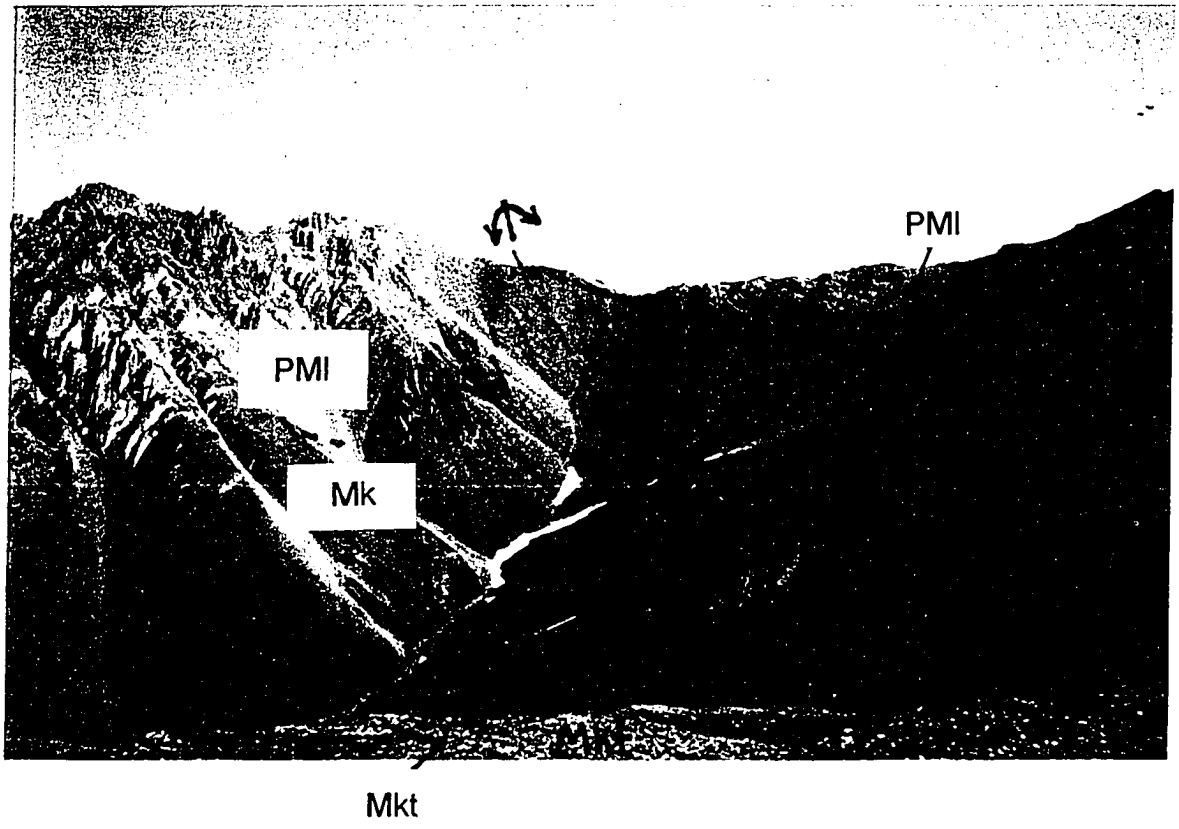

Figure 3.7. Northeastward view of the Straight Creek fold. Note parasitic folds in forelimb to left, eroded hinge in upper Lisburne Limestone, and disharmonic folds in Kayak Shale. Kekiktuk conglomerate in foreground is relatively planar and lies below a detachment in the lowest Kayak Shale. Mkt = Kekiktuk, Mk = Kayak, PMl = Lisburne. Distance across base of mountain is about 1 km.

Reproduced with permission of the copyright owner. Further reproduction prohibited without permission.

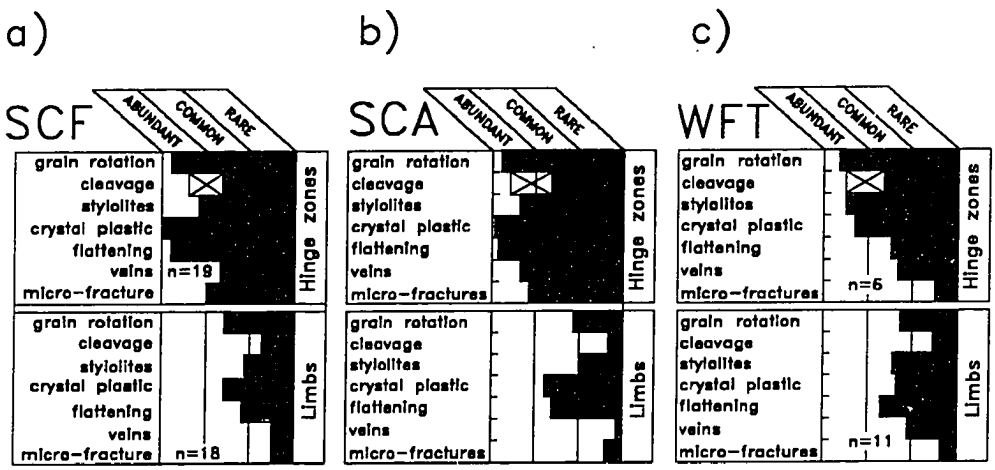

Figure 3.8. Histograms of strain samples from a) the SCA, b) the SCA, and b) the West Fork transect. See Appendix 1 for method. Boxes including an "X" represent the proportion of cleavage that is penetrative.

Reproduced with permission of the copyright owner. Further reproduction prohibited without permission.

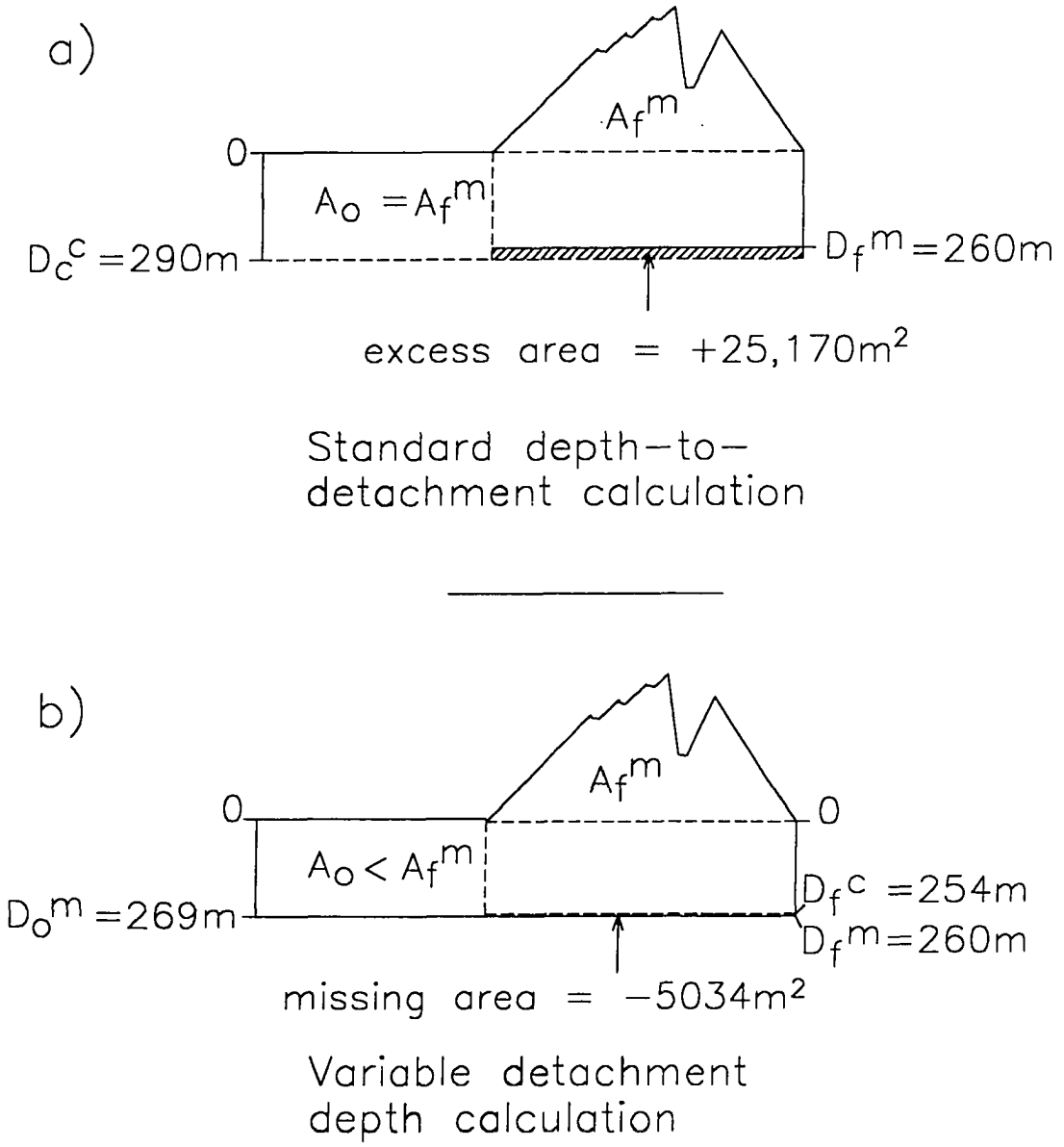

Figure 3.9. Diagram showing the difference between the standard depth-to-detachment technique and the variable detachment depth method as applied to the Straight Creek fold. a) The standard method, where a constant detachment depth (D_o^c) of 290 m is calculated from equation (3.3). This calculation results in a discrepancy of approximately 25,000 m² of excess incompetent material and a 30 m discrepancy between the calculated and measured depths. b) The variable detachment depth method with which a variable "instantaneous" detachment depth of 254 m is calculated from equation (3.6). This method results in a discrepancy of approximately 5000 m² of missing incompetent material and a 6m discrepancy between the calculated and measured depths. See text for more.

Reproduced with permission of the copyright owner. Further reproduction prohibited without permission.

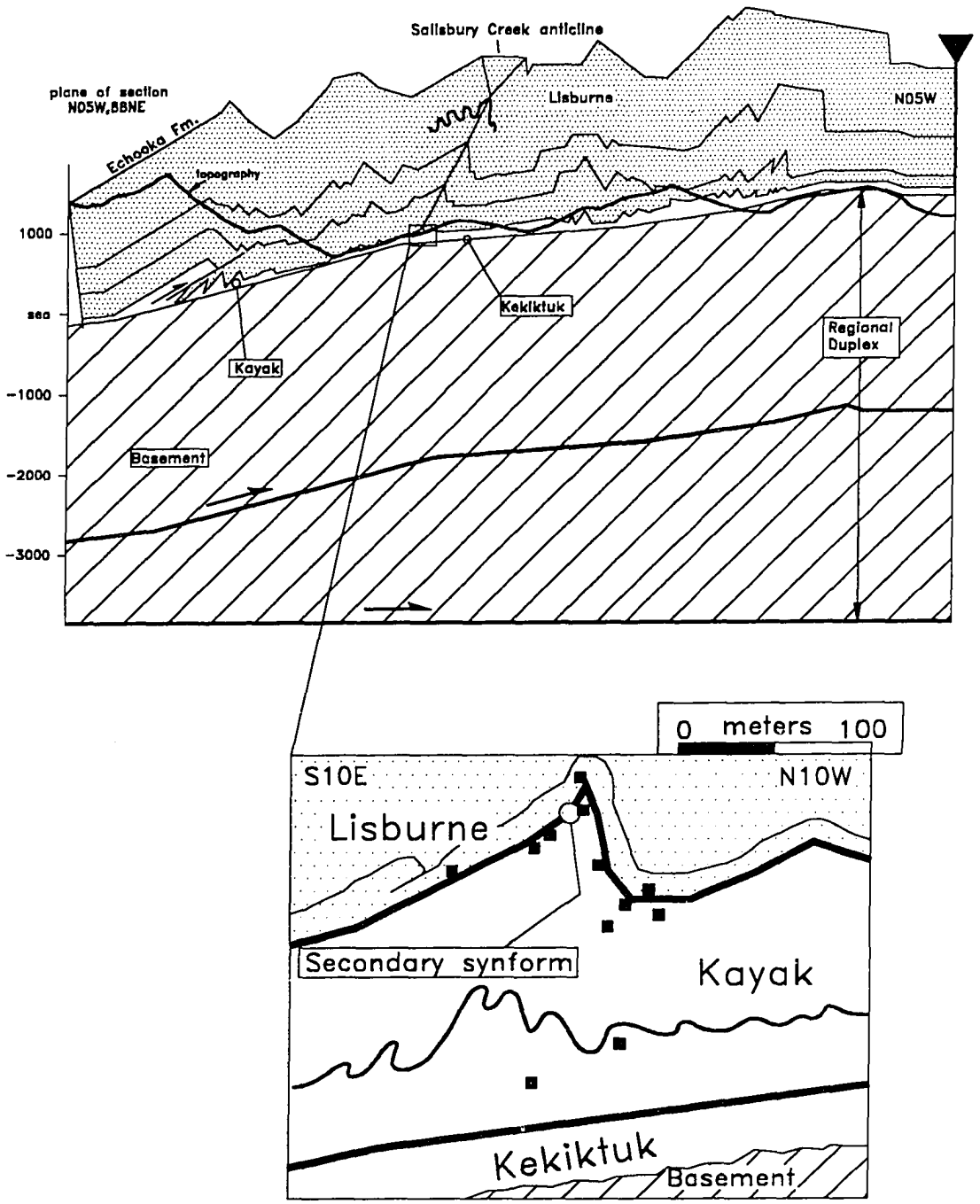

Figure 3.10. Balanced cross section of the Salisbury Creek transect showing Salisbury Creek anticline. See also plates A3.1 & A3.2.

Reproduced with permission of the copyright owner. Further reproduction prohibited without permission.

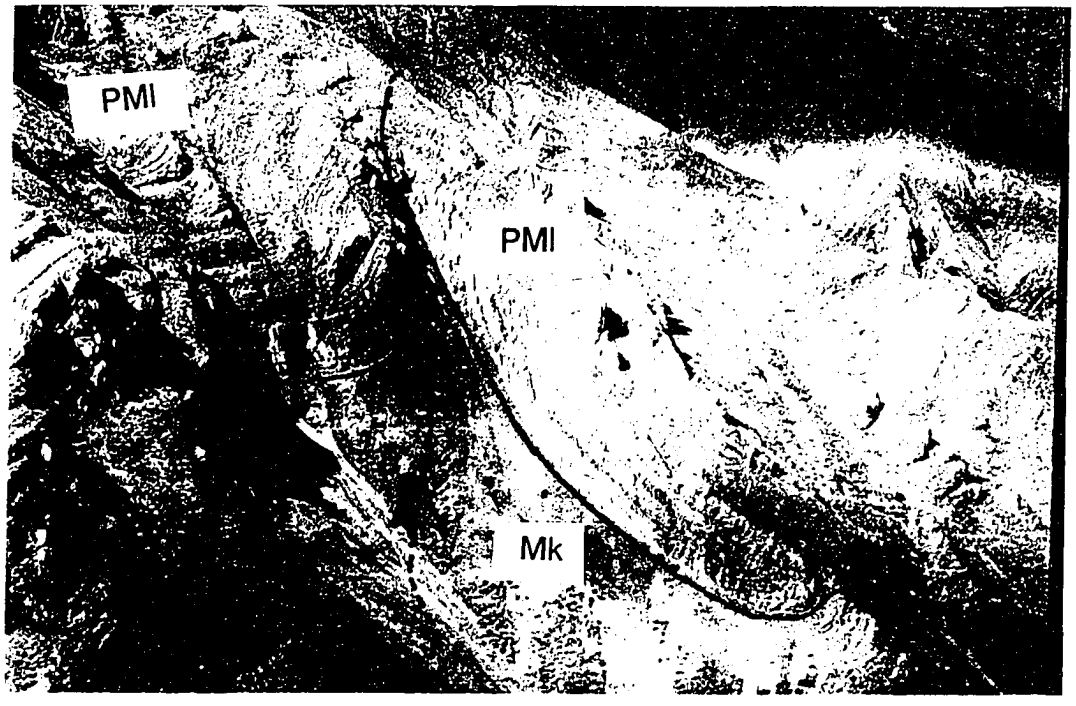

Figure 3.11. Photograph of the Salisbury Creek anticline at the Kayak-Lisburne contact. View is to the northwest, oblique to the fold axis. Horizontal distance across base of photograph is about 200 m. Note thrust fault in the lowest Lisburne on the backlimb. Mk = Kayak, PMl = Lisburne.

Reproduced with permission of the copyright owner. Further reproduction prohibited without permission.

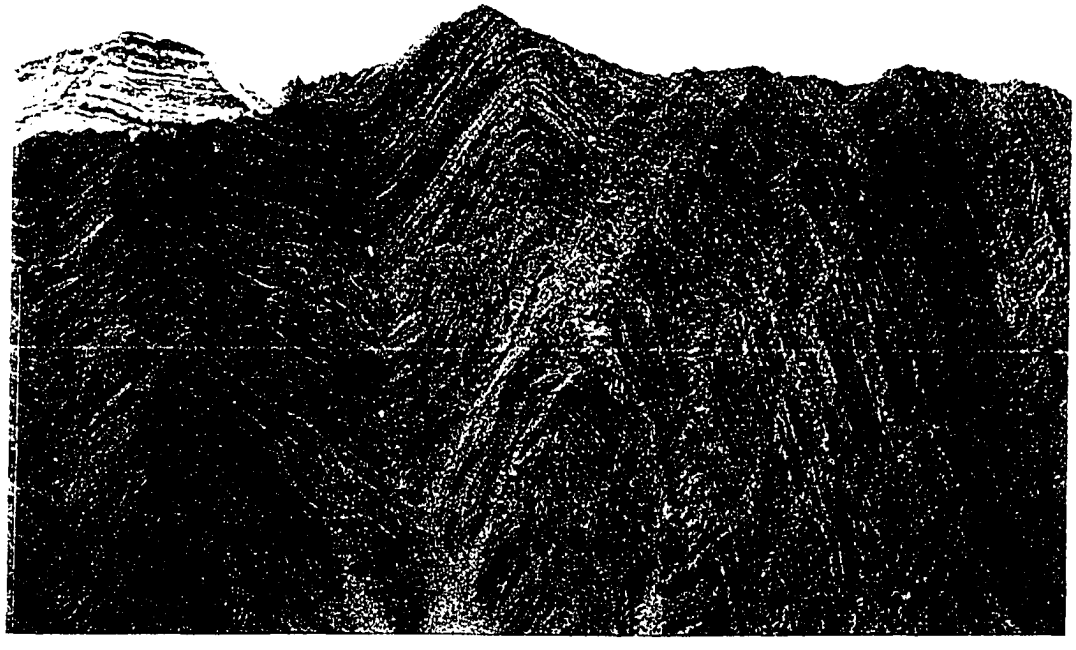

Figure 3.12. Photograph of the Salisbury Creek anticline (center) in the middle part of the Lisburne Limestone. Note parasitic folds on backlimb (to left). The flat crestal panel of the fold in the uppermost Lisburne is exposed on the mountain top in the background. View is to the west-northwest; horizontal distance across base of photo is about 250 m.

Reproduced with permission of the copyright owner. Further reproduction prohibited without permission.

Reproduced with permission of the copyright owner. Further reproduction prohibited without permission.

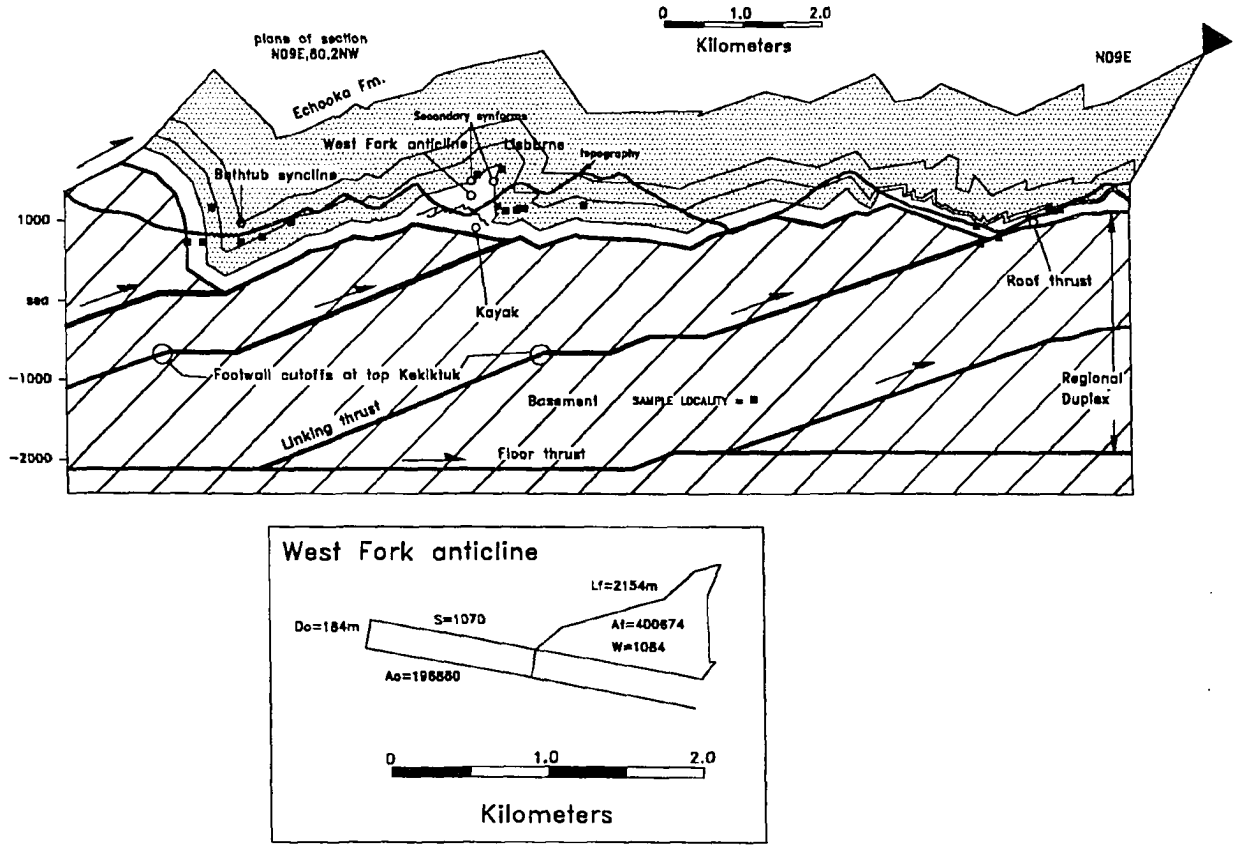

Figure 3.13. Balanced cross section of the West Fork transect showing strain sample localities and the geometry used to calculate values of table 3.2. See also plates A4.1 & A4.2.

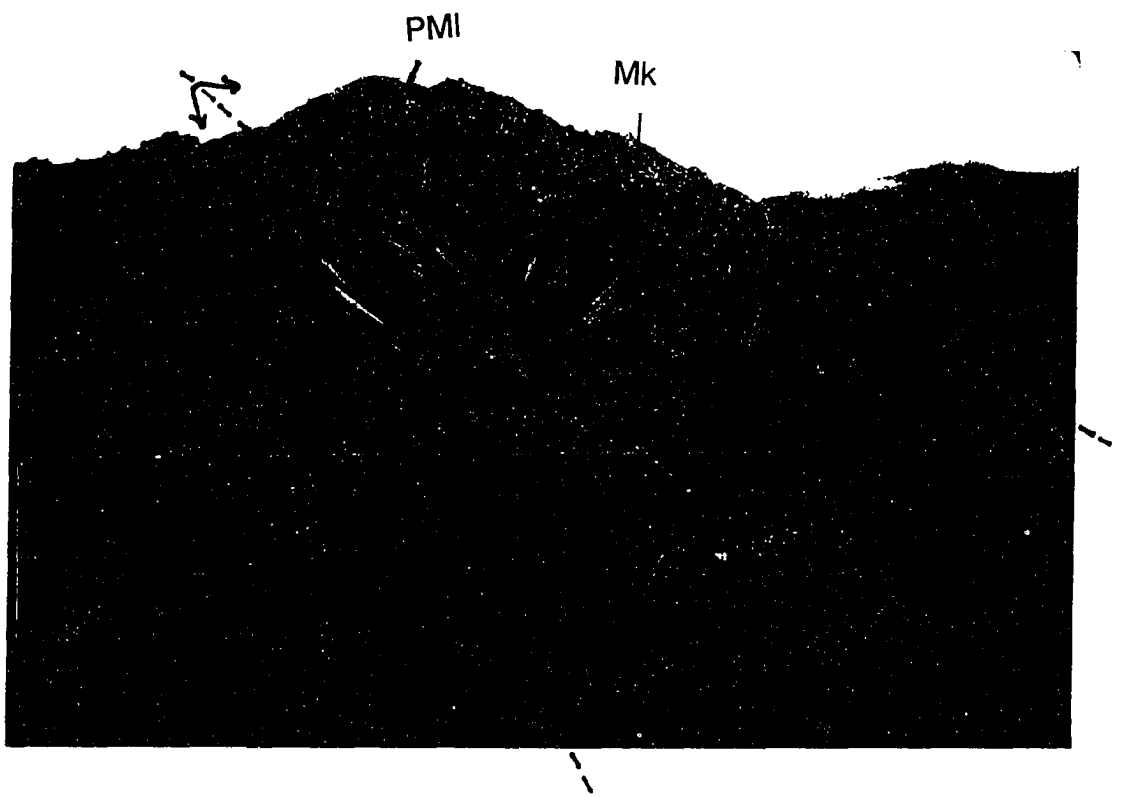

Figure 3.14. Photograph of the West Fork anticline as exposed along the Kayak-Lisburne contact. View is to the east-southeast; horizontal distance across the base of the photograph is about 200 m. Mk = Kayak, PMl = Lisburne.

Reproduced with permission of the copyright owner. Further reproduction prohibited without permission.

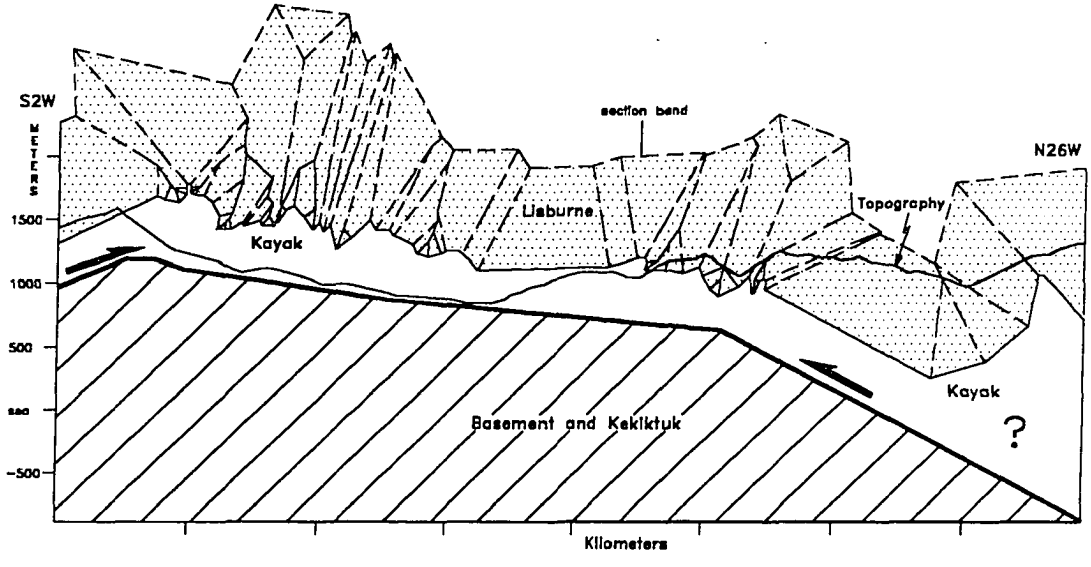

Figure 3.15. Cross section of the Marsh Fork transect. See also plate A3.3.

Reproduced with permission of the copyright owner. Further reproduction prohibited without permission.

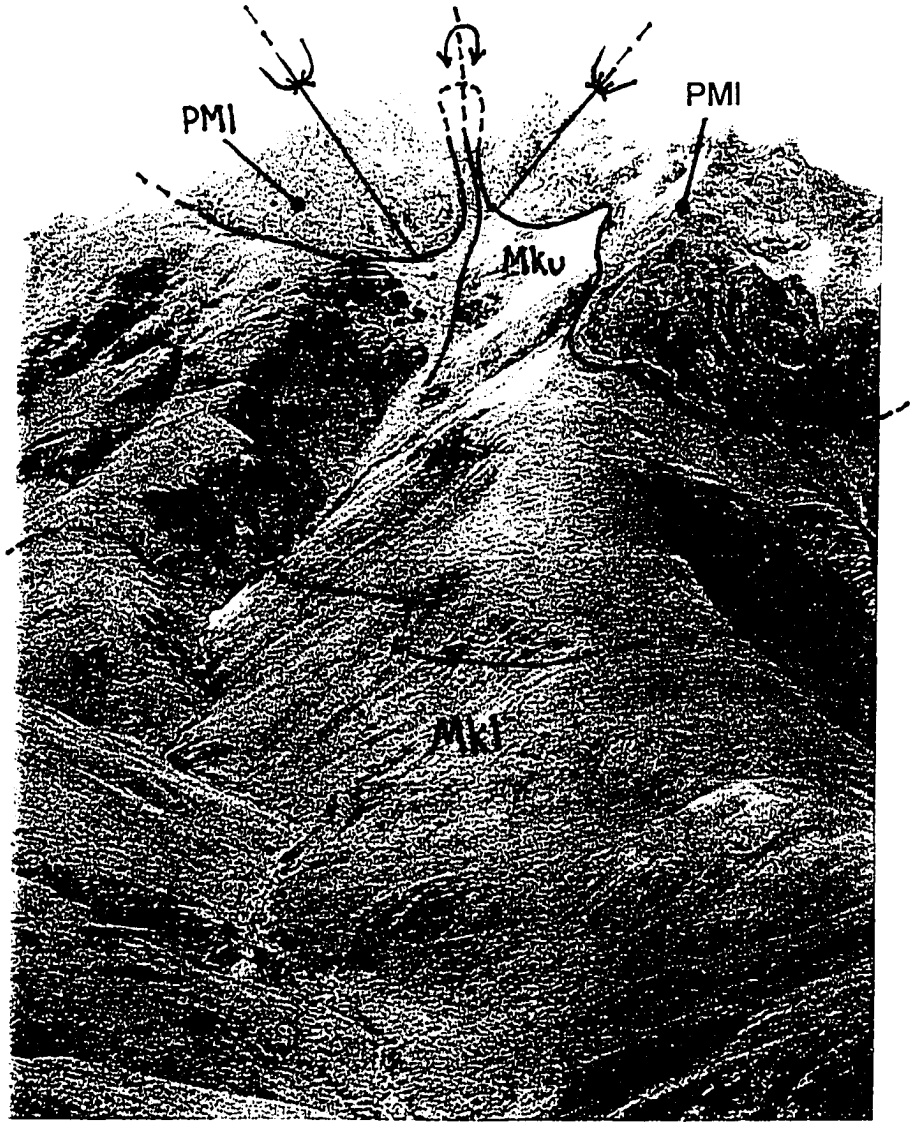

Figure 3.16. Photograph of close-to-isoclinal detachment fold exposed near the southern end of the Marsh Fork transect. View is to the southwest; horizontal distance across the base of the photograph is about 50 m. Mk = Kayak, PMl = Lisburne.

Reproduced with permission of the copyright owner. Further reproduction prohibited without permission.

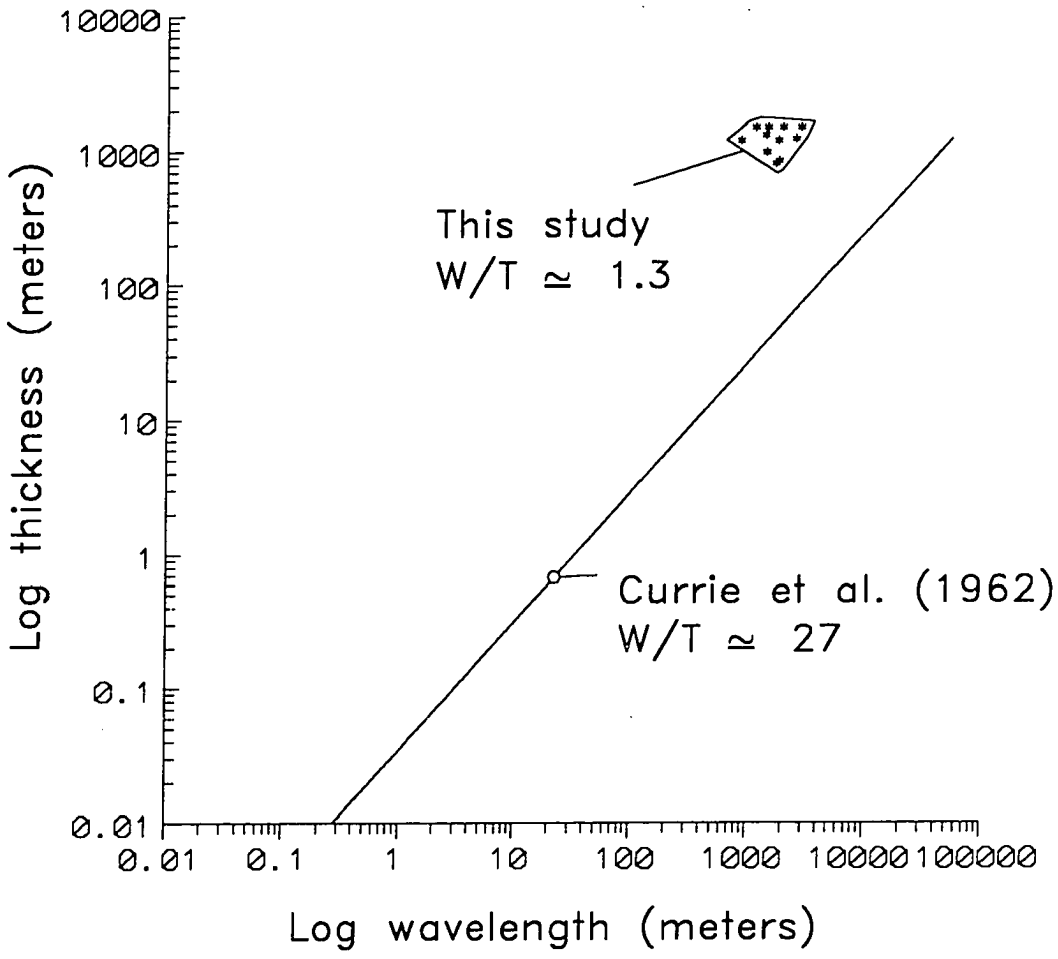

Figure 3.17. Logarithmic plot of wavelength (measured in the competent unit) to competent unit thickness for northeastern Brooks Range detachment folds (in the Lisburne) and the folds discussed by Currie (*et al.* 1962). The folds of this study have a very small wavelength-to-thickness ratio.

Reproduced with permission of the copyright owner. Further reproduction prohibited without permission.

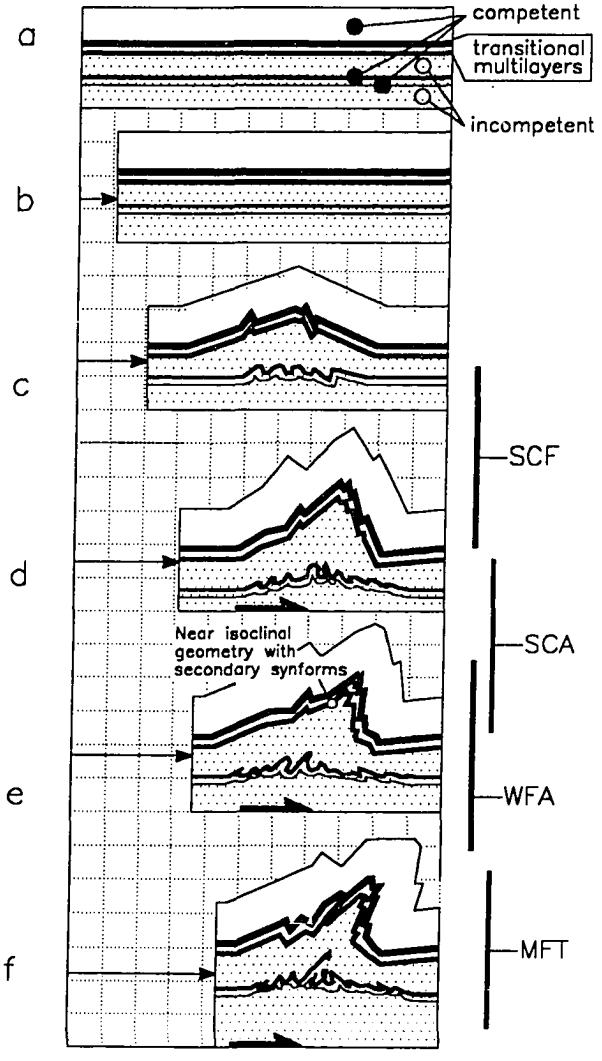

Figure 3.18. Schematic diagram of the evolution of a non-idealized detachment fold incorporating the predictions of the VDDM with features observed in the northeastern Brooks Range. Vertical bars represent the approximate developmental stage of the observed folds. Stage a) Original stratigraphic succession. b) Period of layer-parallel shortening. c) Early phase of fixed-hinge folding with negative $A_{\Delta D}$ ($D_0 > D_f$), parasitic fixed-hinge folds in transitional units, and disharmonic folds in isolated competent units. d) Intermediate phase of folding with $A_{\Delta D} = 0$ ($D_0 \cong D_f$). e) Later phase of folding with positive $A_{\Delta D}$ ($D_0 < D_f$), tightening of folds, especially at the competent-incompetent contact in the anticlinal hinge, and area loss due to solution cleavage in fold cores. f) Very evolved detachment fold with large positive $A_{\Delta D}$ and thrust faults in core and on backlimb.

Reproduced with permission of the copyright owner. Further reproduction prohibited without permission.

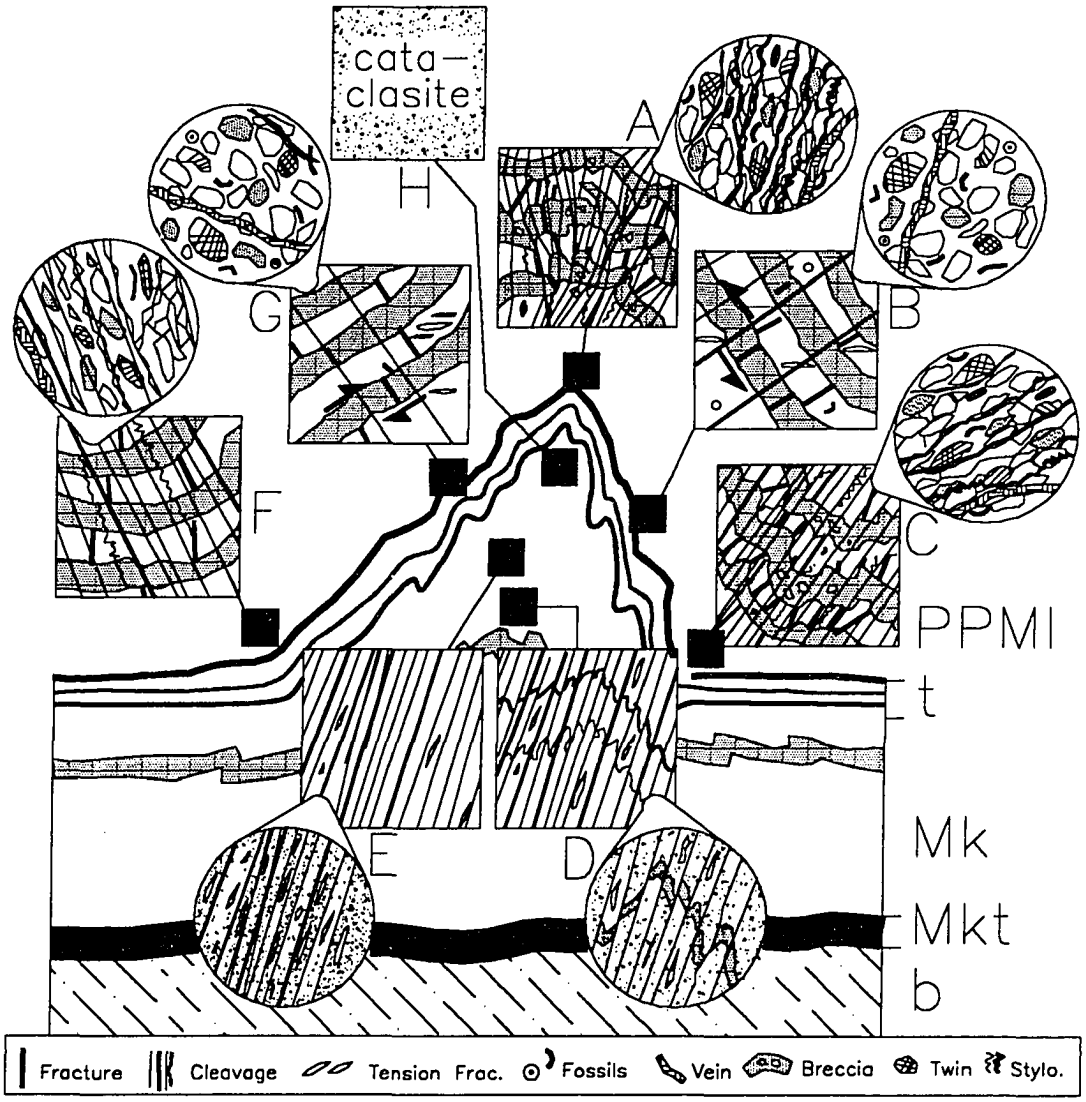

Figure 3.19. Schematic diagram of the distribution of strain indicators in a typical detachment fold in the northeastern Brooks Range. Boxes represent about a square meter of rock and circles represent thin sections. The diagram is simplified and the representation of various structures are intended to reflect their existence rather than their detailed characteristics. Note the high strain indicated by the abundance of structures in the competent hinges (areas A, C, & F), the solution cleavage and cataclasis in the incompetent core (areas D, E, & H) and contrast these areas to the relatively unstrained limbs (areas B & G). The abundance of veins in areas A & C is under-represented for clarity. Arrows in areas B and G represent bed-parallel shear zones. PPMI = Lisburne Limestone, t = mechanically transitional unit, Mk = Kayak Shale, Mkt = Kekiktuk Conglomerate, b = basement rocks.

Reproduced with permission of the copyright owner. Further reproduction prohibited without permission.

Table 3.1. Major structural-stratigraphic units, their structural layering, and the fold types observed in each unit. * - Undetermined thickness.

Structural-stratigraphic unit (structural position)	Thickness	Lithologic/structural layering	Primary fold structures
Sadlerochit (detached above folds)	*	Meter-thick beds of shale and siltstone near base, passing upward into 10s of meters of quartz sandstone in decimeter-thick beds. More calcareous to south, siliceous to north.	2nd order folds (wavelength ≅ 0.1 km) above a secondary detachment at the base of the Sadlerochit. Angular to curved.
Upper Lisburne (primary folded unit)	1200-1600m	Meter-thick massive grainstone beds up section, decimeter-thick laminated wackestone beds down section, beds commonly separated by centimeter-thick mudstone horizons and commonly include chert nodules.	1st order detachment folds (wavelength ≅ 1 km). Angular. Flexural slip along mudstone horizons.
Lowest Lisburne (transitional unit)	≅ 100m	Decimeter-to-meter-thick massive dolomitized wackestone and subordinate grainstone beds interbedded with up-to-meter-thick shale and mudstone. Thicker shales down section.	2nd order folds (wavelength ≅ 0.1 km). Angular and parasitic to 1st order folds. Flexural slip along shale and mudstone layers.
Kayak (detachment unit)	50 - 1000m	Shale up to 10s of meters thick, interbedded with thin siltstone, sandstone, and fossiliferous limestone horizons. Several ≅10-meter-thick units of decimeter-thick quartz sandstone beds within thicker shale units at SCA & SCF. Several ≅ 10-meter-thick units of decimeter-thick fossiliferous limestone beds within thicker shale units at WFA & MFT.	2nd and higher order folds (wavelength < 0.1 km). Disharmonic folds defined by 10-meter-thick competent units within shale. Angular to ptygmatic.
Kekiktuk + basement (sub-detachment unit)	» 1000m	Decimeter-to-meter-thick chert-pebble conglomerate and quartz sandstone beds (Kekiktuk). Heterogeneous, bedded-to-massive quartzite, phyllite, chert, metaconglomerate, and minor volcanic rocks (basement) .	≅ 15 km wavelength folds define anticlinoria marking horses in duplex.

Reproduced with permission of the copyright owner. Further reproduction prohibited without permission.

Table 3.2. Geometric variables associated with major observed detachment folds in the northeastern Brooks Range. D_0^m = measured undeformed thickness of detachment unit outside the fold (original detachment depth). D_f^m = measured depth to detachment beneath fold. H^m = measured fold height. W^m = measured distance between bounding synclines (wavelength). γ = interlimb angle. A_f^m = measured detailed fold area (including parasitic folds). S = shortening calculated using sinuous bed length. D_c = constant detachment depth calculated with conventional technique (*e.g.* equation 3.3). D_f^c = final depth beneath fold calculated with equation (3.5), assuming variable depth. $A_{\Delta D}$ = area differential of VDDM. $\Delta A_{const.\ D.}$ = area change using conventional technique. $\Delta A_{var.\ D.}$ = area change assuming variable depth. * The D_f^m value for the WFA is projected over 0.25 km in the plane of section and is not actually measured.

	Observed geometries							**Calculated depths and areas**				
								Constant depth		**Variable depth**		
	D_0^m	D_f^m	H^m	W^m	γ	A_f^m	S	D_c	$\Delta A_{const.\ D.}$	D_f^c	$A_{\Delta D}$	$\Delta A_{var.\ D.}$
SCF	269	260	398	839	78	179967	621	290	-12918	254	-12918	-5034
SCA	107	115	63	147	40-80	3809	65	59	3146	128	3146	1911
WFA	184	184*	738	1084	60	400674	1070	375	-203794	-4	-203794	-202708
unit	m	m	m	m	degs	m^2	m	m	m^2	m	m^2	m^2

Reproduced with permission of the copyright owner. Further reproduction prohibited without permission.

Table 3.3. Principal results of fold analyses on the folds of the northeastern Brooks Range. (*) The depth to detachment beneath the WFA and the displaced area of the WFA are uncertain, here D_0 is assumed to equal D_f. (**) The area-loss beneath folds of the MFT was not quantified.

Detachment fold	Detachment depth	Uplifted:displaced area
SCF	$D_f < D_o$	$A_f^m > A_o$; small net area gain
WFA*	$D_f = D_o$	$A_f^m > A_o$; large net area gain
SCA	$D_f > D_o$	$A_f^m < A_o$; small net area loss
MFT	$D_f > D_o$	$A_f^m < A_o$; large net area loss**

Reproduced with permission of the copyright owner. Further reproduction prohibited without permission.

CHAPTER 4- IMPLICATIONS

Aside from this study's significance for enhancing the understanding of detachment folding in general (Chapters 2 & 3), this study has significant implications for three separate topics. These topics are: 1) regional tectonics; 2) the structural interpretations in other fold-and-thrust belts; and 3) petroleum exploration and production, both in general and specifically beneath the coastal plain of the Arctic National Wildlife Refuge (Fig. 4.1).

IMPLICATIONS FOR REGIONAL TECTONICS

This research provides information about the tectonic evolution of the northeastern Brooks Range fold-and-thrust belt. The observations of this study support a passive-roof duplex model for the fold-and-thrust belt (Wallace & Hanks 1990), but one with a complex kinematic history.

Duplex model for the northeastern Brooks Range

Two end-member evolutionary models for the northeastern Brooks Range fold-and-thrust belt have been discussed by Wallace and Hanks (1990) (Fig. 4.2). The first model is of a forward-propagating duplex in which a floor thrust is inferred at depth in the basement rocks and there is a roof thrust in the Kayak Shale (Fig. 4.2a). This model has since been refined by Wallace (1993) and Hanks *et al.* (1994) and the western part of the fold-and-thrust belt may now be described as a passive-roof duplex with a complex uplift history (see next section). The second model (Fig. 4.2b) calls on thickening below the Kayak

Reproduced with permission of the copyright owner. Further reproduction prohibited without permission.

Shale by heterogeneous simple shear rather than duplexing (Oldow *et al.* 1987). The critical question for distinguishing between models is "How was shortening accommodated in the Mississippian Kekiktuk Conglomerate?", since this unit lacks the complex pre-Mississippian deformational history of the basement, but has deformed with the basement since Mississippian time (Oldow *et al.* 1987, Wallace & Hanks 1990). The first model requires kilometer-scale thrust duplication of the Kekiktuk whereas the second model requires either penetrative deformation across the sub-Mississippian unconformity and/or major detachment along or closely below the unconformity.

The Kekiktuk Conglomerate and sub-Mississippian unconformity were observed in all of the study areas (Fig. 4.3). The Kekiktuk was observed to be both folded at the meter-scale and thrust faulted with less than 10 m of displacement at one location within the Straight Creek area and at one location within the Marsh Fork Transect. At all other exposures observed in each area, the Kekiktuk Conglomerate is structurally fixed to the basement along a strictly depositional contact and in no place were penetrative structures observed to cut across the unconformity. These observations, and the obvious increase in local shortening from the Kekiktuk upward through the Lisburne Limestone, suggest that the shortening taken up by detachment folding in the Lisburne and Kayak was accommodated in the Kekiktuk and basement by kilometer-scale thrust duplication at depth. Hangingwall cutoffs or other conclusive indications of thrust duplication were not directly observed, but the preceding observations strongly support their existence. The geologic mapping and structural interpretation of both the Salisbury Creek and Marsh Fork transects confirm and

Reproduced with permission of the copyright owner. Further reproduction prohibited without permission.

further constrain the textbook-like fault-bend fold geometry of the form surface of the Kekiktuk that is shown on the cross section of Wallace (1993). Thus, the duplex model (Fig. 4.2a) for the evolution of the northeastern Brooks Range is strongly supported by this study.

Passive-roof duplex along the Canning River

Together, the studies of Wallace and Hanks (1990), Wallace (1993), Ziegler (1989), and this study (Appendices 2, 3, 4 & 5) document the general structural geometry in different structural positions in the western part of the fold-and-thrust belt. Based on this documentation, this section is a synopsis of the general structural style in the areas studied near the Canning River and Marsh Fork (Fig. 4.1) and its tectonic implications.

This area is interpreted as a passive-roof duplex (*e.g.* Banks & Warburton 1986) with a complex kinematic history (Hanks *et al.* 1994) (Figs. 4.1 & 4.4). This *passive-roof* interpretation is based on the following argument (Wallace 1993): The Mississippian Kayak Shale is depositionally absent in the Sadlerochit Mountains to the north of this study area. Where the Kayak is absent, there is no indication of significant relative structural displacement of the basement rocks (duplex horses) with respect to the Lisburne Limestone (roof sequence), as there is where the Kayak is present. Thus, a definitive structural "pin" for the roof thrust is exposed at the forward end of the duplex. This requires that roof-sequence shortening south of the pin be taken up with a backthrust sense of displacement relative to underlying horses, which is supported by restoration of a regional balanced cross section (Wallace 1993). The most recent passive-roof interpretation for the northeastern Brooks Range

Reproduced with permission of the copyright owner. Further reproduction prohibited without permission.

incorporates apatite fission-track data which suggest a complex Cenozoic uplift and unroofing history involving forward propagation followed by hindward backstepping (Hanks *et al.* 1994).

The following observations enable refinement of the passive-roof interpretation for the northeastern Brooks Range:

- In the Canning River-Marsh Fork area, the observed fold asymmetry suggests that deformation was generally north-vergent above the long, gently dipping backlimbs of fault-bend folded horses in the Franklin Mountains, south-vergent above the shorter, steeper forelimbs, and upright above the short crests (Appendix 3) (Fig. 4.5).
- Ziegler (1989) showed evidence for both strongly north-vergent fold asymmetries above the steep forelimb of the southern Franklin Mountains horse and kilometer-scale northward thrust displacements in the cover between the horses.
- Along-strike to the west of Ziegler's (1989) study area at the "Hulahula inlier" (Fig. 4.1, Appendix 5), north-directed thrusts similar to those observed by Ziegler (1989) are exposed in the same structural position with respect to the duplex geometry.
- To the north, the Straight Creek fold lies above the relatively steep forelimb of the northern Franklin Mountains horse and has an upright geometry with respect to the detachment (Chapter 3, Appendix 2)
- Folds north of the Straight Creek fold are also upright but are much tighter in the syncline between the northern Franklin Mountains and Fourth Range

Reproduced with permission of the copyright owner. Further reproduction prohibited without permission.

horses than they are to the north in the Third Range and Shublik Mountains (Fig. 4.4).

- To the south of the Franklin Mountains horses, strongly north-directed folds and thrusts dominate the roof sequence (Wallace 1993).

Taken together, the above information suggests that in the Canning River-Marsh Fork area, roof-sequence shortening was truly passive (*i.e.* the sense of displacement, represented by fold asymmetry, had a significant south-directed component) only in certain structural positions. These include positions above the higher parts of the forelimbs and crests of the Franklin Mountains horses and above horses farther north (Plates A2.2 & A2.4, Fig. 4.5). Fold asymmetry and north-directed thrust faulting indicates that roof deformation was forward-directed, or "active" above both the backlimbs and directly in front of forward-bulldozing fault-bended fold horses (or in the synclinoria) (Appendix 3, Fig. 4.5).

Figure 4.5 shows a model for the structural evolution of the Franklin Mountains area. Since the complex kinematics, together with a general paucity of data on relative timing, preclude construction of accurate sequential balanced models, figure 4.5 is very schematic. Stage 1 shows an undeformed sequence with incipient faults in the basement shown. Emplacement and uplift of the southern Franklin Mountains horse begins in stage 2, with the single horse bounded by a roof thrust in the Kayak Shale and a floor thrust at depth in the basement. The horse deforms with fault-bend fold kinematics (Suppe 1983) and this shortening is accommodated in the roof by fixed-hinge detachment folding. The original position of these folds with respect to the migrating hinges of the

Reproduced with permission of the copyright owner. Further reproduction prohibited without permission.

fault-bend fold is uncertain. North-vergent folding in the roof over the backlimb could be an extension of earlier north-directed thrusting that occurred south of the southern Franklin Mountains horse (Wallace 1993).

As deformation progressed (Fig. 4.5 - stage 3), the detachment folds above the backlimb of the horse developed a north-vergent asymmetry, the folds on the forelimb developed a slight south-vergent asymmetry, and those above the crestal panel were generally upright and symmetrical. This geometry may be explained by "passive roof" (Banks & Warburton 1986) deformation in the forelimb and "active roof" deformation in the backlimb. The north-vergent folding on the backlimb may be the result of either "bulldozing" from the south (as above) and/or it may be an upsection continuation of the north-over-south flexural slip folding involved in the emplacement of the horse. Fold geometry in the crestal panel may represent a continuation of either the active- or passive-roof deformation, or it may describe the spatial intersection of the two.

Apatite-fission track data suggest that the southern Franklin Mountains anticlinorium began to form before the northern Franklin Mountains anticlinorium (Hanks *et al.* 1994). It is likely, however, that displacement of the southern horse continued after displacement of the northern horse began (Wallace, oral comm. 1993) (Fig. 4.5 - stage 3). At this stage, the southern Franklin Mountains horse had reached its full amplitude but forward displacement continued, allowing the roof sequence to be bulldozed northward ahead of the forelimb as south-directed "passive" displacement continued above the forelimb.

In stage 4, deformation associated with the emplacement of both horses overlapped in the intervening syncline. Further northward translation of the

Reproduced with permission of the copyright owner. Further reproduction prohibited without permission.

southern horse caused extreme thickening and northward asymmetry in the roof above its leading edge and contributed to north-directed shear along the backlimb of the northern horse. Northward asymmetry above the forelimb of the southern horse may be related to the north-directed duplexing that Ziegler (1989) described there. The northern Franklin Mountains horse developed like the southern horse, with fold geometry reflecting passive-roof deformation in the forelimb and north-directed shear related to bulldozing and/or fault-bend-folding in the backlimb.

Summary of regional implications

This study generally agrees with the complex passive-roof duplex interpretation for the Canning River-Marsh Fork area of Hanks *et al.* (1994). However, the distribution of detachment fold geometries described above suggests that in addition to the regional north-south transition from upright detachment folds to strongly forward-directed folds and faults described by Wallace (1993), local transitions of similar nature occur in front of each of the Franklin Mountains horses. Thus, although the passive-roof duplex model works for the northern part of the Canning River-Marsh Fork area in the proposed scenario, to the south of the Fourth Range the folds above *each horse* indicate a combination of active (forward-directed bulldozing) and passive (hindward-directed folding) tectonics (Fig. 4.5). This interpretation does not alter the overall geometry or total shortening in Wallace's (1993) cross section, but rather it fills some gaps in the section and suggests revisions to the kinematic details of its interpretation.

Reproduced with permission of the copyright owner. Further reproduction prohibited without permission.

IMPLICATIONS FOR OTHER FOLD-AND-THRUST BELTS

Applicability of the variable detachment depth model

Detailed descriptions of detachment fold evolution are generally sparse in the scientific literature. However, there is enough published information to suggest that the general geometry and kinematics of the folds described in this study are seen in other fold-and-thrust belts, even where they involve different competent and incompetent rock types (see below). For geometric and kinematic analyses of detachment folds, the variable detachment depth model contains fewer assumptions than any other model that I am aware of. Thus, if other models have been successfully applied to an area, it should be possible to successfully apply the variable detachment depth model to the same area, perhaps with more accurate results.

Potential analogs in other fold-and-thrust belts

The detachment folds in the northeastern Brooks Range are defined by Paleozoic carbonates and shale. It is significant to consider the age, rock-type, and structural setting of potential analogs to these folds in other fold-and-thrust belts. In each of the areas mentioned below, competency contrasts are more significant than the actual rock types for controlling fold geometry.

Good analogs in older rocks

Well-studied examples of detachment folds involving other well-indurated rock types of at least Tertiary age include: the Appalachian Plateau folds, which are defined by sandstones and cored by salt (Wiltschko & Chapple 1977); and

Reproduced with permission of the copyright owner. Further reproduction prohibited without permission.

the folds of both the Jura and Zagros Mountains, which are defined by carbonate and clastic rocks and cored by salt (*e.g.* Laubscher 1962, Mitra & Namson 1989). In these cases, the geometries are such that "first order" geometric and kinematic analyses (*i.e.* area change and detachment depth analyses) are possible using geometric-kinematic models because the competent unit controls the fold geometry and the incompetent unit "flows" into/out of anticlinal cores (*e.g.* Wiltschko & Chappie 1977). This scenario is very similar to that in the northeastern Brooks Range.

In the folds of the Pyrenees, which involve Cretaceous and Tertiary carbonates and salt, fixed-hinge kinematics have been suggested based on syn-depositional growth fold patterns (Hardy & Poblet 1994) and paleomagnetic analysis (Holl & Anastasio 1993). Although I am unaware of published detailed geometric and kinematic analyses (using fold models) of Pyrenean detachment folds, they have similarities to those in the northeastern Brooks Range.

However, salt diapirism, where the incompetent unit controls the fold geometry, is also common in older rocks (*e.g.* northern Germany (Trusheim 1960), East Texas (Seni & Jackson 1983)). Salt tectonics may invalidate constant area assumptions incorporated in geometric models. Therefore, if salt diapirism is suspected as a significant driving force for folding, then geometric and kinematic models for fault-related folds may be of little use and alternate models should be explored.

Thus, published work suggests that at least for first order analyses in fold-and-thrust belts involving Tertiary and older rocks, where salt diapirism is not active, the competency contrasts are more significant than the actual rock types

Reproduced with permission of the copyright owner. Further reproduction prohibited without permission.

for controlling fold geometry. Geometric and kinematic analysis using the variable detachment depth model may be applied to detachment folds that do not involve diapiric salts.

Poor analogs in recent sediments

In contrast, very young, actively dewatering sediments (including incipient competent sandstones) undergoing compression may not follow the constant area assumptions of the variable detachment depth model, and perhaps more importantly, overpressured diapiric salts may flow to lower-pressure regimes without tectonic shortening. Such situations would lead to significant departures from the assumptions of geometric models where the shortening represented in the competent unit is used as a baseline for calculations of area in the incompetent unit. Dewatering and diapirism may be expected in active toe-of-slope contractional zones, like those in the deep-water Gulf of Mexico petroleum province or in active accretionary wedge fold-and-thrust systems, such as the Andean or Aleutian accretionary complexes. Thus, in active toe-of-slope contractional zones or accretionary wedges, constant area geometric and kinematic modeling may be useful only for estimating not be applicable.

Detachment depth

The question of whether detachment folds form with fixed or variable detachment depths (Fig. 4.6) is very fundamental and has implications for the interpretations of detachment folds in other fold-and-thrust belts. Some detachment fold geometries that are possible to generate with a variable detachment depth are geometrically impossible to generate if constant depth is

Reproduced with permission of the copyright owner. Further reproduction prohibited without permission.

assumed. I have shown that assumption to be invalid for the folds observed here (Chapters 2 & 3). Thus, some workers may discard a correct *geometric interpretation* if they make an invalid assumption of constant detachment depth.

The assumption of constant detachment depth has a direct bearing on the question of fold kinematics. A fold that forms above a constant detachment depth requires a migrating hinge mechanism. However, a fold that forms above a variable detachment depth does not require hinge migration. Thus, *kinematic interpretations* in other fold-and-thrust belts are directly affected by whether constant or variable detachment depth is assumed.

Fixed or migrating hinges?

The question of whether detachment folds form with fixed or migrating hinges (Fig. 4.7) is also very fundamental. It clearly has implications for the interpretation of detachment folds in other fold-and-thrust belts. In order to trace the *kinematic path* of any fold accurately, the *kinematic mechanism* must be understood. This section outlines the basic evidence for both fixed- and migrating-hinge detachment fold kinematics.

Although evidence of hinge-migration in kink bands and finely laminated rocks is well documented (*e.g.* Weiss 1968, Stewart & Alvarez 1991), there is much more published geologic evidence for fixed-hinge *detachment fold* kinematics than for migrating-hinge kinematics. Some often-cited studies *imply* or *assume* that detachment folds form with migrating hinges (*e.g.* Laubscher (1962), Dahlstrom (1990), Jamison (1987), Mitra & Namson (1989), Butler (1992)). However, I have not any seen published, conclusive evidence

Reproduced with permission of the copyright owner. Further reproduction prohibited without permission.

supporting hinge-migration in studies of either artificial or natural detachment folds.

One geologic relationship that seems essential in order to verify the migration of a hinge through a layer of competent rock (Fig. 4.7*b*) is *limb-type* structures overprinting hinge-type structures (as described in Chapter 1). An example of such a progression in deformation phases (as recorded by syntectonic pressure shadows and cleavage fanning) has been provided by Beutner *et al.* (1988) for fault-bend folds. However, fault-bend folds are kinematically very different than detachment folds and the rationale for hinge-migration in fault-bend folds is clear: rock layers are transported over a bend in a fault. Hinge-migration is not so self-evident in detachment folding, thus strong geologic evidence is needed for its verification.

Conversely, many studies explicitly provide geologic evidence of, and/or strong theoretical support for, fixed-hinge kinematics or limb-rotation. These data include:

- the theoretical predictions and geological observations of de Sitter (1956), Biot (1961), Currie *et al.* (1962), Ramsay (1967, 1974), Johnson (1977), Mancktelow and Abassi (1992) and many others, which support fixed-hinge buckling and limb-rotation in outcrop scale folds.
- the physical models of Dixon and Tirrul (1991) and Dixon and Liu (1992) which document a fixed-hinge buckling mechanism for artificial detachment folds.

Reproduced with permission of the copyright owner. Further reproduction prohibited without permission.

- the strain observations of Fischer *et al.* (1992), which support fixed-hinge buckling for a natural detachment fold in the Rocky Mountain fold-and-thrust belt (Montana).
- the strain observations of Thompson (1989), which document a lack of overprinting structures in the limbs of natural detachment folds in the Rocky Mountain fold-and-thrust belt (British Columbia).
- the strain observations of Rowan and Kligfield (1992), which indicate fixed hinges in Alpine detachment folds.
- the paleomagnetic study of Holl and Anastasio (1993), which indicates that a detachment fold in the Pyrenees formed by limb-rotation.
- the stratigraphic studies of Poblet and Hardy (1994) and Vergis *et al.* (in review), which support limb-rotation in Pyrenean detachment folds.

Other studies that imply or assume fixed-hinge buckling for detachment folds include: Wiltschko & Chapple (1977), Mitchell & Woodward (1988), and many other early fold studies (see Willis & Willis 1934). In this study, the specific evidence from northeastern Brooks Range detachment folds which supports fixed-hinge kinematics are shown schematically in figure 4.8. The evidence includes:

- a lack of limb-type structures overprinting hinge-type structures
- the dramatic increase in the abundance of strain indicators and the intensity of strain from limbs to hinges (and the preferential erosion of all anticlinal hinges)

Reproduced with permission of the copyright owner. Further reproduction prohibited without permission.

- the exposure of parasitic folds near the competent-incompetent contact with opposite asymmetry beneath each fold limb (these are difficult to account for with migrating hinge kinematics)

Fixed-hinge kinematics for northeastern Brooks Range folds is further supported by the general agreement of fold geometries and the predictions of the variable detachment depth model for fixed-hinge detachment folds (Chapter 3). There is, however, a discrepancy between another buckle-fold model and the observed fold geometries: According to the model of Currie (*et al.* 1962), the ratio fold wavelength-to-competent unit thickness should be about 27. In contrast, the observed ratio is much smaller in the northeastern Brooks Range (~ 1.0) (Fig. 4.9). However, this could be easily explained by the lack of a great thickness of incompetent rock below *and above* the folds observed in the Brooks Range since this represents a major difference from the model assumptions of Currie (*et al.* 1962) (Chapter 3). Nonetheless, this study suggests that folds can form by fixed-hinge buckling even where a great thickness of incompetent rock is not present and the wavelength-to-thickness ratio is very small.

In conclusion, I believe that many detachment folds form with fixed hinges and above a detachment unit that varies in thickness during deformation. Thus, the fixed-hinge, variable detachment depth geometric-kinematic development described here for the detachment folds in the northeastern Brooks Range may be used as an analogy for many other fold-and-thrust belts.

Reproduced with permission of the copyright owner. Further reproduction prohibited without permission.

The significance of lithologic stratigraphy

As mentioned in chapter 3, in the northeastern Brooks Range, the boundary between the detachment shale and the competent limestone is commonly sedimentologically (LePain 1993) and mechanically gradational (Fig. 4.3). This stratigraphy results in an upward gradation in structural style from penetrative, "ductile" deformation in the lowest, finest-grained rocks, to fixed arc-length flexural-slip parasitic folding in the transitional strata, to longer-wavelength fixed arc-length flexural-slip folding in the upper part of the competent unit. Such gradations in structural style are probably common in detachment folds in other fold-and-thrust belts involving shale since lateral facies changes that lead to vertical stratigraphic gradations are common in terrigenous clastic and carbonate rocks typical of fold-and-thrust belts. Thus, similar stratigraphically controlled gradations in fold geometry and kinematics are to be expected in detachment folds involving shale as the incompetent unit and should be accounted for in geometric-kinematic interpretations.

BEARING ON PETROLEUM GEOLOGY

This study is significant for constraining the geometry of anticlinal petroleum traps known to be detachment folds or traps for which insufficient data exist to determine whether or not they are detachment folds. It is less relevant to folds involving only competent rocks, except to emphasize that models appropriate to folds in competent rocks are commonly misapplied to detachment folds. Some general comments about a single hypothetical illustration of variation among reservoirs in different fold-types are presented here.

Reproduced with permission of the copyright owner. Further reproduction prohibited without permission.

Bearing on interpretations of trap geometry

Figure 4.10a is a hypothetical seismic reflection line suggesting the presence of an anticline. Based on the seismic data alone, the structure may be interpreted as either a fault-bend fold (FBF) (Fig. 4.10b), a fault-propagation fold (FPF) (Fig. 4.10c), or a detachment fold (Figs. 4.10d & 4.10e). Since incompetent rock is very common in many oil-bearing stratigraphic successions, and since incompetent units commonly underlie folds, it is certainly possible that the fold depicted on the seismic line of figure 4.10a is a detachment fold. The detachment fold interpretation is intrinsically more variable than either the FBF or the FPF interpretation. Since the detachment depth can vary during folding, the depth of a sub-detachment reservoir is more difficult to define in a detachment fold. This is especially true when the undeformed thickness of the incompetent unit is unknown. Also, the detailed geometry of the fold may involve disharmonic or parasitic folds that will affect the interpreted shortening and hence the interpreted geometry. The detachment folds in the northeastern Brooks Range consistently show evidence of long-term fluid flow in their incompetent cores (Chapter 3). This may allow for post-folding source-to-reservoir migration (Fig. 4.10d). Alternatively, incompetent rock is generally of very low permeability and may tend to define impermeable structural highs that may be barriers to short-term fluid flow and are devoid of recoverable resources. Thus, overpressured fluid may migrate down-structure, around the incompetent core and along the limbs of a detachment fold (Fig. 4.10e). Further, high strain in the hinge of the competent unit may either enhance or hamper flow there. If the reservoir is determined to be a thrust-truncated detachment fold, then the

Reproduced with permission of the copyright owner. Further reproduction prohibited without permission.

likelihood of an effective footwall trap is high since thrusts involving large amounts of shale are typically impermeable (Fig. 4.10e).

If the seismic line is supplemented with data indicating that no incompetent rocks are present, then the detachment fold model may be discarded and a FBF or FPF model may be more appropriate. The seismic data alone provide good constraints on the ramp geometry and detachment depth for the FBF and FPF models. The distribution of fluid will vary depending on whether the fold is a FBF or a FPF and these structures may involve footwall traps and/or along-fault or across-fault permeability (Figs. 4.10b & 4.10.c). However, if shale or salt, for example, is believed to stratigraphically underlie the folded unit, or if the rock types are unknown, then the fold involving the reservoir may be a detachment fold and a detachment fold model could be used.

Bearing of trap geometry on enhanced oil recovery methods

The fold geometry (*i.e.* FBF, FPF, or detachment fold) will also influence secondary and tertiary recovery methods. If a waterflood is planned for the folded reservoir, it would necessarily be very different for a FBF or FPF than for a detachment fold. Since good vertical pressure communication between the competent and incompetent rocks in a detachment fold is unlikely, water injection into the incompetent unit may be difficult and unproductive (Fig. 4.10d). The permeability barrier between units in a detachment fold may allow a high pressure waterflood within the competent reservoir unit, which may be a thin conduit in pressure isolation. Such good pressure support may not be as easily attainable in either a FBF or FPF because lesser permeability contrasts and

Reproduced with permission of the copyright owner. Further reproduction prohibited without permission.

better communication among units in those folds (perhaps resulting, in part, from hinge-migration) represents a larger conduit to pressurize (Figs. 4.10b & 4.10c).

In summary, selection of the correct fold model may be relatively simple depending upon how much is known about the stratigraphy. A detachment fold model should be considered when the stratigraphy is poorly defined and especially when incompetent rocks are known to underlie the reservoir. The critical variables needed for further evaluation will be dictated by the amount of data available for a particular structure.

Speculations about oil exploration and production in the Arctic National Wildlife Refuge "1002" area

To the north of the study area lies the portion of the Arctic National Wildlife Refuge that may be leased for hydrocarbon development, the controversial "1002" area (Fig. 4.1). Since the tectonic regime is contractional in this area (the Cenozoic deformation front of the northeastern Brooks Range lies offshore (Grantz *et al.* 1990, Moore *et al.* 1994)), it is likely that map-scale contractional structures similar to those exposed in the northeastern Brooks Range are present in the subsurface of the 1002 area. Thus, this study provides a basis for speculations relevant to oil exploration in the 1002 area.

Studies of both the sand intervals in the Kayak Shale (LePain 1993) and the upper parts of the Lisburne Limestone (Krumhardt 1992) suggest that these units could provide good reservoir rock in the 1002 area. However, it is likely that exploration will be targeted higher in the stratigraphic section, either in the Permian-Triassic Sadlerochit Group (Crowder 1990), Lower Cretaceous Kemik

Reproduced with permission of the copyright owner. Further reproduction prohibited without permission.

Sandstone (Mull 1987, Reifenstuhl 1995), or younger rocks. This research not only has economic implications for potential detachment fold reservoirs in the Kayak-Lisburne interval, but also for the geometry of units upsection that may be structurally affected by Kayak-Lisburne folds. The general suggestions of this study for the geometry and kinematics of detachment folds may be significant (as in the preceding sections on "other fold-and-thrust belts") for folds structurally removed from the influence of Kayak-Lisburne folds. Such folds are likely to be smaller than those in the Lisburne because the competent unit intervals up-section are thinner than the Lisburne. However, this discussion focuses on units that directly overlie, and are directly affected by, folds in the Kayak-Lisburne interval.

Three important questions for assessing structures directly affected by Kayak-Lisburne detachment folds are discussed here.

1) What is the depositional distribution of the Kayak and Lisburne in the 1002 area?

The Lisburne Limestone and Kayak Shale depositionally thin northward (Watts *et al.* 1988, LePain 1993). The Kayak Shale depositionally pinches out in the Sadlerochit Mountains in the southwestern part of the 1002 area, but Kayak could be present in the subsurface to the east (Fig. 4.11). The pinch-out is located on a Paleozoic and younger structural high, the Sadlerochit high, which may be related to another, larger, long-lived structural high: the Barrow arch (Moore *et al.* 1994). The Barrow arch is a regional structure that trends southeastward from Barrow to Prudhoe Bay, where it forms petroleum traps. East of Prudhoe Bay, the arch plunges gently southeastward, beneath the 1002

Reproduced with permission of the copyright owner. Further reproduction prohibited without permission.

area, but its geometry is poorly constrained east of the Canning River. Thus, question 1 can be stated as: "Do the Kayak and Lisburne depositionally onlap, or wrap-around, the Barrow arch beneath the 1002 area (Fig. 4.11)"? In order for detachment folds to exist in the Kayak-Lisburne interval in the 1002 area, these units must have been deposited. Thus, in order for detachment folds in the Lisburne to be associated with an exploration target in the 1002 area, the Lisburne and the Kayak must at least depositionally onlap the Barrow arch.

2) Are the Kayak and/or the Lisburne truncated by the regional Lower Cretaceous unconformity in the 1002 area?

This question is just as critical as the first question, but its answer is also not known. In order for detachment folds to exist in the Kayak-Lisburne interval, these units must not have been eroded, thus we must assume that they were at no time truncated by an unconformity.

Thus, if the Kayak and Lisburne were deposited on the Barrow arch and were not subsequently eroded, then there is a strong possibility that detachment folds exist in the sub-surface. If this is true, then rock units up section must also accommodate that fold shortening.

3) How do the geometry and kinematics of folds observed in this study influence the structural geometry immediately up section?

The very existence of an anticlinal detachment fold implies that overlying stratigraphy will share the same general form as the detachment fold (*e.g.* Fig. 4.12). This is because the overlying unit must take up the same amount of shortening as is accommodated by the detachment fold. Specifically *how* the

Reproduced with permission of the copyright owner. Further reproduction prohibited without permission.

overlying stratigraphy accommodates the shortening defined by the detachment fold (*e.g.* folding, faulting, penetrative deformation) is dependent on the mechanical stratigraphy of the overlying rocks (see Ramsay & Huber 1987).

The Sadlerochit Group overlies the detachment folds described in this study (Fig. 4.3) but was only observed at a few locations (Figs. A2.7, Plates A2, A3 & A4). The Ivishak Formation in the Sadlerochit accommodates the super giant Prudhoe Bay oil and gas field some 100 km northwest of this study area but was not observed in this study. However, I can speculate about its geometry. The Ivishak Formation contains a competent-incompetent couplet similar to the Kayak-Lisburne couplet (Ledge Sandstone member - competent, Kavik Shale member - incompetent (Crowder 1990)). In a variety of places in the northeastern Brooks Range, the structural geometry of the Ivishak is observed to be characterized by detachment folds involving the Ledge and Kavik members, that are generally parasitic to the detachment folds in the Lisburne (Hanks 1991, Homza 1992a, E. Pavia oral comm. 1994).

However, in some places, for example at Bathtub syncline to the southeast of this study area, these smaller-scale detachment folds in the Ivishak are separated from the Lisburne folds by another competent-incompetent couplet within the Permian Echooka Formation of the Sadlerochit Group that also forms detachment folds (Homza 1992a). In general, the geometry of the Ivishak in the Arctic National Wildlife Refuge will be determined by the geometry of the Echooka, which in turn is determined by the geometry of the Lisburne. In this scenario, which may be common in the 1002 area (given the multilayer nature of the Sadlerochit (Crowder 1990)), the whole structural sequence may

Reproduced with permission of the copyright owner. Further reproduction prohibited without permission.

be termed polyharmonic (Ramsay & Huber 1987) (Fig. 4.12), with the Lisburne folds representing "1st order" detachment folds.

The geometry of folds in the Lisburne is not discussed further here (see Chapter 3). Since the Ivishak was not observed in this study, I can only discuss the common structural characteristics of the Echooka Formation that I observed in a variety of areas in the northeastern Brooks Range in this and previous studies (*e.g.* Homza 1992a) (Plates 3 & 4). These features are important because, although the Lisburne folds indirectly affect the structure of the Ivishak, the Ivishak responds directly to structures in the Echooka Formation. The Echooka Formation in most areas:

- is less than 100 meters thick and includes a lower detachment shale and an upper mixed carbonate, clastic, and chert-bearing succession
- forms detachment folds defined by this internal competent-incompetent couplet with wavelengths on the order of 10s of meters
- accommodates more shortening above detachment fold synclines (a duplex is exposed in the Sadlerochit at Bathtub syncline to the southeast (Homza 1992a) and out-of-syncline thrust faults are exposed above the Lisburne detachment synclines in the Franklin Mountains synclinoria (Appendix 3)) and overturned forelimbs than it does above detachment fold crests or backlimbs. This relationship between shortening and structural position is analogous to that observed for the Lisburne detachment folds with respect to their positions above the Franklin Mountains anticlinoria (Fig. 4.5).

Reproduced with permission of the copyright owner. Further reproduction prohibited without permission.

- accommodates a significant amount of shortening by small-scale deformation in the finer-grained rocks, primarily in the form of centimeter-scale kink folds and crenulation cleavage

Given its mechanical stratigraphy, I suspect that the Ivishak forms detachment folds and thrust-faulted detachment folds above the Echooka in a manner similar to that described for the Echooka above the Lisburne. If the stratigraphy beneath the Arctic National Wildlife Refuge 1002 area is similar to that in the northeastern Brooks Range, then the very general geometry shown in figures 4.11 and 4.12 may be expected in the subsurface.

Summary of implications for petroleum geology in the Arctic National Wildlife Refuge 1002 area

Detachment fold geometries similar to those described in this study may exist in the sub-surface of the 1002 area (Fig. 4.11). If detachment folds exist in the Lisburne beneath the 1002 area, then the geometry of the principal reservoir rock, the Ivishak Formation, is expected to form parasitic (or polyharmonic) detachment folds that follow the general form of the underlying structures. The amount of deformation accommodated in the reservoir may be expected to decrease from positions above detachment fold synclines to those above forelimbs to those above crests and backlimbs (Fig. 4.12).

Reproduced with permission of the copyright owner. Further reproduction prohibited without permission.

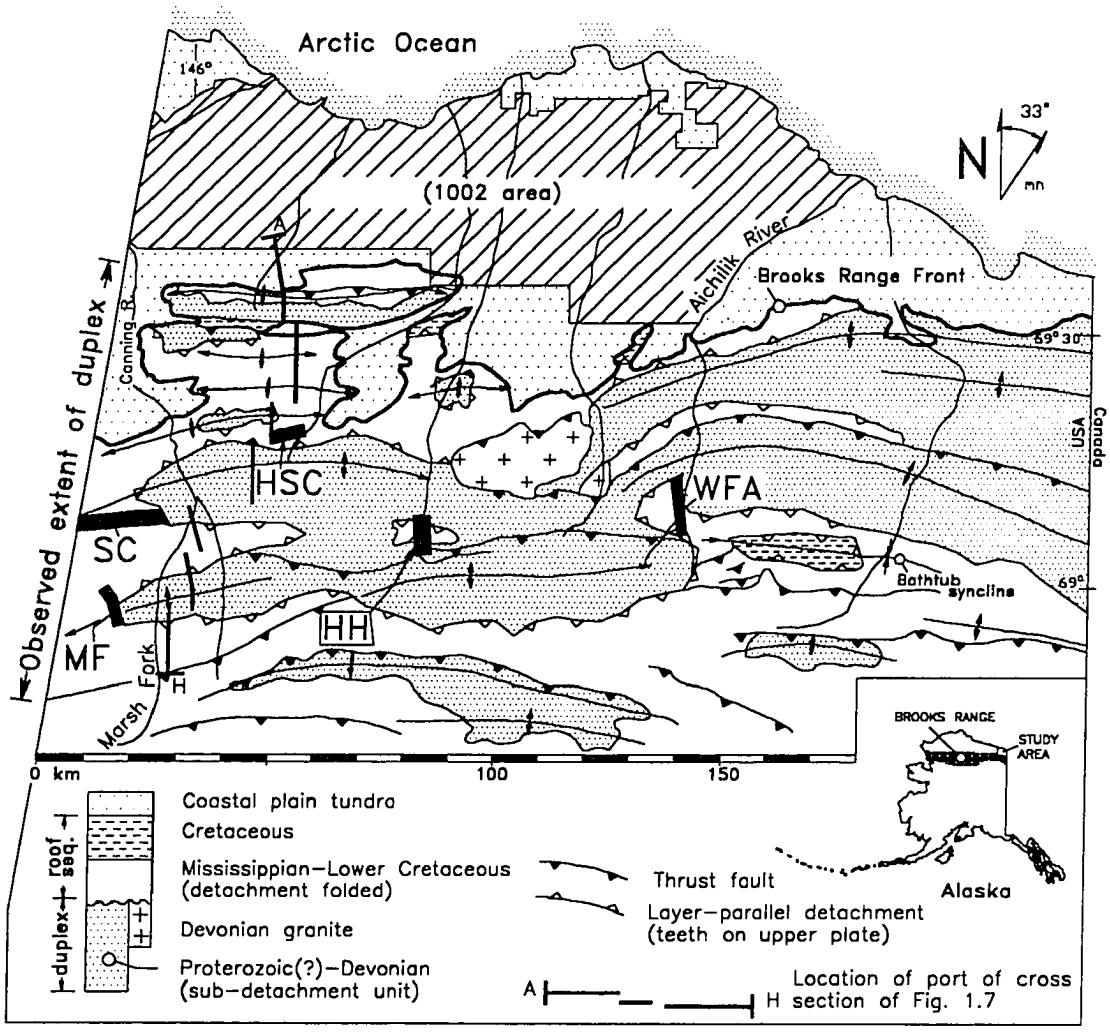

Figure 4.1. Simplified structural map of the northeastern Brooks Range and coastal plain of the Arctic National Wildlife Refuge showing the study areas and the regional anticlinoria. HSC = Headwaters of Straight Creek area, SC = Salisbury Creek, MF = Marsh Fork area, WFA = West Fork Aichilik River area, HH = Hulahula River area.

Reproduced with permission of the copyright owner. Further reproduction prohibited without permission.

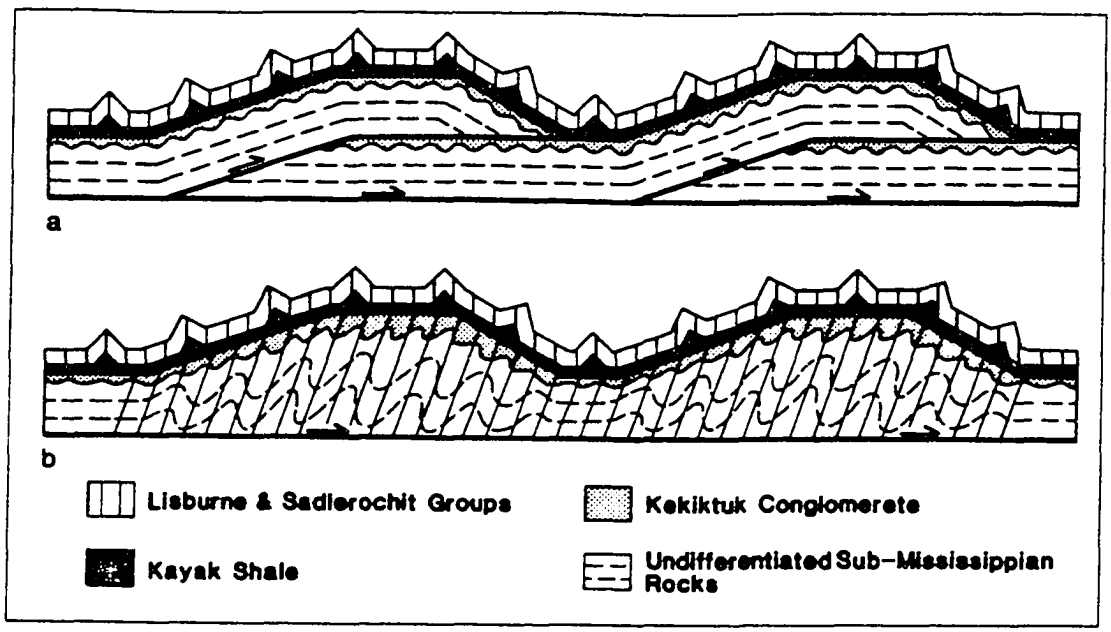

Figure 4.2 Two end member tectonic models for the northeastern Brooks Range: a) the duplex model, b) the heterogeneous simple shear model (from Wallace & Hanks 1990).

Reproduced with permission of the copyright owner. Further reproduction prohibited without permission.

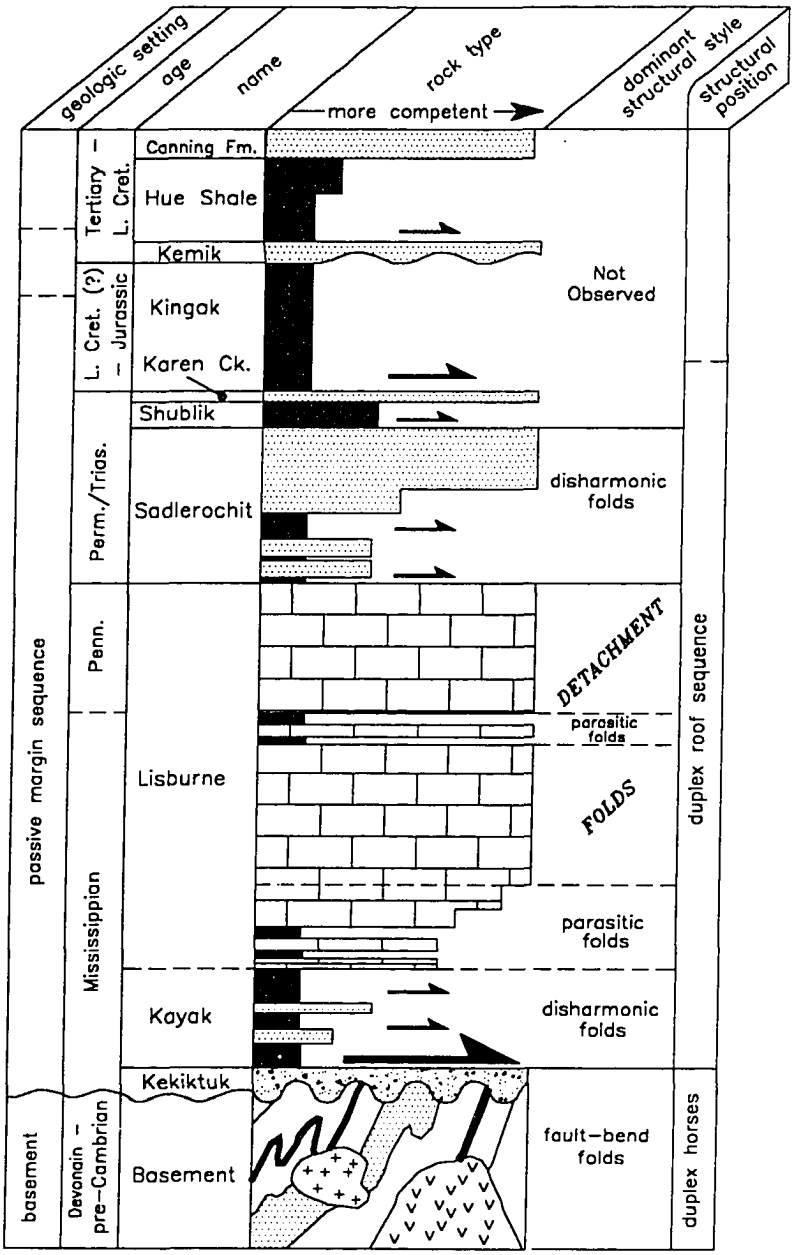

Figure 4.3. Generalized column of the stratigraphy involved in detachment folding in the northeastern Brooks Range. The large arrow indicates the location of the duplex roof thrust and the detachment beneath the detachment folds.

Reproduced with permission of the copyright owner. Further reproduction prohibited without permission.

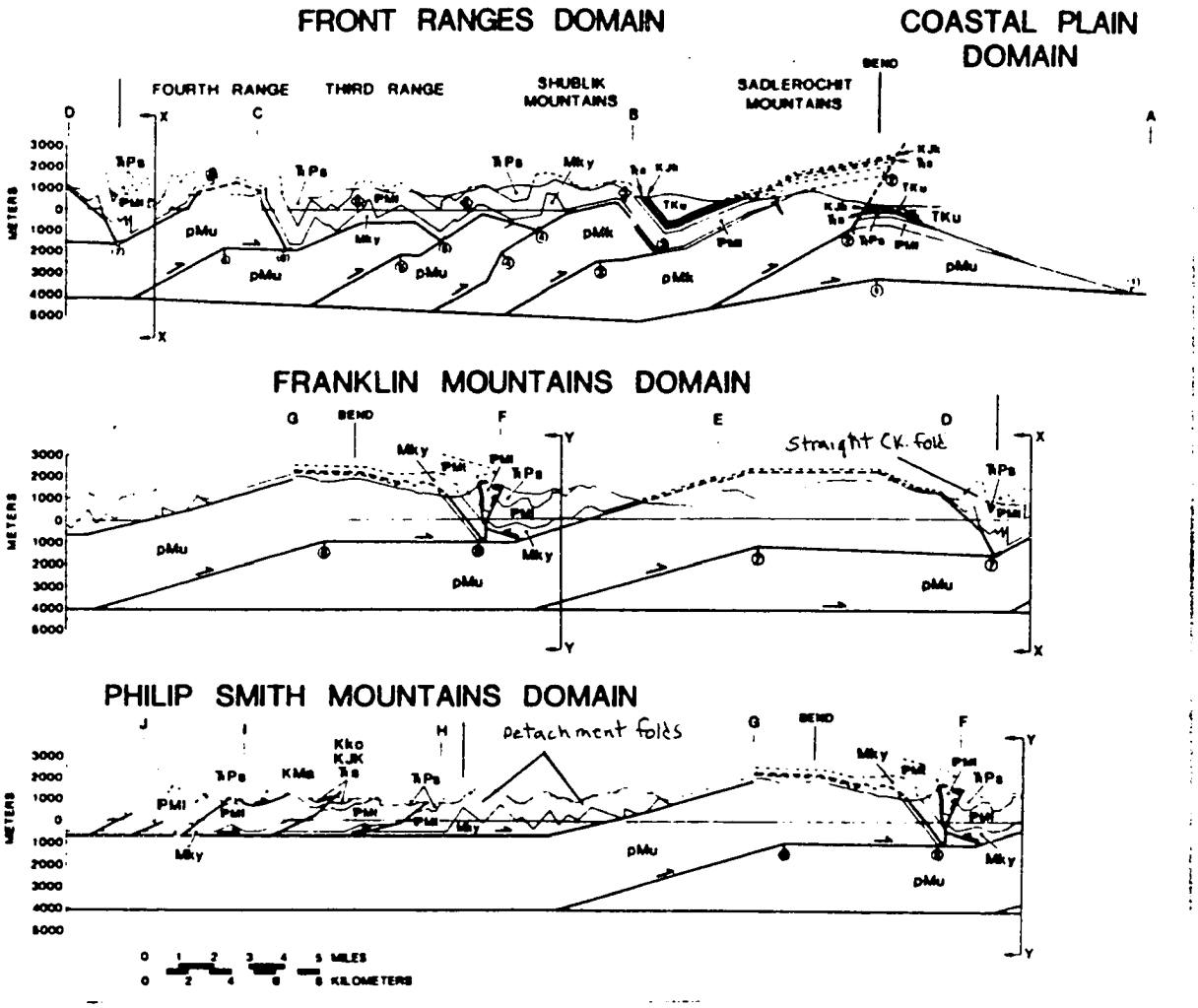

Figure 4.4. Balanced Cross section across the northeastern Brooks Range near the Canning River showing both the interpreted fault-bend folded horses in the regional duplex and the relative structural position of the detachment folds in the roof sequence (from Wallace 1993).

Reproduced with permission of the copyright owner. Further reproduction prohibited without permission.

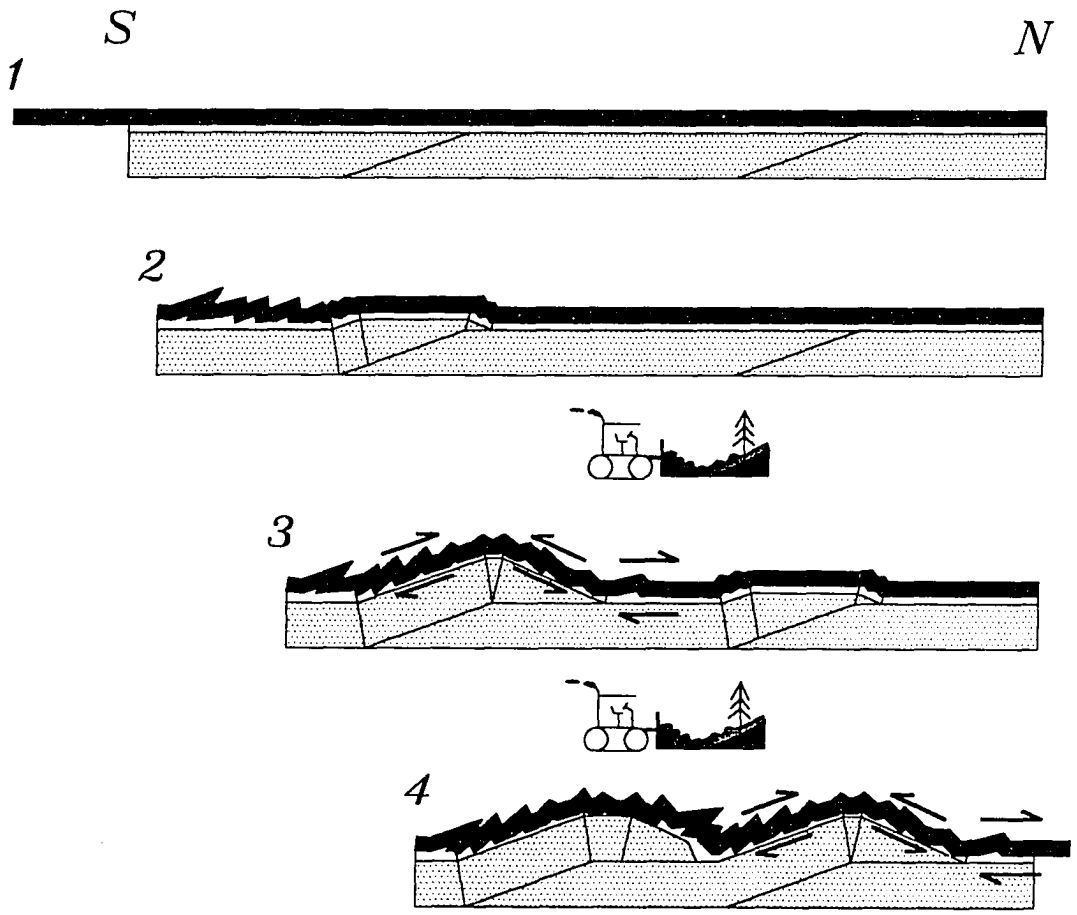

Figure 4.5 Schematic diagram representing the kinematic evolution of the Franklin Mountains anticlinoria.

Reproduced with permission of the copyright owner. Further reproduction prohibited without permission.

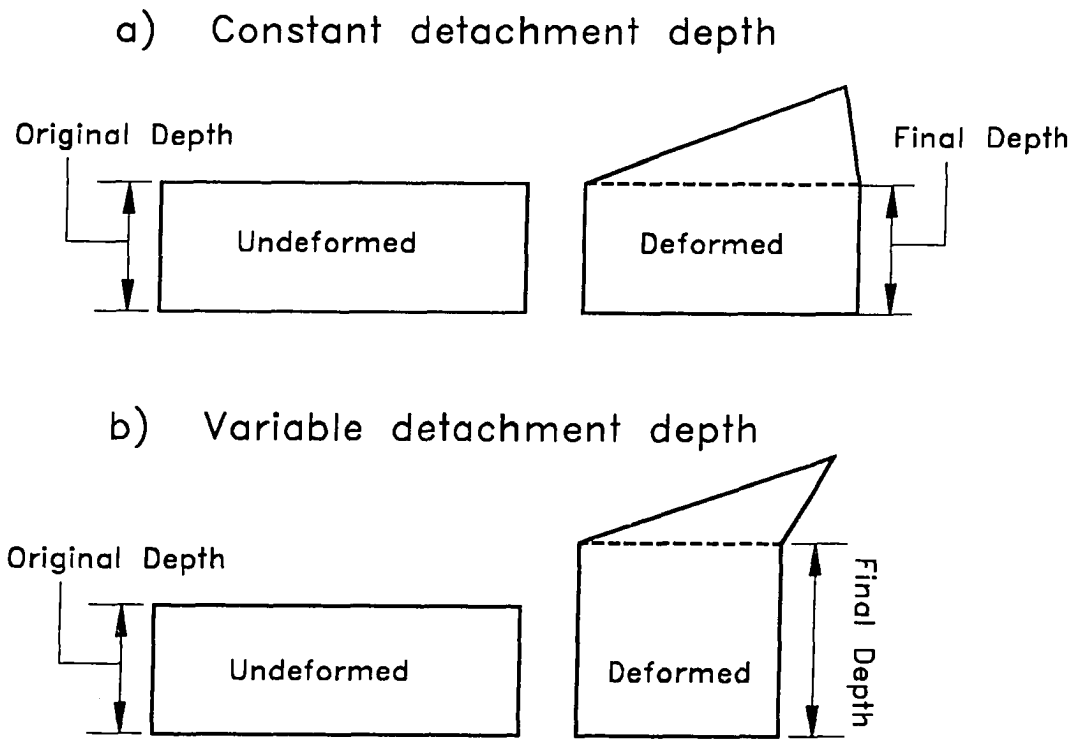

Figure 4.6. Diagram illustrating the concept of detachment depth variation as measured at the hinges of the synclines bounding the detachment anticline. a) The thickness of the detachment unit remains constant during folding - constant detachment depth. b) The thickness of the detachment unit changes during folding (increases in this case) - variable detachment depth.

Reproduced with permission of the copyright owner. Further reproduction prohibited without permission.

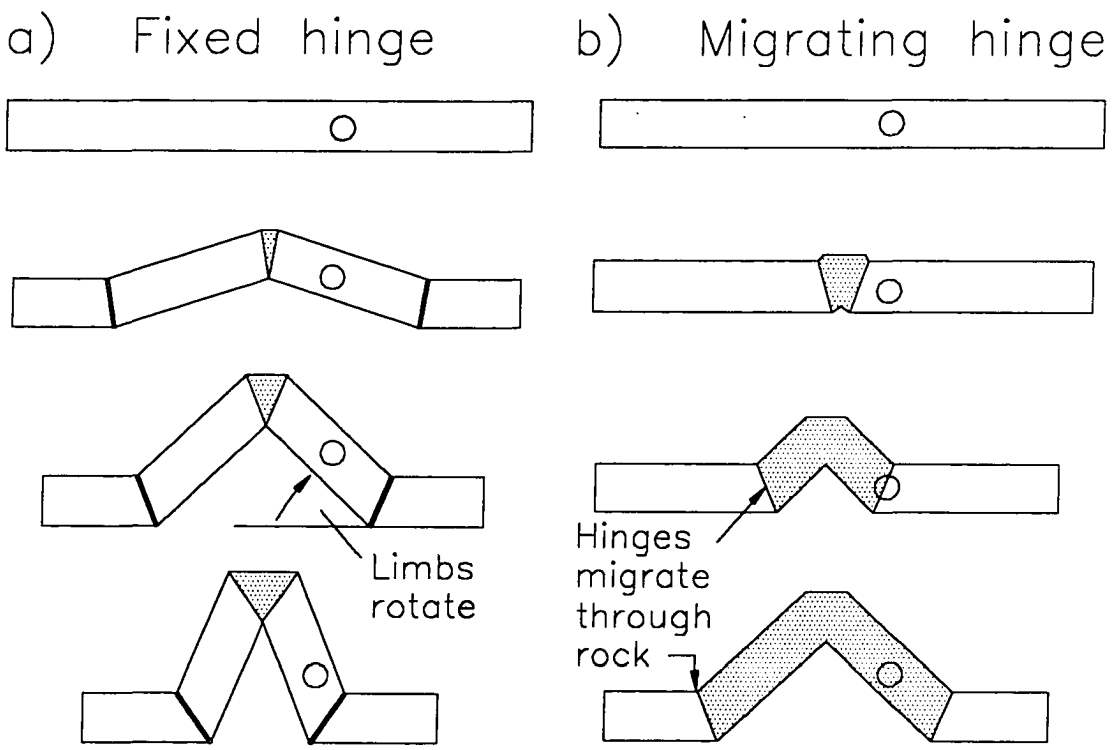

Figure 4.7. Diagram showing the fundamental difference in kinematics between fixed arc-length and migrating-hinge folding. The circle represents a particle path and the shaded area represents rock that has experienced hinge-type deformation. (a) The arc-length remains constant and hinges are fixed throughout the evolution of the fold, the particle experiences only limb-type deformation. (b) The arc-length increases and the particle is rolled through a hinge and experiences hinge-type deformation followed by limb-type deformation.

Reproduced with permission of the copyright owner. Further reproduction prohibited without permission.

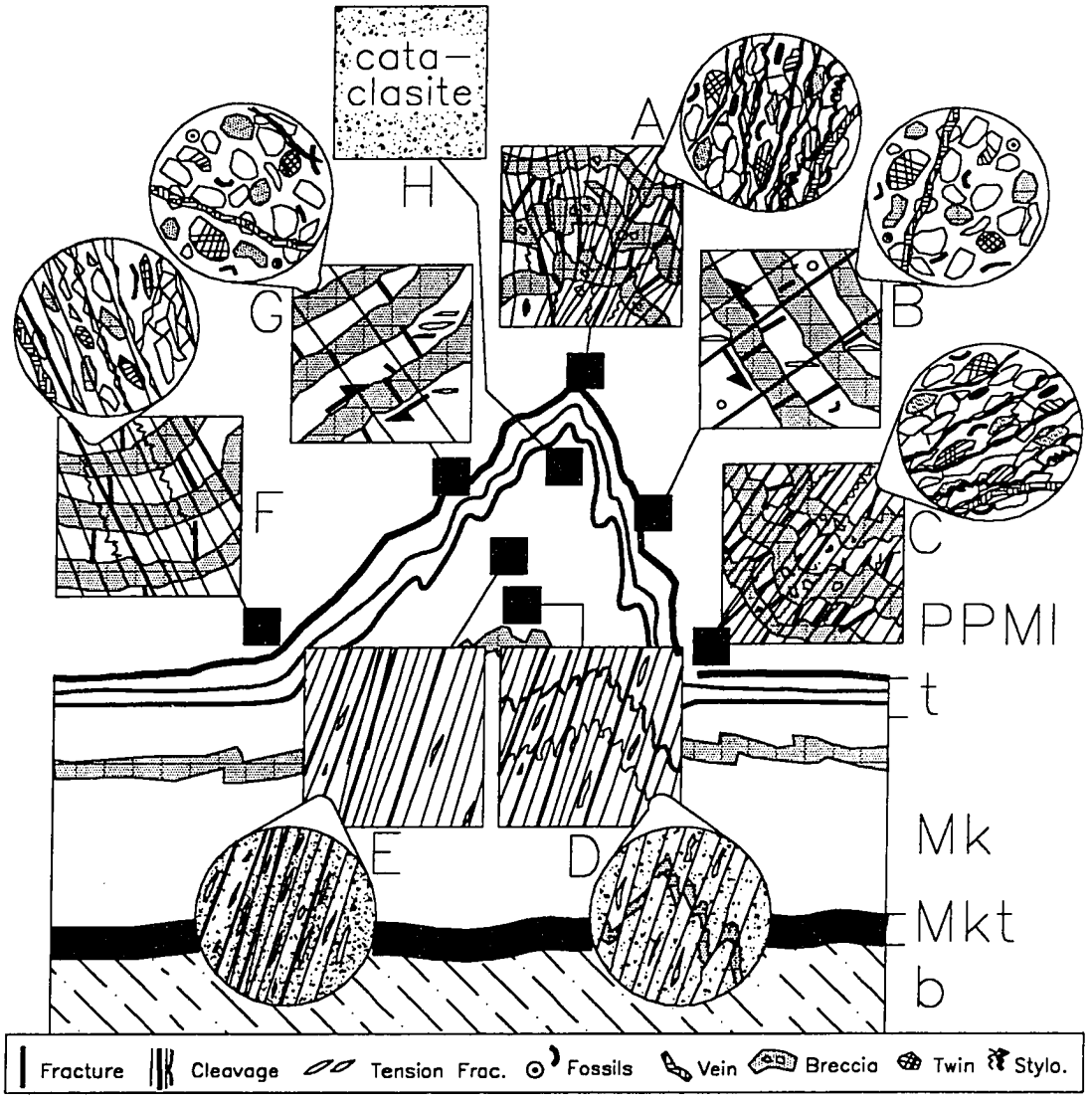

Figure 4.8. Schematic diagram of the distribution of strain indicators in a typical detachment fold in the northeastern Brooks Range. Boxes represent about a square meter of rock and circles represent thin sections. The diagram is simplified and the representation of various structures are intended to note their existence rather than their detailed characteristics. Note the high strain indicated by the abundance of structures in the competent hinges (areas A, C, & F), the solution cleavage and cataclasis in the incompetent core (areas D, E, & H) and contrast these areas to the relatively unstrained limbs (areas B & G). The abundance of veining in areas A & C is under-represented for clarity. Arrows in areas B and G represent bed-parallel shear zones. This distribution strongly supports fixed-hinge kinematics. PPMI = Lisburne Limestone, t = mechanically transitional unit, Mk = Kayak Shale, Mkt = Kekiktuk Conglomerate, b = basement rocks.

Reproduced with permission of the copyright owner. Further reproduction prohibited without permission.

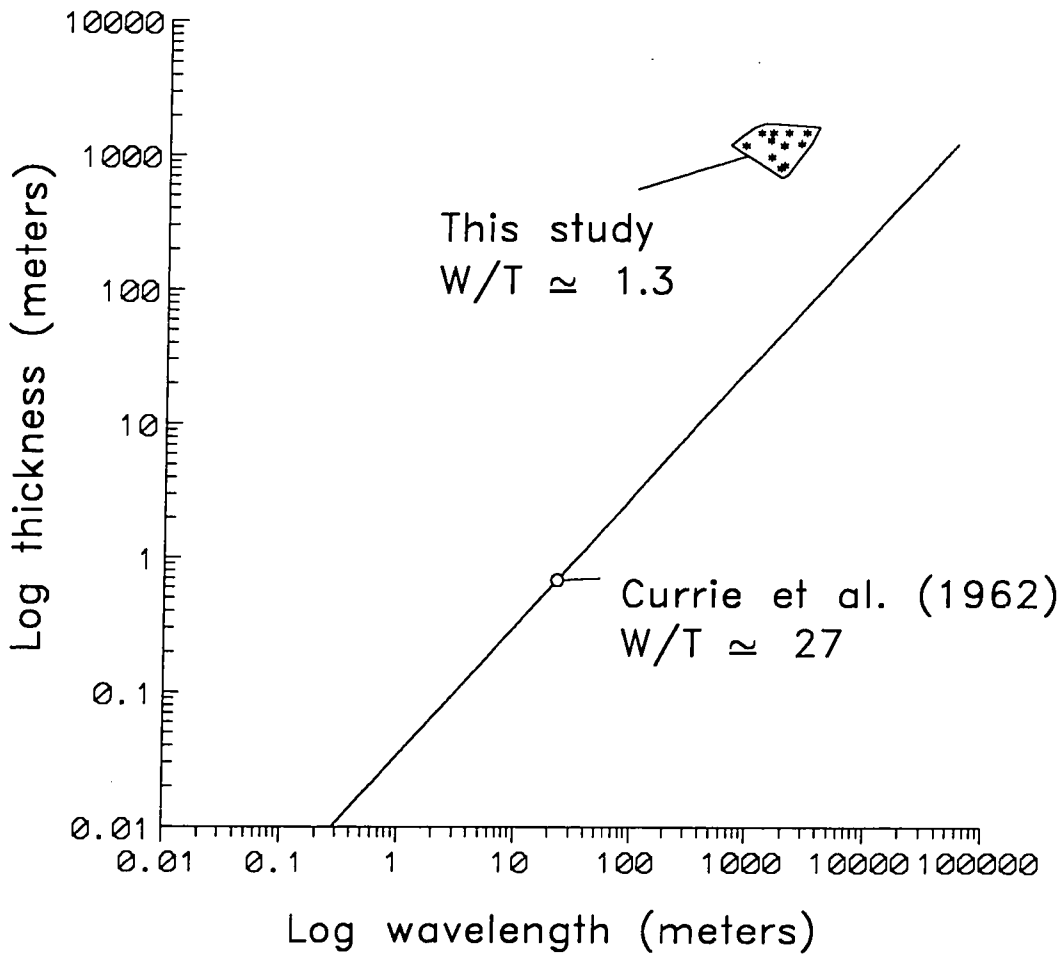

Figure 4.9. Logarithmic plot of wavelength (measured in the competent unit) to competent unit thickness for northeastern Brooks Range detachment folds (in the Lisburne) and the folds discussed by Currie (*et al.* 1962). The folds of this study have a very small wavelength-to-thickness ratio, perhaps due to the lack of great thicknesses of incompetent rock above or below the Lisburne Limestone.

Reproduced with permission of the copyright owner. Further reproduction prohibited without permission.

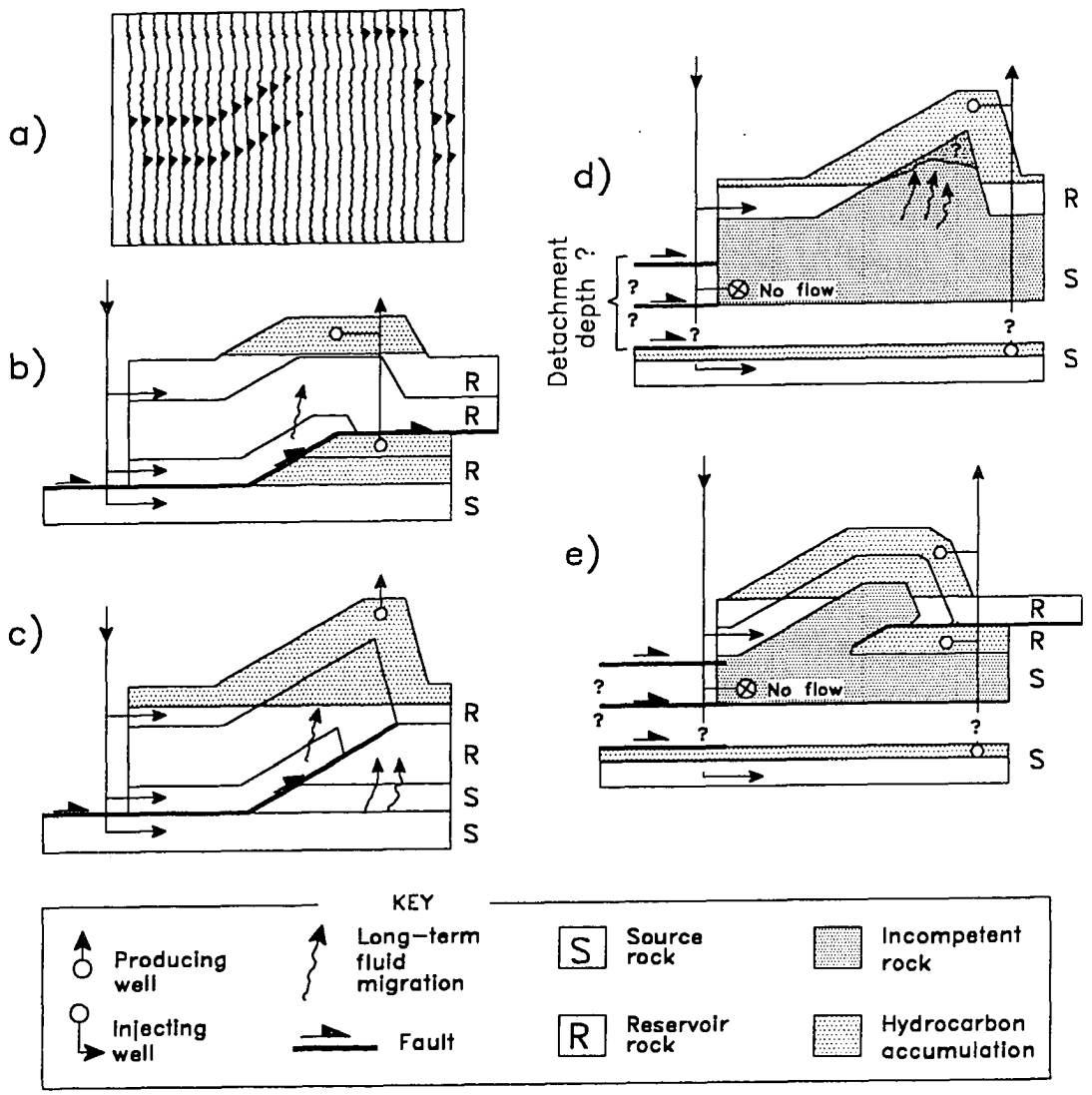

Figure 4.10 a) Schematic diagram of a hypothetical seismogram. Several possible geometric interpretations of the seismic data: b) a fault-bend fold, c) a fault-propagation fold, d) a detachment fold, and e) a thrust-truncated detachment fold. See text for discussion.

Reproduced with permission of the copyright owner. Further reproduction prohibited without permission.

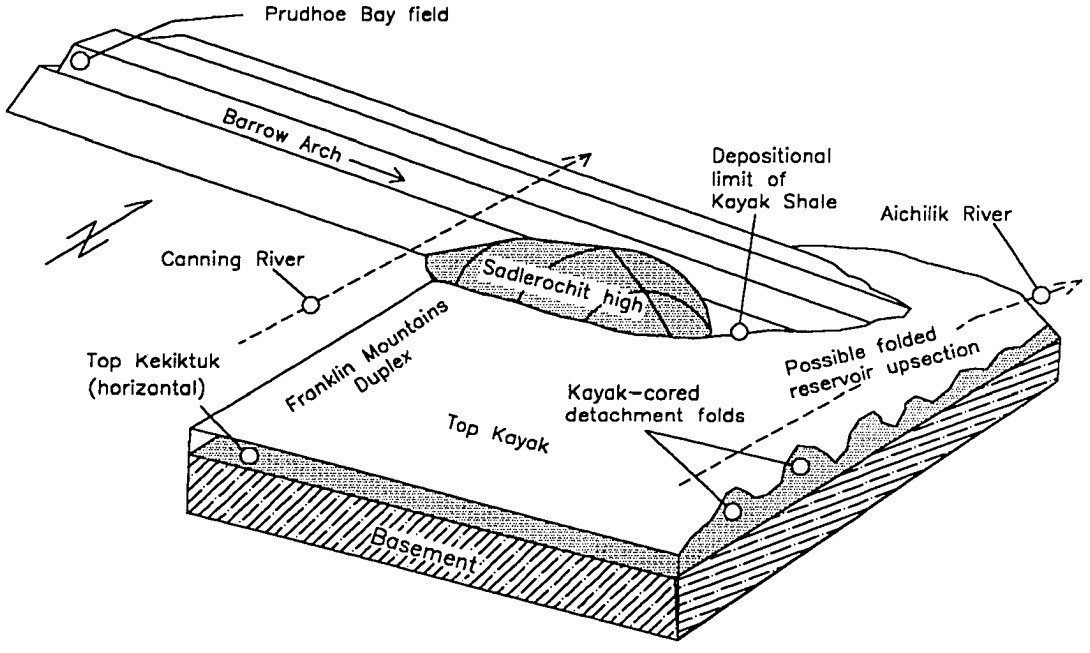

Figure 4.11 Schematic block diagram of the general structural geometry expected in the subsurface of the Arctic National Wildlife Refuge if the Kayak Shale depositionally overlies the Barrow Arch there. Note Prudhoe Bay, the Aichilik River and the Canning River for location. Diagram is not to scale.

Reproduced with permission of the copyright owner. Further reproduction prohibited without permission.

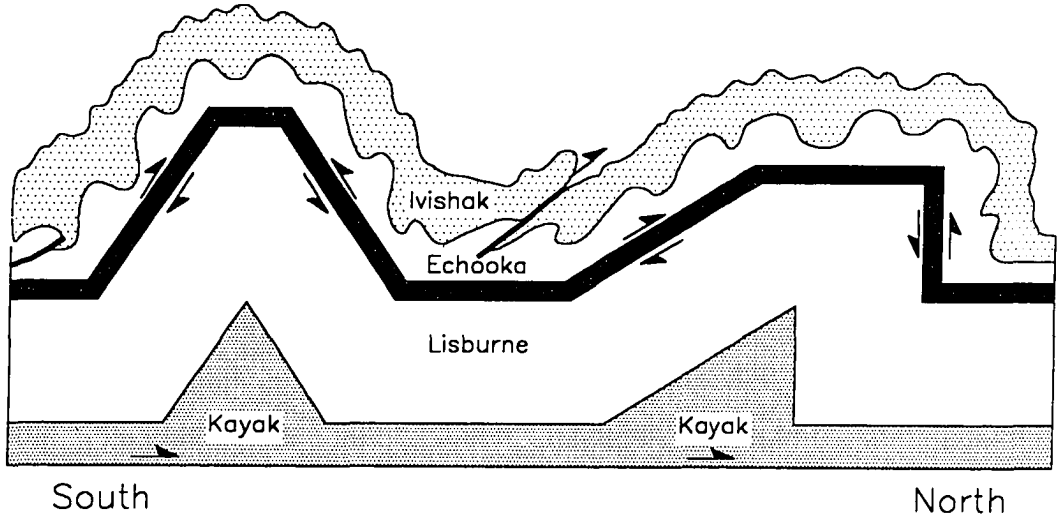

Figure 4.12 Schematic diagram of the general structural geometry expected above detachment folds in the Lisburne Limestone.

Reproduced with permission of the copyright owner. Further reproduction prohibited without permission.

CHAPTER 5- CONCLUSIONS

Although not demonstrated with examples in this study, I assert that detachment folds are likely to be very common in fold-and-thrust belts. This is because: a) detachment folds are the only major fault-related fold type that involves incompetent rock units and b) mechanical stratigraphies of alternating competent and incompetent units are common in fold-and-thrust belts.

THE SIGNIFICANCE OF THE GEOMETRIC-KINEMATIC MODEL PRESENTED

The study presents a versatile tool for geometric and kinematic detachment fold analysis. The tool, the variable detachment depth model for detachment folds, is less restrictive than others that have been published (Jamison 1987, Mitra & Namson 1989). The reason that the model is less restrictive is that it eliminates two assumptions about detachment folds that are incorporated in published models:

1) the assumption of constant detachment depth during folding and

2) the assumption of a migrating-hinge kinematic mechanism for fold evolution.

This is significant because it suggests that the variable detachment depth model, rather than other published models, should be used for the geometric-kinematic analysis of any detachment fold. However, because of the mobility of incompetent material (including mobility into/out of the confines of the fold in the

Reproduced with permission of the copyright owner. Further reproduction prohibited without permission.

plane of section or into/out of the plane of section), the variable detachment depth model is more useful for fold analysis than for the reconstruction of geometry.

OBSERVATIONS AND INTERPRETATIONS OF NATURAL FOLDS

The research includes detailed geometric observations and kinematic interpretations of several natural detachment folds exposed in the northeastern Brooks Range fold-and-thrust belt:

- The detachment folds are defined by the mechanically competent Mississippian-Pennsylvanian Lisburne Limestone and cored by the incompetent Mississippian Kayak Shale.
- A detachment exists at the base of the Kayak Shale that separates the detachment folds from underlying competent rocks.
- The detachment folds are generally angular and represent a range of geometries and evolutionary stages.
- Each detachment fold formed by a fixed-hinge kinematic mechanism (Figs. 5.1 & 5.2).
- The depth-to-detachment varied during the evolution of each detachment fold.
- The detailed fold geometry is controlled by multilayer rheology (bed thickness, competency, and percent competent beds), with the size and spacing of folds reflecting the overall competency and thickness of the multilayer.

Reproduced with permission of the copyright owner. Further reproduction prohibited without permission.

- Constant-depth, migrating-hinge models do not work for the folds observed in the northeastern Brooks Range.

GENERALIZED DETACHMENT FOLD MODEL

The above observations, together with the variable detachment depth model suggest that the evolution of a typical detachment fold generally follows a sequential pattern (Fig. 5.3). Typical detachment folds:

1) may initially take up shortening by layer-parallel shortening;

2) buckle with the hinges fixed with respect to the rock (Figs. 5.1, 5.2, & 5.3);

3) rapidly increase in anticline area, which is accommodated by material transport into the core and a decrease in incompetent unit thickness beneath synclines (Fig. 5.3);

4) reach a maximum anticline area at an interlimb angle of about 90°;

5) decrease in fold area as the fold tightens, at least in part by formation of solution cleavage in fold cores. As the fold tightens further local conditions may cause the fold to respond in any or all of the following ways:

a) it may lose more area by ductile flow or solution, causing isoclinal geometries and, perhaps, lift-off folding (Mitra & Namson 1989);

b) it may lose area by non-plane strain;

c) it may become elevated above the regional elevation and/or;

d) it may be truncated by a thrust fault.

During detachment fold evolution, the thickness of the incompetent unit as measured beneath the synclines (*i.e.* the detachment depth), varies in a

Reproduced with permission of the copyright owner. Further reproduction prohibited without permission.

predictable way that is generally inversely related to the amount of area accommodated in the fold core (Fig. 5.3). Since this evolutionary scenario is intrinsically variable, it is not viewed as "ideal", but rather "typical" of detachment folds developed in fold-and-thrust belts. Model predictions, together with the observed fold geometries, suggest general characteristics of detachment folds that are difficult to model accurately. These include layer-parallel shortening, non-uniform structural stratigraphy that promotes parasitic folding, area-loss, variation in detachment depth, and fixed-hinge kinematics.

SECONDARY IMPLICATIONS OF THIS STUDY

The results of this study also suggest that:

1) Structurally, the western part of the northeastern Brooks Range (Wallace & Hanks 1990) is generally a passive-roof duplex with components of active, or forward-propagating, roof deformation localized forward of fault-bend-folded horses.

2) The observations and models discussed are relevant to detachment fold analyses in other fold-and-thrust belts that did not form while dewatering or diapiric tectonics were active.

3) Detachment folds may form petroleum traps. Detachment folds that are targeted for petroleum exploration or production must be treated differently than fault-bend or fault-propagation folds that are similarly targeted (Fig. 5.4). Ivishak Formation that forms parasitic folds with respect to the Lisburne detachment folds may represent potential reservoirs beneath the 1002 area (Figs. 5.5 & 5.6).

Reproduced with permission of the copyright owner. Further reproduction prohibited without permission.

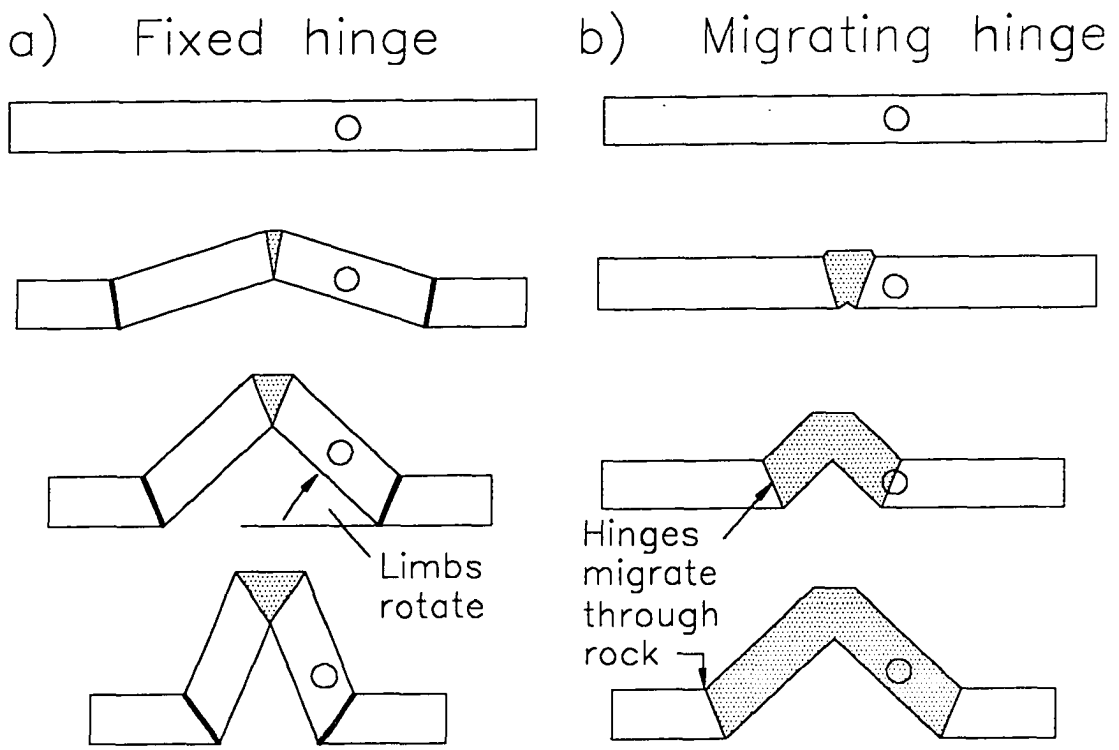

Figure 5.1. Diagram showing the fundamental difference in kinematics between fixed arc-length and migrating-hinge folding. The circle represents a particle path and the shaded area represents rock that has experienced hinge-type deformation. (a) The arc-length remains constant and hinges are fixed throughout the evolution of the fold, the particle experiences only limb-type deformation. (b) The arc-length increases and the particle is rolled through a hinge and experiences hinge-type deformation followed by limb-type deformation.

Reproduced with permission of the copyright owner. Further reproduction prohibited without permission.

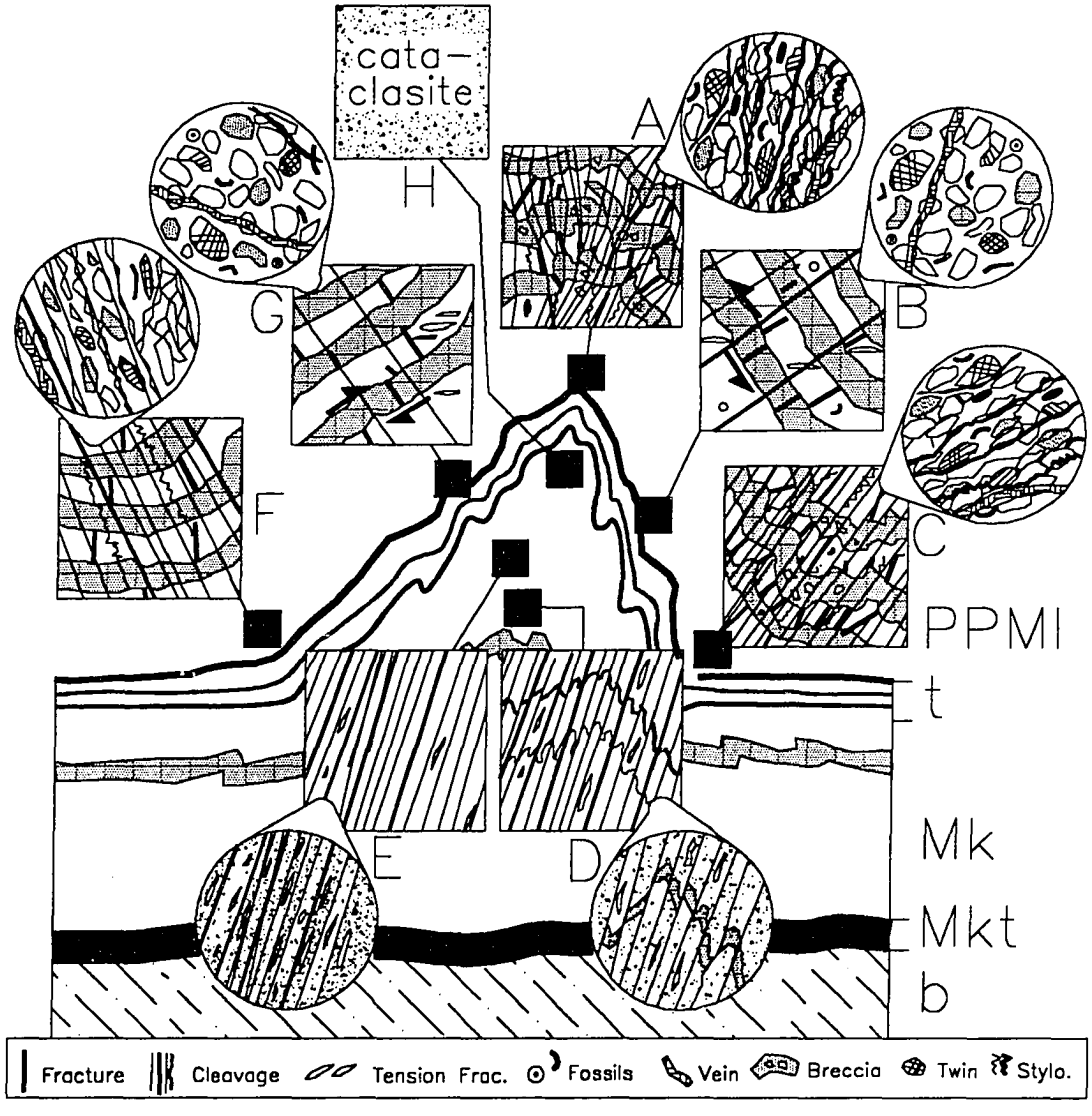

Figure 5.2. Schematic diagram of the distribution of strain indicators in a typical detachment fold in the northeastern Brooks Range. Boxes represent about a square meter of rock and circles represent thin sections. The diagram is simplified and the representation of various structures are intended to note their existence rather than their detailed characteristics. Note the high strain indicated by the abundance of structures in the competent hinges (areas A, C, & F), the solution cleavage and cataclasis in the incompetent core (areas D, E, & H) and contrast these areas to the relatively unstrained limbs (areas B & G). The abundance of veining in areas A & C is under-represented for clarity. Arrows in areas B and G represent bed-parallel shear zones. This distribution strongly supports fixed-hinge kinematics. PPMI = Lisburne Limestone, t = mechanically transitional unit, Mk = Kayak Shale, Mkt = Kekiktuk Conglomerate, b = basement rocks.

Reproduced with permission of the copyright owner. Further reproduction prohibited without permission.

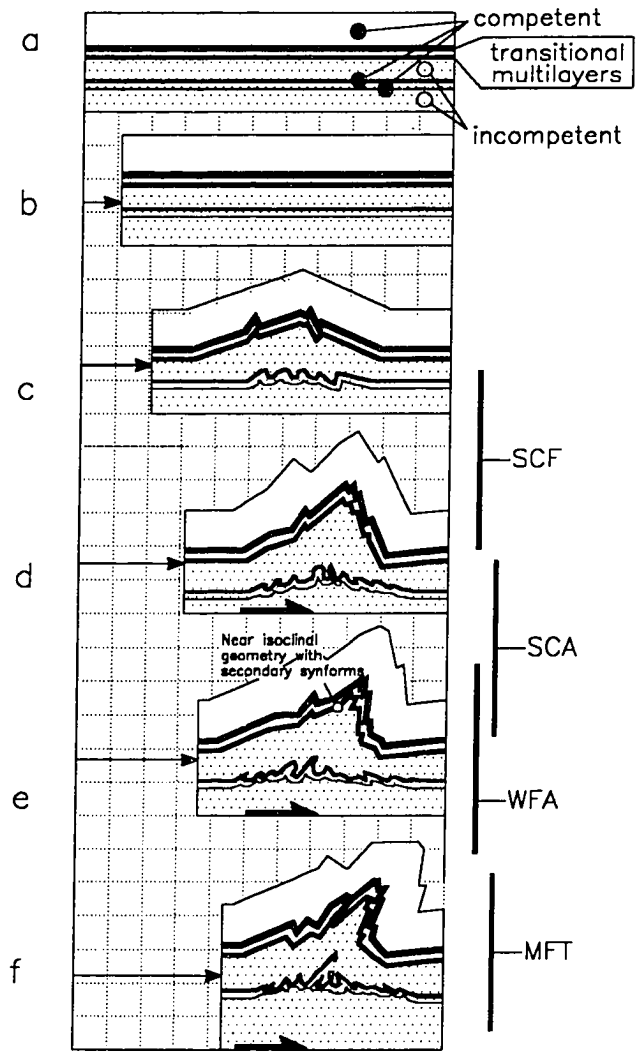

Figure 5.3. Schematic diagram of the evolution of a typical detachment fold incorporating the predictions of the variable detachment depth model with features observed in the northeastern Brooks Range. Vertical bars represent the approximate developmental stage of the observed folds. Stage a) Original stratigraphic succession. b) Period of layer-parallel shortening. c) Early phase of fixed-hinge folding with excess area in the fold core and decrease in detachment depth, parasitic fixed-hinge folds in transitional units, and disharmonic folds in isolated competent units. d) Intermediate phase of folding with final detachment depth equal to original depth. e) Late phase of folding with area deficit in core and tightening of folds, especially at the competent-incompetent contact in the anticlinal hinge. f) Very evolved detachment fold with large area deficit in core and thrust faults in core and on backlimb.

Reproduced with permission of the copyright owner. Further reproduction prohibited without permission.

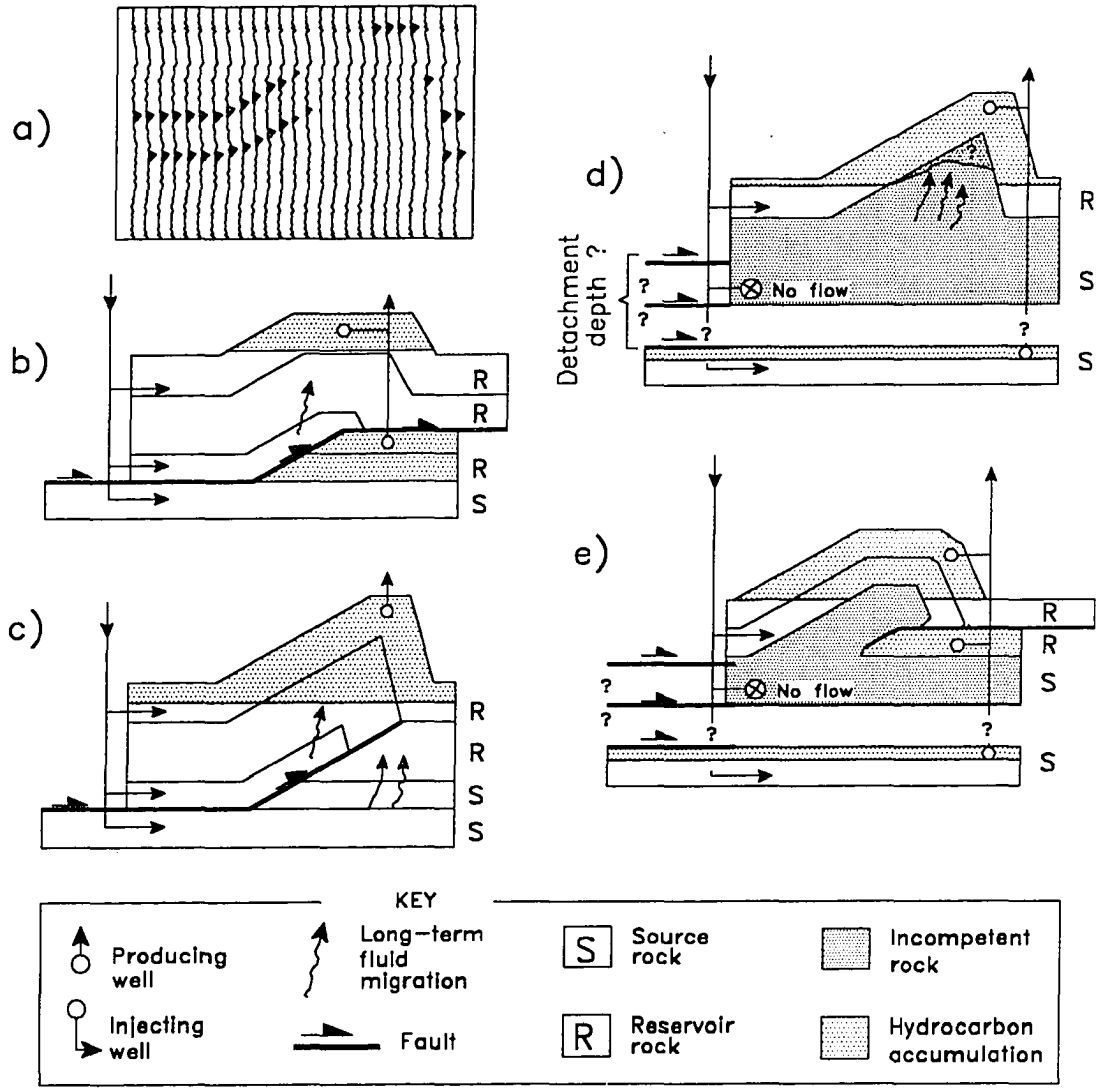

Figure 5.4 a) Schematic diagram of a hypothetical seismogram. Several possible geometric interpretations of the seismic data: b) a fault-bend fold, c) a fault-propagation fold, d) a detachment fold, and e) a thrust-truncated detachment fold. See text for discussion.

Reproduced with permission of the copyright owner. Further reproduction prohibited without permission.

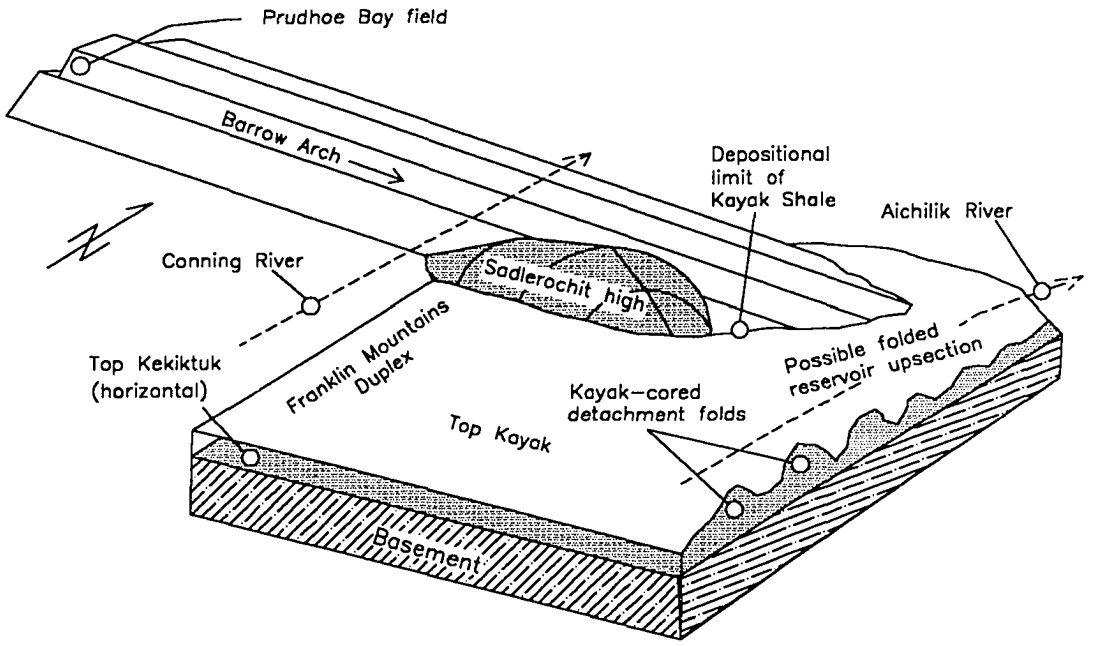

Figure 5.5 Schematic block diagram of the general structural geometry expected in the subsurface of the Arctic National Wildlife Refuge if the Kayak Shale depositionally overlies the Barrow Arch there. Note Prudhoe Bay, the Aichilik River and the Canning River for location. Diagram is not to scale.

Reproduced with permission of the copyright owner. Further reproduction prohibited without permission.

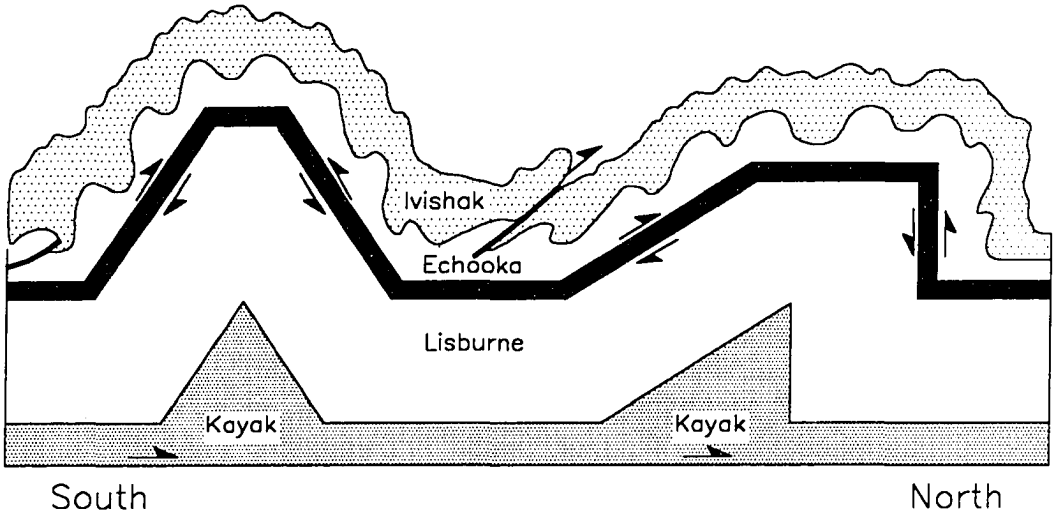

Figure 5.6 Schematic diagram of the general structural geometry expected above detachment folds in the Lisburne Limestone.

Reproduced with permission of the copyright owner. Further reproduction prohibited without permission.

CHAPTER 6- SUGGESTIONS FOR FUTURE RESEARCH

This study addresses many fundamental issues in structural geology and some issues pertinent only to the northeastern Brooks Range and Arctic Slope. However, several important questions in both of these subject areas remain unanswered. This section directly poses some of these questions and suggests possible ways of approaching them.

FUTURE RESEARCH QUESTIONS ABOUT DETACHMENT FOLDS

1) What factors control whether a fold forms by hinge-migration or fixed-hinge buckling?

This study addresses questions of geometry and kinematics, which represent building blocks or starting points for studies about fold mechanics. The detachment fold geometries in the northeastern Brooks Range were described and kinematic models were suggested herein. Thus, I have described *what* geometries detachment folds may form and *how* these geometries evolve, however I have not researched *why* the folds evolve the way they do.

Migrating-hinge fold kinematics is best documented in finely laminated media (*e.g.* Weiss 1968, Stewart & Alvarez 1991). Fixed-hinge kinematics is best understood where it involves a single competent unit lying between two incompetent units that are much thicker than the competent unit (*e.g.* Currie *et al.* 1962, Ramsay & Huber 1987). I suspect these two different mechanical scenarios represent two end members in a spectrum of possible kinematic

Reproduced with permission of the copyright owner. Further reproduction prohibited without permission.

evolutions. Thus, I suggest that the mechanical stratigraphy is the primary controlling factor for fold kinematics.

Another controlling factor may be overburden (*i.e.* confining pressure). Folds with very little overburden may tend toward buckling as suggested by Ramsay & Huber (1987), whereas folds with a large overburden may tend toward "kinking" (hinge-migration). I suspect this is true because more physical work is required to deflect fold limbs via buckling beneath a heavy overburden than beneath a relatively light overburden. It *may* be that the dynamics of hinge-migration and buckling are such that kinking requires less work beneath a heavy overburden than buckling does. This is purely conjectural and is included only to suggest a starting point for further research.

Thus, I suggest mechanical experiments involving variation in both mechanical stratigraphy and confining pressure to approach the question. The hypothesized kinematic spectrum between pure fixed-hinge buckling and pure migrating-hinge kinking may be quantifiable using Newtonian physics or finite element analysis in such controlled experiments. The results of such a study may then be compared with natural examples of folds formed in different mechanical stratigraphies at a variety of depths.

2) What is the detailed kinematic path followed by the incompetent unit during detachment folding?

This questions stems from two limiting assumptions of the variable detachment depth model (Chapters 2 & 3). The model assumes:

a) plane strain (constant area) and

Reproduced with permission of the copyright owner. Further reproduction prohibited without permission.

b) no material moves through the synclines (*e.g.* Fig. 3.4 and related text)

These assumptions are related and are certainly not entirely valid, yet they may be explored quantitatively through 3-dimensional geometric and kinematic modeling. A 3-dimensional model would probably assume constant volume rather than constant area, enabling assessment of a possible relationship between along-strike fold elevation and detachment depth. I suspect that detachment depths may be greater beneath the "domes" than beneath the "saddles" (*e.g.* Ramsay & Huber 1987). This would suggest that material moves from beneath the lowest saddle in a 3-dimensional detachment fold upward to the dome of the structure. This approach would provide data about the non-plane strain assumption, however limiting geometric boundaries to the system would still need to be defined in a 3-dimensional model. A multi-fold system needs to be analyzed in order to constrain the details of flow from beneath synclines. Such a system may be best analyzed using physical models (*e.g.* Dixon & Tirrul 1991).

3) What controls detachment fold asymmetry?

This question stems from observations about the variation in detachment fold asymmetry across the Franklin Mountains anticlinoria (Chapters 3 & 4, Appendix 3). There is a relationship between structural position and fold asymmetry in this area. I suspect this relationship may be explained by some quantifiable relationship among shortening, fold asymmetry, simple shear, and thrust faulting. Some very tight, highly shortened folds are upright and not faulted (*e.g.* Marsh Fork transect, Chapter 3, Plate A3.4) whereas other,

Reproduced with permission of the copyright owner. Further reproduction prohibited without permission.

asymmetric, but less tight folds are truncated by thrust faults (*e.g.* West Fork anticline, Chapter 3, Appendix 4, Plate A4.2). This is a very complex issue that is likely strongly related to the local structure. That is, if a fault exists in the sub-detachment unit, as at the West Fork anticline, then thrusting may be preferred. A detailed answer to this question involves many variables, including the hinge-migration vs. fixed-hinge issue of question 1.

FUTURE RESEARCH QUESTIONS ABOUT THE STUDY OF NORTHERN ALASKA DETACHMENT FOLDS

1) Are detachment folds likely in other parts of the northern Alaskan stratigraphy?

Detachment folds involving different rock units in northern Alaska are probably common, given the multilayer nature of the regional mechanical stratigraphy (see Moore *et al.* 1994 for northern Alaska stratigraphy and references). Some folds, for example those involving the Cretaceous Nanushuk Group and Torok Formation on the Alaskan North Slope, form above very thick detachment units (C. G. Mull, oral comm. 1995). These folds, and others like them, probably formed in a way similar to the folds in the Lisburne. That is, there were likely fixed-hinges and a variable detachment depth during folding and the variable detachment depth model is applicable to constrain the detachment depth.

The incompetent unit will likely be a zone shear which decreases in intensity farther beneath the competent unit. Thus, the detachment "surface"

Reproduced with permission of the copyright owner. Further reproduction prohibited without permission.

may be manifested as the limit of this thick shear zone within the incompetent unit (*i.e.* the limit of the "zone of contact strain" of Ramsay and Huber (1987)).

This question is related to question 1 in the preceding section inasmuch as the local mechanical stratigraphy is likely the primary controlling factor for fold geometries higher in the northern Alaska stratigraphy.

2) Are there other detachment folds involving the Lisburne and Kayak in the northeastern Brooks Range, and what data might a further study of them yield?

Other detachment folds involving the Kayak-Lisburne interval are exposed in the northeastern Brooks Range that were not evaluated in this study. Examples include folds in the "Third" and "Fourth" ranges, folds north of the Okpilak batholith (Hanks 1991), and folds at the headwaters of the Marsh Fork and south of Bathtub Ridge that involve thrust faults. An analysis of their geometry and strain-indicator distribution, similar to this study, would build on the data base provided by this study, help address the question of controls on fold asymmetry, and provide additional data about the details of the tectonic evolution of the northeastern Brooks Range.

Reproduced with permission of the copyright owner. Further reproduction prohibited without permission.

APPENDIX 1- EXPLANATION OF THE MICRO-STRAIN ANALYSIS TECHNIQUE OF CHAPTER 3

In the Lisburne Limestone and Kayak Shale near the anticlinal cores of detachment folds in the northeastern Brooks Range, a lack of natural fossils or geologic features precludes conventional strain ellipse analysis (*e.g.* Ramsay & Huber 1983). Thus, a counting technique apparently very similar to that used by Fischer *et al.* (1992) (Fischer *et al.* (1992) did not describe their technique in this publication) was used to estimate the abundance of 7 separate microscopic strain features, or micro-structures. The method is designed to determine the number and distribution of strained features in a fold in order to determine whether the detachment folds formed by hinge-migration or fixed-hinge kinematics (Chapters 1 & 4). Fischer *et al* (1992) conducting their analysis for the same purpose (and arrived at similar results).

The abundance of each micro-structure was rated as either absent, rare (r), common (c), or abundant (a) based on the number of occurrences in a single, representative field of view at 2X magnification power (Figs. A1.1 - A1.7). Both plane and polarized light were used to identify micro-structures. In fine-grained samples, 10X magnification was used to identify smaller features and these features were included in the total number of micro-structures in a field of view at 2X magnification. The distribution was classified as either hinge or limb, depending on whether the sample was retrieved from a hinge zone or limb *of either parasitic or primary folds.*

Reproduced with permission of the copyright owner. Further reproduction prohibited without permission.

Figures A1.1 through A1.7 show that the number of features that constitute a particular rating varies from feature to feature and in some cases, the rating is based on the ratio of unstrained grains to strained grains. This procedure eliminates bias introduced by grain-size variation between samples and sorting within a single sample. The relative fractions of the sample population classified as fine, medium, and coarse were later differentiated (*e.g.* Fig. A1.8).

Reproduced with permission of the copyright owner. Further reproduction prohibited without permission.

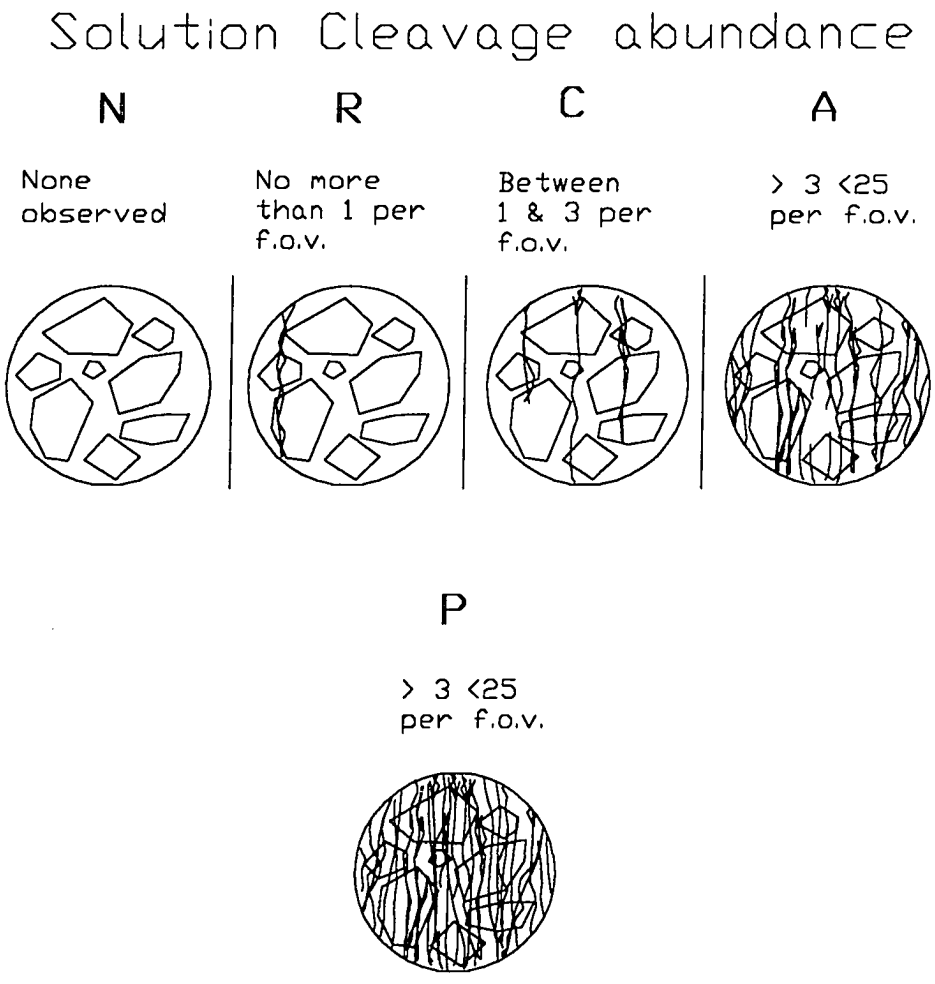

Figure A1.1. Schematic diagram showing the counting technique used in chapter 3 to classify the abundance of solution cleavage features per microscopic field of view (f.o.v). The four columns represent, from left to right: none seen (N), rare (R), common (C), and abundant (A). Solution cleavage was classified as pervasive (or penetrative, P) on figure 3.8 if more than 25 cleavage planes were observed. Circles represent the microscopic field of view.

Reproduced with permission of the copyright owner. Further reproduction prohibited without permission.

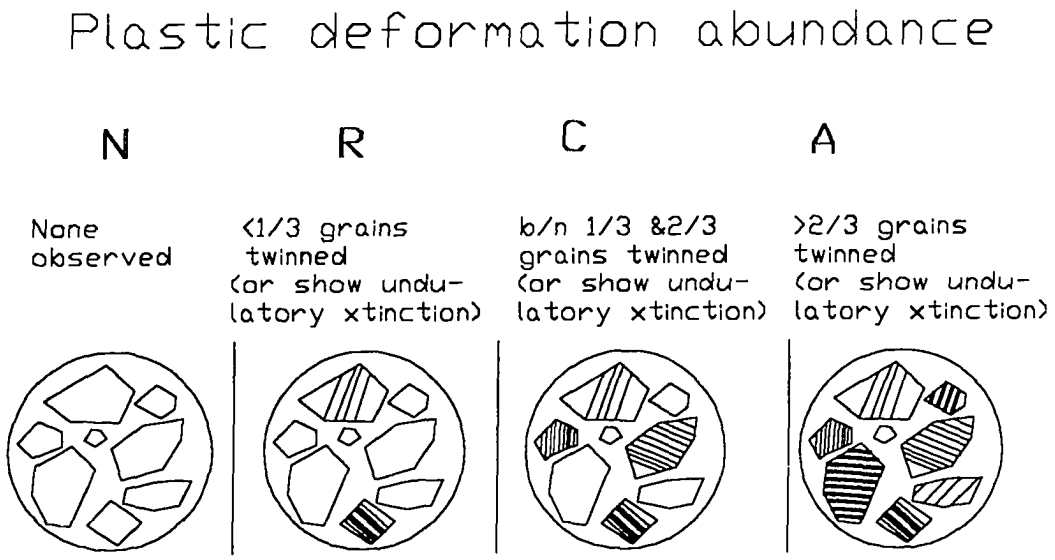

Figure A1.2. Schematic diagram showing the counting technique used in chapter 3 to classify the abundance of features indicating plastic deformation per microscopic field of view. The four columns represent, from left to right: none seen (N), rare (R), common (C), and abundant (A). Circles represent the microscopic field of view.

Reproduced with permission of the copyright owner. Further reproduction prohibited without permission.

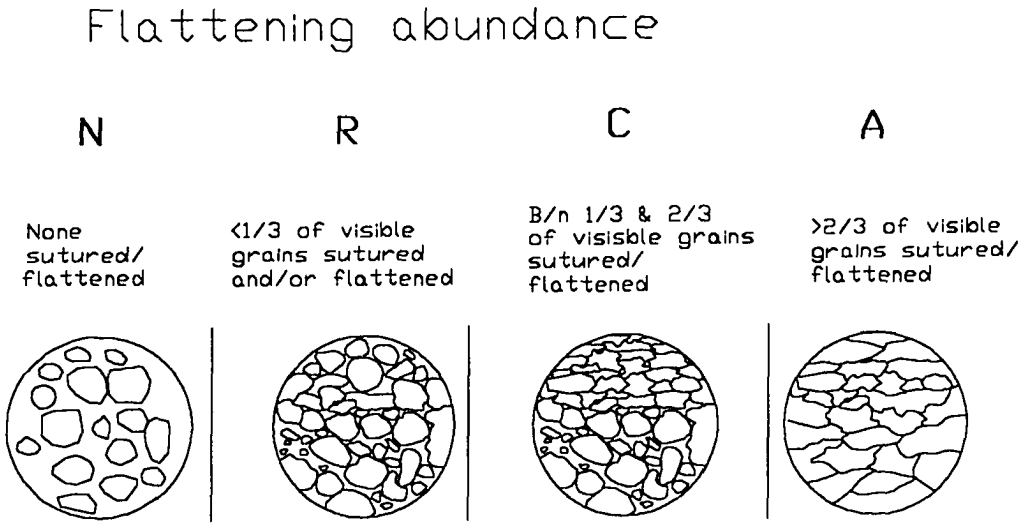

Figure A1.3. Schematic diagram showing the counting technique used in chapter 3 to classify the number of features indicating flattening per microscopic field of view. The four columns represent, from left to right: none seen (N), rare (R), common (C), and abundant (A). Circles represent the microscopic field of view.

Reproduced with permission of the copyright owner. Further reproduction prohibited without permission.

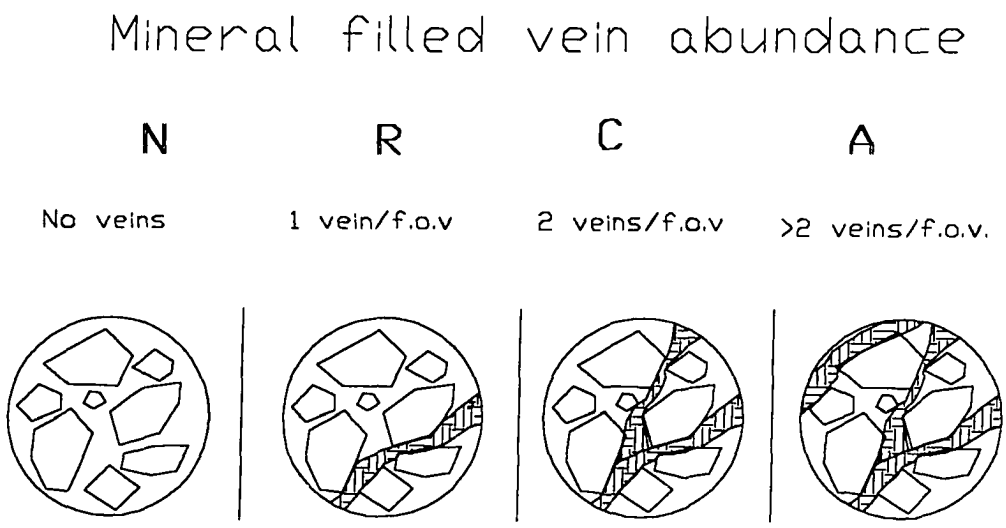

Figure A1.4. Schematic diagram showing the counting technique used in chapter 3 to classify the number of mineral-filled veins per microscopic field of view (f.o.v). The four columns represent, from left to right: none seen (N), rare (R), common (C), and abundant (A). Circles represent the microscopic field of view.

Reproduced with permission of the copyright owner. Further reproduction prohibited without permission.

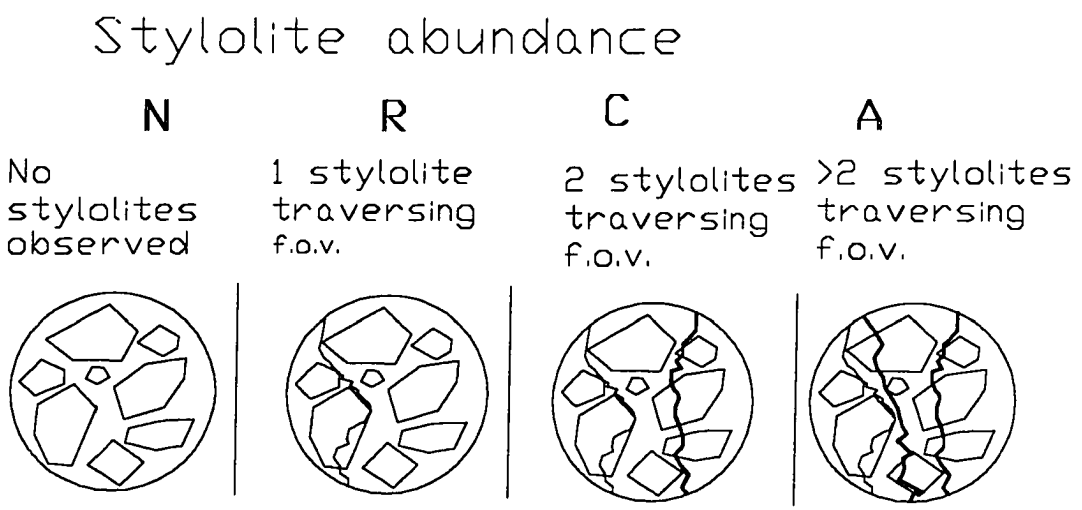

Figure A1.5. Schematic diagram showing the counting technique used in chapter 3 to classify the number of stylolites per microscopic field of view (f.o.v). The four columns represent, from left to right: none seen (N), rare (R), common (C), and abundant (A). Circles represent the microscopic field of view.

Reproduced with permission of the copyright owner. Further reproduction prohibited without permission.

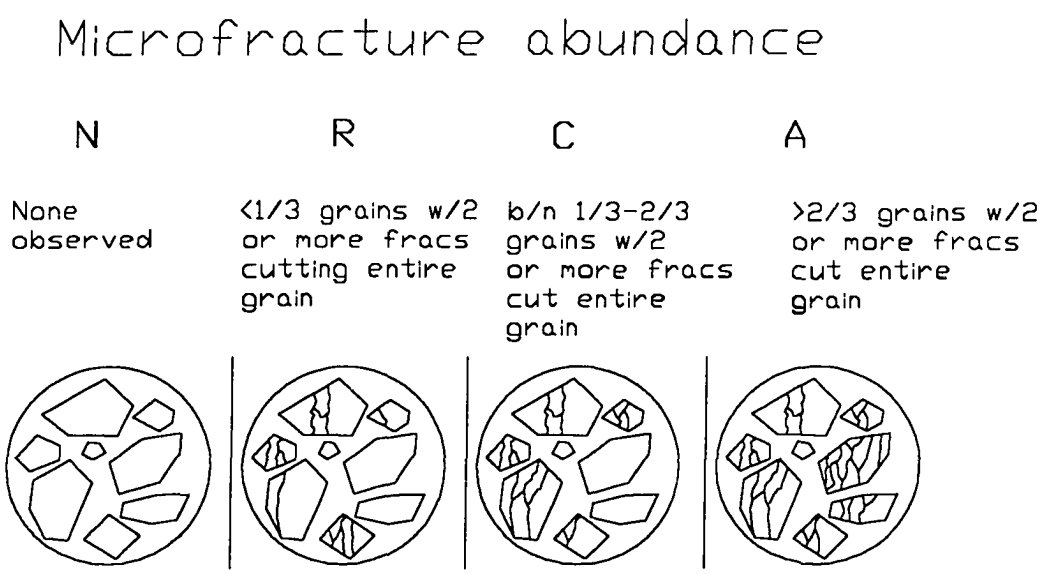

Figure A1.6. Schematic diagram showing the counting technique used in chapter 3 to classify the number of intra-grain microfractures per microscopic field of view. The four columns represent, from left to right: none seen (N), rare (R), common (C), and abundant (A). Circles represent the microscopic field of view.

Reproduced with permission of the copyright owner. Further reproduction prohibited without permission.

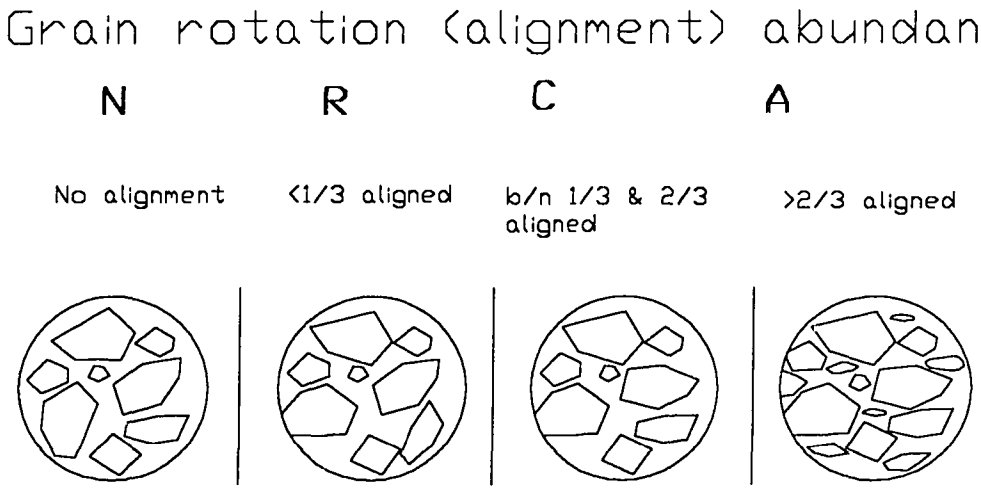

Figure A1.7. Schematic diagram showing the counting technique used in chapter 3 to classify the number of rotated grains per microscopic field of view. The four columns represent, from left to right: none seen (N), rare (R), common (C), and abundant (A). Circles represent the microscopic field of view.

Reproduced with permission of the copyright owner. Further reproduction prohibited without permission.

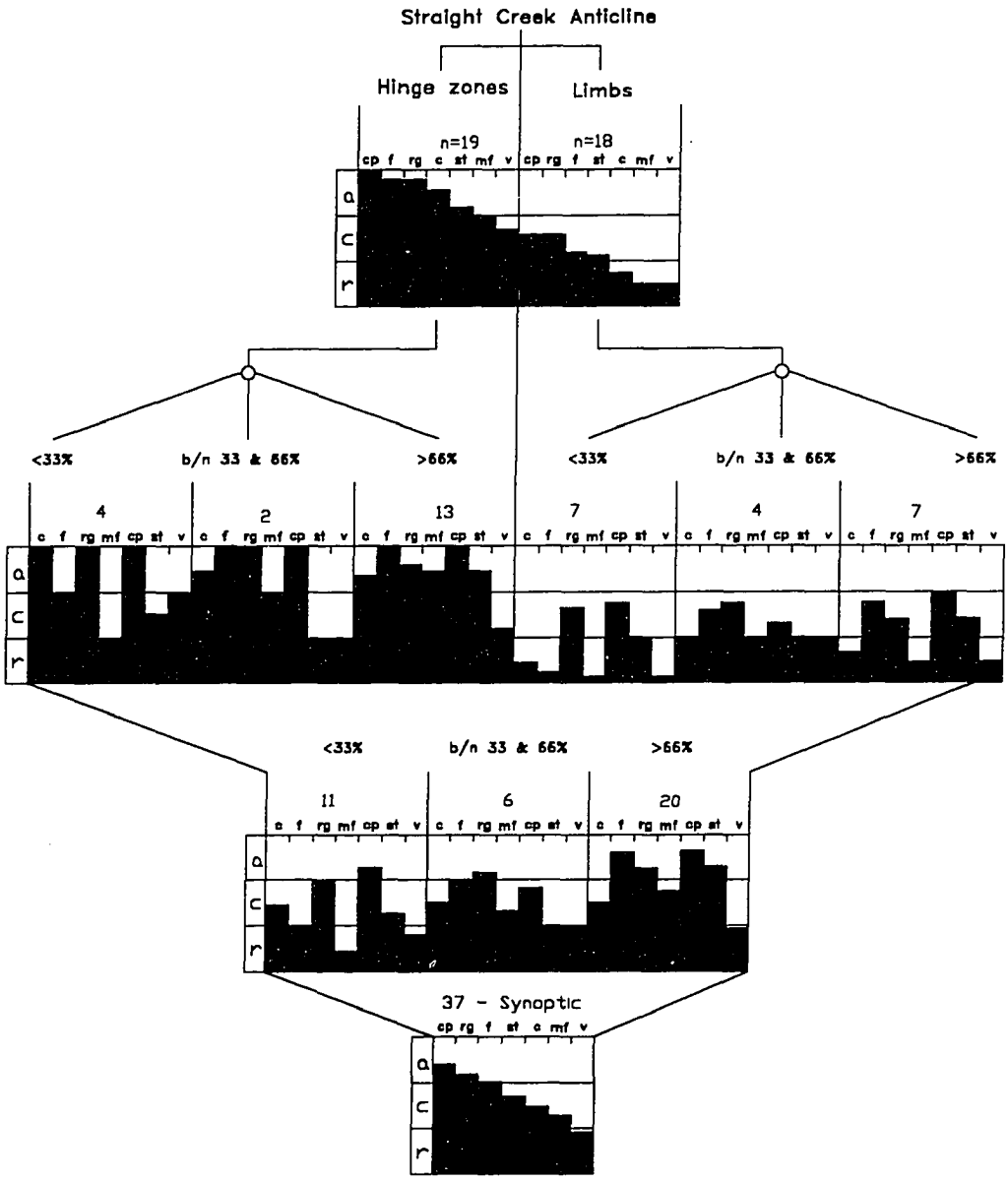

Figure A1.8. Histogram from the Straight Creek fold illustrating the distribution of grain sizes in samples and the relative abundance of the various microstructures in different size fractions. cp = crystal plastic (Fig. A1.2), f = flattened grains (Fig. A1.3), rg = rotated grains (Fig. A1.7), c = cleavage (solution) (Fig. A1.1), st = stylolites (Fig. A1.5), mf = microfracture (intragrain) (Fig. A1.6), v = veins (Fig. A1.4). Percentages refer to the percent visible grains at 2X magnification.

Reproduced with permission of the copyright owner. Further reproduction prohibited without permission.

APPENDIX 2*- PRELIMINARY OBSERVATIONS OF THE STRAIGHT CREEK DETACHMENT ANTICLINE

This report presents preliminary findings of the 1992 field studies conducted at the Straight Creek detachment anticline (SCDA) in the northeastern Brooks Range of Alaska. The SCDA is being analyzed as part of a general, multi-faceted study of the geometric and kinematic properties of detachment folds. The purpose of this report is to describe the geometry and internal deformational features of the SCDA and to discuss its significance in the context of the general study.

The SCDA is an excellent example of a detachment fold. A detachment fold is defined as "a fold in a relatively competent rock unit that is accommodated by internal deformation of a less competent unit that is, in turn, separated by a surface or zone of displacement (detachment horizon or décollement) from another competent unit that bounds the fold" (Homza & Wallace 1995) (Fig. A2.1). Detachment folds are probably very common in fold-and-thrust belts worldwide but commonly are not recognized as detachment folds and thus are currently poorly understood (Homza & Wallace 1995).

In the general study, the geometry and strain distribution of detachment folds in the northeastern Brooks Range are being analyzed in order to develop a

---

* Published by the Alaska Division of Geological and Geophysical Surveys as Public Data File 93-43: "Preliminary observations of the Straight Creek detachment anticline-northeastern Brooks Range, Alaska: a basis for geometric and kinematic detachment fold models", by Thomas X. Homza.

Reproduced with permission of the copyright owner. Further reproduction prohibited without permission.

consistent and quantitative means of describing and reconstructing their evolution. This work aims ultimately to provide one or more actualistic geometric and kinematic models for detachment folds that will be comparable to existing models for two other common types of fault-related folds: fault-bend folds (Suppe, 1983) and fault-propagation folds (Suppe & Medwedeff 1990, Mitra 1990) (Fig. A2.2). These models have been used successfully in analyzing fault-bend and fault-propagation folds, which, together with detachment folds, represent common structural hydrocarbon trap types. However, no comparable detailed models currently exist for detachment folds. Thus, unlike the other two fold types, there is neither a widely used standard for identifying detachment folds nor a model that allows consistent and quantitative reconstructions of detachment folds. The current study seeks to develop such a model (or models) using the well-exposed detachment folds in the northeastern Brooks Range (*e.g.* the SCDA) as the primary guide in an iterative process of geometric/kinematic modeling. The main objectives of the general study are to provide:

1) a better basis for the recognition of natural detachment folds and a better understanding of their evolution.

2) a more general and applicable basis for consistent and quantitative reconstructions of natural detachment folds than is provided by existing models.

3) a model that can easily be modified to fit observed detachment fold geometries and the character and distribution of internal structures and strain within those folds.

Reproduced with permission of the copyright owner. Further reproduction prohibited without permission.

The SCDA is the first fold in the general study to be analyzed in detail. The starting point for the forthcoming modeling process is the current idealized model for detachment folds of Homza and Wallace (1995), which provides general constraints on the geometry and kinematic evolution of detachment folds. That model is very idealized because it is based on untested assumptions. The explicit assumptions of that model will be systematically tested and modified in this study, guided by the observations of natural folds, in order to produce more actualistic models. Our idealized model for detachment folds (Homza & Wallace 1995) assumes:

- Parallel folding of the competent unit (constant bed-length and thickness)
- A triangular fold form
- Constant cross-sectional area
- Constant detachment depth
- No overlap of adjacent detachment folds
- No bed-parallel shear outside of detachment anticlines
- Evolution of detachment folds by hinge migration (a consequence of some of the assumptions above)

The SCDA will be used as a guide in the process of modifying these assumptions in order to produce a "first-order" geometric and kinematic model for detachment folds. Other folds will be analyzed and all of the data will be combined in order to produce higher-order best-fit models that are designed to provide a basis for the quantitative assessment of detachment folds.

Reproduced with permission of the copyright owner. Further reproduction prohibited without permission.

The main objectives of the Straight Creek portion of the general study are to:

1) describe, in detail, the structural geometry of the SCDA.

2) assess the distribution and relative age of internal structures and strain within the SCDA.

3) develop a balanced cross section across the SCDA, incorporating geometric and strain data, to be used as a guide in developing more refined geometric and kinematic models for detachment folds.

4) identify and mathematically evaluate the natural factors that require modification of the explicit assumptions of our current model.

This project will ultimately yield a very useful tool for both understanding the evolution of external regions of mountain belts in general, and for assessing the potential of particular hydrocarbon traps. This preliminary report describes only the geometric aspects of the SCDA while the strain analyses needed for a complete kinematic description are being conducted. Since this is only a preliminary description of the first fold analyzed in the current study, no modifications to our current model are offered herein.

LOCATION AND GEOLOGIC SETTING

The SCDA is located at the headwaters of the north-flowing Straight Creek, along the eastern boundary of that watershed in the Mt. Michelson B-3 Quadrangle, Townships 2S and 1S, Ranges 27E and 28E of northeastern Alaska (Fig. A2.3). The study area covers approximately 25 km^2 in the northern Franklin Mountains of the northeastern Brooks Range (Fig. A2.3, Plate A2.1).

Reproduced with permission of the copyright owner. Further reproduction prohibited without permission.

REGIONAL STRATIGRAPHY

The rocks of the northeastern Brooks Range are divided into three sequences. In ascending stratigraphic order, these are the poly-deformed "pre-Mississippian rocks" (low-grade metasedimentary and metavolcanic basement), the Mississippian-Neocomian Ellesmerian passive continental margin sequence, and the Hauterivian-present foredeep deposits of the Brookian sequence (Fig. A2.4). A regional sub-Middle Devonian angular unconformity separates the pre-Mississippian rocks from the Ellesmerian sequence everywhere in the northeastern Brooks Range.

TECTONIC SETTING

The Brooks Range is a more than 100-km wide, east-west trending orogenic belt in northern Alaska that extends from the Yukon Territory in the east to the Chukchi Sea in the west (Moore *et al.* 1994) (Fig. A2.3). The northeastern Brooks Range fold-and-thrust belt extends north of the main axis of the Brooks Range, east of the Sagavanirktok River, as a northward convex arcuate topographic salient. The study area is part of the "western structural province" of the northeastern Brooks Range, as defined by Wallace and Hanks (1990).

The outcrop pattern in the western structural province defines a series of arcuate (northward convex) east-west trending belts alternating between pre-Mississippian rocks and Ellesmerian sequence rocks. The pre-Mississippian rocks are exposed in anticlinoria that represent horses in a regional forward

Reproduced with permission of the copyright owner. Further reproduction prohibited without permission.

(northward)-propagating duplex that extends from at least the continental divide area in the south, north to the Arctic coastal plain (Figs. A2.3 & A2.5) (Namson & Wallace 1986, Wallace & Hanks 1990). The geometry of the duplex suggests that these anticlinoria are fault-bend folded horses formed between a floor thrust in the pre-Mississippian rocks and a roof thrust in the Mississippian Kayak Shale (Namson & Wallace 1986, Wallace & Hanks 1990). The duplex has been described by Wallace (1992) as a "passive roof duplex", a duplex in which displacement on the roof thrust is in a hindward direction (Banks & Warburton 1986).

Shortening above the roof thrust in the Kayak Shale has been accommodated primarily by kilometer-scale detachment folds with a distinct lack of thrust faults (Wallace & Hanks 1990, Wallace 1992). The detachment folds are defined by the competent carbonates of the Mississippian-Pennsylvanian Lisburne Group while the Kayak Shale serves as the detachment horizon. A south-directed, or back-thrust, sense of displacement (with respect to the underlying duplex) is accommodated by these detachment folds (Wallace 1992). The SCDA represents a well-exposed example of one of these detachment folds and it is thought to be located structurally above the hangingwall ramp of the "northern Franklin Mountains horse" of the regional duplex. This is the second major horse north of the currently recognized southern limit of the duplex (Wallace 1992).

Reproduced with permission of the copyright owner. Further reproduction prohibited without permission.

PREVIOUS REGIONAL WORK

Significant summary studies

Moore *et al.* (1994) present an overview of the geologic history of the northeastern Brooks Range. An overview of, and model for, the structure of the northeastern Brooks Range is presented by Wallace and Hanks (1990), and an alternative model by Oldow *et al.* (1987). Regional geologic maps include Bader and Bird (1986) and Reiser *et al.* (1980).

Local geologic work

A sedimentologic study of the Mississippian Endicott Group was carried out near the headwaters of Straight Creek by LePain (1993). Structural studies, focusing on the nature of the sub-Mississippian rocks and sub-Mississippian unconformity (SMU) were conducted by Oldow *et al.* (1987) with the aim of addressing more regional tectonic issues. Wallace (1992) described the structure along a north-south transect across the northeastern Brooks Range, including the study area, and defined the geometry of a passive roof duplex overlain by detachment folds.

DETACHMENT FOLDS

Alternating mechanically competent and incompetent rock units constitute the stratigraphy in most fold-and-thrust belts, and folds in relatively competent units with thickened internally deformed weaker rock in their cores - detachment folds - are very common structural features. The SCDA is an excellent example of a detachment fold with all of the defining features exposed (compare Fig. A2.1

Reproduced with permission of the copyright owner. Further reproduction prohibited without permission.

& Plate A2.2), including the competent unit (the Lisburne Limestone), the incompetent unit (the Kayak Shale), the detachment zone (near the base of the Kayak Shale), and the bounding competent unit (the Mississippian Kekiktuk Conglomerate together with the pre-Mississippian rocks).

Previous studies of detachment folds

Structural geometries characteristic of detachment folds have been recognized since the 19th century (see Willis & Willis 1934 for a review). Dahlstrom (1969, 1990) described the fundamental geometric characteristics of detachment folds and qualitatively suggested inherent kinematic constraints upon them. Homza and Wallace (1995) have developed a succinct definition for detachment folds, as given above.

Using the conservation of bed-length and area, Jamison (1987) and Mitra and Namson (1989) presented trigonometric analyses of detachment folds. Although these were important conceptual studies, these models address a relatively restricted range of detachment fold geometries and they do not consider the full range of variables that influence the geometry and kinematic behavior of detachment folds. Homza and Wallace (1995) also used the conservation of bed-length and area in developing a very idealized geometric model for detachment folds that allows calculation of either shortening or detachment depth using fold geometry and requires hinge-migration kinematics. This model provides the conceptual basis for the present study.

Reproduced with permission of the copyright owner. Further reproduction prohibited without permission.

Significance of detachment folds

Detachment folds are one of three currently recognized thrust-related folds observed in fold-and-thrust belts (Jamison 1987) (Fig. A2.2). The other two types are fault-bend folds (Suppe 1983) and fault-propagation folds (Suppe & Medwedeff 1990, Mitra 1990). Detachment folds differ from the other two types in that detachment folds do not initially involve thrust ramps in their cores, but rather involve structurally thickened incompetent rock in that position. Detachment folds may be truncated by thrust faults after their formation making them difficult to distinguish from fault-propagation folds (Homza 1992a).

The importance of distinguishing among these three thrust-related fold types stems from the fact that they each evolve along significantly different kinematic paths resulting in different geometries. In order to predict subsurface geometries accurately, the petroleum geologist must correctly identify the fold-type and apply a quantitative model to constrain the possible geometric solutions for the target. Also, balancing structural cross sections to understand the evolution of the external regions of mountain belts requires the correct choice of fold-type and model. Thus, from both an applied and purely scientific standpoint, the nature of detachment folds is of significance.

The kinematics of detachment folds - hinge migration or fixed arc-length folding?

Empirical observations and mechanical considerations suggest that buckle folds in a competent layer bounded by incompetent material nucleate with an arc-length that is a function of rheology and competent layer thickness, and retain a constant arc-length (and hence, fixed hinges) as shortening increases

Reproduced with permission of the copyright owner. Further reproduction prohibited without permission.

and the fold grows (de Sitter 1956, Biot 1961, Currie *et al.* 1962, Ramberg 1964, Ramsay 1967, 1974, Johnson 1977, Abassi & Mancktelow 1992, Fischer *et al* 1992, Mancktelow & Abassi 1992) (Fig. A2.12a). Mitchell and Woodward (1988) assumed that detachment folds form by this fixed arc-length buckling mechanism, and Fischer *et al.* (1992) provide evidence for fixed-hinge growth of several natural folds that could be interpreted as detachment folds.

Dahlstrom (1990) pointed out that fixed arc-length folding is incompatible with the fundamental concept of conservation of cross-sectional area, which implies a linear relationship between shortening and cross-sectional area uplifted above base level (*e.g.* Fig. A2.13). In contrast, Wiltschko and Chapple (1977) documented a non-linear relationship between uplifted area and shortening for symmetrical fixed arc-length folds (Fig. A2.14). The apparent contradiction is particularly obvious for folds with interlimb angles less than about 60^{o}, for which there is an inverse non-linear relationship between uplifted area and shortening (Wiltschko & Chapple 1977). These relationships suggest that a fixed arc-length fold cannot evolve with a fixed detachment depth and still obey the law of conservation of cross-sectional area. Wiltschko and Chapple (1977) resolved this apparent contradiction by assuming that incompetent material moves from synclines to anticlines as uplifted area initially increases, then flows out of the anticlines as area decreases with increasing shortening. In this case, the detachment depth is not fixed.

In order for a detachment fold to grow with a fixed detachment depth, the uplifted area in its core must increase linearly as shortening increases. This requires an increase in the length of at least one fold limb, which in turn requires

Reproduced with permission of the copyright owner. Further reproduction prohibited without permission.

hinge migration (Fig. A2.12b). Growth of folds by hinge migration has been documented for kink bands (Weiss 1968, Stewart & Alvarez 1991), and has been used to model fault-bend folds (Suppe 1983) and fault-propagation folds (Suppe & Medwedeff 1984, 1990). Dahlstrom (1990) concluded that growth of detachment folds by hinge migration is likely, and the geometric models of Jamison (1987) and Mitra and Namson (1989) both assume a fixed detachment depth and fold growth by hinge migration. Hinge-migration kinematics are not an initial assumption of the current idealized model of Homza and Wallace (1995), hinge migration is a required consequence of the model.

Thus, a very fundamental question remains unanswered: What geometric and kinematic paths do detachment folds follow? The present study aims to address this question by evaluating natural fold geometries and kinematic indicators and to produce a better kinematic model for detachment folds based on the natural constraints. Some of the preliminary observations of the SCDA that bear on fold kinematics are noted below.

METHODS

This general study of detachment folds uses several distinct but related techniques. Geologic mapping (scale:1:25,000) is the essential data base, since it provides the basis for creating balanced cross sections which, in turn, establish a first-order approximation of the fold geometry. The cross section of the SCDA (Plate A2.2) represents such a first-order approximation. This geometry will be refined on the basis of detailed strain analyses carried out on a variety of strain indicators using the Rf-ϕ method (Ramsay & Huber 1983, 1987).

Reproduced with permission of the copyright owner. Further reproduction prohibited without permission.

The modeling process involves use of trigonometry to relate fold geometry and conservation of mass. A series of iterations will be done in which observations will guide changes in assumptions of Homza and Wallace (1995). Such changes limit the viable geometries and a best-fit match between natural folds and the model will be derived. The AutoCAD graphics package is used in constructing both the balanced cross sections and the geometric and kinematic models (Homza 1992b).

GEOMETRY AND INTERNAL STRUCTURES OF THE STRAIGHT CREEK DETACHMENT ANTICLINE

The SCDA is an open, inclined, angular anticline that plunges 15 degrees to N87E. Competent carbonates of the Lisburne Group define the fold with a wavelength of about 840m, and the incompetent shales of the Kayak Shale are about 1.5 times thicker in the core than beneath the limbs of the SCDA (Plate A2.2). Plate A2.2 is a balanced cross-section of the SCDA that is considered preliminary since it does not yet include strain data. The fold sits structurally above a relatively planar, north-dipping detachment surface near the base of the Kayak Shale that separates it from an underlying structurally competent package of rock. This lower structural package includes the Kekiktuk Conglomerate, the sub-Mississippian unconformity, and the pre-Mississippian rocks. Figure A2.6 displays the stratigraphy of the SCDA.

Although its axial surface dips about 58°S, the SCDA is relatively symmetrical and its axial surface is near-perpendicular to the underlying detachment surface. Its north limb (forelimb) is steep to overturned and its

Reproduced with permission of the copyright owner. Further reproduction prohibited without permission.

backlimb dips gently northward. A more complete numerical description of the fold is provided on plate A2.2. Observations of outcrop-scale structures are discussed below. Microscopic features have not yet been analyzed and, as a result, the amount of layer-parallel shortening and the distribution and significance of strain and incompetent flow are currently undetermined.

Internal structures of the Lisburne Limestone

The overall structural character of the Lisburne Limestone is dependent on both its internal stratigraphy and its structural position within the SCDA. A much greater frequency and degree of strain is observed near the hinge of the fold than is seen on the limbs and flexural-slip folding is indicated by limb structures. A N-S striking, essentially vertical joint set is everywhere in the Lisburne Group at Straight Creek.

The Lisburne Limestone in this area is divided into informal "lower" and "upper" structural units that are separated by a zone of weakness controlled by a competency contrast that displays structures indicating primarily bed-parallel displacement (minor shear zones, slickenfibers). The 60m thick lower Lisburne is composed of red-stained wackestone and packstone beds that are up to 1 meter thick whereas the 700m-thick upper Lisburne is characterized by 1m-5m thick beds of gray and tan mudstone to grainstone. The nature of folds that are parasitic to the SCDA defines the primary structural difference between the upper and lower Lisburne Group. The thinner beds of the lower Lisburne are commonly tightly folded (interlimb angles commonly less than 60^0), especially near the hinge of the SCDA, their axial surfaces are inclined toward the core of the larger fold. The thicker upper Lisburne beds display fewer folds that are

Reproduced with permission of the copyright owner. Further reproduction prohibited without permission.

gentle (interlimb angles about 130^0) with axial surfaces also inclined toward the core of the fold with no obvious sense of vergence.

Limb structures

Outcrop-scale internal deformational features within the Lisburne Group on the limbs of the SCDA include parasitic folds (with wavelengths of meters in the lower Lisburne and 10's of meters in the upper Lisburne), en echelon tension fractures, slickenfibers on interbed fault zones, minor thrust faults, and stylolites. The distribution and orientation of these features suggest flexural-slip folding: a north-over-south sense shear on the north limb (forelimb) and a south-over-north sense of shear on the southern limb (Fig. A2.7).

Hinge structures

The Lisburne Limestone in the hinge area of the SCDA is highly strained. As a result, the upper Lisburne has been eroded, leaving only the lower Lisburne exposed. Tight, overturned folds with calcite-filled saddle reefs (Ramsay 1974), penetrative slatey cleavage, and minor south-over-north thrust faults are densely distributed in the hinge zone (Fig. A2.7). In outcrop, the pervasive cleavage obliterates macrofossils and all but the most distinct bedding surfaces; microscopic observations are pending. It is important to note that the structures distinguishing the hinge and limb areas were nowhere observed to overprint each other.

Internal structures of the Kayak Shale

Like the Lisburne Limestone, the structural character of the Kayak Shale is dependent on both its internal stratigraphy and its structural position within the

Reproduced with permission of the copyright owner. Further reproduction prohibited without permission.

SCDA. The variation in structural character as a function of structural position is particularly evident in the Kayak where two mechanically competent siliceous units approximately 10m thick are present between thicker incompetent units of shale that contain many meter-thick competent sand horizons (LePain 1993). These different lithologies/competencies record different deformational features with the most important being the spectacularly folded competent units (Fig. A2.8). These folds are disharmonic with respect to the SCDA and are an order of magnitude smaller. The same N-S striking, steeply dipping joint set present in the Lisburne Limestone is evident in the Kayak Shale, especially in the competent units.

Limb structures

Structures within the Kayak Shale beneath the limbs of the SCDA include parasitic folds, minor thrust faults, "ductile" shear zones in shale units, and minor stylolites. Shear indicators, especially small scale folds in meter-thick sand horizons, show a south-over-north sense of shear on the backlimb of the SCDA and a north-over-south sense of shear on the forelimb.

Hinge structures

The hinge zone of the SCDA in the Kayak Shale is dominated by intense penetrative solution cleavage in shale units and tight folds in competent sand units (up to 10m in wavelength). Although centimeter-scale parasitic isoclinal folds are recognizable in shale horizons beneath the limbs of these folds, bedding in the shale horizons that occupy fold cores is transposed and nearly obliterated by the cleavage (Fig. A2.9). Shale units have been nearly

Reproduced with permission of the copyright owner. Further reproduction prohibited without permission.

completely squeezed out of the cores of these folds (Fig. A2.10). The folded thicker competent units show randomly distributed, closely spaced, quartz-filled fractures and minor thrust faults in the hinge zones (Fig. A2.10). These folds in the SCDA hinge zone show no dominant sense of vergence.

The bounding synclines of the Straight Creek detachment anticline

Establishing the geometry of adjacent folds in both the competent and incompetent units is critical in the analysis of any one detachment fold because this geometry influences the modeling process. In other words, the geometry and kinematics of adjacent folds are intimately related to that of the fold under consideration.

The syncline adjacent to the forelimb of the SCDA - the "forelimb syncline" - is a multi-panel, gentle, upright (with respect to the detachment) fold. The most significant hinge of this fold, in terms of modeling, is the southernmost hinge because this is the closest hinge to the SCDA and it is the hinge that marks the transition in the thickness in the Kayak Shale: south of this hinge, the Kayak drastically thickens toward the anticlinal core of the SCDA. Poor exposures north of the southernmost hinge of the forelimb syncline limit accurate estimations of the thickness of the Kayak Shale in this area. However, north-over-south shear indicators in the Kayak in the vicinity of the southernmost hinge of the forelimb syncline are present. In the Lisburne Limestone, the southernmost hinge zone is composed of angular parasitic folds rather than a single hinge. The hinge zones of each of these folds display structures indicative of irreversible strain such as penetrative cleavage, minor faults, and abundant veins.

Reproduced with permission of the copyright owner. Further reproduction prohibited without permission.

The "backlimb syncline" of the SCDA is fully exposed at Straight Creek. It is a gentle and upright (with respect to the detachment) fold (Plate A2.2). The Lisburne Limestone is folded in the hinge area into several open folds that display only minor penetrative fabrics, and south-over-north shear indicators in the Kayak Shale beneath this fold suggest thinning beneath the hinge. This thinning is not directly observed, but instead, the thickness of the Kayak beneath the panel south of the hinge of the backlimb syncline is approximately equal to (or even less than) that beneath the hinge. Thus, the observed geometry shows a gradational increase in the thickness of the Kayak from south of the backlimb syncline north to the anticlinal core.

Structural significance of the Kekiktuk Conglomerate, the detachment, and the sub-Mississippian unconformity

A form surface defined by the top of the Kekiktuk Conglomerate traces a north-dipping panel (27^{o}) in the area and is thought to reflect the geometry of the forelimb of the underlying northern Franklin Mountains horse (Namson & Wallace 1986, Wallace 1992). The upper part of the Kekiktuk displays several tight, north-vergent folds (Fig. A2.11), but Their bases are not exposed. These folds may have formed above a detachment within the Kekiktuk or they could reflect deformation in the pre-Mississippian rocks. Overall, the Kekiktuk appears to accommodate much less shortening than the overlying Kayak and Lisburne. Only local indications of significant internal penetrative strain (crenulation cleavage, quartz veining) are apparent within the Kekiktuk and are associated exclusively with the tight folds.

Reproduced with permission of the copyright owner. Further reproduction prohibited without permission.

Shortening in the Kekiktuk is about 43% that of the Kayak (Plate A2.2). This change in the amount of shortening occurs over a narrow stratigraphic zone. This situation requires detachment between the Kayak and the Kekiktuk and that the detachment horizon exist in this narrow zone near the bottom of the Kayak Shale or directly along the stratigraphic contact.

The erosional sub-Mississippian unconformity is exposed in several places in the study area. There is no observed indication of shear along the unconformity, nor are there any faults observed to truncate the unconformity. This, coupled with the general lack of internal strain observed in the Kekiktuk, suggests that the conglomerate accommodates the same amount of Brookian shortening as the underlying pre-Mississippian rocks. This is consistent with observations from other parts of the northeastern Brooks Range by Wallace and Hanks (1990), but is inconsistent with observations very near this study area by Oldow *et al.* (1987), who noted areas both of no shear and of "substantial shear" along the unconformity.

Preliminary conclusions

Observations from the SCDA require modification of the constant-area assumption of our current model (Homza & Wallace 1995) and may or may not require modification of the kinematic consequence of our model: hinge migration kinematics. These issues are discussed separately below.

1) The presence of significant penetrative solution cleavage in the Kayak Shale in the core of the anticline strongly suggests that there was a component of mass-movement out of the core of the SCDA during fold formation. If this is true, then the modeling assumption of constant cross-sectional area is invalid

Reproduced with permission of the copyright owner. Further reproduction prohibited without permission.

here. The significance of this will be more fully understood when thin-section analyses provide quantitative estimates of the amount of area that was lost to solution.

2) There is excess material within the Kayak Shale in the anticlinal core of the fold that cannot be accounted for elsewhere. That is, there is not an observed area deficiency elsewhere in the Kayak (this deficiency may exist beneath the forelimb of the SCDA, but this area is not exposed). This geometry is relatively consistent with a hinge-migration kinematic model for detachment folds since a linear increase in limb-length as shortening increases could accommodate the excess area without a decrease in area beneath the limbs or adjacent synclinal hinges. In contrast, the observation of no apparent overprinting relationships between hinge and limb structures in the Lisburne Limestone of the SCDA suggests that the hinges of the SCDA did not migrate since a) the current anticlinal forelimb synclinal hinge zones display penetrative and irreversible strain, and b) evidence of similar strain (*i.e.* tight folds, penetrative cleavage) would be expected to be overprinted in fold limbs by structures indicative of limb deformation if hinges migrated. This observation argues for a fixed arc-length kinematic model for the SCDA. Thus, it is not clear whether the SCDA evolved only by a fixed arc-length process or by a combination of fixed arc-length and migrating-hinge processes, but at least two hinges appear to have been fixed during folding. Future detailed modeling including strain data may clarify this uncertainty.

Reproduced with permission of the copyright owner. Further reproduction prohibited without permission.

SUMMARY AND FUTURE RESEARCH

The Straight Creek Detachment Anticline (SCDA) is a well-exposed detachment fold at the headwaters of Straight Creek in the northeastern Brooks Range. This study of the SCDA has produced much useful data about the geometry and kinematics of detachment folds. These data are presented here in the form of a preliminary balanced cross section of the SCDA. Strain analyses are not yet complete and thus, are not incorporated in the present cross section.

Study of the SCDA represents the first stage in a general study of detachment folds and the information gleaned from the SCDA will provide important constraints concerning the geometry and kinematics of detachment folds. The results thus far suggest that the folding occurred mainly by flexural-slip, that the fold evolved with at least some fixed hinges, and that at least one of the common geometric assumptions about detachment folds (*i.e.* constant area) may be invalid.

Data obtained at Straight Creek will be incorporated with similar data from other detachment folds in the northeastern Brooks Range. All of this information will be used in an iterative modeling process involving modification of the assumptions of our current model (Homza & Wallace 1995) in order to develop an actualistic quantitative geometric and kinematic model (or models) for detachment folds. Such a model may be used to provide constraints on the evolution of fold-and-thrust belts worldwide and to better define the geometry of common structural hydrocarbon traps.

Reproduced with permission of the copyright owner. Further reproduction prohibited without permission.

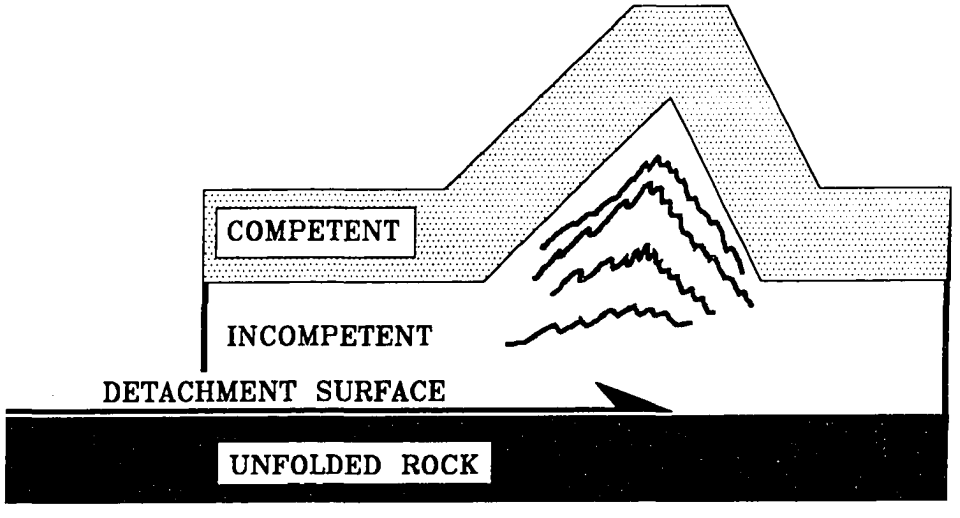

Figure A2.1. Schematic diagram showing the essential elements of a detachment fold.

Reproduced with permission of the copyright owner. Further reproduction prohibited without permission.

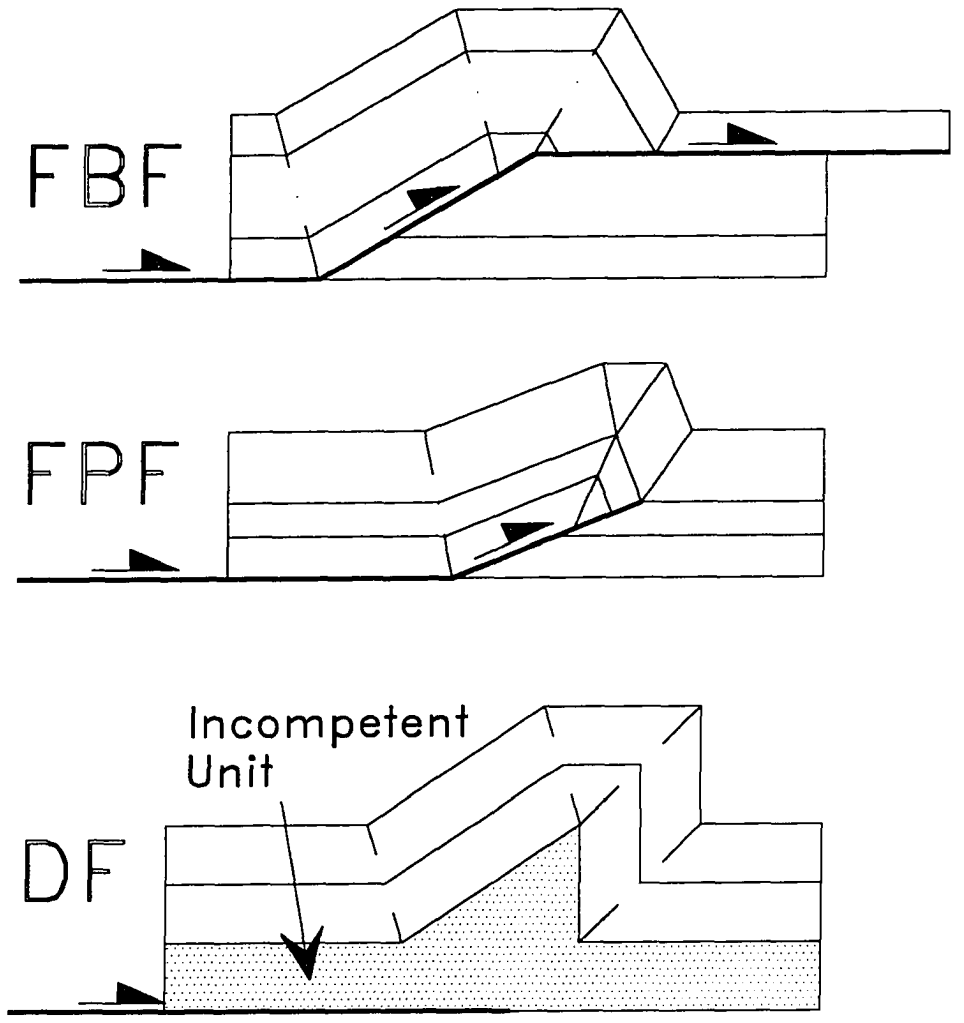

Figure A2.2. Three generic types of thrust-related folds in fold-and-thrust belts: Fault-bend folds (FBF), fault-propagation folds (FPF), and detachment folds (DF).

Reproduced with permission of the copyright owner. Further reproduction prohibited without permission.

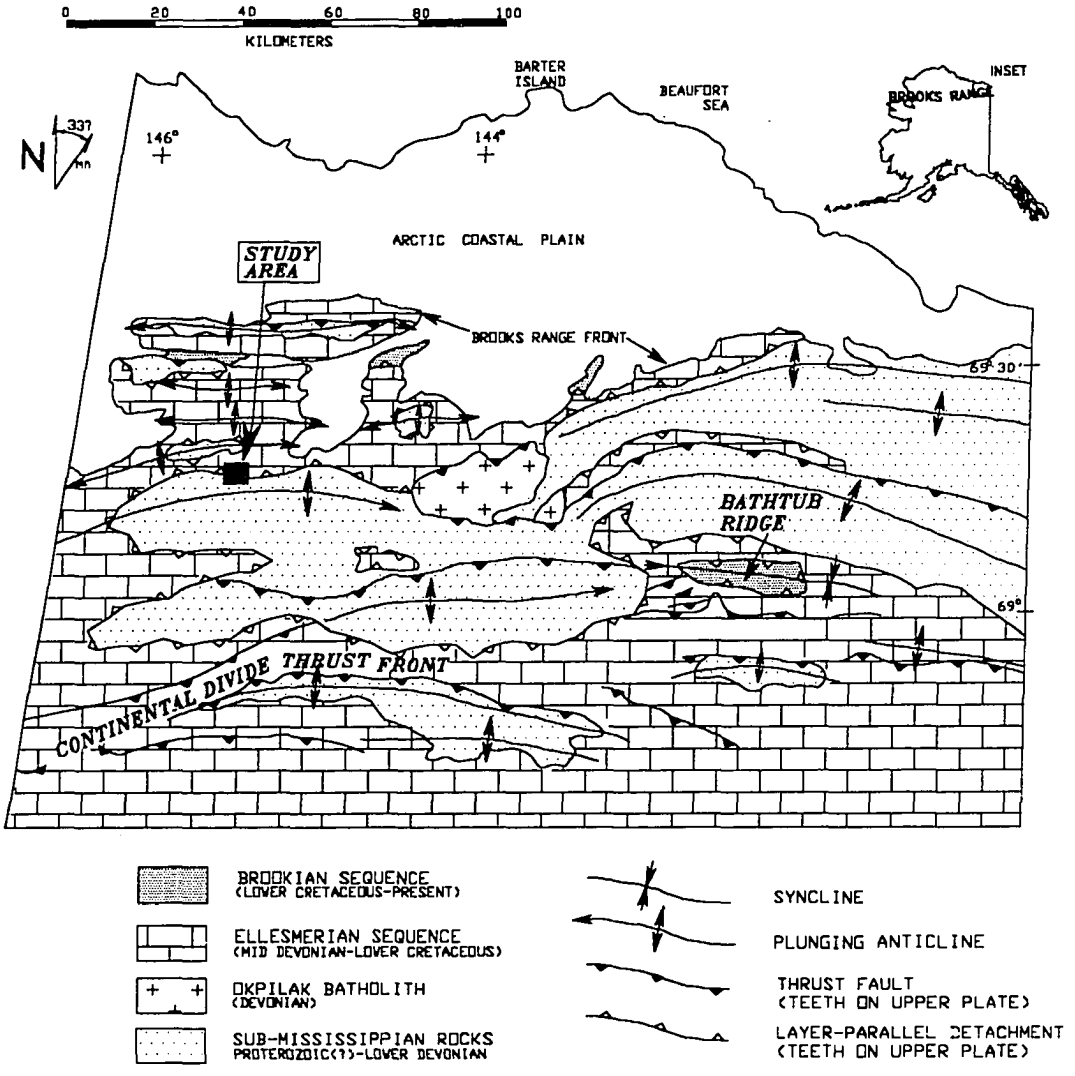

Figure A2.3. Tectonic map of the northeastern Brooks Range, showing location of the study area.

Reproduced with permission of the copyright owner. Further reproduction prohibited without permission.

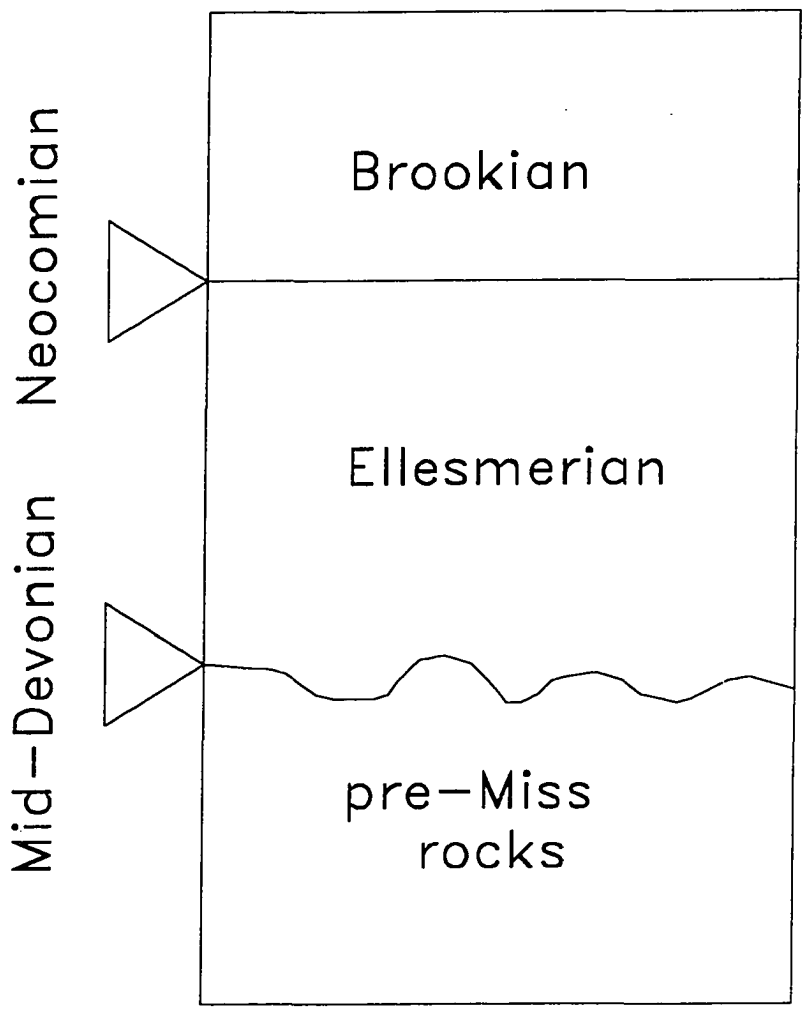

Figure A2.4. Stratigraphic column of the 3 general sequences of rock in the northeastern Brooks Range.

Reproduced with permission of the copyright owner. Further reproduction prohibited without permission.

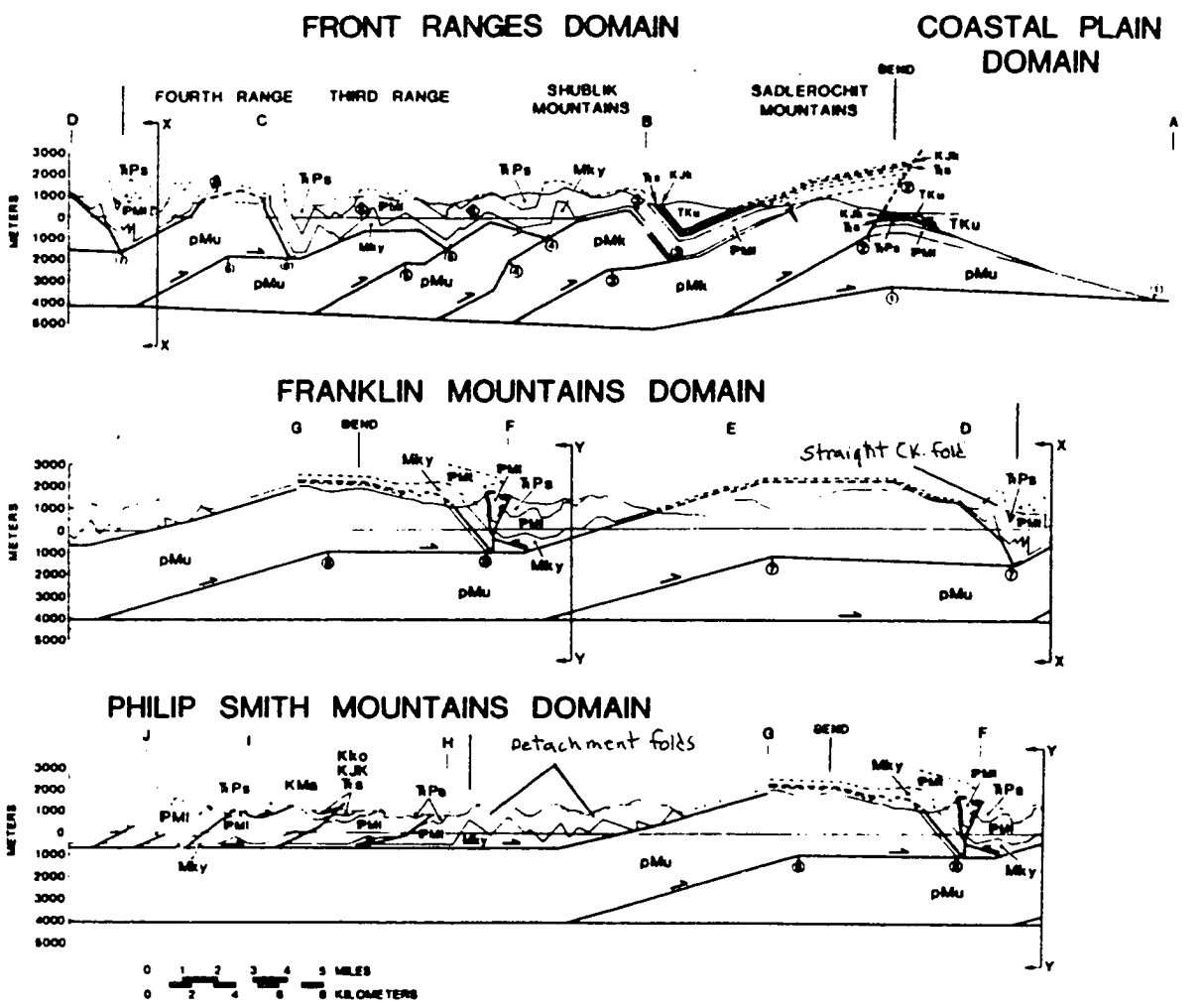

Figure A2.5. Balanced cross section across the western structural province of the northeastern Brooks Range (Wallace & Hanks 1990). Section is from the continental divide area (Fig. A2.1.) north to the coastal plain. From Namson & Wallace (1986).

Reproduced with permission of the copyright owner. Further reproduction prohibited without permission.

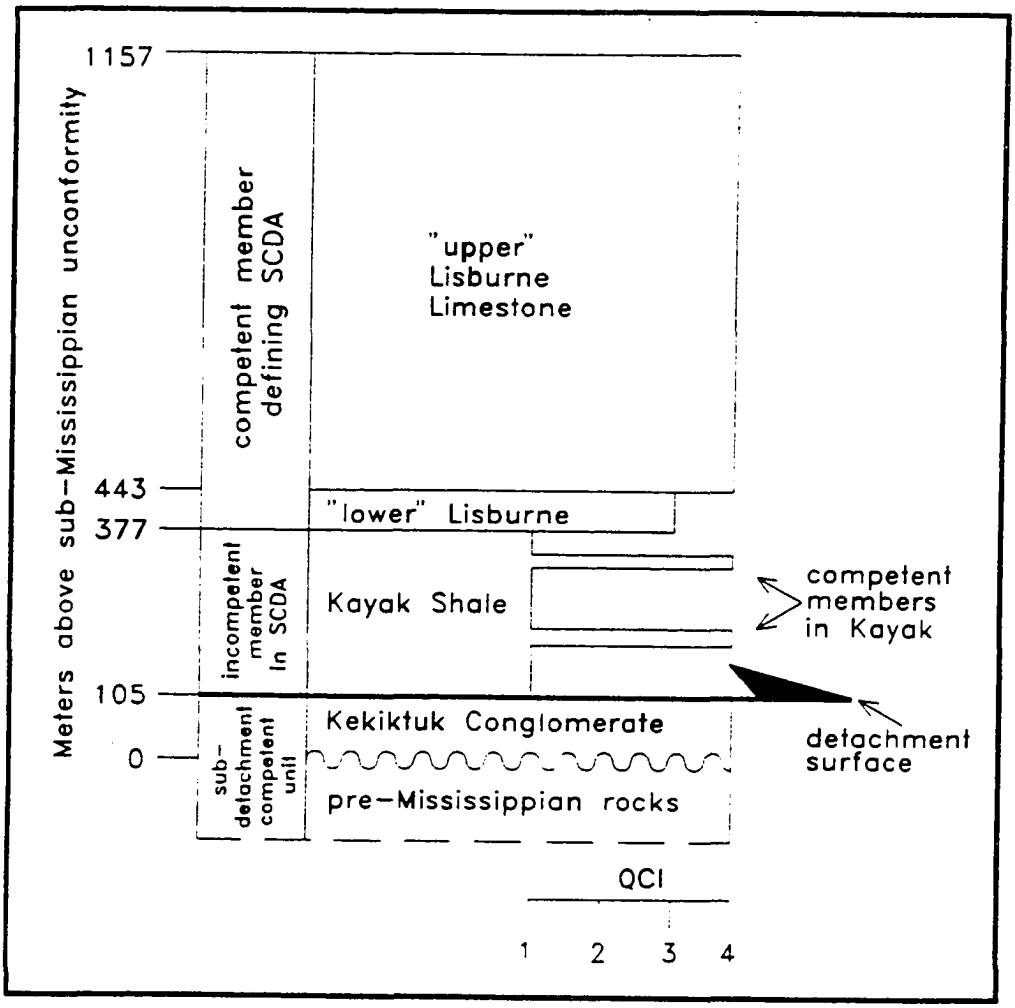

Figure A2.6. General stratigraphic column of structural stratigraphy in the Straight Creek headwaters area. QCI = Qualitative competency index, larger values indicate more competent units. That is, a QCI of 1 means the unit has between 0 and 25% competent beds and that the average thickness of the competent beds is less than 0.25m. A QCI of 4 is used to describe a unit made up of more than 75% competent beds that are greater than 0.25m thick. QCIs of 2 and 3 are of intermediate competency (after Homza 1992a).

Reproduced with permission of the copyright owner. Further reproduction prohibited without permission.

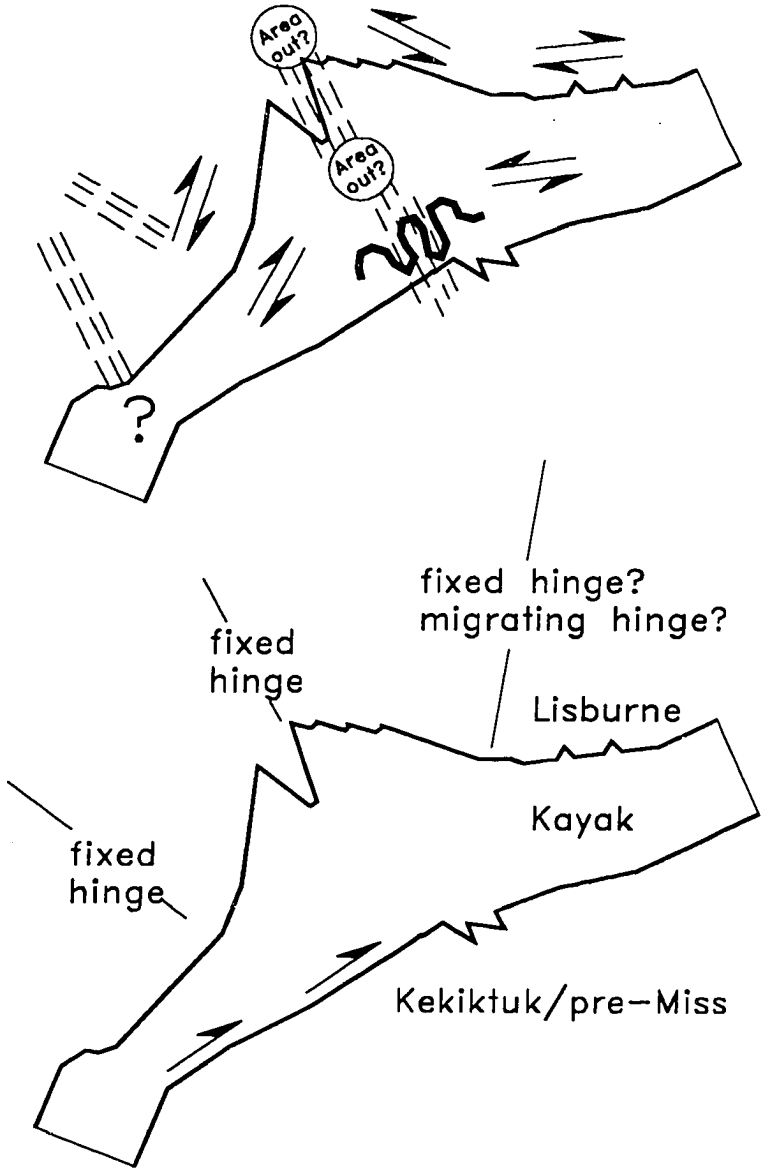

Figure A2.7. Diagrammatic sketch of the distribution of the significant outcrop-scale structures observed across the Straight Creek detachment anticline (upper sketch) and the interpreted kinematic constraints imposed upon the modeling process by these observations (lower sketch).

Reproduced with permission of the copyright owner. Further reproduction prohibited without permission.

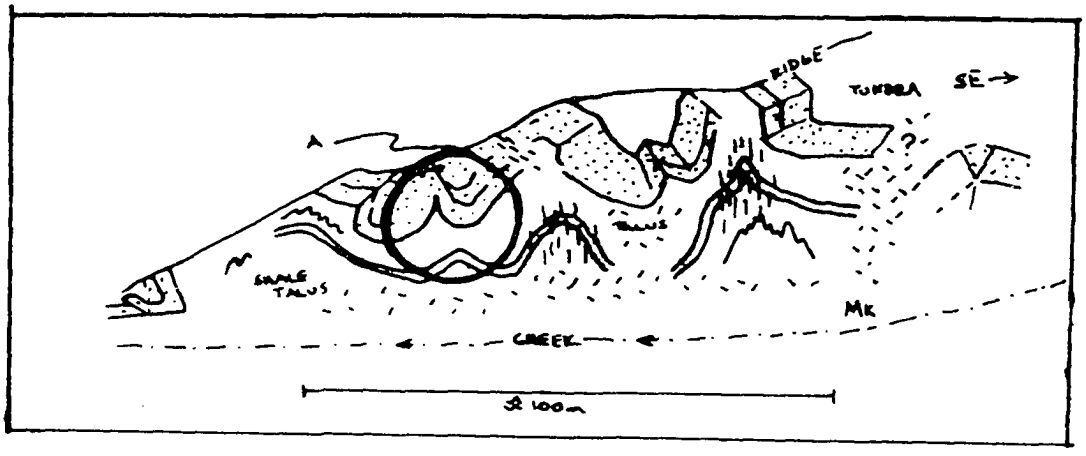

Figure A2.8. Sketch of the folds observed in the lower siliceous unit of the Kayak Shale observed in the lower parts of the core of the Straight Creek detachment anticline. Area A is shown in figure A2.10.

Reproduced with permission of the copyright owner. Further reproduction prohibited without permission.

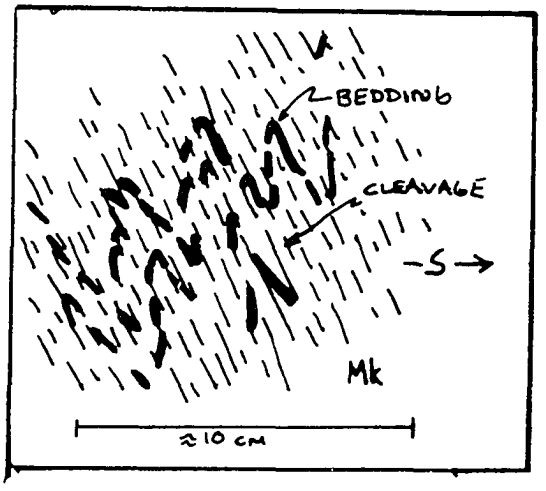

Figure A2.9. Sketch of transposed bedding observed in the shale units in the upper parts of the Kayak Shale in the core of the Straight Creek detachment anticline.

Reproduced with permission of the copyright owner. Further reproduction prohibited without permission.

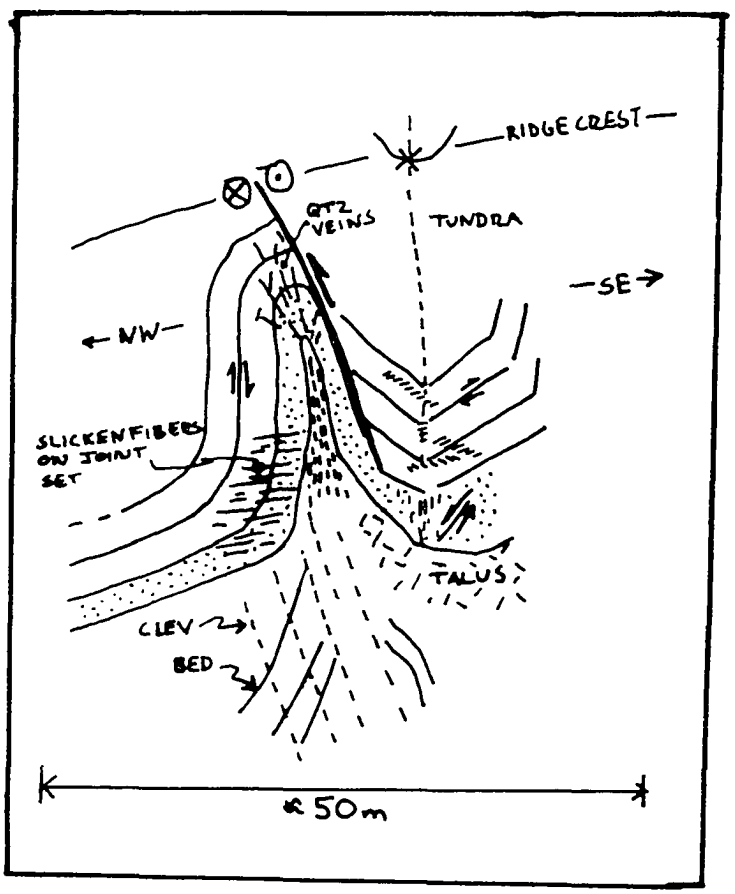

Figure A2.10. Sketch showing an example of the distribution of structures associated with the tight folds of the lower siliceous unit of the Kayak Shale (Fig. A2.8).

Reproduced with permission of the copyright owner. Further reproduction prohibited without permission.

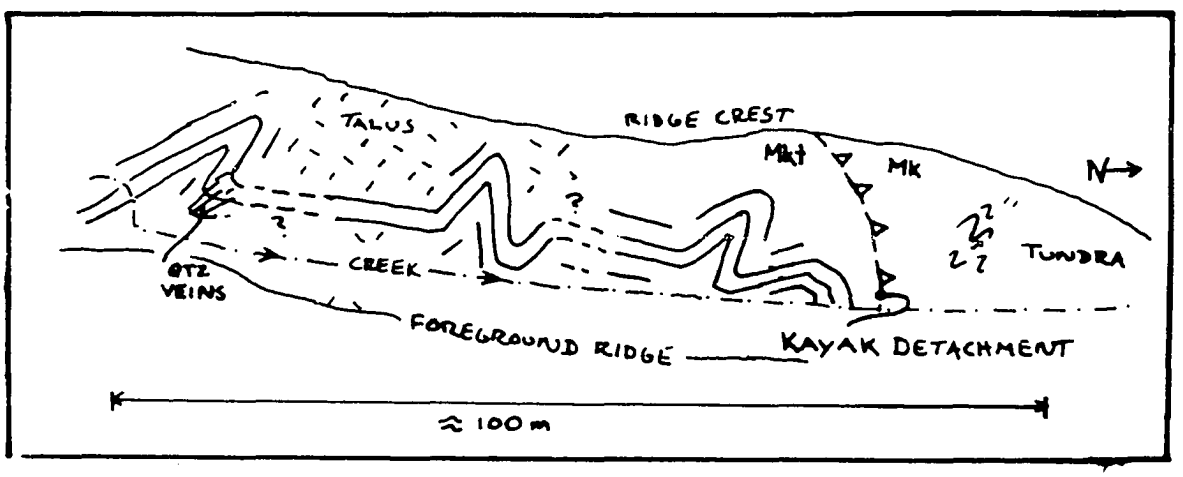

Figure A2.11. Sketch of the tight folds observed in the upper Kekiktuk Conglomerate beneath the detachment horizon in the Kayak Shale.

Reproduced with permission of the copyright owner. Further reproduction prohibited without permission.

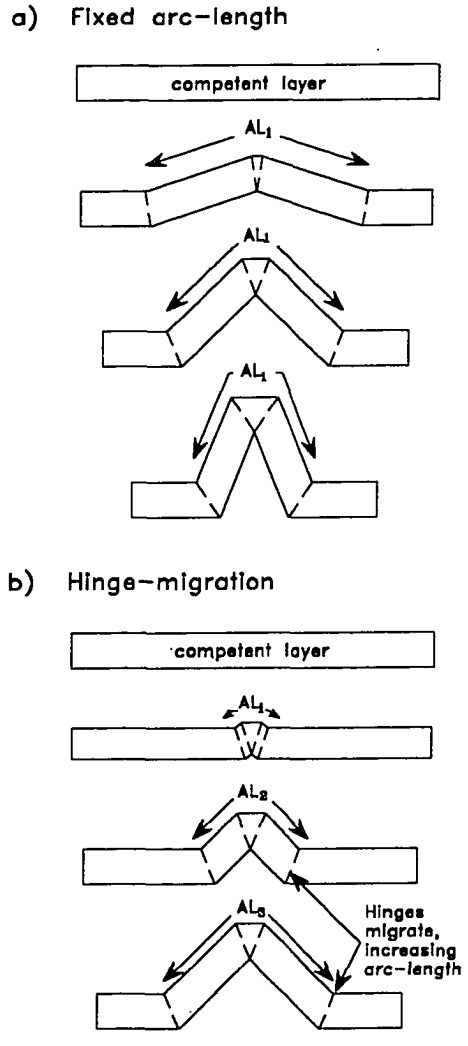

Figure A2.12. Diagram illustrating the kinematic distinction between fixed-arc length folding and migrating-hinge folding. Migrating hinge kinematics suggests the existence of overprinting relationships on the limbs of folds (limb structures overprinting hinge structures).

Reproduced with permission of the copyright owner. Further reproduction prohibited without permission.

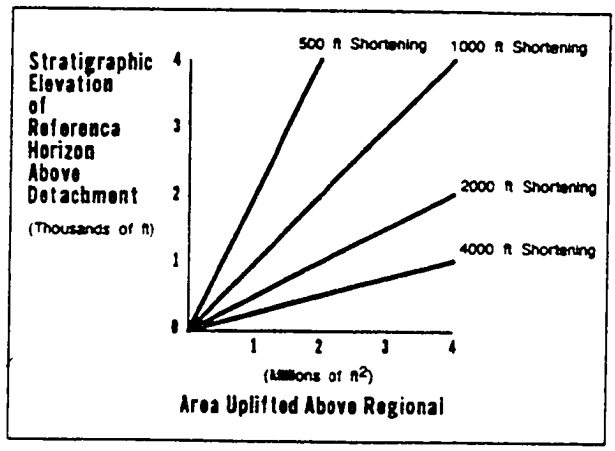

Figure A2.13. Linear relationship among shortening (S), detachment depth (D), and area uplifted beneath an idealized detachment anticline (A) (SD=1/2(A)). From Dahlstrom (1990).

Reproduced with permission of the copyright owner. Further reproduction prohibited without permission.

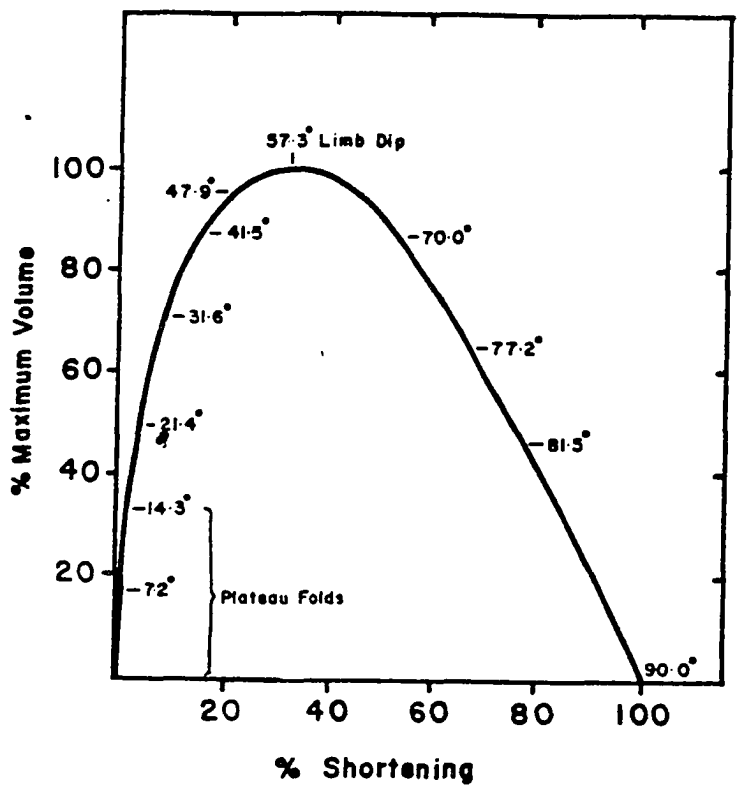

Figure A2.14. Non-linear relationship between cross-sectional area and shortening for a fixed arc-length fold (From Wiltschko & Chapple 1977).

Reproduced with permission of the copyright owner. Further reproduction prohibited without permission.

APPENDIX 3*- THE DETACHMENT FOLDS IN THE FRANKLIN MOUNTAINS WEST OF THE CANNING RIVER

The purpose of this report is to present the results of field work conducted during the summer of 1993 at two localities near the Canning River in the northeastern Brooks Range of Alaska (Fig A3.1). The two study areas each expose part of a regional north-directed duplex, which extends from the continental divide of the northeastern Brooks Range northward to the Arctic coastal plain (Namson and Wallace 1986; Wallace and Hanks, 1990; Wallace, 1993). Overlying the duplex are kilometer-scale detachment folds which record deformation in the detached roof sequence. The field work was specifically directed toward documenting and interpreting the geometry and kinematic history of these detachment folds.

This study addresses two primary questions:

1) What is the geometry and kinematic history of individual detachment folds in the area? It is unclear whether detachment folds form by a process of hinge-migration (*i.e.* kinking) (Dahlstrom 1990) above a detachment unit of constant thickness or by a process of fixed-hinge buckling above a detachment unit that changes thickness during folding. This study suggests that at least some of the major detachment folds formed as a result of fixed-hinge buckling

* Published by the Alaska Division of Geological and Geophysical Surveys as Public Data File 94-43: "The structural geometry of detachment folds above a duplex in the Franklin Mountains, northeastern Brooks Range", by Thomas X. Homza.

Reproduced with permission of the copyright owner. Further reproduction prohibited without permission.

above a detachment unit that changed thickness during deformation (Homza & Wallace 1995).

2) What constraints does the geometry of both the duplex and the roof sequence place on the kinematic history of the duplex? Wallace (1993) suggested that many of the detachment folds in the northeastern Brooks Range formed in response to a southward, or backthrust, sense of displacement due to the northward emplacement of horses in the underlying duplex. Results based on the geometric analyses and qualitative strain observations of this study agree with Wallace's (1993) conclusions but also show that a significant portion of the deformation in this area was north-directed. This suggests that the system formed by a process involving both forward and hindward displacements (*e.g.* Dunne & Ferrill 1988).

This report is organized as follows: First, a general geologic description of the region is provided, then pertinent observations from the two study areas, the "northern area" and "southern area", are presented. Finally, conclusions are discussed about 1) the geometry and kinematics of the detachment folds in the area and 2) the relationship between the emplacement of the underlying duplex and the kinematics of the roof sequence.

LOCATION, METHODS, AND GENERAL STRUCTURAL SETTING

The northern area covers approximately 100 km^2 in the central part of the Mt. Michelson A-4 quadrangle along the drainage divide between Salisbury Creek and Plunge Creek (Fig. A3.1, Plate A3.1). The southern area includes about 80 km^2 of the south-central portion of the Mt. Michelson A-4 quadrangle

Reproduced with permission of the copyright owner. Further reproduction prohibited without permission.

and the north-central part of the Arctic D-4 quadrangle (Fig. A3.1, Plates A3.3 & A3.4). The areas are separated by about 10 km. Geologic maps (scale = 1:25,000, Plates A3.1 & A3.3) and cross sections (Plates A3.2 & A3.4) were constructed using AutoCAD software.

Both study areas are part of the North Slope subterrane of the Arctic Alaska terrane (Moore *et al.* 1992, 1994) and include both pre-Middle Devonian rocks, here loosely referred to as "basement", and younger cover rocks consisting mainly of the lower part of the Mississippian to Neocomian Ellesmerian sequence (Plate A3.1). The dominant structures of the areas are part of a north-directed fold-and-thrust belt formed during the Cenozoic Romanzof uplift of Moore *et al.* (1992). Two regional structural highs, the "northern Franklin Mountains anticlinorium" and the "southern Franklin Mountains anticlinorium" occur in the northern and southern study areas, respectively. Structural contours in each area define a westward convex map pattern reflecting the westward plunge of the anticlinoria (Wallace & Hanks 1990) (Fig. A3.1). Each anticlinorium is composed of two elements: 1) a basement core, interpreted to be an east-west trending fault-bend folded horse in a regional-scale northward-directed duplex with a roof thrust in the Mississippian Kayak Shale and a floor thrust at an unknown depth in the basement (Namson & Wallace 1986, Wallace & Hanks 1990, Wallace 1993). These basement cores are referred to as the northern and southern Franklin Mountains horses; and 2) a roof sequence deformed into kilometer-scale detachment folds and defined by the competent Mississippian-Pennsylvanian Lisburne Limestone formed above the incompetent and internally deformed

Reproduced with permission of the copyright owner. Further reproduction prohibited without permission.

Kayak Shale (Wallace 1993, Homza & Wallace 1995) (Plates A3.2 & A3.4). The Mississippian Kekiktuk Conglomerate is beneath the roof thrust in the Kayak Shale and thus is not directly involved in the detachment folding but instead deformed with the basement as part of the horses in the duplex (Wallace & Hanks, 1990) (Plates A3.2 & A3.4). A balanced (Plate A3.2) and a schematic (Plate A3.4) cross section have been constructed across the northern and southern areas, respectively. The region between study areas includes the hangingwall cut-off of southern Franklin Mountains horse and the footwall cut-off of the northern Franklin Mountains horse (Ziegler 1989). The balanced cross section of Ziegler (1989) is used in this study to characterize the structural geometry between the horses.

THE NORTHERN STUDY AREA - THE WESTERN END OF THE NORTHERN FRANKLIN MOUNTAINS ANTICLINORIUM

Local stratigraphy

Sedimentary rocks of pre-Middle Devonian to Permian age are exposed in the northern study area (Plates A3.1 & A3.2) and are briefly described here in ascending stratigraphic order. The basement is composed of an unknown thickness of polydeformed chert and a chlorite-rich phyllitic argillite. It is unconformably (?) overlain by up to 100 m of resistant silt- to gravel-size, ripple cross-laminated, dark colored, quartz/lithic arenite that displays distinctive plumose fractures. Meter-thick beds of these rocks are interbedded with shale horizons and may represent a local deltaic or fluvial facies. This "sub-Kekiktuk

Reproduced with permission of the copyright owner. Further reproduction prohibited without permission.

(?) clastic unit" lacks the polydeformational history of the basement and is separated from the Kekiktuk Conglomerate by a low-angle erosional (?) unconformity that is best exposed in outcrops in Salisbury Creek. Since no fossils were found to constrain the age of this unconformity, the stratigraphic correlation of the sub-Kekiktuk (?) clastic unit is uncertain. The sub-Kekiktuk (?) clastic unit may be equivalent to the unconformity-bounded Middle to Upper (?) Devonian marine to non-marine succession found between the basement and the Kekiktuk to the south (Anderson & Wallace 1990) or it may represent a thick basin-fill succession within the basal part of the Kekiktuk (LePain 1993).

Overlying the sub-Kekiktuk (?) clastic unit, the Kekiktuk Conglomerate (LePain 1993) varies from a nearly 40 m thick cobble conglomerate in the northern part of the area to a 3 to 4 m thick quartz arenite at Salisbury Creek to the south. Clasts of the sub-Kekiktuk (?) clastic unit and, more commonly, of the basement chert, are observed in the Kekiktuk and the unit is commonly channelized with well-developed channel-lag deposits. Where it is a sandstone, bedding is generally on the order of 10s of cm thick and contains poorly developed ripple cross laminae. Plant fossils and coal lenses are common in the coarser fraction of the Kekiktuk, which is composed of beds up to 1 m thick in this area. The Kekiktuk Conglomerate grades upward into the Kayak Shale.

Kayak Shale in this area is characterized by black fissile shale interbedded with carbonate beds up to 10 cm thick and meter-thick calcareous sandstone beds. The 10-20 m thick sandstone beds observed in the Kayak elsewhere in the northeastern Brooks Range (Homza 1993, LePain 1993) are lacking in this area. Here, the Kayak Shale varies in thickness from about 100 m

Reproduced with permission of the copyright owner. Further reproduction prohibited without permission.

to nearly 500 m and this variation represents primarily contractional strain and not stratigraphic thickness changes. Abruptly and conformably overlying the Kayak Shale are beds of the "lower" Lisburne Limestone.

The "lower" Lisburne Limestone is marked by 10 to 20 m of resistant crinoidal wackestone with abundant black chert nodules that grades upward into non-resistant limestone beds some 100 m thick and into another resistant unit of massive calcareous mudstone-to-crinoidal wackestone at the top. The entire unit thickens from 140 m at Plunge Creek in the north to nearly 300 m along Salisbury Creek in the south.

The "middle" Lisburne Limestone is generally recessive and composed of fossiliferous limestone and calcareous mudstone which reaches thicknesses of over 500 m. It passes up section into the massive beds of the "upper" Lisburne Limestone. Meter-thick beds of massive gray wackestone and grainstone characterize the "upper" Lisburne, which has a thickness exceeding 800 m. The entire Lisburne Group exceeds 1500 m in thickness in this area. This thickness is determined from the balanced cross section that is based on map data from an extensive dip panel that exposes easily discernible stratigraphic contacts immediately south of Salisbury Creek (Plate A3.2), and thus is considered a reliable thickness estimate. However, it is considered a maximum estimate because it may include some covered folded intervals related to sub-surface structural thickening in the lower parts of the Lisburne in that area.

The Echooka Formation, which disconformably overlies the Lisburne Limestone, consists of brown-weathering lithic arenite and shale and is exposed

Reproduced with permission of the copyright owner. Further reproduction prohibited without permission.

only in isolated outcrops along the western and southern boundaries of the study area.

Local structural style

Two structural domains are defined in the northern area by distinct structural geometries (Plate A3.2). The regional duplex defines the "duplex" structural domain. In this area it lies generally east of, and structurally beneath, the "roof" structural domain, which corresponds to the roof sequence (Wallace, 1993), or all rocks stratigraphically above the Kekiktuk Conglomerate.

The duplex structural domain

Rocks within the duplex structural domain include the polydeformed basement, the sub-Kekiktuk (?) clastic unit, and the Kekiktuk Conglomerate. The duplex domain is defined by the northern Franklin Mountains horse, which forms a regional antiform that trends approximately S85°W and has a wavelength of about 15 km. The northern Franklin Mountains antiform is defined by three well-defined dip panels. From south to north and from most-exposed to least-exposed these are: a gently dipping backlimb (Fig. A3.2a), a nearly horizontal crestal panel, and a moderately dipping forelimb. This geometry matches well with Suppe's (1983) mode 1 fault-bend fold model and led Namson and Wallace (1986) to interpret the northern Franklin Mountains antiform as a fault-bend fold with the change in dip between the two southernmost dip panels reflecting the underlying footwall ramp-flat transition. Although Namson and Wallace's (1986) study was more regional, the remarkable continuity and lateral extent of the dip panels (*e.g.* Fig. A3.2a) allowed them to make predictions about

Reproduced with permission of the copyright owner. Further reproduction prohibited without permission.

detachment depth beneath the northern Franklin Mountains horse that match very closely with those of this more detailed study (Plate A3.2). Both studies interpret the detachment to lie at approximately 4 km subsea.

The roof structural domain

The structural style of the roof structural domain is controlled primarily by the local mechanical stratigraphy. Rocks overlying the competent northern Franklin Mountains horse define a gradient in mechanical competency from least competent in the Kayak Shale at the bottom to most competent in the "upper" Lisburne Limestone at the top. This mechanical stratigraphy lends itself to detachment folding (Jamison 1987) and the roof structural domain is characterized by detachment folds (Plate A3.2).

In the roof structural domain, four kilometer-scale symmetrical-to-north-vergent anticlinal detachment folds are defined by the Lisburne Limestone and cored by the Mississippian Kayak Shale (Plate A3.2). The Kayak Shale is thickened in the cores of these anticlines by disharmonic folding, small-displacement thrust faulting, and penetrative strain (Fig. A3.3). Straight dip panels that parallel the backlimb of the underlying northern Franklin Mountains horse separate the detachment folds. In general, the folds have single, close, angular hinges in their structurally lower parts that give way up section to multi-hinged, open, angular folds (Plate A3.2). The two major folds in the northern part of the study area are more upright and symmetrical than those to the south, which are more northward-inclined and asymmetrical. One of these north-vergent folds, the Salisbury Creek anticline, is discussed in more detail below.

Reproduced with permission of the copyright owner. Further reproduction prohibited without permission.

The Salisbury Creek anticline

The Salisbury Creek anticline is well exposed for more than 10 km along strike (Plate A3.1) and its crest in the "upper" Lisburne Limestone defines Mt. Salisbury (7,060'). At the contact between the Kayak Shale and the Lisburne Limestone, the fold is asymmetrical and north-vergent, with a single, tight, angular hinge and planar limbs (Fig. A3.4a). The fold increases in wavelength from ≅160 m near the core to ≅ 1.5 km in the uppermost Lisburne at Mt. Salisbury, where it is a multi-panel, open anticline with a nearly horizontal crest (Fig. A3.5). The limbs, although complicated by parasitic folds, generally maintain a constant dip both down plunge and up structural section (Fig. A3.4b). The forelimb dips ≅ 85° N, the backlimb dips ≅ 25° S, and the interlimb angle is ≅ 69°. The Kayak Shale is thickened by about 50% in the fold core (Fig. A3.4) and the depth to the base of the Kayak (depth-to-detachment) is about 115 m (Homza & Wallace 1995).

Qualitative analysis of the distribution of strain in the Salisbury Creek anticline provides constraints on its kinematic evolution. Little solution cleavage and only very minor stylolitization are apparent in the backlimb. Centimeter-thick chert beds that make up the base of the Lisburne Limestone record only a few poorly developed veins and no tectonic brecciation in the backlimb. The only significant deformation in the backlimb is recorded by bed-parallel slickensides that indicate flexural slip and by a late-stage thrust fault with about 10 m of displacement (Fig. A3.4a). The anticlinal hinge is extremely strained and includes many minor contractional faults with a variety of orientations and offsets, abundant cm-scale folds, well-developed calcite-filled veins that parallel

Reproduced with permission of the copyright owner. Further reproduction prohibited without permission.

and cross-cut bedding, tectonic brecciation, solution cleavage, and stylolitization (Fig. A3.6).

The synclines bounding the forelimb and the backlimb are similarly very strained. The hinges of these synclines include each of the strain indicators listed for the anticlinal hinge, although here there are fewer indicators and they are not as well developed as in the anticlinal hinge. Forelimb deformation includes tectonically brecciated and boundinaged chert beds, minor cleavage, bed-parallel veins of stretched calcite fibers, and stretched bed-parallel slickenfibers indicating north-over-south flexural slip.

There are no structural relationships suggesting hinge-migration through the backlimb nor is there any definitive indication of hinge-migration in the forelimb (*e.g.* Thompson 1989, Fischer *et al.* 1992). The intensity of tectonic brecciation and interbed shear in the forelimb permits the possibility that either adjacent hinge migrated through the forelimb during the early stages of fold growth. However, a fixed-hinge interpretation is preferred because the contractional faults, cross-cutting veins, minor folds, and intense solution cleavage that characterize the adjacent fold hinges are lacking in the forelimb.

The Salisbury Creek anticline is interpreted to have formed by fixed-hinge buckling, with late-stage strain related to clockwise (north-over-south) flexural-slip rotation of the forelimb, late-stage north-directed thrust faulting in the backlimb and an increase in the thickness of the detachment unit (Homza & Wallace 1995). The north-vergent asymmetry of the fold, together with the north-directed thrust fault along the backlimb suggest that this deformation involved a significant component of north-directed motion.

Reproduced with permission of the copyright owner. Further reproduction prohibited without permission.

THE SOUTHERN STUDY AREA - THE WESTERN END OF THE SOUTHERN FRANKLIN MOUNTAINS ANTICLINORIUM

Local stratigraphy

Rocks as old as the pre-Middle Devonian basement and as young as the Mississippian-Pennsylvanian Lisburne Limestone are exposed in the southern area (Plate A3.3) and are briefly described here in ascending stratigraphic order. An undetermined thickness of pre-Middle Devonian basement is composed primarily of massive beds of light-colored chert in this area and is unconformably overlain by the Kekiktuk Conglomerate. No sub-Kekiktuk (?) clastic unit was observed in the southern study area. The Kekiktuk Conglomerate consists of about 20 m of cobble and lesser pebble conglomerate and quartz sandstone. Well-developed channels and, in the sand-rich beds, ripple cross-laminations are apparent. Up to 100 m of tan-weathering highly crenulated siltstone overlies the Kekiktuk, is informally referred to as the "lower" Kayak, and may represent the "Ms" unit of Bader and Bird (1986). The "upper" Kayak is a black fissile shale that includes minor orange-weathering carbonate beds but lacks the significant thicknesses of sandstone observed near the range front (Homza 1993, LePain 1993). The entire Kayak Shale is about 500 m thick but, as in the northern area, is significantly thickened in the cores of anticlines.

The thickness of the Lisburne Limestone in the southern area is only estimated on the schematic cross section (Plate A3.4) because its upper contact is not exposed in the area and up-plunge projections from the nearest upper-

Reproduced with permission of the copyright owner. Further reproduction prohibited without permission.

contact exposures yield unreasonable and inconsistent thickness values. Also, individual structural units in the Lisburne are poorly defined in the south.

Local structural style

As in the northern study area, two structural domains are identified in the southern area: the "duplex" and "roof" structural domains (Plate A3.4). Here, the duplex domain is defined by the southern Franklin Mountains horse and the roof domain is defined by the roof sequence, including all rocks stratigraphically above the Kekiktuk Conglomerate.

The duplex structural domain -

The southern Franklin Mountains horse includes the polydeformed basement and the Kekiktuk Conglomerate and, like the northern Franklin Mountains horse, it approximates the geometry of a fault-bend fold (Wallace & Hanks 1990, Wallace 1993) (Plate A3.3). The flat crestal panel that characterizes the southern horse east of this area narrows westward toward this area where the horse has only a very narrow crestal panel, a gently dipping backlimb that extends eastward and southward from the study area (Fig. A3.2b), and a gently dipping forelimb. Rocks in the duplex domain of this area are nearly entirely in the forelimb position of the fault-bend fold.

No detachment is observed between the basement and the Kekiktuk in this domain. Although a meter-displacement thrust fault occurs in the Kekiktuk (Plate A3.3), there are no other indications of significant shortening in the well-exposed straight dip panels of Kekiktuk save for that due to its overall fault-bend fold geometry.

Reproduced with permission of the copyright owner. Further reproduction prohibited without permission.

The roof structural domain -

The roof domain is characterized by detachment folds defined by Lisburne carbonates deformed above the internally deformed and thickened Kayak Shale (Plate A3.4). Roof sequence rocks in the map area lie mostly above the forelimb of the southern Franklin Mountains horse enabling characterization of detachment folds in that structural position. The lower parts of the Lisburne and the Kayak-Lisburne contact are well exposed in the area and, together with the well-defined geometry of the lower parts of the detachment folds, yield information about the development of the folds.

The kilometer-scale detachment folds in the southern area occur in three sub-domains defined by fold trains with distinctive geometries that are separated by straight panels which roughly parallel panels in the underlying duplex domain. These three sub-domains are, in decreasing structural elevation and from south to north: the crestal, forelimb, and cut-off sub-domains. The sub-domains are named for their position above the southern Franklin Mountains horse.

The crestal sub-domain

The crestal sub-domain is directly above and immediately forward of the narrow crest of the underlying horse and is characterized by several generally close, north-vergent to symmetrical, northward-overturned to upright folds. Each fold has a complex angular to curved geometry with numerous parasitic folds on the limbs (Fig. A3.7). As in the northern study area, penetrative strain in the form of solution cleavage and stylolitization and distributed strain in the form of meter-scale faults and folds are very common in the hinge areas and there is less strain on the limbs. Although the difference in the intensity of strain

Reproduced with permission of the copyright owner. Further reproduction prohibited without permission.

between hinge and limb areas is less in this sub-domain than in others due to the multitude of parasitic folds and their associated structures here, many of the largest anticlinal closures along the Lisburne-Kayak contact have eroded away (*e.g.* Fig. A3.7), leaving local topographic lows and suggesting decreased resistance to erosion due to strain. Several north-vergent out-of-syncline thrust faults with displacements measured in meters occur in this sub-domain.

The vergence of meter-scale fold-trains in the carbonate beds in the Kayak Shale in the crestal sub-domain indicates top-toward-the-anticline simple shear (Fig. A3.8). This suggests that the detachment unit was tectonically transported into anticlines from beneath synclines. The Kayak Shale in anticlinal cores is thickened and extremely strained by minor faulting and folding and by intense solution cleavage with carbonate precipitated as an orange rind surrounding centimeter-scale gray siliceous lenticular bodies resembling fault asperities.

The forelimb sub-domain

Detachment folds in the forelimb sub-domain are clustered above a change in dip in the forelimb of the underlying horse and they grade in geometry from a close, north-vergent fold in the hindward position to an upright isoclinal fold in the forward position (Plate A3.4). Although the amount of thickening in the Kayak Shale beneath these folds is uncertain, top-toward-the-anticline simple shear is indicated by small scale fold trains in the Kayak (as in Fig. A3.8). As in the crestal sub-domain, the Kayak in anticlinal folds is contractionally strained by solution cleavage and minor faults and folds.

Reproduced with permission of the copyright owner. Further reproduction prohibited without permission.

Outcrop-scale observations of the distribution of strain in these folds show a drastic decrease in strain from hinges to limbs and there are few parasitic folds. This difference in strain is most obvious in the tighter anticlines where intense solution cleavage, stylolites, and small-scale folds and faults in the hinges give way to coherent, planar beds on the limbs.

The cut-off sub-domain

The cut-off sub-domain was accessed only at a few locations within the Lisburne Limestone. The domain is dominated by a single, large anticline-syncline pair which can be traced at least 6 km down plunge to the west where spectacular exposure was observed from a distance. The anticline is slightly asymmetrical and, unlike other folds in this study area, is slightly south-vergent.

KINEMATICS OF THE DETACHMENT FOLDS

Outcrop-scale geometric and strain observations in both the northern and southern areas show that fold hinge zones have been intensely and irreversibly strained during deformation. If the folds grew by migration of the hinges through the rock, remnants of such hinge strain should be recognizable in fold limbs (Thompson 1989, Fischer *et al.* 1992, Homza & Wallace 1995). No such overprinting relationships were observed in fold limbs. In order for the folds in the area to have formed by fixed-hinge kinematics and obey the assumption of constant cross-sectional area, then the Kayak Shale is required to have changed thickness during deformation (Homza & Wallace 1995). The wide variety of thicknesses determined for the Kayak Shale on the cross sections and the

Reproduced with permission of the copyright owner. Further reproduction prohibited without permission.

observed internal deformational features (*e.g.* top toward the anticline shear, solution cleavage, core stylolites and precipitation rinds) support the interpretation that the Kayak changed thickness, and perhaps cross-sectional area, during deformation. Thus, the observations reported here suggest that the kinematic evolution of detachment folds in the Franklin Mountains anticlinoria involved changes in the thickness of the detachment unit and a significant component of fixed-hinge buckling (see Homza 1993 and Homza & Wallace 1995). This conclusion is incompatible with most geometric models for detachment folds (*e.g.* Jamison 1987, Mitra & Namson 1989), which are based on assumptions of fixed detachment depth and hinge-migration kinematics, but is compatible with Homza and Wallace's (1995) more general model for detachment anticlines above a detachment unit that changes thickness during deformation.

GEOMETRY AND KINEMATICS OF THE ROOF SEQUENCE

The roof sequence in the northern study area lies structurally above the backlimb and crest of the northern Franklin Mountains horse whereas the roof sequence in the southern study area lies above the crest and forelimb of the southern Franklin Mountains horse. Ziegler (1989) constructed a north-striking balanced cross section across the hangingwall cutoff of the southern Franklin Mountains horse in the area between the Canning River and the Marsh Fork (northeast of the southern area, Fig. A3.1). Thus, taken together, observations from these areas are well suited to analyze the nature of roof sequence

Reproduced with permission of the copyright owner. Further reproduction prohibited without permission.

deformation in terms of its position above horses in the regional duplex (Fig. A3.9).

Detachment folds above the backlimb of the northern Franklin Mountains horse are north-vergent and are generally separated by straight panels that parallel the backlimb of the horse. Folds above the forelimb of the southern Franklin Mountains horse are north-vergent to south-vergent in the southern area but are strongly north-vergent east of the Marsh Fork (Ziegler 1989), where the forelimb of the horse is steeper and is defined by a smaller-scale duplex within the basement (Fig. A3.9). More symmetrical and upright geometries characterize the detachment folds that lie above the sub-horizontal crestal panels of both horses. Folds are more abundant and complex where there is a change in dip between panels of the underlying horse than they are above straight panels. These geometric observations suggest a complex deformation history for the roof sequence that is related to the geometry and kinematics of the underlying horses, the details of which are beyond the scope of this report. However, a general interpretation of the overall geometric and kinematic evolution of the Franklin mountains anticlinoria is presented below.

Structural evolution of the Franklin Mountains anticlinoria

In interpreting the structural evolution of the Franklin Mountains anticlinoria, two general observations must be explained. First, the drastic difference in both structural geometry and apparent shortening between the duplex and roof domains must be accounted for. This is best accomplished by calling on the fault-bend fold duplex model (Wallace & Hanks 1990, Wallace 1993), as described above. Second, the form, distribution, and apparent

Reproduced with permission of the copyright owner. Further reproduction prohibited without permission.

kinematic path (*i.e.* fixed-hinge buckling) of detachment folds in the roof sequence must be explained, preferably in the context of the fault-bend fold model.

Figure A3.10 shows a simplistic model for the structural evolution of the area. Since the complex kinematics, together with a general paucity of relative timing data, preclude construction of accurate sequential, balanced models, figure A3.10 is very schematic. Stage 1 shows an undeformed sequence with incipient faults in the basement shown. Emplacement and uplift of the southern Franklin Mountains horse begins in stage 2 with the single horse bounded by a roof thrust in the Kayak Shale and a floor thrust at depth in the basement. Fault-bend fold kinematics (Suppe 1983) occurs in the horse itself and the associated shortening is accommodated in the roof by fixed-hinge detachment folding concentrated above the bends and growing dip panels of the underlying horse. The original position of these folds with respect to the migrating hinges of the fault-bend fold is uncertain. North-vergent folding in the roof over the backlimb could have been related to north-directed thrusting that occurred south of the southern Franklin Mountains horse (Wallace 1993), which may have resulted in northward displacement of the roof as far north as the barrier created by the backlimb of the southern Franklin Mountains anticlinorium.

As deformation progressed (Fig. A3.10 - stage 3) the detachment folds above the backlimb of the horse developed a north-vergent asymmetry, the folds on the forelimb developed a slight south-vergent asymmetry, and those above the

Reproduced with permission of the copyright owner. Further reproduction prohibited without permission.

crestal panel were generally upright and symmetrical. This geometry may be explained by "passive roof" (Banks & Warburton 1986) deformation in the forelimb and "active roof" deformation in the backlimb. The north-vergent folding on the backlimb may be the result of either "bulldozing" from the south (as above) and/or it may be an upsection continuation of the north-over-south flexural slip folding involved in the emplacement of the horse. Fold geometry in the crestal panel may represent a continuation of either the active or passive roof deformation, or it may describe the spatial intersection of the two.

Apatite-fission track data suggest that the southern Franklin Mountains anticlinorium began to form before the northern anticlinorium (Wallace *et al.* in prep.). It is likely, however, that displacement of the southern horse continued after displacement of the northern horse began (Wallace oral comm. 1993) (Fig. A3.10, stage 3). At this stage, the southern Franklin Mountains horse had reached its full amplitude but forward displacement continued, allowing the roof sequence to be bulldozed northward ahead of the forelimb as south-directed "passive" displacement continued above the forelimb.

In stage 4, deformation associated with the emplacement of both horses overlapped in the intervening syncline. Further northward translation of the southern horse caused extreme thickening and northward asymmetry in the roof above its leading edge and contributed to north-directed shear along the backlimb of the northern horse. Northward asymmetry above the hangingwall cut-off of the southern horse may be related to the north directed duplexing in the forelimb of the southern horse that Ziegler (1989) described. The northern Franklin Mountains horse developed like the southern horse, with fold geometry

Reproduced with permission of the copyright owner. Further reproduction prohibited without permission.

reflecting passive roof deformation in the forelimb and north-directed shear related to bulldozing and/or fault-bend-folding in the backlimb.

LOCALIZATION OF DETACHMENT FOLDS ABOVE BENDS IN THE HORSES

The detachment folds in the roof sequence are concentrated above bends in the underlying horses and commonly the sense of shear indicated by the asymmetry of these folds changes across the underlying bend. This geometry is clear in the southern study area where straight non-folded panels in the roof sequence lie above panels in the horse and trains of folds in the roof sequence lie above bends in the horse (Plate A3.4).

This geometry suggests a general kinematic relationship between the fold trains and the bends in underlying structures. However, this relationship is problematic because the fold trains in the roof sequence must move relative to the bends in the horse whether or not the horses formed by ideal fault-bend-folding. If ideal fault-bend-folding is assumed for the horse, then the fact that the fault-bend-fold hinges (bends) migrate through the basement during folding introduces a further complexity. One speculative kinematic scenario is that the bends in the fault-bend-fold horses served as nucleation points for the detachment folds and the fold trains moved with the migrating hinges of the fault-bend-fold and accumulated shortening as the total shortening increased.

CONCLUSIONS

Structural relationships in a regional duplex along the Canning River in the northeastern Brooks Range suggest that detachment folds in the roof

Reproduced with permission of the copyright owner. Further reproduction prohibited without permission.

sequence formed in response to both forward- and hindward-directed contraction. Qualitative strain analysis indicates that at least some of the detachment folds formed by fixed arc-length kinematics above a detachment unit that changed thickness during deformation. The horses in the duplex are fault-bend folds and the distribution of detachment fold asymmetries relative to the horses constrains the kinematic relationship between the horses and the roof sequence. Detachment fold trains may have nucleated above, and migrated with, hinges in the fault-bend-folds.

Reproduced with permission of the copyright owner. Further reproduction prohibited without permission.

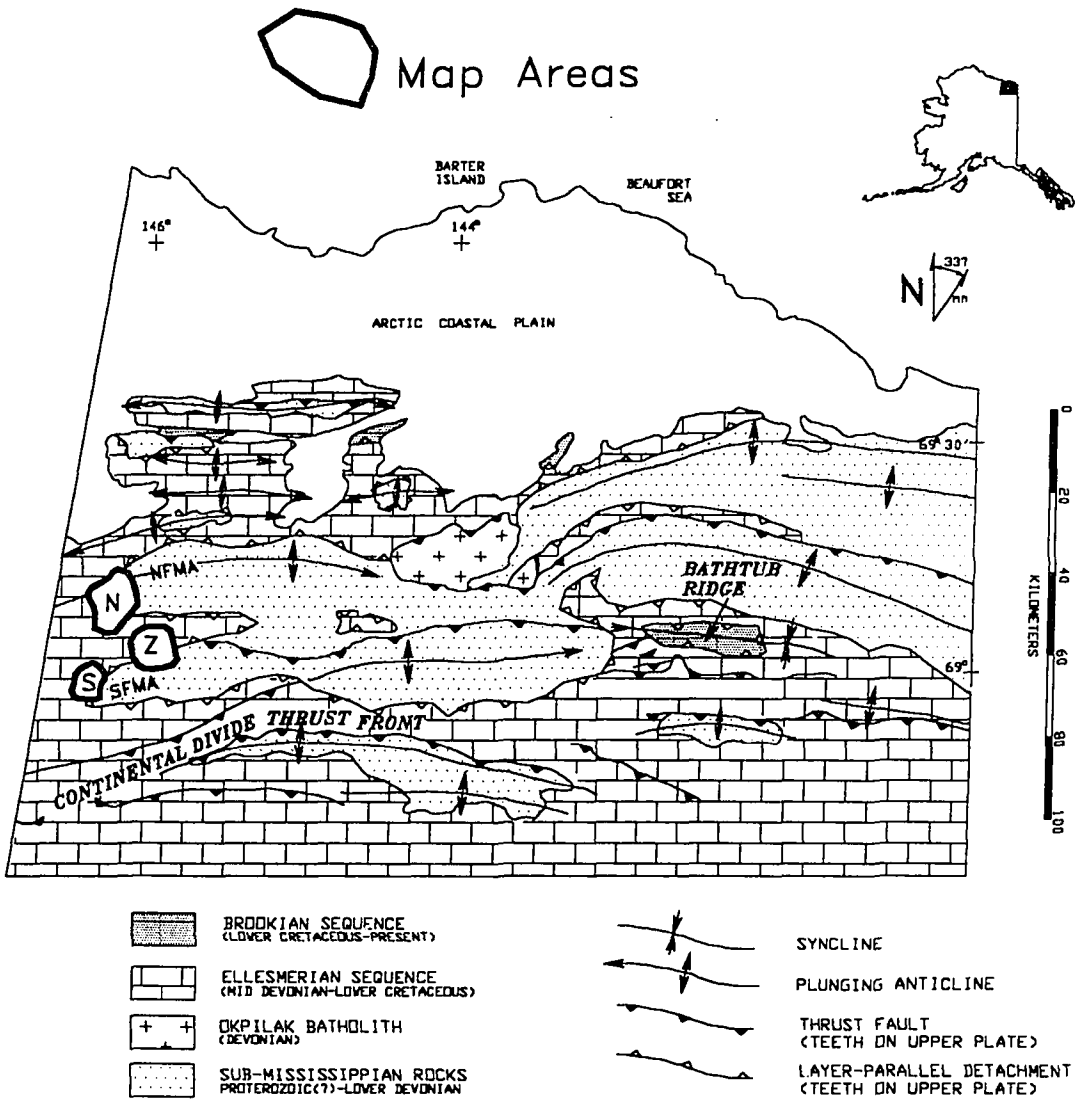

Figure A3.1. Generalized tectonic map of the northeastern Brooks Range showing the location of the northern study area (N), the southern study area (S), Ziegler's (1989) study area (Z), and the observed extent of the regional duplex.

Reproduced with permission of the copyright owner. Further reproduction prohibited without permission.

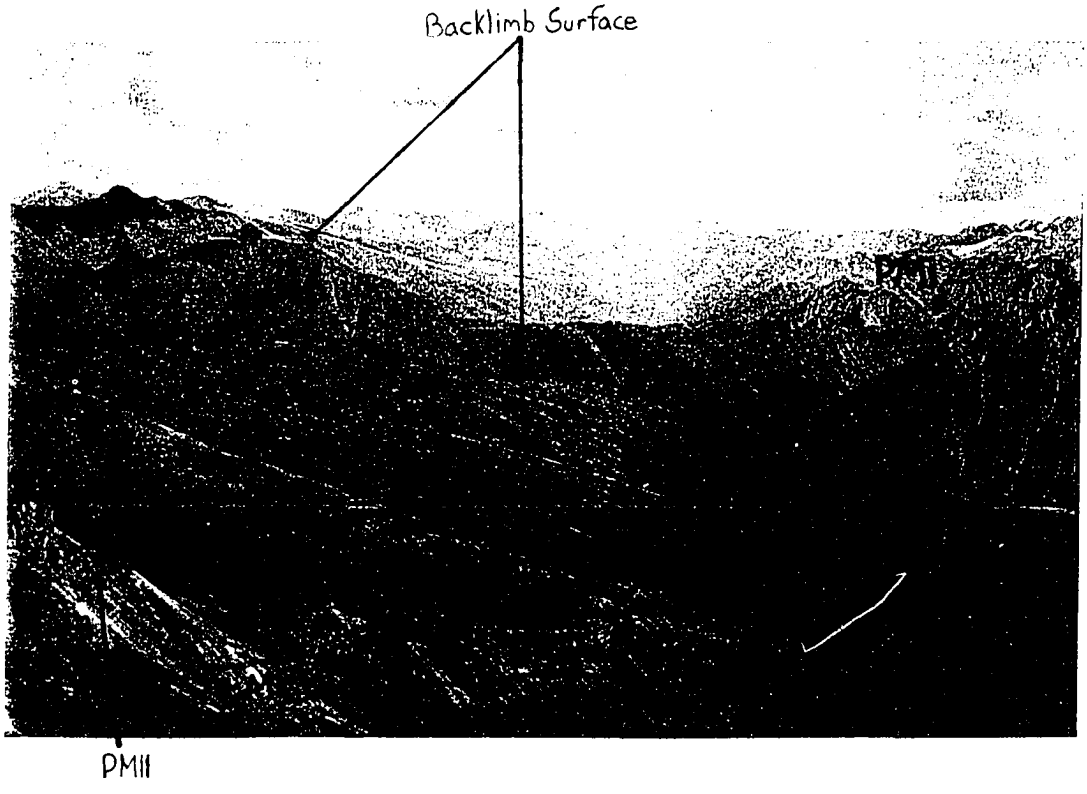

Figure A3.2.a. Photograph of the backlimb of the northern Franklin Mountains horse taken from locality 2a on Plate A3.1. View is eastward and the base of the photo is about 1 km. pMD = basement, Mkt = Kekiktuk Conglomerate, Mk = Kayak Shale, PMII = "lower" Lisburne Limestone, PMI = Lisburne Limestone (undivided).

Reproduced with permission of the copyright owner. Further reproduction prohibited without permission.

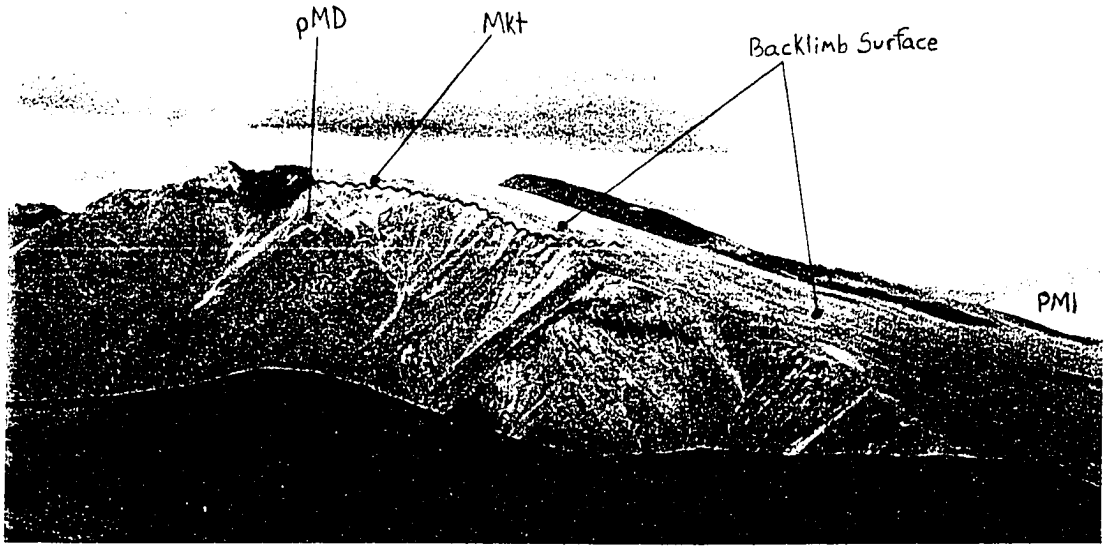

Figure A3.2.a. Photograph of the backlimb of the southern Franklin Mountains horse taken from locality 2b on plate A3.3.a. View is eastward and the base of the photo is about 1 km. pMD = basement, Mkt = Kekiktuk Conglomerate, Mk = Kayak Shale, PMll = "lower" Lisburne Limestone, PMl = Lisburne Limestone (undivided).

Reproduced with permission of the copyright owner. Further reproduction prohibited without permission.

Figure A3.3. Photograph of structurally thickened Kayak Shale in the core of a kilometer-scale detachment fold in the roof domain of the northern study area.

Reproduced with permission of the copyright owner. Further reproduction prohibited without permission.

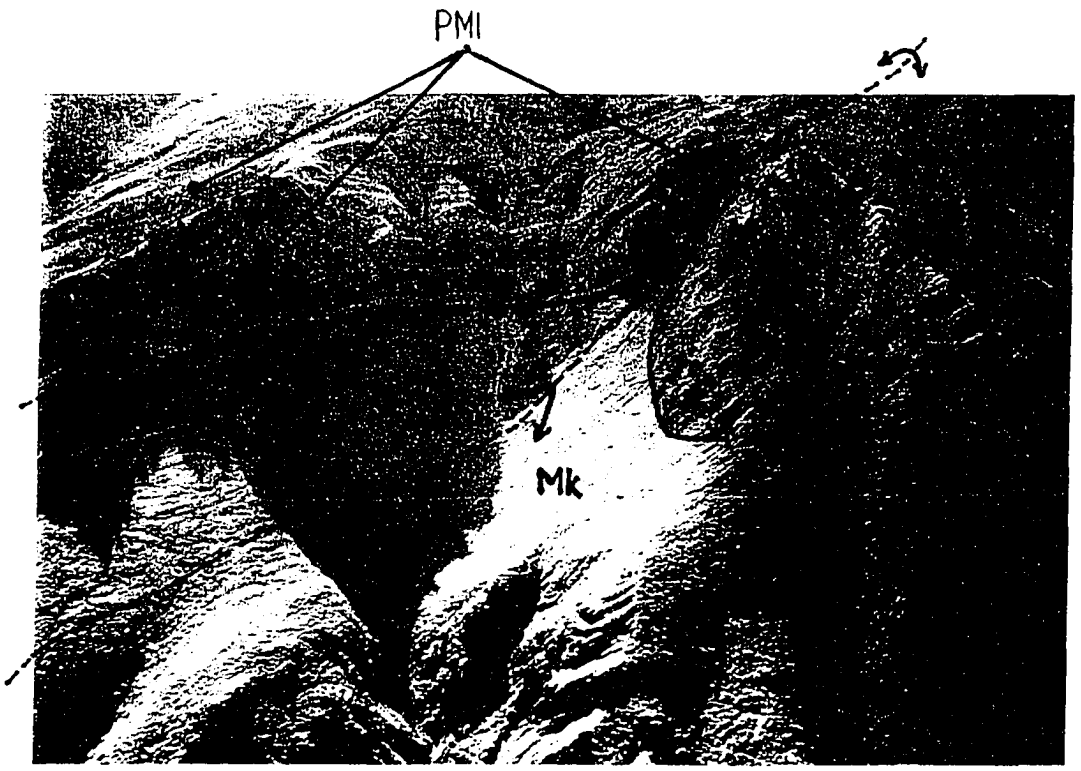

Figure A3.4.a Photograph of the core of the Salisbury Creek anticline taken from locality 4a on plate A3.1. The base of the photograph is about 150 m and the view is westward. The area in this photo is outlined in figure A3.4.b. Mk = Kayak, PMI = Lisburne.

Reproduced with permission of the copyright owner. Further reproduction prohibited without permission.

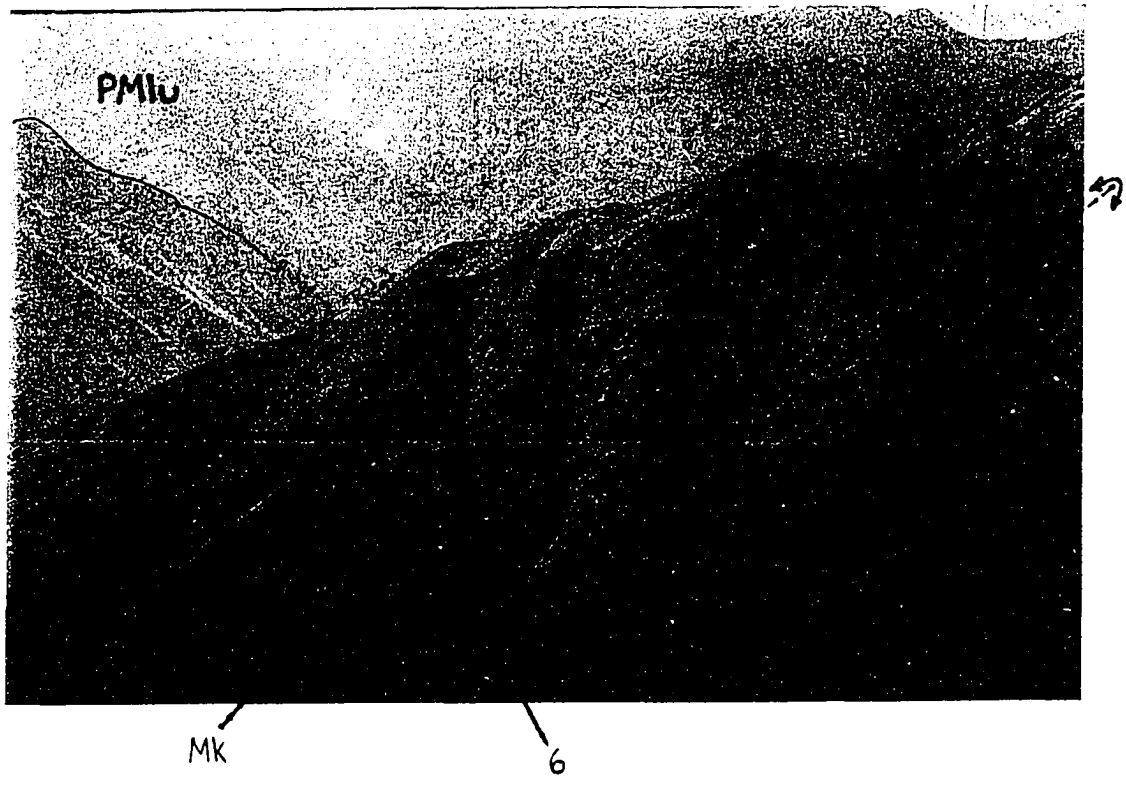

Figure A3.4.b Photograph of the structurally lower parts of the Salisbury Creek anticline taken from locality 4b on plate A3.1. The base of the photograph is about 200 m and the view is to the west-northwest. Mk = Kayak Shale, PMll = "lower" Lisburne Limestone, PMlm = "middle" Lisburne Limestone, PMlu = "upper" Lisburne Limestone, "PMl" = Lisburne limestone (undivided). The box indicates the location of figure A3.4.a. (6) indicates the location of the photograph in figure A3.6.

Reproduced with permission of the copyright owner. Further reproduction prohibited without permission.

Figure A3.5. Photograph of structurally high parts of the Salisbury Creek anticline and the adjacent syncline and flat panel that lie to the north. All of the rocks in this photograph are part of the Lisburne Limestone. Photograph taken from locality 5 on plate A3.1, the view is southwestward, and the base of the photograph is about 1 km.

Reproduced with permission of the copyright owner. Further reproduction prohibited without permission.

Figure A3.6. Photograph of the intense small-scale folding and penetrative deformational features in the hinge of the Salisbury Creek anticline in the "lower" Lisburne Limestone. See figure A3.4.b for location, hammer head for scale.

Reproduced with permission of the copyright owner. Further reproduction prohibited without permission.

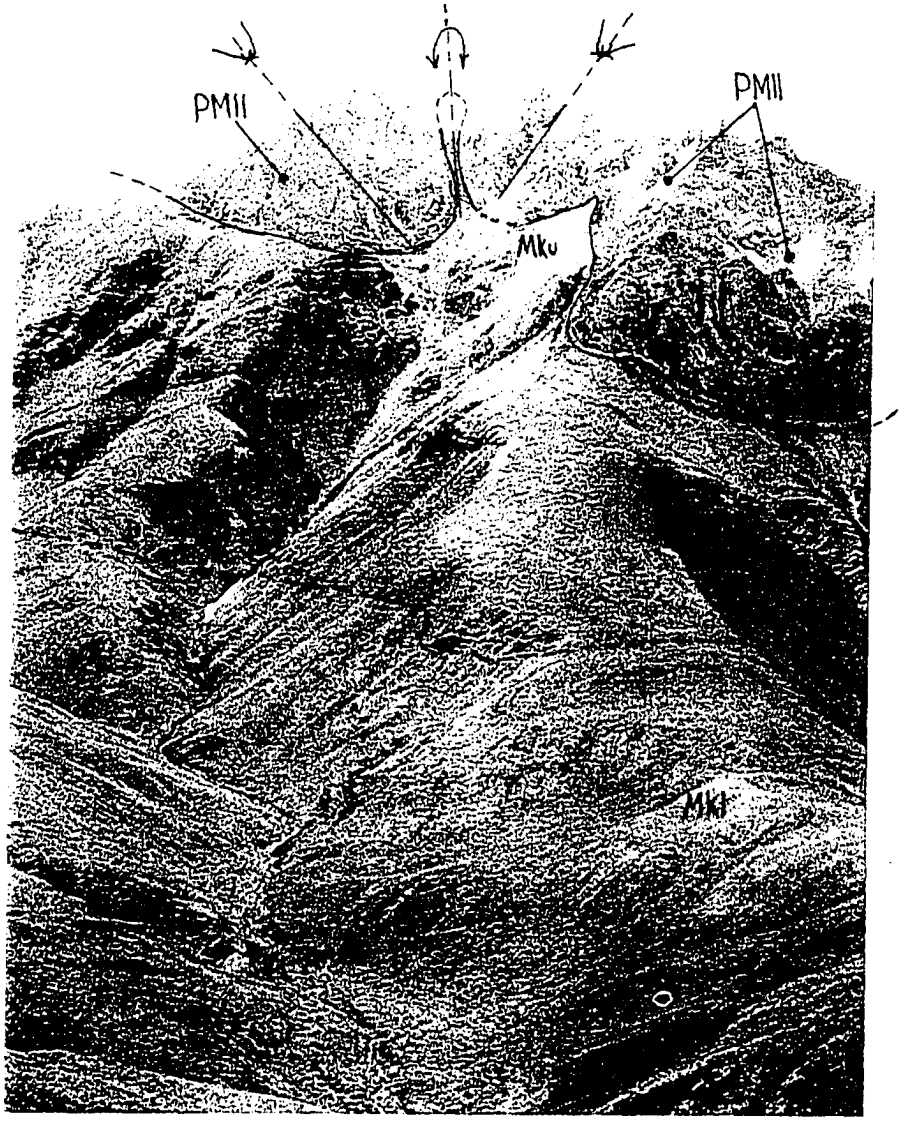

Figure A3.7. Photograph of a large upright, symmetrical detachment anticline in the crestal subdomain of the roof domain in the southern area taken from locality 7 on plate A3.3. The view is southwestward and the horizontal distance across the photograph at the level of the mountain in the foreground is about 50 m. The fold lies above the narrow crestal panel of the southern Franklin Mountains horse. Mkl = "lower" Kayak Shale, Mku = "upper" Kayak Shale, PMll = "lower" Lisburne Limestone.

Reproduced with permission of the copyright owner. Further reproduction prohibited without permission.

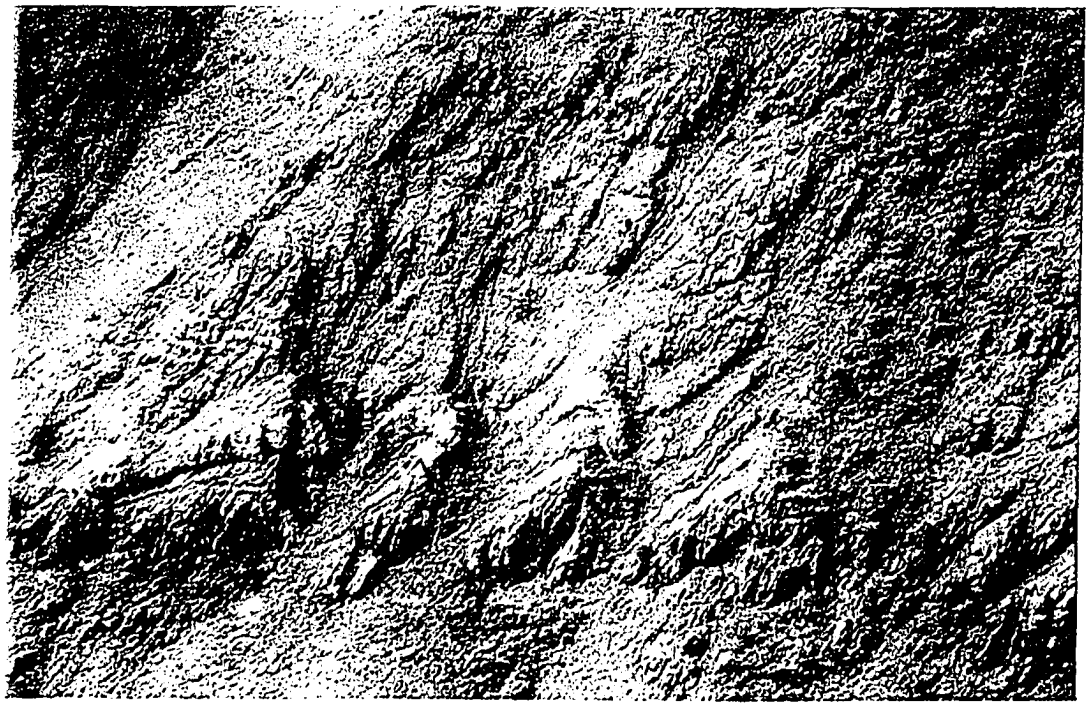

Figure A3.8. Photograph of a small-scale fold train in the Kayak Shale with vergence toward the core of a larger-scale detachment fold that lies structurally upsection. The distance across the base of the photograph is about 7 m.

Reproduced with permission of the copyright owner. Further reproduction prohibited without permission.

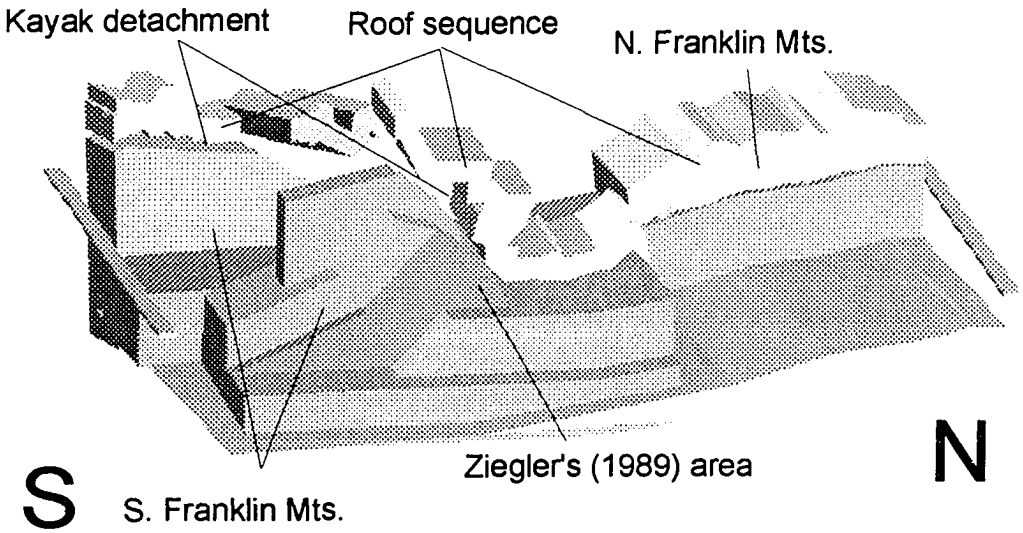

Figure A3.9. 3-dimensional view of the Franklin Mountains anticlinoria, looking northwestward. The bar at the southern end of the diagram runs east-west at sea level and the N-S extent of the figure is about 40 km.

Reproduced with permission of the copyright owner. Further reproduction prohibited without permission.

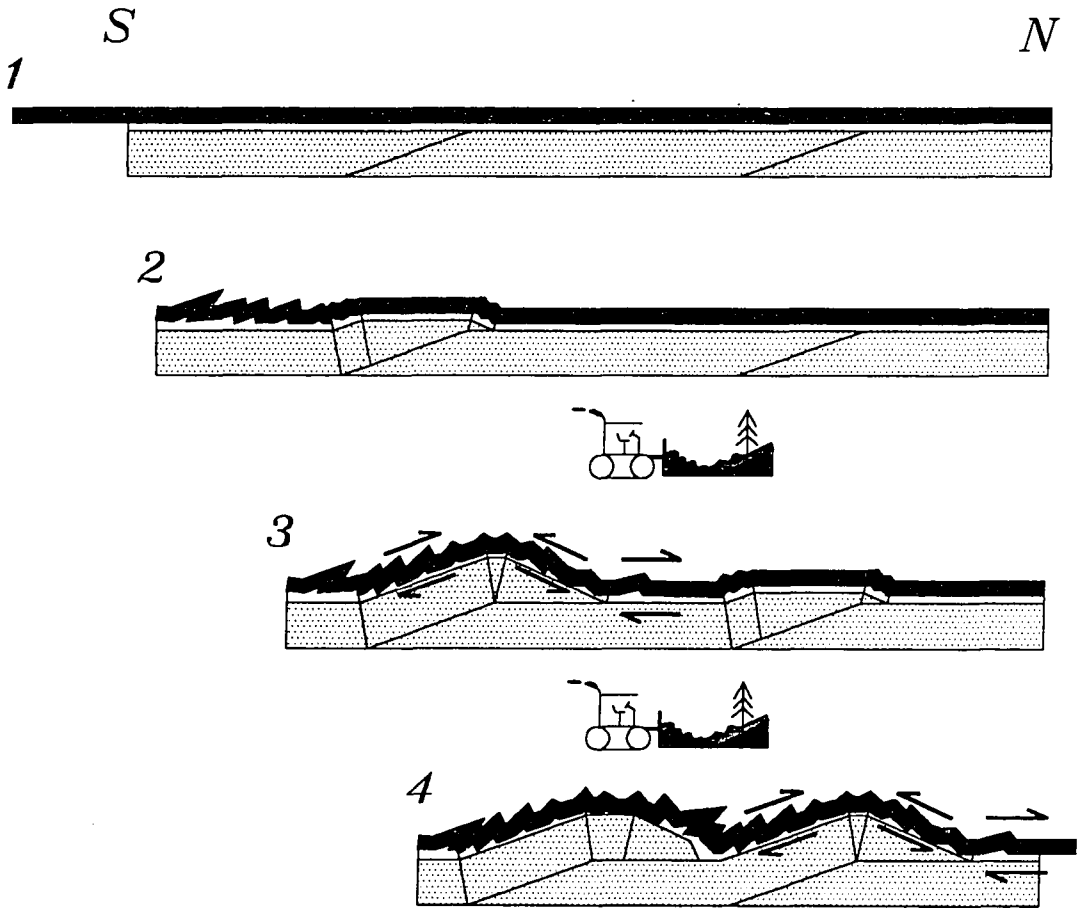

Figure A3.10. Schematic diagram representing the kinematic evolution of the Franklin Mountains anticlinoria. Detachment folds form by fixed-hinge buckling above a detachment unit that changes thickness (see text for explanation).

Reproduced with permission of the copyright owner. Further reproduction prohibited without permission.

APPENDIX 4 GEOLOGIC MAP AND BALANCED CROSS SECTION OF THE AICHILIK FORKS REGION

See plates A4.1 and A4.2

Reproduced with permission of the copyright owner. Further reproduction prohibited without permission.

APPENDIX 5- GEOLOGIC MAP AND STRUCTURAL GEOMETRY OF AN ELLESMERIAN SEQUENCE INLIER ALONG THE HULAHULA RIVER

An inlier of Ellesmerian sequence rocks within an extensive outcrop belt of older, basement rocks along the middle reaches of the Hulahula River in the northeastern Brooks Range (Mt. Michelson A1 and A2 Quadrangles) is shown in reconnaissance maps by Reiser *et al.* (1971), Bader & Bird (1986), and Imm *et al.* (1993). The purpose of this report is to provide more detail about the geometry and internal structure of the inlier. The primary contributions of this study are a geologic map of the central part of the inlier (Plate A5.1) and a north-south cross section through the inlier (Plate A5.2).

PHYSIOGRAPHY AND EXPOSURE IN THE STUDY AREA

Roughly rectangular, the inlier extends about 15 km in the east-west direction and 5 km from north to south. The inlier consists primarily of the Mississippian-Pennsylvanian Lisburne Limestone and the Mississippian Kayak Shale, although the Mississippian Kekiktuk Conglomerate has been mapped along the northeastern contact (Bader & Bird 1986). The west-central part of the area is covered by alluvium from the north-flowing Hulahula River. Relative to surrounding basement rocks, the inlier is topographically and structurally low. Exposed outcrop constitutes less than about 10% of the area, which is mostly covered by a combination of tundra, alluvium, and talus.

Reproduced with permission of the copyright owner. Further reproduction prohibited without permission.

STRUCTURAL STRATIGRAPHY

Three primary rock units are distinguished in the study area. In ascending stratigraphic order these are sub-Middle Devonian (Anderson & Wallace 1990) metasedimentary rocks (basement), fissile black shale and decimeter-thick carbonate beds of the Kayak Shale, and the Lisburne Limestone. Although it is not directly observed in this area, the basement and the Kayak Shale are inferred to be separated by the same regional, angular "sub-Middle Devonian unconformity" observed throughout the northeastern Brooks Range (Moore *et al.* 1994). The lower part of the Lisburne in this area consists of decimeter-thick wackestone beds with up to 70% replacement chert. The Lisburne becomes gradationally less cherty and coarser grained up section until meter-thick grainstone beds dominate. The upper contact of the Lisburne is not exposed in the study area.

STRUCTURE OF THE AREA

Reiser *et al.* (1971) and Imm *et al.* (1993) show the perimeter contacts of the inlier as erosional and Bader & Bird (1986) show its southern contact as a high-angle normal fault. However, in this study the southern contact of the inlier was clearly observed to be a south-dipping reverse fault with an associated northward-overturned footwall syncline in the Ellesmerian sequence.

Within the inlier, south-dipping thrust faults and northward-asymmetric thrust-truncated detachment folds with south-dipping axial surfaces indicate structures internal to the inlier verge strongly northward. Detachment folds are

Reproduced with permission of the copyright owner. Further reproduction prohibited without permission.

best defined by the lower part of the Lisburne Limestone and cored by structurally thickened Kayak Shale. The areal distribution of penetrative deformation in the Lisburne indicates a region of relatively high strain directly beneath the thrust fault that bounds the inlier on its south side. This strain is probably associated with displacement on the fault.

Reproduced with permission of the copyright owner. Further reproduction prohibited without permission.

APPENDIX 6*: METHODS FOR ELIMINATING UNNECESSARY ERROR WHEN PROJECTING DATA ONTO CROSS SECTIONS

This article discusses two aspects of the process of projecting data onto a geologic cross section that introduce errors. We suggest methods for eliminating some error associated with: 1) projecting data onto a profile plane in areas of high topographic relief and 2) projecting data onto an inclined plane that is parallel to the direction of tectonic transport.

In this discussion, "plunge angle" refers to the mean inclination angle of fold axial trend measured relative to a horizontal plane and in the vertical plane that contains the axial trend, "profile sections" refer to cross sections that are both perpendicular to the regional plunge angle (*i.e.* normal to the plunge direction or mean axial trend). "Transport azimuth" refers to the mean tectonic transport direction determined by either detailed analysis of kinematic indicators (*e.g.* slickenfibers, stretching lineations, fault grooves, ect.) or by the Hansen (1971) separation arc method.

INCLINED SECTIONS IN MOUNTAINOUS TERRAIN

Two separate problematic aspects of projecting data onto an inclined cross section in mountainous terrain are discussed. First, the trace of the intersection of the profile plane and the ground surface (*i.e.* the line of section)

---

* To be published as "Eliminating unnecessary error when projecting data onto cross sections", by Thomas X. Homza and Wesley K. Wallace.

Reproduced with permission of the copyright owner. Further reproduction prohibited without permission.

will not define a *straight* line unless there is no topographic relief (Fig. A6.1). Second, when the elevation of the projection point is not considered, error associated with approximating the ground surface as horizontal is introduced on profile sections (Fig. A6.2).

The first problem primarily effects correspondence between map locations near the line of section and data on the cross section. An inclined plane that intersects mountainous topography defines a circuitous line in map view. Thus, it is unclear exactly where the inclined section intersects the earth, or stated differently, it is unclear what topography should be represented on the cross section (Fig. A6.1). Until a solution to this problem is developed, perhaps with computer techniques, we suggest showing no topography on the cross section and depicting the line of section as the zero-elevation line of Ramsay and Huber (1987) (see-below).

There is a published solution for the second problem (Fig. A6.2) (Ramsay & Huber 1987), but because its use is not widely cited, we present a more extensive explanation of the method and the reasons for its use. Many geologic cross sections are drawn through mountainous terrain and all but the simplest structural settings involve plunging structures that require profile sections to be represented accurately. Most discussions of cross section-balancing methods make no mention of the effects of topographic relief on the projection of data onto the cross section (Dahlstrom 1969, Woodward *et al.* 1985, 1989, Suppe 1985, De Paor 1988). It is unclear to what extent workers routinely and correctly account for this relief. In mountainous areas, the process of projecting onto a plane-of-section requires a simple trigonometric correction (Ramsay & Huber

Reproduced with permission of the copyright owner. Further reproduction prohibited without permission.

1987 - see below) in order to account for the error introduced by topographic relief. When the correction is not used, the projected point will lie at an incorrect low elevation on the cross section. This error (*e*), in linear units, is:

$$e = a \cos p \qquad \text{(A6.1)}$$

where (*a*) is the difference between the real elevation of the data point and the elevation of the line of section and (*p*) is the plunge angle (Fig. A6.2).

The Ramsay and Huber (1987) method

We suggest using the Ramsay and Huber (1987) projection method (Fig. A6.2) to eliminate error associated with the elevation of the projection point. The method uses the average regional plunge angle (*p*), the elevation of the point to be projected (*h*), and the distance (*d*) of that point *from the zero-elevation line* measured perpendicular to the zero-elevation line in the zero-elevation plane:

$$y = h \cos p \pm d \sin p \qquad \text{(A6.2)}$$

where *y* is the elevation above the zero-elevation plane on the profile plane (*x'* of Ramsay and Huber (1987) is changed here to *y* in order to coincide with a Cartesian system, see below). The equation is additive if point (*h*) lies down-plunge from the profile plane and subtractive if (*h*) lies up-plunge of the profile plane.

PROJECTING DATA ONTO AN INCLINED PLANE THAT IS PARALLEL TO THE TECTONIC TRANSPORT DIRECTION

The assumption of plane strain in a particular plane-of-section can be valid only if the plane-of-section is constructed parallel to the transport azimuth.

Reproduced with permission of the copyright owner. Further reproduction prohibited without permission.

Thus, ideally, balanced cross sections are drawn both parallel to the transport azimuth (Woodward *et al.* 1985, 1989) and inclined so that the plane of section is normal to the axial trend. In some cases, for example where the local structural trend is arcuate (Fig. A6.3), it is difficult to satisfy both of these criteria. Here we propose a technique for constructing a plane-of-section parallel to the transport azimuth (defined by kinematic indicators) and inclined at 90 degrees minus the plunge angle. We refer to this plane of section as the "transport-parallel, inclined" (TI) plane (Fig. A6.4). In order to locate the TI plane, one must first refer to the plane that contains both the transport azimuth and the structural trend and plunge angle and then construct the TI plane such that it is both perpendicular to that reference plane and contains the transport azimuth (Fig. A6.5). The TI plane is the most suitable plane on which to construct a balanced cross section and the components of Ramsay and Huber's equation (equation A6.2) are measured relative to it and its zero-elevation line (Fig. A6.4).

The Ramsay and Huber (1987) projection technique is modified in order to accommodate the fact that the plane-of-section is not perpendicular to the plunge. The modification involves projecting along plunge onto the TI plane where ϕ = the angle between the profile plane and the TI plane, measured in a horizontal reference frame (Fig. A6.6). If we consider the TI plane to define a Cartesian coordinate system with the origin at the intersection of its zero-elevation line and the line of length d (Fig. A6.4), then we may project any point to a second point (x, y) on the TI plane and maintain the appropriate plunge angle (Fig. A6.6):

$$x = d \tan \phi \qquad \text{(A6.3)}$$

Reproduced with permission of the copyright owner. Further reproduction prohibited without permission.

$$y = h \cos p \pm (d/\cos \phi) \sin p \qquad \text{(A6.4)}.$$

Thus, in mountainous terrain where the transport azimuth is not perpendicular to the regional structural trend, we construct a TI plane-of-section, use equation (A6.3) to define the X-axis position of the projected point (Figs. A6.4 & A6.7), and use equation (A6.4) to define the Y-axis position of the point (Fig. A6.4). Apparent dip on this new plane is treated in the usual way and any non-parallel fold-forms resulting from projection onto a plane that is not perpendicular to plunge will require area-balancing.

CONCLUSIONS

In order to produce balanced cross sections without introducing unnecessary error, the plane-of-section must be inclined at 90 degrees minus the plunge angle and parallel to the direction of tectonic transport and distortion due to the topographic relief must be corrected. Although constructing such sections requires several additional steps in the already-tedious process of data-projection, the incorporation of these steps into computer programs can streamline the process and allow more accurate balanced sections.

Reproduced with permission of the copyright owner. Further reproduction prohibited without permission.

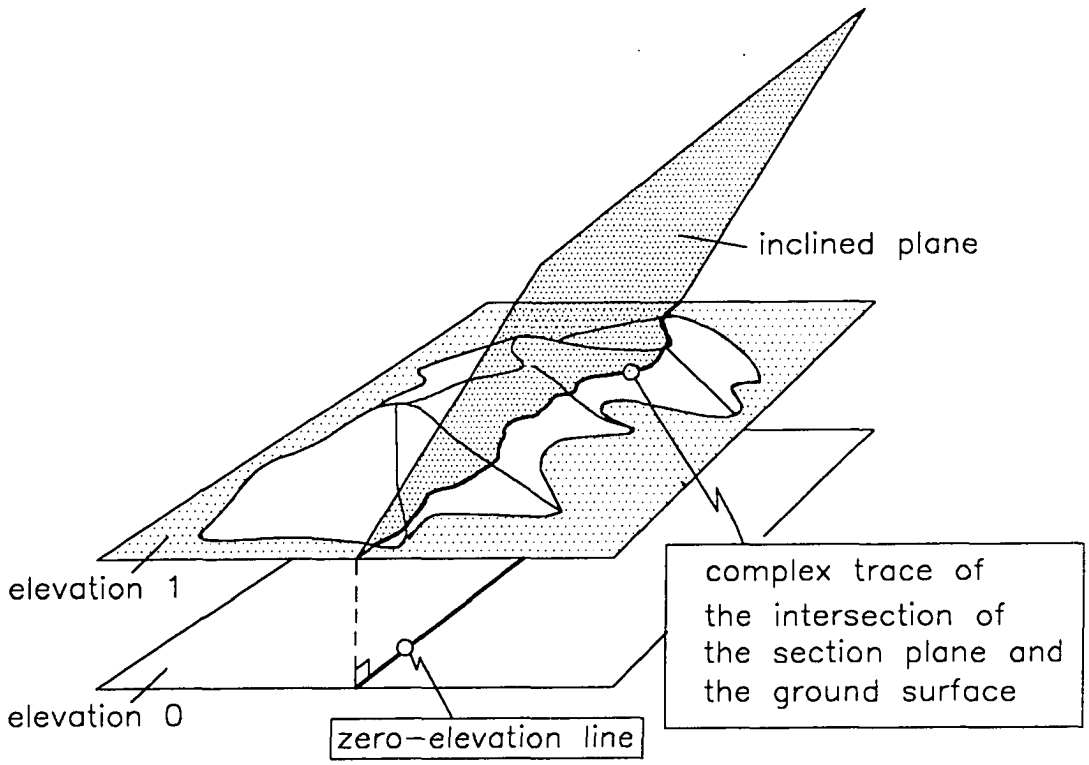

Figure A6.1 - Diagram illustrating that the line defined by the intersection of mountainous terrain and an inclined plane is not straight.

Reproduced with permission of the copyright owner. Further reproduction prohibited without permission.

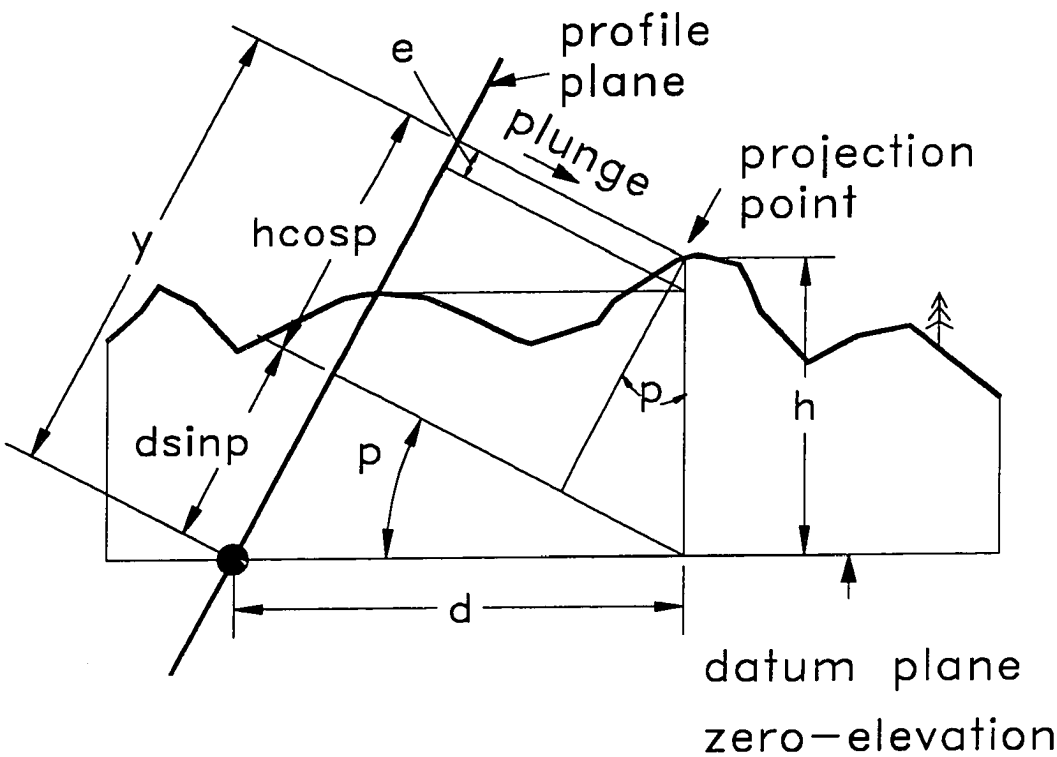

Figure A6.2 - Ramsay and Huber's (1987) method for projecting data along plunge onto a profile section in mountainous areas. The dark circle is the trace of the zero-elevation line, which lies perpendicular to the page, *d* = the horizontal distance of the projection point from the zero-elevation line, *h* = the height of the projection point above the datum plane, *p* = the plunge angle, *y* = the distance in the profile plane above the zero-elevation line of the final position of the projection point, *e* = the error of approximating the topography as a horizontal plane (after Ramsay and Huber (1987)).

Reproduced with permission of the copyright owner. Further reproduction prohibited without permission.

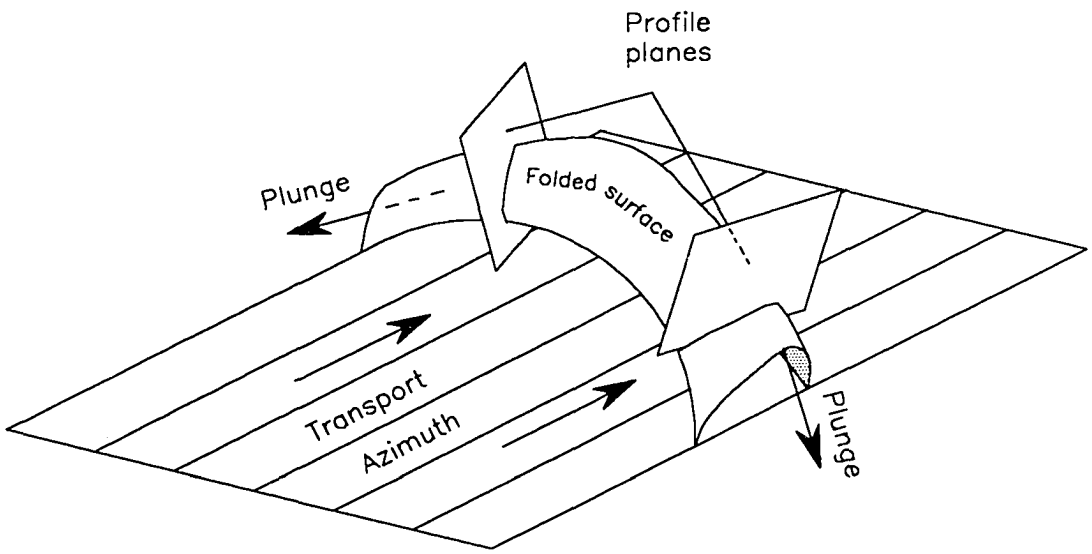

Figure A6.3 - Diagram illustrating the relationship between the profile plane and the direction of tectonic transport in an arcuate structure.

Reproduced with permission of the copyright owner. Further reproduction prohibited without permission.

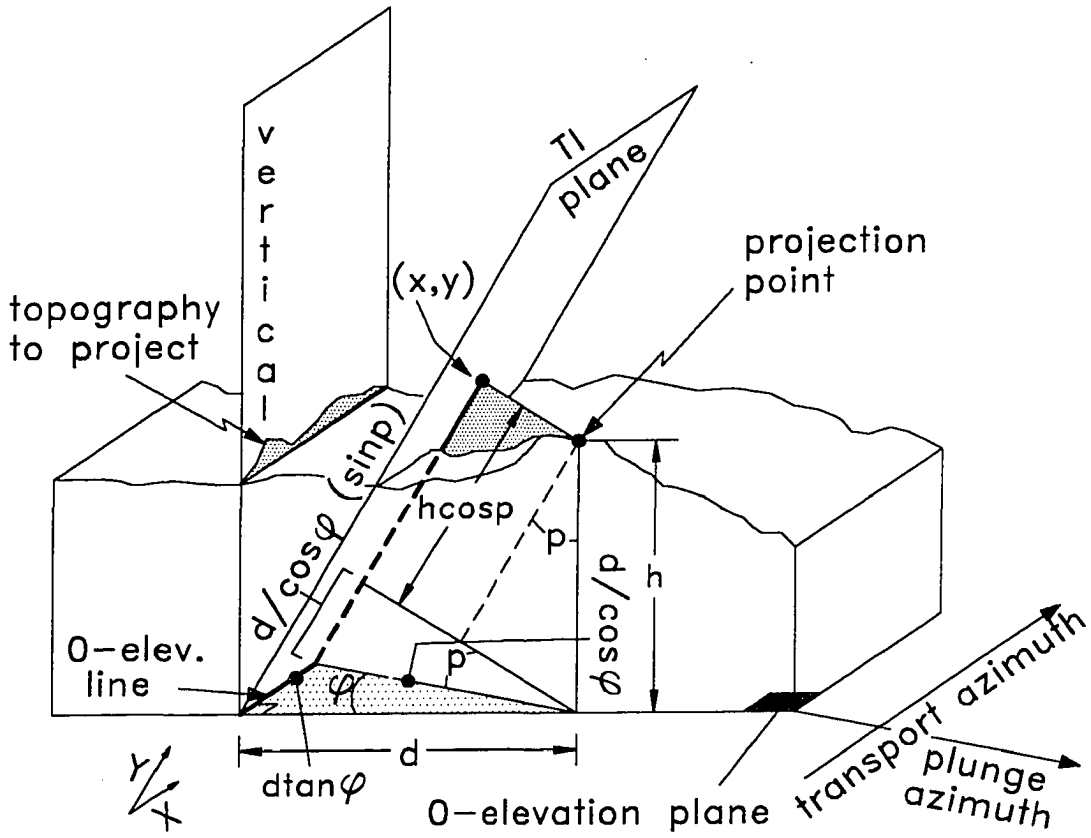

Figure A6.4 - Diagram showing the technique of projecting a point up-plunge onto an inclined "transport-parallel, inclined plane" (TI plane). *d* = distance measured from, and perpendicular to, the zero-elevation line in the zero-elevation plane. ϕ = the angle between the structural trend (plunge azimuth) and *d*, which is perpendicular to the transport azimuth. *h* = the height of projection point above zero-elevation plane. *p* = the plunge angle. The point projects to *(x, y)* on the TI plane according to equations (A6.3) and (A6.4). The profile plane, normal to the plunge, is removed for clarity.

Reproduced with permission of the copyright owner. Further reproduction prohibited without permission.

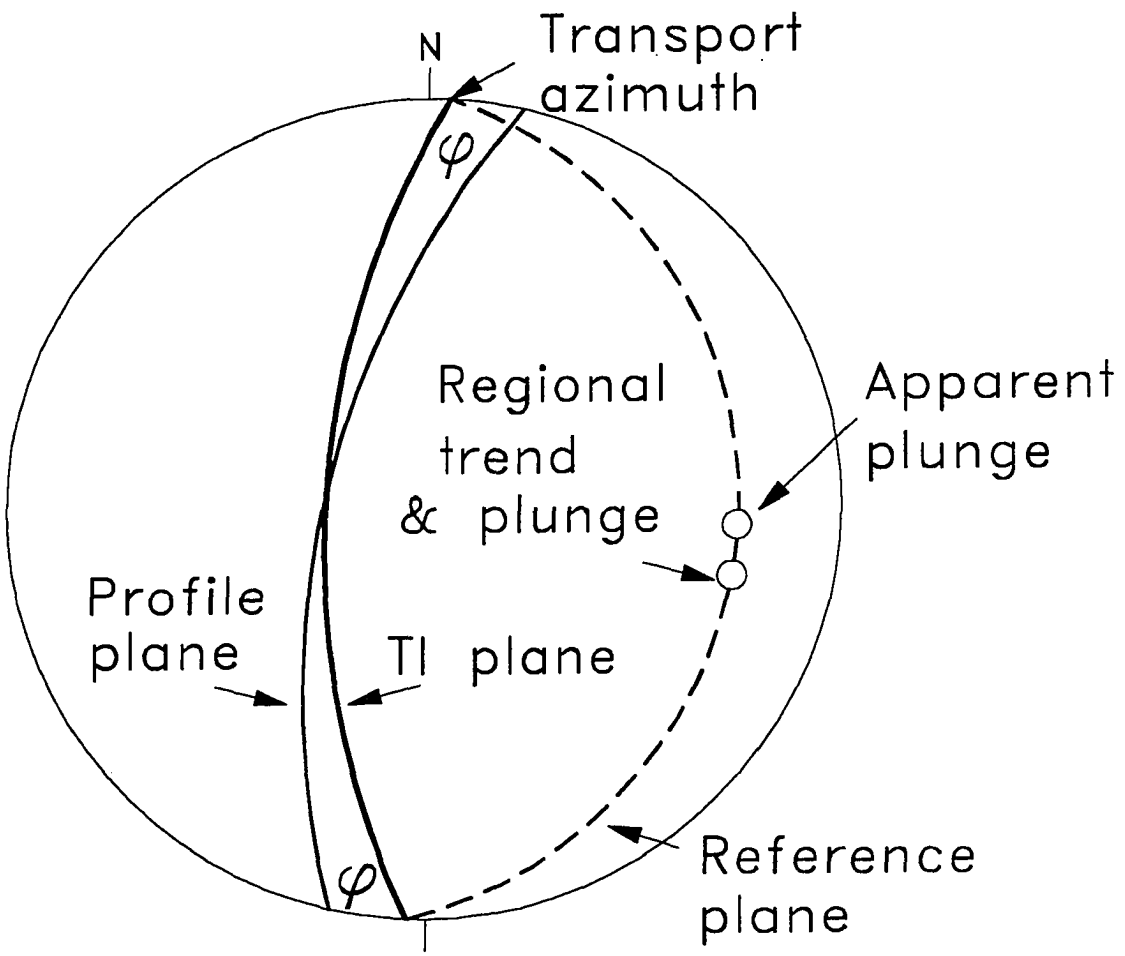

Figure A6.5 - Hypothetical lower hemisphere equal-area stereogram showing determination of ϕ based on both the regional structural trend and plunge angle and the transport azimuth. The dashed line is the projection of the reference plane (see text) and the profile plane is perpendicular to both the structural trend and the structural plunge angle. The TI plane is perpendicular to the apparent plunge angle and contains the transport azimuth.

Reproduced with permission of the copyright owner. Further reproduction prohibited without permission.

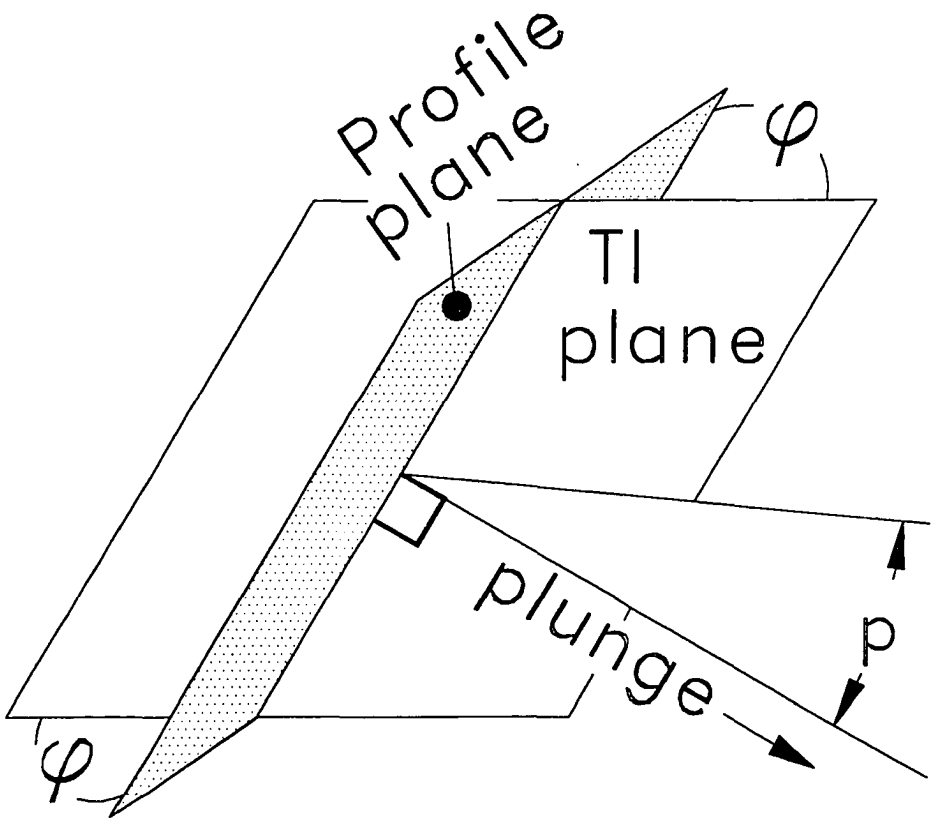

Figure A6.6 - Angular relationship between hypothetical profile and TI planes. The plunge is normal to the profile plane so that any point may be projected with equation (A6.4) along plunge onto the transport-parallel, inclined plane.

Reproduced with permission of the copyright owner. Further reproduction prohibited without permission.

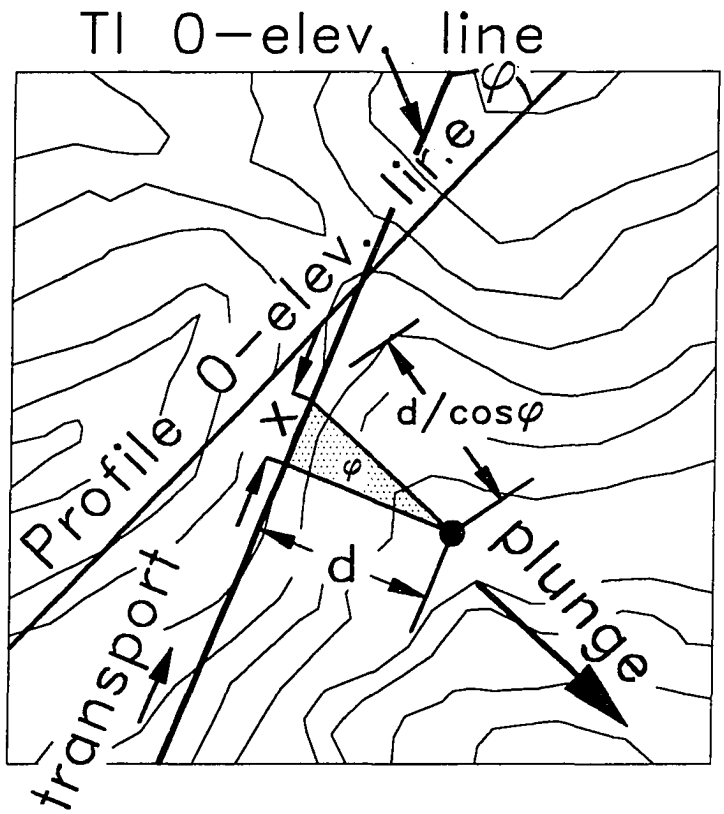

Figure A6.7 - Hypothetical map view showing relationships among the structural trend, the zero-elevation lines of the TI plane and the profile plane. d = the horizontal distance of the projection point measured from, and perpendicular to, the zero-elevation line, ϕ = the angle between the profile and TI planes, x = the X-axis value of the final position of the point projected onto the TI plane ($x = d \tan\phi$).

Reproduced with permission of the copyright owner. Further reproduction prohibited without permission.

APPENDIX 7*- THE PROJECT!© COMPUTER PROGRAM (USERS' GUIDE)

PROject! is an AutoLISP program designed to streamline the process of constructing a geologic cross section. It is fully compatible with AutoCAD r12 and AutoCAD for windows. Project! runs within AutoCAD, allowing the user to modify the cross section with standard AutoCAD commands. The program accepts information from a topographic map (or geologic map with topography) that is secured to a digitizing tablet and has a line of section[1] drawn on it (Fig. A7.1). *PROject!* also interfaces with dialogue boxes and the AutoCAD command line.

PROject! provides easy and accurate techniques for 1) constructing a topographic profile above a cross section line and 2) projecting point and planar data onto a vertical or inclined plane of section. *PROject!* utilizes the Ramsay and Huber (1987) technique for projecting geologic data onto an inclined plane of section in areas of high topographic relief. The program assumes cylindrical folding and accepts bedding data that have been previously converted to apparent dip.

---

* Currently avaliable through RockWare, Inc., Golden, Colorado as: "PROject!".

[1] The line of section or "section line" is a line defined by the intersection of the "plane of section" on which the cross section is drawn, and a plane at elevation zero (e.g. sea level). It is not the intersection of the plane of section and topography, since that line is only straight if the plane of section is vertical. The topography created by PROject! represents the topography directly above the line of section. That is, the topography on a vertical plane above the section line is projected down-plunge onto the section (see also Fig. 5).

Reproduced with permission of the copyright owner. Further reproduction prohibited without permission.

LOADING *PROJECT!*

PROject! requires AutoCAD release 12 or higher, a math co-processor, 40 kb hard disk space, a digitizing tablet, and about 4 MB RAM. To run the program, copy all of the files supplied on the *PROject!* disk into the \acad\support subdirectory. Next, launch AutoCAD and load the program by typing (load "proj") at the AutoCAD command prompt. The program is launched by typing proj. The units setting in AutoCAD determines the units and resolution of both angles and lengths. Before running *PROject!*, be sure that length and angle units are set to decimal and decimal degrees, respectively. You are free to select any resolution.

USING *PROJECT!*

Before running *PROject!*, secure the geologic/topographic map on the digitizing tablet (Fig. A7.1). Upon typing proj, the "PROject! parameters" dialogue box appears (Fig. A7.2). This is the "root" dialogue for *PROject!* and it prompts for information about the general dimensions of the cross section and for instructions about which action you wish to perform.

Contour interval

The contour interval usually equals that of the topographic map on which the line of section is drawn (Fig. A7.1) (see *Calibrate the tablet*). A contour interval is required for all calculations; it is entered as a non-zero integer or real number. The contour interval units (either meters or feet) are chosen below the edit box.

Reproduced with permission of the copyright owner. Further reproduction prohibited without permission.

Section length

Section length is the length of the line of section, it is best to have both ends of the line of section terminate at a contour line. A value for section length is required for *PROject!* to run. Enter this length as a non-zero real or integer and select the units below the box.

Plunge

The plunge is also entered as a real or integer value with no units or directions permitted. The units are assumed to be degrees and the directions are accounted for in other parts of the input process. A value of 0, or no value at all, is acceptable.

Calibrate the tablet

Calibrate the tablet must be selected before any other option in order to calibrate the digitizing tablet in terms of the current contour interval and section length. This selection calls the AutoCAD tablet command, and selects "cal" for calibrate. But first, the "Tablet parameters" dialogue box appears informing you exactly how to calibrate the tablet (not shown). This dialogue includes a highlighted value that will become the X-coordinate defining the right end of your line of section. This value is the section length you selected in the "PROject parameters" dialogue corrected for unit-type and expressed in the same units as the contour interval (*i.e.* feet or meters). This conversion is required in order to produce a section with zero vertical exaggeration. Upon selecting "OK" from the "Tablet parameters" dialogue you will see the following at the AutoCAD command prompt:

Reproduced with permission of the copyright owner. Further reproduction prohibited without permission.

Digitize point #1:

At this point select the left end of the line of section drawn on your map with the puck. The coordinates (0,0) are automatically provided by the program and you are then asked to

Digitize point #2:

Select the right end of the section line in response. *PROject!* enters the value highlighted in the "Tablet parameters" dialogue box as the X-coordinate and "0" as the Y-coordinate of the right end of the section line. For example, if you chose a contour interval of 100 feet and a section length of 2 miles in the "PROject! parameters" dialogue box, then the right end of the section line is automatically calibrated as point (10560,0). When you press "enter" to exit the AutoCAD tablet command after selecting the second point, the tablet is calibrated to the map and the cross section will be drawn with no vertical exaggeration[2]. Project! will always turn *and leave* tablet mode on. To re-enter *PROject!* after calibrating, press 'enter'.

Construct topographic profile

After the tablet has been calibrated, an accurate topographic profile can be drawn from the map data. The resolution on the profile is determined by the contour interval you chose, usually the one on the map. By following the instructions that follow this selection, you will draw a polyline that represents the topography from the left end of the section to the right end of the section. The smoothness of this profile line is determined by the vertex spacing, which in turn

[2] You are free to recalibrate the tablet with other values later in the PROject! session, although digitized points will be assumed to be in units of meters or feet by all PROject! operators.

Reproduced with permission of the copyright owner. Further reproduction prohibited without permission.

is determined by the spacing between contour line/section line intersection points (Fig. A7.1). If you are dealing with a very long line of section and many contour/section line intersection points, you may want to select only every major contour. In this case, a new contour interval needs to be supplied in the "PROject! parameters" dialogue box and the tablet will need to be re-calibrated to account for this change. For instance, if the contour interval on the topographic map is 100' and you wish to use only 500' increments, then the contour interval input into the "PROject! parameters" dialogue box must be 500, not 100.

Upon selecting *Construct topographic profile* you are prompted, at the AutoCAD command line, for the elevation of the left end of the section:

What is the elevation of the left end of the section?

In response to this prompt, enter the topographic elevation at the extreme left end of the section. It is best to place the left end of the section exactly on a contour line and enter the value of that contour line at this prompt. For example, the appropriate response to this question for the section line in figure A7.1 is 250.

Next, *PROject!* zooms to a readable scale. If you are constructing a short cross section, but one that includes a significant vertical component (*i.e.* height:length ~1:1) some of the polylines may be drawn out of the field of view. You can regain a proper perspective after you construct the topographic profile by using standard AutoCAD zoom commands. At this stage, you are asked to select the left end of the section.

Select the left end of the section:

Reproduced with permission of the copyright owner. Further reproduction prohibited without permission.

PROject! now switches to osnap mode "end". Select the left end of the section on the calibrated digitizing board. *PROject!* draws the base and left hand side of the cross section and then prompts:

Pick the next contour line/section line intersection point to the right:

The intersection point on the map that you choose must be *immediately to the right* of the left end of the section, unless you chose a contour interval that differs from that on the map. After this point is selected, you are asked where this point lies relative to the left end of the section:

Is this point Higher than (H), Lower than (L), or at the same (S) elevation as the last point?

Any contour line that intersects the section line must satisfy one of these three conditions. If you respond with (H) or (L), then *PROject!* draws a polyline from the last point (*i.e.* the left end of the section if this is your first intersection selection) to a new point and this polyline represents the slope of the topography between the two points. This polyline is yellow and is drawn on a layer named "topo", which can be modified using standard AutoCAD commands.

If you respond to the last prompt with (S), then you are asked a further question:

Did you just cross a valley (V), a ridge (R), or does the contour line parallel the contact? (C)?

Reproduced with permission of the copyright owner. Further reproduction prohibited without permission.

Responding appropriately allows *PROject!* to draw a polyline which represents the intervening valley or ridge and connect that polyline to the one created in response to the last pick point[3]. You are then asked whether you wish to continue. Answering "yes" (enter) repeats the process, while responding "no" (n) ends *PROject!* At the end of the *Construct a topographic profile* command sequence, the topography is represented by a single polyline with many vertices that can be treated as a normal AutoCAD polyline entity. Tablet mode remains on. IMPORTANT - If you make a mistake during construction of the topographic profile, start from the beginning (*i.e.* the left end of the section) and don't try to restart the construction process midway along the section line.

Project planes (*e.g.* contacts, fault planes)

PROject! treats separate lithologic contacts as separate layers within AutoCAD. Layer, plunge, and elevation data are input using the "Contact/fault information" dialogue box (Fig. A7.3) in order to project a contact or fault onto a cross section.

A contact is selected at each contour/section line intersection, so that large numbers of points along a contact may be projected easily. The result of this operation on the cross section is a polyline, on a user-defined layer, that represents the along-plunge projection of a lithologic boundary.

---

[3] Any valley or ridge is assumed to lie at 1/2 the distance between contour lines, in both a vertical and horizontal sense. If this is not the case (e.g. the valley is much closer to the more recently selected contour than to the previous selected contour - rather than exactly midway between them), then you may want to go back to this point after you finish creating the profile and edit the coordinates of this point using the AutoCAD pedit/edit vertex/move command sequence.

Reproduced with permission of the copyright owner. Further reproduction prohibited without permission.

In the "Contact/fault information" dialogue you specify a layer name and color for the contact to be projected, the elevation of the first point you wish to project, and the position of the contact relative to the section line. When this information is supplied in an acceptable form, *PROject!* prompts for points of intersection between the contact and consecutive contour lines. These prompts are similar to those used in creating the topographic profile. You are asked whether each selection point is topographically higher than, lower than, or at the same elevation as the previous point.

The number you enter as "Elevation of 1st digitized point on this contact/fault" is treated as a starting elevation. It is assumed to be in the same units as the contour interval entered in the "PROject! parameters" dialogue box. The first contact/contour intersection may lie anywhere on the digitizing board. For example, in figure A7.1, if the labeled contour/contact intersection is the first to be selected, then the proper response to the elevation prompt is 300. *PROject!* determines the shortest distance (d) between the point and the line of section (*i.e.* the perpendicular distance). Next, with the plane of section represented by a Cartesian coordinate system, *PROject!* determines the x-coordinate of the pick point, solves for the y-coordinate (y') using the plunge angle (p), elevation (h), and the Ramsay and Huber (1987) equation for data-projection:

$$y' = h \cos p \pm d \sin p \qquad \text{(A7.1)}$$

which is additive while "Down plunge" is selected and subtractive while "Up plunge" is selected (Fig. A7.4).

Reproduced with permission of the copyright owner. Further reproduction prohibited without permission.

Very few geologic cross sections traverse areas of perfect cylindrical folding and the projections performed with this, or any program are rarely 100% accurate. Also, "S" or "Z"-shaped map patterns may result in "S" or "Z"-shaped cross section patterns, which may be geologically implausible. If you suspect such distortion, it is recommended to that you select only that part of the "S" or "Z" shape on the map that lies closest to the section line and discard the other points. The accuracy of any projection decreases with distance from the section line and projection distances (d) of several kilometers or more are not recommended.

Project strike/dip symbols

PROject! inserts standard strike/dip symbols in the form of AutoCAD block entities. A separate block is created for each layer and the strike/dip block on a particular layer has the name of that layer. Upon selecting *Project strike/dip symbols* button, a dialogue box like figure A7.5 appears and prompts for strike/dip symbol specifications.

Dip-direction buttons

These buttons insert a strike/dip symbol with an open circle on one end and a line extending from the circle toward the dip-direction[4] (Fig. A7.6). For example, use the *Dips to the left* selection for upright beds that dip to the left as seen on the section plane. Note, this is not to be confused with "dips to the west" since *PROject!* is concerned only with relative directions. Overturned

[4] The form of the bedding symbols is convenient for cross section balancing, since the "tail" of the symbol is exactly parallel to the dip. This enables easy extrapolation and determination of fold hinges in cross section using AutoCAD osnap modes and the extend command.

Reproduced with permission of the copyright owner. Further reproduction prohibited without permission.

beds are represented by strike/dip symbols with the circle at the bottom (Fig. A7.6).

The symbols are each scaled to be visible on the section. If you wish to alter the size of a strike/dip symbol, you may do so with the AutoCAD scale command. Alternatively, you may explode and re-create the block at a more suitable size, remembering that the block name must be the same as the layer name if *PROject!* is to automatically insert it and that this modification affects all other strike/dip blocks on that layer. The insertion point is the center of the circle.

Degrees of apparent dip

This numerical editor accepts real or integer values between 0 and 90 inclusive, or no value at all. The value represents the apparent dip of a plane when projected into the plane of section. *PROject!* does not solve for apparent dip, since this is more easily accomplished in a spread sheet format. See an introductory structural geology text for more about apparent dip.

Elevation of the data point

Any real or integer value, or no value, is acceptable for entry in the *Elevation of the data point* numerical editor. This elevation is used as the variable (h) in the Ramsay and Huber (1987) equation. The elevation is read directly off of the topographic map so that the data point in figure A7.1 has an elevation of 300.

Reproduced with permission of the copyright owner. Further reproduction prohibited without permission.

Relative plunge position

As in other *PROject!* dialogue boxes, you must specify the relative position of the data point with respect to the plane of section. This selection determines whether the projection equation is additive or subtractive. In figure A7.1, you would select "Down plunge".

Project text, points or numerical data

Annotations and point symbols are projected onto the plane of section using the *Project text, points or numerical data* button. Upon selecting this option, the "Annotate projection points" dialogue box appears (Fig. A7.7).

The components of this box are very similar to those of other dialogues, except that this one contains the toggle switch *Enable automatic point scaling. PROject!* uses the AutoCAD point command with the point style defined by the AutoCAD system variable "pdmode" 32. The size of the point is determined by the relative sizes of the horizontal and vertical dimensions of the plane of section (similar to the strike/dip symbol size). When the *Enable automatic point scaling* toggle is active, *PROject!* will automatically scale the size of the point symbol. If this toggle is deactivated, then you are free to experiment with other sizes and shapes using the pdsize and pdmode AutoCAD commands. Note that such changes affect all previous and subsequent point commands.

The text size for projected text or numbers is determined manually by the *Text size* numerical editor. Since the dimensions of the cross section are always expressed in terms of meters or feet, choosing the best text size may require a bit of trial and error. Text is projected onto the cross section using the AutoCAD dtext command.

Reproduced with permission of the copyright owner. Further reproduction prohibited without permission.

PROJECT! MESSAGES

When your input is invalid or incomplete, a message box appears, points out the problem, and (except when constructing the topographic profile) returns you to the AutoCAD command line. After a *PROject!* message, the AutoCAD command line reads:

Press 'enter' to restart PROject!: quit/exit abort *Cancel*

If a message box appears while you're performing an action other than constructing topography, press "enter" 2 or 3 times and you will return to the box where the problem occurred.

Reproduced with permission of the copyright owner. Further reproduction prohibited without permission.

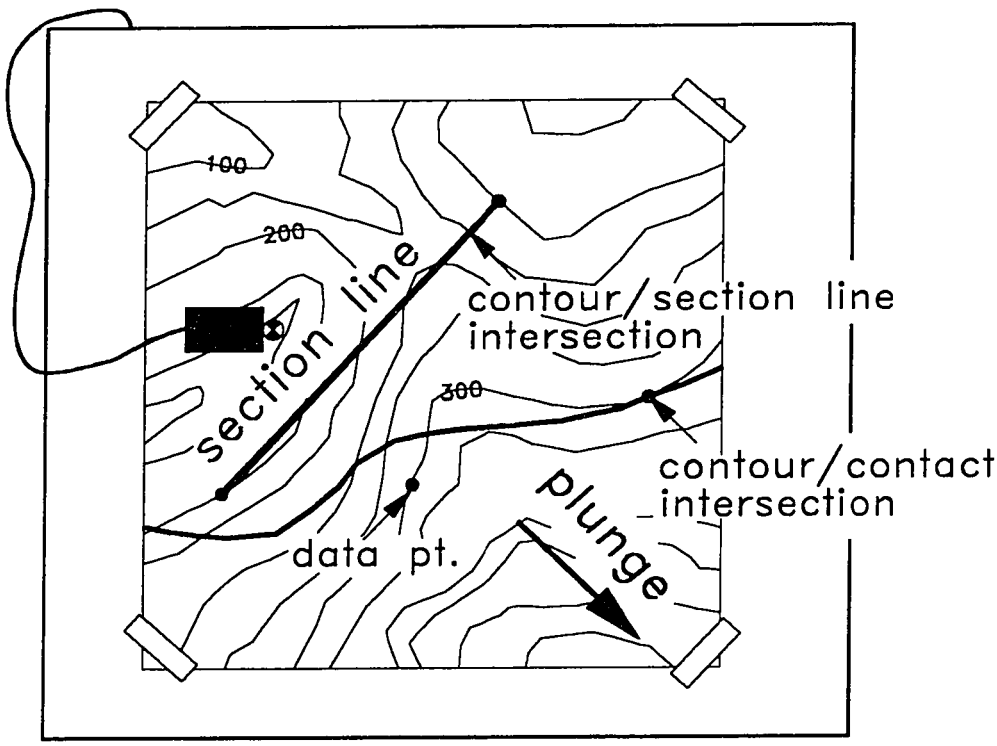

Figure A7.1 - An example of a section line drawn perpendicular to the plunge on a geologic map that is taped to a digitizing board. Note that the section line terminates at a contour line and that the contour interval is 50. The heavy curved line represents a lithologic contact.

Reproduced with permission of the copyright owner. Further reproduction prohibited without permission.

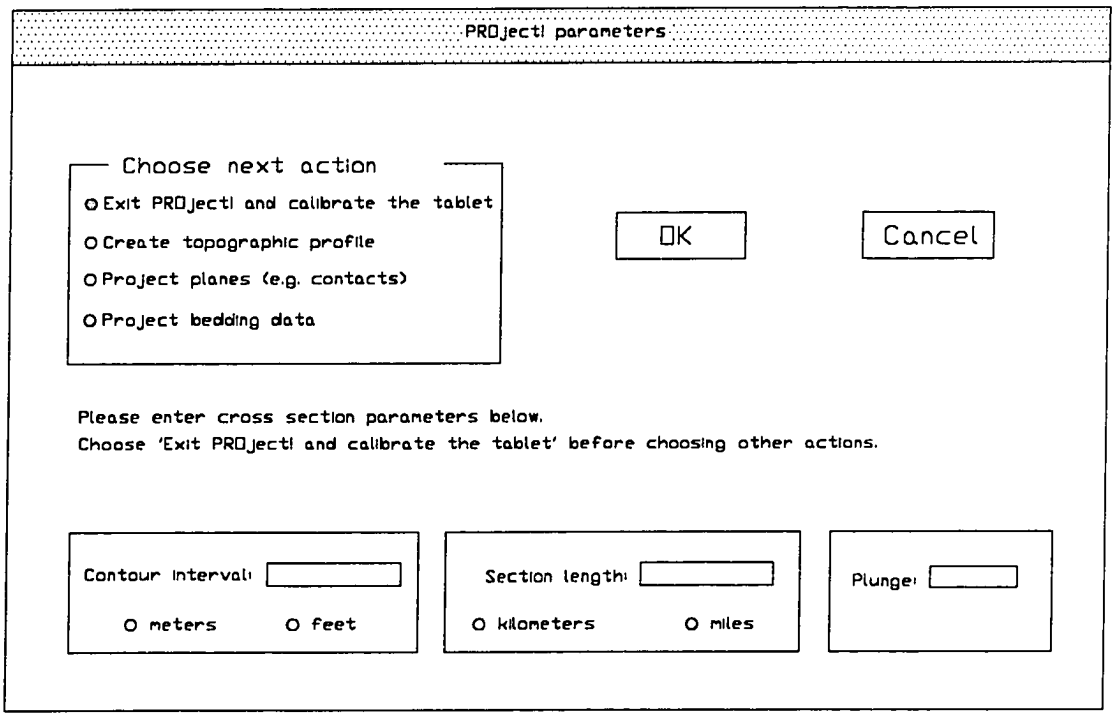

Figure A7.2 - The "PROject! parameters" dialogue box.

Reproduced with permission of the copyright owner. Further reproduction prohibited without permission.

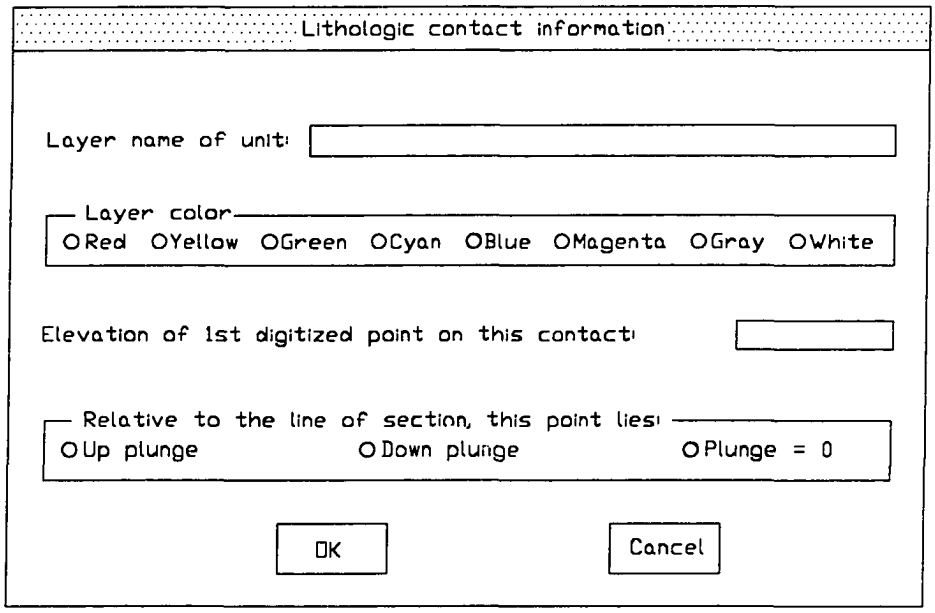

Figure A7.3 - The "Contact/fault information" dialogue box.

Reproduced with permission of the copyright owner. Further reproduction prohibited without permission.

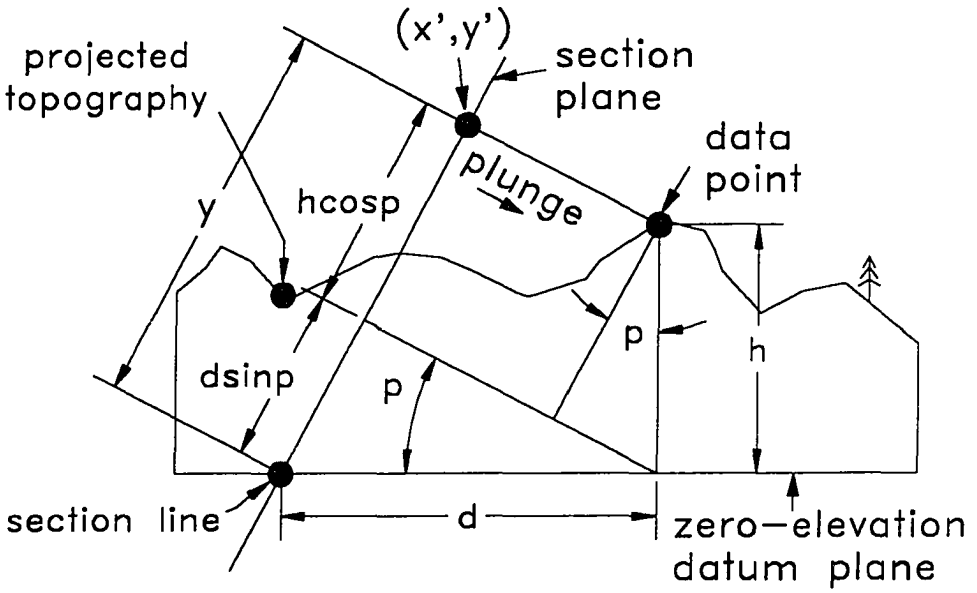

Figure A7.4 - The Ramsay and Huber (1987) method for projecting data onto a profile section in regions of high relief. The method assumes cylindrical folding so that any point may be projected along the normal to the section plane. Here the data point lies down plunge of the line of section and is projected to point (x', y'). The trend of the section is perpendicular to the best fit regional fold axis and the dip of the section is (90° - plunge angle). (After Ramsay and Huber (1987, p. 368, Fig. 18.5a)).

Reproduced with permission of the copyright owner. Further reproduction prohibited without permission.

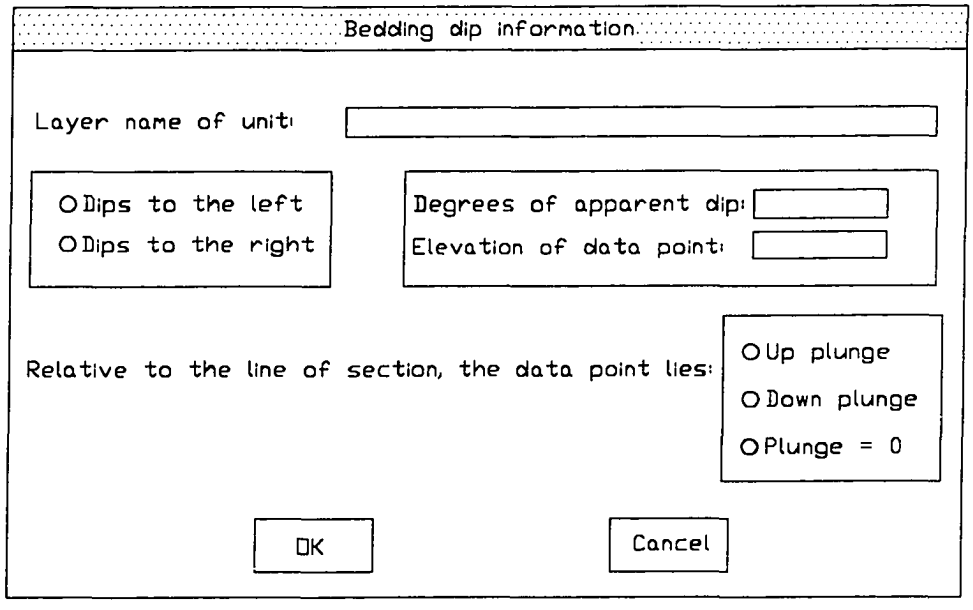

Figure A7.5 - The "bedding dip information" dialogue box.

Reproduced with permission of the copyright owner. Further reproduction prohibited without permission.

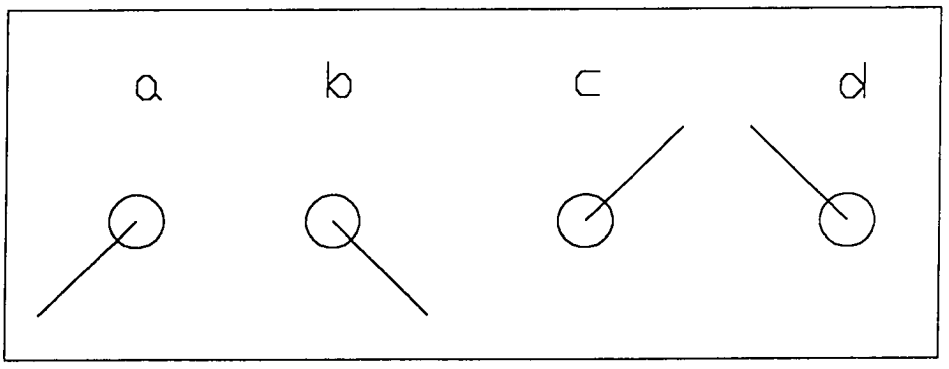

Figure A7.6 - The strike/dip symbols constructed by *PROject!* Four separate symbols are used which represent beds that a) dip to the left, b) dip to the right, c) are overturned to the left, and d) are overturned to the right.

Reproduced with permission of the copyright owner. Further reproduction prohibited without permission.

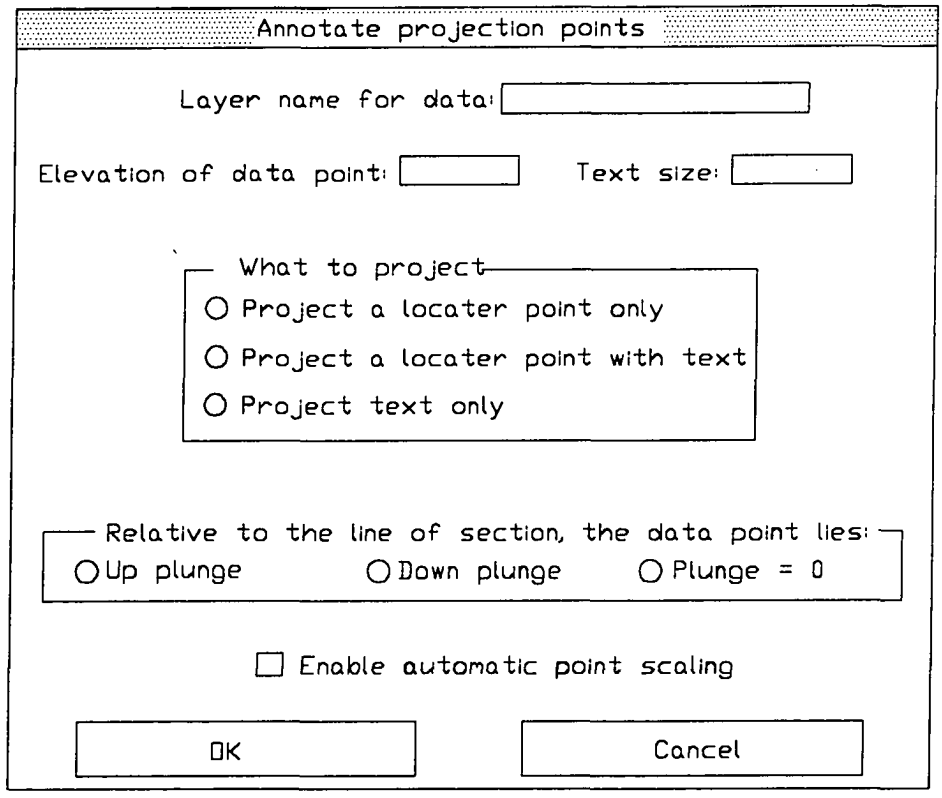

Figure A7.7 - The "Annotate projection points" dialogue box.

Reproduced with permission of the copyright owner. Further reproduction prohibited without permission.

APPENDIX 8 - THE DETFOLD COMPUTER PROGRAM (USERS' GUIDE)*

Detfold is a simple AutoLISP routine that solves for the detachment depth beneath a triangular detachment anticline above a horizontal detachment. The program is useful for assessing detachment fold geometries because it calculates and precisely draws a balanced fold geometry very quickly. Since the program is a simple AutoCAD command, it is very helpful for users already working in the AutoCAD environment (on detachment fold analyses or balanced cross sections). *Detfold* requires AutoCAD release 10 (or later) and a negligible amount of disk space and memory.

Input consists of 1) picking 6 points to define the geometry, 2) answering the question "Do you know *either* the original or final detachment depth (Yes or No)?", and 3) supplying an "original" or "final" depth (if you answer question #2 positively). The routine uses equations 2.4, 2.18, and 2.19 to determine the constant depth, area differential, and variable depth, respectively. In this program, the elevation of the top of the incompetent unit outside the anticline represents the "regional" elevation, as in figures. 2.8 and 2.10 (contrast with Figs. 2.6 & 3.4).

LOADING *DETFOLD*

To load the program:

---

* The program *Detfold.lsp* is considered "shareware". It may be copied and freely distributed.

Reproduced with permission of the copyright owner. Further reproduction prohibited without permission.

1) Copy the file *detfold.lsp* from the disk provided into the acad\support directory.

2) Type: (load "detfold") at the AutoCAD command line.

To run the program, type detfold and press <enter>.

INPUT

All input is supplied at the AutoCAD command line or by picking points, there are no dialogue boxes, as in *PROject!* After typing detfold at the command prompt, you are asked to pick a point:

pick the first point:

Here, you choose a point representing point 1 on figure A8.1. This prompt continues until six points are selected sequentially. You may choose these points in a variety of standard ways (*e.g.* enter coordinates, choose endpoints of an existing fold-drawing, or pick isometric points with the AutoCAD "snap" mode - recommended for first-time users). The selections define points along the competent-incompetent contact and the thickness of the competent unit as follows (Fig. A8.1):

- Point (1) = left-hand extent of horizontal contact
- Point (2) = left-hand synclinal hinge at the contact
- Point (3) = anticlinal hinge at the contact
- Point (4) = right-hand synclinal hinge at the contact
- Point (5) = right-hand extent of horizontal contact
- Point (6) = competent unit thickness

Points (1), (5), and (6) are not necessary to define the triangle, but are included to aid in constructing a clear diagram (*e.g.* Fig. A8.2). Points (1), (2), (4), and (5)

Reproduced with permission of the copyright owner. Further reproduction prohibited without permission.

should lie on the same horizontal (all should have the same Y-axis coordinates) but their spacing can vary. Thus, when superimposing these points on a diagram of a natural fold, the diagram may have to be rotated first. Point (3) can lie anywhere above the horizontal defined by points (2), (4), and (5). Point (6) should be on a vertical line above point (5). To ensure that the points are orthogonal, it is helpful to have the AutoCAD "snap" mode on (press F9 to do this).

After selecting or entering the six points, you are asked:

Do you know EITHER the original or final depth <N=no/Return=yes>?

and, if yes:

Do you know the original (O) or final (F) depth?

Answer by entering O or F. Then you are accordingly asked:

What is the original depth?

or

What is the final depth?

You must respond to these questions with real or whole number input at the command line. *Detfold* is independent of specific units (*e.g.* meters, miles, ect.).

OUTPUT

Output takes the form of 1) a geometrical representation of a balanced detachment fold and 2) a list of the calculated geometrical values. The list of calculated values enables variables to be directly plotted on the variable depth

Reproduced with permission of the copyright owner. Further reproduction prohibited without permission.

diagram (Fig. 2.7). This list is not explained further here[1]. The geometrical representation is briefly outlined here (but see Figs. A8.2, A8.3, & A8.4).

For a constant detachment depth fold (Fig. A8.2):

- The constant depth is represented as a continuous horizontal line along the base of the diagram.

For variable depth folds (Figs. A8.3 & A8.4):

- The displaced area, (A_O) in Chapters 2 and 3, is the rectangle on the lower left of the diagram.
- The original depth (undeformed stratigraphic thickness of the incompetent unit) is the base of the A_O rectangle.
- The area differential is shown as a rectangle with a cross in it.
- The final depth, (D_f) in Chapters 2 & 3, is the side of the area differential rectangle that is *not* on the same horizontal as the original depth.

All other variables are as in figures 2.2, 2.6, and 3.4.

Detfold is a single routine. When the drawing is completed and the values listed, you are returned to the AutoCAD command prompt.

[1] The default text size is set to "0.3" for this program. Thus, the text size may be too large or small, depending on your current setting. To fix this, scale the list -after it is printed- to a more suitable text size (use the scale command to do this) or alter line 14 of the code (setvar "textsize" 0.3) to a more suitable size (Appendix 9).

Reproduced with permission of the copyright owner. Further reproduction prohibited without permission.

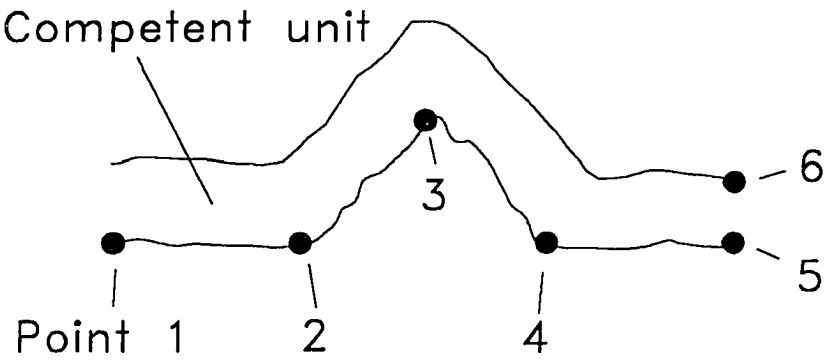

Figure A8.1 - Diagram showing where to pick points for *Detfold.* Points must be selected (or input) in sequential order from 1 to 6. Points (1), (2), (4), and (5) must define a horizontal line and points (5) and (6) must define a vertical line. This diagram shows that these selections can be overlain "on top of" a cross section of a natural fold (lines represent geologic contacts in cross-sectional view).

Reproduced with permission of the copyright owner. Further reproduction prohibited without permission.

Uplifted fold area (Af) (units squared)=
4.00
Displaced area (Ao) (units squared)=
4.02
Wavelength (W)=
4.00
Amplitude (H)=
2.01
Shortening (S)=
1.66
Detachment Depth (D)=
2.42
Thickness=
1.00
Gamma=
90.00
Alpha=
45.00
S/D=
0.68
W/H=
1.99

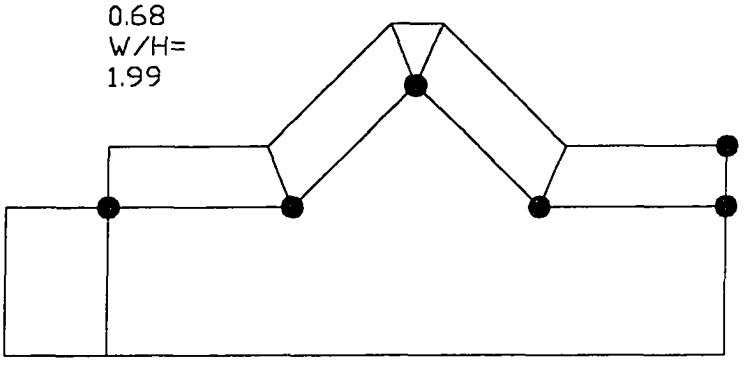

Figure A8.2 - An example of output from *Detfold* for a constant depth solution (see Fig. 2.2). Output does not include the dark points, which represent input (Fig. A8.1).

Reproduced with permission of the copyright owner. Further reproduction prohibited without permission.

```
Uplifted fold area (Af) (units squared)=
7.06
Displaced area (Ao) (units squared)=
2.13
Area Diff. (units squared)=
-4.96
Final Detachment Depth (Df)=
1.30
Original Detachment Depth (Do)=
2.00
Amplitude (H)=
2.01
Shortening (S)=
1.07
Wavelength=
7.06
Thickness=
1.00
Df/Do=
0.65
Delta D=
-0.70
S/H=
0.53
S/W=
0.15
```

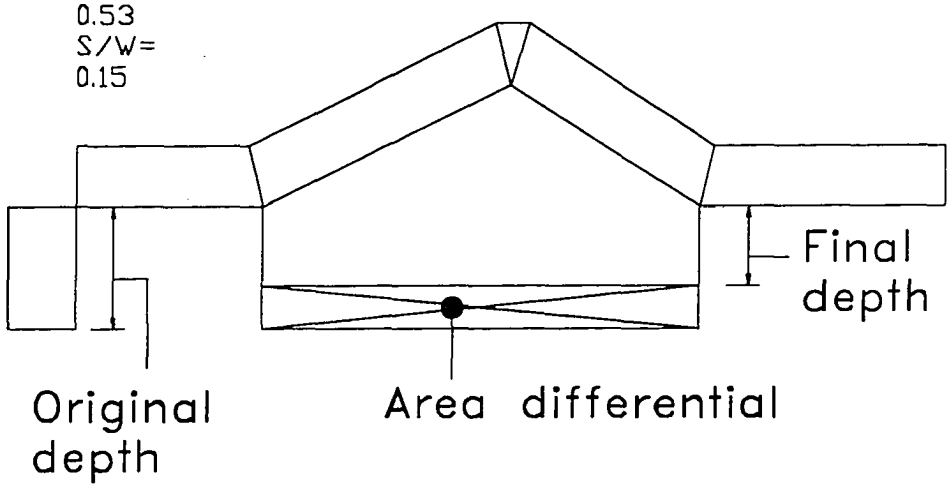

Figure A8.3 - An example of output from *Detfold* for a variable depth solution where the final depth is less than the original depth ($D_f < D_o$, an early-stage, open fold) (*e.g.* Fig. 3.4). Final depth is always measured from the side of the area-differential rectangle that is at a different elevation from the original depth. Output does not include the large-print annotations on this diagram.

Reproduced with permission of the copyright owner. Further reproduction prohibited without permission.

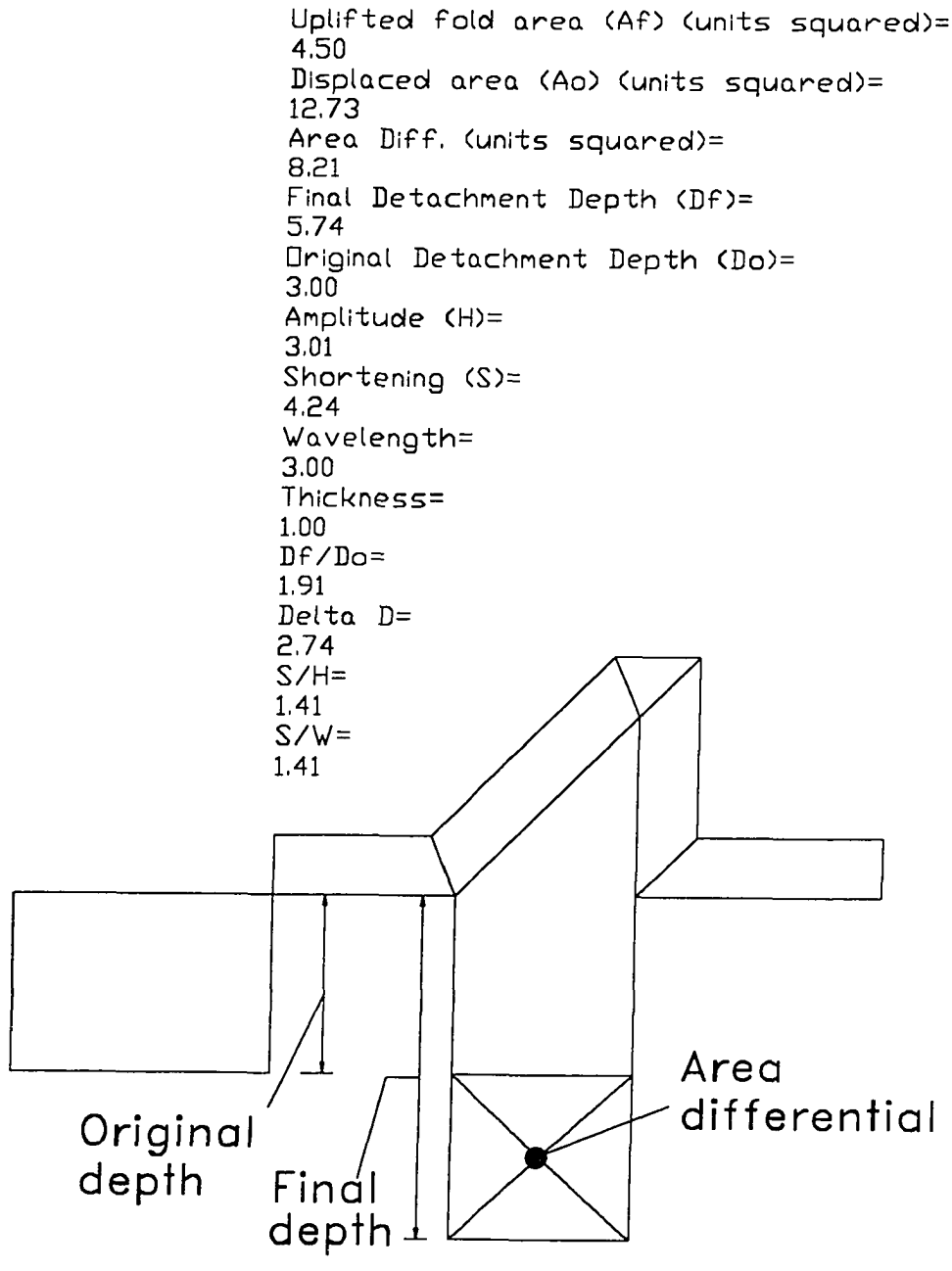

Figure A8.4 - An example of output from *Detfold* for a variable depth solution where the final depth is greater than the original depth ($D_f > D_0$, a late-stage tight fold) (*e.g.* Fig. 3.4). Final depth is always measured from the side of the area-differential rectangle that is at a different elevation from the original depth. Output does not include the large-print annotations on this diagram.

Reproduced with permission of the copyright owner. Further reproduction prohibited without permission.

APPENDIX 9- DETFOLD.LSP (COMPUTER CODE)

This AutoLISP code is not as streamlined and efficient as possible and if any reader chooses to update and streamline it, please send an updated version to me. I can be contacted through the University.

```
(defun restore()
(setvar "textsize" oldsize)
(quit)
(princ)
(princ)
(princ)
   )
(defun c:detfold (/ pt1 pt2 pt3 pt4 pt5 pt6 alpharad gamrad cotalpha omegarad
cotomega omega alpha W H short S D obtuse sinobtuse acute sinacute
thickness
dist1 pt7 pt8 dist2 dist3 dist4 pt9 pt10 pt11 pt12 pt13 pt14 pt15)
(setq oldsize (getvar "textsize"))
(setvar "textsize" 0.3)
(setq pt1 (getpoint "\npick the first point:"))
(setq pt2 (getpoint "\npick the second point:"))
(setq pt3 (getpoint "\npick the third point:"))
(setq pt4 (getpoint "\npick the fourth point:"))
(setq pt5 (getpoint "\npick the fifth point:"))
(setq pt6 (getpoint "\npick the sixth point:"))
(setq alpharad (angle pt2 pt3))
(setq gamrad (- (angle pt3 pt4) (angle pt3 pt2)))
(setq cotalpha (/ (cos alpharad) (sin alpharad)))
(setq omegarad (- 3.145927 (+ gamrad alpharad)))
(setq cotomega (/ (cos omegarad) (sin omegarad)))
```

Reproduced with permission of the copyright owner. Further reproduction prohibited without permission.

```
(setq omega (* omegarad 57.2958))
(setq alpha (* alpharad 57.2958))
(setq gamma (* gamrad 57.2958))
(setq W (distance pt2 pt4))
(setq H (/ W (+ cotomega cotalpha)))
(setq short (+ (distance pt2 pt3) (distance pt3 pt4)))
(setq S (- short W))
(setq D (/ (* W H) (* 2 S)))
(setq obtuse (+ (/ (- (angle pt2 pt1) (angle pt2 pt3)) 2) alpharad))
(setq sinobtuse (sin obtuse))
(setq acute (/ (+ (angle pt4 pt5) (angle pt4 pt3)) 2))
(setq sinacute (sin acute))
(setq thickness (distance pt5 pt6))
(setq dist1 (/ thickness sinacute))
(setq pt7 (polar pt4 acute dist1))
(setq pt8 (polar pt3 acute dist1))
(setq dist2 (distance pt3 pt4))
(setq dist3 (/ thickness sinobtuse))
(setq dist4 (distance pt2 pt3))
(setq pt9 (polar pt3 obtuse dist3))
(setq pt10 (polar pt2 obtuse dist3))
(setq pt11 (polar pt1 (/ pi 2) thickness))
(setq pt12 (polar pt1 pi S))
(setq pt13 (polar pt12 4.71239 D))
(setq pt14 (polar pt1 4.71239 D))
(setq pt15 (polar pt5 4.71239 D))
(setq pt16 (polar pt11 (/ pi 2) thickness))
(setq pt17 (polar pt16 (/ pi 2) 0.5))
(setq pt18 (polar pt17 (/ pi 2) 0.5))
(setq pt19 (polar pt18 (/ pi 2) 0.5))
(setq pt20 (polar pt19 (/ pi 2) 0.5))
(setq pt21 (polar pt20 (/ pi 2) 0.5))
```

Reproduced with permission of the copyright owner. Further reproduction prohibited without permission.

```
(setq pt22 (polar pt21 (/ pi 2) 0.5))
(setq pt23 (polar pt22 (/ pi 2) 0.5))
(setq pt24 (polar pt23 (/ pi 2) 0.5))
(setq pt25 (polar pt24 (/ pi 2) 0.5))
(setq s/d (/ S D))
(setq w/h (/ W H))
(setq pt26 (polar pt25 (/ pi 2) 0.5))
(setq pt27 (polar pt26 (/ pi 2) 0.5))
(setq pt28 (polar pt27 (/ pi 2) 0.5))
(setq pt29 (polar pt28 (/ pi 2) 0.5))
(setq pt30 (polar pt29 (/ pi 2) 0.5))
(setq pt31 (polar pt30 (/ pi 2) 0.5))
(setq pt32 (polar pt31 (/ pi 2) 0.5))
(setq pt33 (polar pt32 (/ pi 2) 0.5))
(setq pt34 (polar pt33 (/ pi 2) 0.5))
(setq pt35 (polar pt34 (/ pi 2) 0.5))
(setq pt36 (polar pt35 (/ pi 2) 0.5))
(setq pt37 (polar pt36 (/ pi 2) 0.5))
(setq pt38 (polar pt37 (/ pi 2) 0.5))
(setq pt39 (polar pt38 (/ pi 2) 0.5))
(setq pt40 (polar pt39 (/ pi 2) 0.5))
(setq pt41 (polar pt40 (/ pi 2) 0.5))
(setq sh/de (rtos s/d 2 2))
(setq wa/am (rtos w/h 2 2))
(setq sh (rtos S 2 2))
(setq de (rtos D 2 2))
(setq wa (rtos W 2 2))
(setq am (rtos H 2 2))
(setq al (rtos alpha 2 2))
(setq ga (rtos gamma 2 2))
(setq th (rtos thickness 2 2))
(setq sooh (/ S H))
```

Reproduced with permission of the copyright owner. Further reproduction prohibited without permission.

```
(setq soow (/ S W))
(setq soh (rtos sooh 2 2))
(setq sow (rtos soow 2 2))
(command "area" pt2 pt3 pt4 "")
(setq afu (getvar "area"))
(setq af (rtos afu 2 2))
(setq sxd (* S D))
(setq sd (rtos sxd 2 2))
(setq xgraph (* w/h 1.66))
(setq ygraph (* s/d 0.70))
(setq depth (getstring "\nDo you know EITHER the original or final depth
<N=no/Return=yes>?"))
 (if (or (equal depth "n") (equal depth "N"))
  (progn
   (command "line" pt1 pt12 pt13 pt14 pt15 pt5 pt4 pt3 pt2 pt1 pt11 pt10 pt9
    pt8 pt7 pt6 pt5 ""
    "line" pt10 pt2 ""
    "line" pt9 pt3 pt8 ""
    "line" pt1 pt14 ""
    "line" pt4 pt7 ""
    "text" pt16 "" "" wa/am
    "text" pt17 "" "" "W/H="
    "text" pt18 "" "" sh/de
    "text" pt19 "" "" "S/D="
    "text" pt20 "" "" al
    "text" pt21 "" "" "Alpha="
    "text" pt22 "" "" ga
    "text" pt23 "" "" "Gamma="
    "text" pt24 "" "" th
    "text" pt25 "" "" "Thickness="
    "text" pt26 "" "" de
    "text" pt27 "" "" "Detachment Depth (D)="
```

Reproduced with permission of the copyright owner. Further reproduction prohibited without permission.

```
    "text" pt28 "" "" sh
    "text" pt29 "" "" "Shortening (S)="
    "text" pt30 "" "" am
    "text" pt31 "" "" "Amplitude (H)="
    "text" pt32 "" "" wa
    "text" pt33 "" "" "Wavelength (W)="
    "text" pt34 "" "" sd
    "text" pt35 "" "" "Displaced area (Ao) (units squared)="
    "text" pt36 "" "" af
    "text" pt37 "" "" "Uplifted fold area (Af) (units squared)=" )
   );end progn
  (progn
   (setq foro (getstring "\nDo you know the original (O) or final (F) depth?"))
     (if (or (equal foro "o") (equal foroh "O"))
      (progn
       (setq do (getreal "\nWhat is the original depth?"))
       (setq df (- (+ (/ (* do S) W) do) (/ H 2)))
      ); end progn
      (progn
       (if (or (equal foro "f") (equal foro "F"))
        (progn
        (setq df (getreal "\nWhat is the final depth?"))
        (setq do (/ (+ df (/ H 2)) (+ (/ S W) 1)))
        ); end progn
        (progn
        (alert "Try again - please enter F or D.")
        (restore)
        );end progn
       );end if
      );end progn
     );end if
(setq adiff (* W (- df do)))
```

Reproduced with permission of the copyright owner. Further reproduction prohibited without permission.

```
 (setq pt15 (polar pt4 4.71239 df))
 (setq pt14 (polar pt2 4.71239 df))
 (setq pt103 (polar pt4 4.71239 do))
 (setq pt104 (polar pt2 4.71239 do))
 (setq pt13 (polar pt12 4.71239 do))
 (setq pt100 (polar pt13 0 S))
 (setq add (rtos adiff 2 2))
    (setq sxd (* S do))
    (setq sd (rtos sxd 2 2))
    (setq od (rtos do 2 2))
    (setq fd (rtos df 2 2))
    (setq dfodo (/ df do))
    (setq deltd (- df do))
    (setq dfdo (rtos dfodo 2 2))
    (setq dd (rtos deltd 2 2))
(if (> deltd 1)
 (progn
   (setq pt101 (polar pt14 (/ pi 2) deltd))
   (setq pt102 (polar pt15 (/ pi 2) deltd))
 );end progn
 (progn
   (setq pt101 (polar pt14 4.71239 deltd))
   (setq pt102 (polar pt15 4.71239 deltd))
 );end progn
 );end if
(command "line" pt1 pt12 pt13 pt100 pt1 pt2 pt14 pt15 pt4 pt5 pt6 pt7 pt8 pt9
pt10 pt11 pt1 ""
"line" pt8 pt7 pt6 pt5 ""
"line" pt10 pt2 pt3 pt4 ""
"line" pt9 pt3 pt8 ""
"line" pt4 pt7 ""
"line" pt103 pt15 pt14 pt104 pt103 pt14 pt104 pt15 ""
```

Reproduced with permission of the copyright owner. Further reproduction prohibited without permission.

```
 "text" pt16 "" "" sow
 "text" pt17 "" "" "S/W="
 "text" pt18 "" "" soh
 "text" pt19 "" "" "S/H="
 "text" pt20 "" "" dd
 "text" pt21 "" "" "Delta D="
 "text" pt22 "" "" dfdo
 "text" pt23 "" "" "Df/Do="
 "text" pt24 "" "" th
 "text" pt25 "" "" "Thickness="
 "text" pt26 "" "" wa
 "text" pt27 "" "" "Wavelength (W)="
 "text" pt28 "" "" sh
 "text" pt29 "" "" "Shortening (S)="
 "text" pt30 "" "" am
 "text" pt31 "" "" "Amplitude (H)="
 "text" pt32 "" "" od
"text" pt33 "" "" "Original Detachment Depth (Do)="
"text" pt34 "" "" fd
"text" pt35 "" "" "Final Detachment Depth (Df)="
"text" pt36 "" "" add
"text" pt37 "" "" "Area Diff. (units squared)="
"text" pt38 "" "" sd
"text" pt39 "" "" "Displaced area (Ao) (units squared)="
"text" pt40 "" "" af
"text" pt41 "" "" "Uplifted fold area (Af) (units squared)=")
);end progn
);end if
(setvar "textsize" oldsize))
```

Reproduced with permission of the copyright owner. Further reproduction prohibited without permission.

REFERENCES CITED

Abbassi, M. R. & Mancktelow, N. S. 1992. Single layer buckle folding in non-linear materials-I, experimental study of development from an isolated initial perturbation. *J. Struct. Geol.* **14**, 85-104.

Anderson, A. V. & Wallace, W. K. 1990. Middle Devonian to Mississippian clastic depositional cycles southwest of Bathtub Ridge, northeastern Brooks Range, Alaska. *Program with Abstracts for Annual Meeting of Geological Association of Canada/Mineralogical Association of Canada,* **15**, p. A2.

Anderson, A. V., Wallace, W. K. & Mull, C. G. 1994. Depositional record of a major tectonic transition in northern Alaska: Middle Devonian to Mississippian rift-basin margin deposits, upper Kongakut River region, eastern Brooks Range, Alaska. In: *Proceedings Intl. Conf. Arctic Margins* (edited by Thurston, D. & Fujita, K.), *US Minerals Mngmt. Serv. outer continental shelf study.*

Bader, J.W. & Bird, J.K. 1986. Geologic map of the Demarcation Point, Mt. Michelson, Flaxman Island, and Barter Island Quadrangles, northeastern Alaska. *USGS misc. investigations map I-1791,* 1 sheet, scale 1:250,000.

Banks, C. J. & Warburton, J. 1986. "Passive-roof" duplex geometry in the frontal structures of the Kirthar and Sulaiman mountain belts, Pakistan. *J. Struct. Geol.* 8, 229-237.

Beutner, E. C., Fisher, D. M. & Kirkpatrick, J. L. 1988. Kinematics of deformation at a thrust fault ramp (?) from syntectonic fibers in pressure shadows. *Geol. Soc. Am. Special paper 222.*

Biot, M. A. 1961. Theory of folding of stratified viscoelastic media and its implication in tectonics and orogenesis. *Bull. Geol. Soc. Am.* **72**, 1595-1620.

Bucher, W. H. 1933. *Deformation of the Earth's crust.* Princeton, New Jersey, Princeton University Press, 518p.

Reproduced with permission of the copyright owner. Further reproduction prohibited without permission.

Butler, R. W. H. 1992. Evolution of Alpine fold-thrust complexes: a linked kinematic approach. In: *Structural geology of fold and thrust belts* (edited by Mitra, S. and Fisher, G. W.). *The Johns Hopkins University Press,* 29-44.

Chamberlin, R. T. 1910. The Appalachian folds of central Pennsylvania. *J. Geol.* **18**, 228-251.

Crowder, R. K. 1990. Permian and Traissic sedimentation in the northeastern Brooks Range, Alaska: Deposition of the Sadlerochit Group. *AAPG Bull.,* **74**, 1351-1370.

Currie, J. B., Patnode, H. W. & Trump, R. P. 1962. Development of folds in sedimentary strata. *Bull. Geol. Soc. Am.* **73**, 655-674.

Dahlstrom, C. D. A. 1969. The upper detachment in concentric folding. *Bull. Can. Petrol. Geol.* **17**, 326-346.

Dahlstrom, C. D. A. 1970. Structural geology in the eastern margin of the Canadian Rocky Mountains. *Bull. Can. Petrol. Geol.* **18**, 322-406.

Dahlstrom, C. D. A. 1990. Geometric constraints derived from the law of conservation of volume and applied to evolutionary models for detachment folding. *Bull. Am. Ass. Petrol. Geol.* **74**, 336-344.

Davis, D. M. & Engelder, T. 1985. The role of salt in fold-and-thrust belts. *Tectonophysics.* **119**, 67-88.

De Paor, D. G. 1988. Balanced section in thrust belts part 1: construction. *AAPG Bull.,* **72**, 73-90.

de Sitter, L. U. 1956. *Structural geology.* McGraw Hill Inc., New York.

Dixon, J. M. & Tirrul, R. 1991. Centrifuge modeling of fold-thrust structures in a tripartite stratigraphic succession. *J. Struct. Geol.* **13**, 3-20.

Dixon, J. M. & Liu, S. 1992. Centrifuge modelling of the propagation of thrust faults. In: *Thrust Tectonics* (edited by McClay, K. R.). Chapman and Hall, London, 53-70.

Dunne, W. M. & Ferrill, D. A. 1988. Blind thrust systems, *Geology,* **6**, 33-36.

Reproduced with permission of the copyright owner. Further reproduction prohibited without permission.

Epard, J. L. & Groshong, R. H. 1993. Excess area and depth to detachment. *Bull. Am. Ass. Petrol. Geol.* **77**, 1291-1302.

Fischer, M. P., Woodward, N. B. & Mitchell, M. M. 1992. The kinematics of break-thrust folds. *J. Struct. Geol.* **14,** 451-460.

Geiser, P. A. 1988. The role of kinematics in the construction and analysis of geologic cross sections in deformed terranes. In: *Geometries and mechanisms of thrusting, with special reference to the Appalachians* (edited by Mitra, G. & Wojtal, S.). *Geol. Soc. Am. Special paper 222*, 47-76.

Goguel, J. 1962. *Tectonics.* Freeman, San Francisco.

Grantz, A., May, S. D. & Hart, P. E. 1990. Geology of the Arctic continental margin of Alaska. In *The Arctic Ocean Region,* (edited by Grantz, A., Johnson, L. & Sweeney, J. F.), *GSA DNAG L.*

Groshong, R. H. & Epard, J. Jr. 1994. The role of strain in area-constant detachment folding. *J. Struct. Geol.* **16**, 613-618.

Hanks, C. L. 1991. A comparative study of contrasting structural styles in the range-front region of the northeastern Arctic National Wildlife Refuge, northeastern Brooks Range, Alaska. Unpublished Ph.D. dissertation, University of Alaska Fairbanks, 271p.

Hanks, C. L., Wallace, W. K. & O'Sullivan, P. 1994. The Cenozoic structural evolution of the northeastern Brooks Range, Alaska. In: *Proceedings Intl. Conf. Arctic Margins* (edited by Thurston, D. & Fujita, K.), *US Minerals Mngmt. Serv. outer continental shelf study 94-0040,* 263-268.

Hansen, E. 1971. *Strain Facies.* Springer-Verlag, New York.

Hardy, S. & Poblet, J. 1994. Geometric and numerical model of progressive limb rotation in detachment folds. *Geology.* **22**, 371-374.

Holl, J. E. & Anastasio, D. J. 1993. Paleomagnetically derived folding rates, southern Pyrenees, Spain. *Geology.* **21**, 271-274.

Reproduced with permission of the copyright owner. Further reproduction prohibited without permission.

Homza, T. X. 1991. Geologic map, cross section, and structural geology of an area southwest of Bathtub Ridge, northeastern Brooks Range, Alaska. *Alaksa Div. Geol. and Geophys. Surv., Public Data File 91-9.*

Homza, T. X. 1992a. A detachment fold-truncation duplex southwest of Bathtub Ridge-northeastern Brooks Range, Alaska. Unpublished M.S. thesis, University of Alaska, Fairbanks.

Homza, T. X. 1992b. Digitizing field maps and constructing balanced cross sections with AutoCAD. *Alaksa Div. Geol. and Geophys. Surv., Public Data File 92-14.*

Homza, T. X. 1993. Preliminary observations of the Straight Creek detachment anticline-northeastern Brooks Range, Alaska: a basis for geometric and kinematic detachment fold models. *Alaska Div. Geol. and Geophys. Surv., Public Data File 93-43.*

Homza, T. X. 1994. The structural geometry of detachment folds above a duplex in the Franklin Mountains, northeastern Brooks Range, *Alaska, Alaska Div. Geol. and Geophys. Surv., Public Data File 94-43*, 33p., 4 plates.

Homza, T. X. & Wallace, W. K. 1991a. Thrust-truncated detachment folds and duplex evolution southwest of Bathtub Ridge, northeastern Brooks Range, Alaska. *Geol. Soc. Am. Abstr. Programs,* **23**, *2.*

Homza, T. X. & Wallace, W. K. 1991b. A duplex formed by the thrust-truncation of detachment folds in the Arctic National Wildlife Refuge (ANWR), northeastern Alaska. *Geol. Soc. Am. Abstr. Programs,* **23,** 5.

Homza, T. X. & Wallace, W. K. 1995. Geometric and kinematic models for detachment folds with fixed and variable detachment depths. *J. Struct. Geol.* **17**, 575-588.

Hossack, J. R. 1979. The use of balanced cross-sections in the calculation of orogenic contraction: A review. *J. Geol. Soc. Lond.* **136**, 705-711.

Imm, T. A., Dillon, J. T. & Bakke, A. A. 1993. Generalized geologic map of the Arctic National Wildlife Refuge, northeastern Brooks Range, Alaska. *Alaska Div. Geol. and Geophys. Surv., Special Report 42*, 1 sheet.

Reproduced with permission of the copyright owner. Further reproduction prohibited without permission.

Jamison, W. R. 1987. Geometric analysis of fold development in overthrust terranes. *J. Struct. Geol.* **9**, 207-219.

Johnson, A. M. 1977. *Styles of folding.* Elsevier, Amsterdam.

Krumhardt, A. P. 1992. Conodont biostratigraphy and biofacies of the Carboniferous Wahoo Limestone, eastern Sadlerochit Mountains, Arctic National Wildlife Refuge, northeastern Brooks Range, Alaska. Unpublished masters thesis, University of Alaska Fairbanks, 158pp.

Laubscher, H. P. 1962. Die Zweiphasenhypothese der Jurafaltung. *Eclog. geol. Helv.* **55**, 1-22.

LePain, D. L. 1993. Transgressive sedimentation in rift-flank region: deposition of the Endicott Group (Early Carboniferous), northeastern Brooks Range, Alaska. Unpublished Ph.D. dissertation, University of Alaska, Fairbanks.

Mancktelow, N. S. & Abbassi, M. R. 1992. Single layer buckle folding in non-linear materials-II, comparison between theory and experiment. *J. Struct. Geol.* **14**, 105-120.

Marshak, S. & Mitra, G. 1988. *Basic methods of structural geology.* Prentice Hall, Englewood Cliffs N. J., 446p.

Mitchell, M. M. & Woodward, N. B. 1988. Kink detachment fold in the southwestern Montana fold and thrust belt. *Geology* **16**, 162-165.

Mitra, S. 1990. Fault-propagation folds: geometry, kinematic evolution, and hydrocarbon traps. *Bull. Am. Ass. Petrol. Geol.* **74**, 921-945.

Mitra, S. 1992. Balanced structural interpretations in fold and thrust belts. In: *Structural geology of fold and thrust belts* (edited by Mitra, S. & Fisher, G. W.). *The Johns Hopkins University Press,* 53-77.

Mitra, S. & Namson, J. S. 1989. Equal-area balancing. *Am. J. Sci.* **289**, 563-599.

Moore, T. E., Wallace, W. K., Bird, K. J., Karl, S. M., Mull, C. G. & Dillon, J. T. 1992, Stratigraphy, structure, and geologic synthesis of northern Alaska. *USGS Open-file Report 92-330.*

Reproduced with permission of the copyright owner. Further reproduction prohibited without permission.

Moore, T. E., Wallace, W. K., Bird, K. J., Karl, S. M., Mull, C. G. & Dillon, J. T. 1994. Stratigraphy, structure, and geologic synthesis of northern Alaska. In *Geology of North America,* (edited by Plafker, G. & Berg, H. C.), *GSA DNAG* ***G-1.***

Mull, C. G. 1987. Kemik Formation, Arctic National Wildlife Refuge, northeastern Alaska, In: *Alaskan North Slope Geology* (edited by Tailleur, I. L. & Weimer, P.), *Pacific section of Soc. of Econ. Paleo. and Min. and Alaska Geol. Soc.* **50**, 405-431.

Namson, J. S. & Wallace, W. K. 1986. A structural transect across the northeastern Brooks Range, Alaska. *Geol. Soc. Am. Abtsr. Programs.* **18**, 163.

Oldow, J. S., Avé Lallemant, H. G., Julian, F. E. & Seidensticker. C. M. 1987. Ellesmerian (?) and Brookian deformation in the Franklin Mountains, northeastern Brooks Range, Alaska, and its bearing on the origin of the Canada Basin. *Geology.* **15**, 37-41.

Ramberg, H. 1964. Selective buckling of composite layers with contrasted rheological properties, a theory for simultaneous formation of several orders of folds. *Tectonophysics.* **1**, 307-341.

Ramsay, J. G. 1967. *Folding and fracturing of rocks.* McGraw Hill, New York.

Ramsay, J. G. 1974. Development of chevron folds. *Bull. geol. Soc. Am.* **85**, 1741-1754.

Ramsay, J. G. & Huber, M. I. 1983. The techniques of modern structural geology, vol. 1: strain analysis. *Academic Press,* 307p.

Ramsay, J. G. & Huber, M. I. 1987. The techniques of modern structural geology, vol. 2: folds and fractures. *Academic Press,* 393p.

Reifenstuhl, R. R. 1995. Lithofacies, petrology, and petrophysics of the Kemik Sandstone (Lower Cretaceous), eastern Arctic Slope, Alaska. In: *Short Notes on Alaskan Geology 1995* (edited by Combellick, R., A. & Tannian, F.). *Alaska Div. Geol. & Geophys. Surv. Professional Report 117*, 53-67.

Reproduced with permission of the copyright owner. Further reproduction prohibited without permission.

Reiser, H.N., Brosgé, W.P., Dutro, J.T., Jr. & Detterman, R.L. 1971. Preliminary geologic map of the Mt. Michelson Quadrangle, Alaska. *USGS open-file report OF-71-237,* 1 sheet, scale 1:250,000.

Reiser, H. N., Brosgé, W. P., Dutro J. T. Jr. & Detterman, R. L. 1980. Geologic map of the Demarcation Point Quadrangle, Alaska. *USGS Misc. Inv. Series Map I-1133,* scale 1:250,000, 1 sheet.

Rowan, M. G. & Kligfield, R. 1992. Kinematics of large-scale asymmetric buckle folds in overthrust shear: an example from the Helvetic nappes. In: *Thrust Tectonics* (edited by McClay, K. R.). *Chapman Hall* 165-173.

Seni, S. J. & Jackson, M. P. A. 1983. Evolution of salt structures, East Texas diapir province, part 1: sedimentary record of halokinesis. *AAPG Bull.* **67**, 1219-1244.

Stewart, K. G. & Alvarez, W. 1991. Mobile-hinge kinking in layered rocks and models. *J. Struct. Geol.* **13**, 243-259.

Suppe, J. 1983. Geometry and kinematics of fault-bend folding. *Am. J. Sci.* **283**, 684-721.

Suppe, J. 1985. *Principles of structural geology.* Prentice Hall, Englewood Cliffs N. J., 537p.

Suppe, J. & Medwedeff, D. A. 1984. Fault-propagation folding, *Geol. Soc. Am. Abstr. Programs,* **16**, 670.

Suppe, J. & Medwedeff, D. A. 1990. Geometry and kinematics of fault-propagation folding. *Eclog. geol. Helv.* **83**, 409-454.

Thompson, R. I. 1989. Stratigraphy, tectonic evolution and structural analysis of the Halfway River map area (94 B), northern Rocky Mountains, British Columbia. *Geol. Surv. Can. Memoir* 425.

Trusheim, F. 1960. Mechanism of salt migration in northern Germany, *AAPG Bull.*, **44**, 1519-1540.

Vergis, J., Burbank, D. W. & Meigs, A. in review at *Geology.* Unfolding: An inverse approach to fold kinematics.

Reproduced with permission of the copyright owner. Further reproduction prohibited without permission.

Wallace, W. K. 1992. Detachment folds above a passive-roof duplex: An example from the northeastern Brooks Range, Alaska. *Alaska Div. Geol. & Geophys. Surv, Public Data File 92-9,* 41 p.

Wallace, W. K. 1993. Detachment folds and a passive-roof duplex: Examples from the northeastern Brooks Range, Alaska. In: *Short Notes on Alaskan Geology 1993* (edited by Solie, D. N. & Tannian, F.). *Alaska Div. Geol. & Geophys. Surv. Professional Report 113*, 81-99.

Wallace, W. K. & Hanks, C. L. 1990. Structural provinces of the northeastern Brooks Range, Arctic National Wildlife Refuge, Alaska. *AAPG Bull.* **74**, 1100-1118.

Watts, K. F., Carlson, R., Imm, T., Gruzlovic, P. & Hanks, C. L. 1988. Influence of pre-Mississippian paleogeography on the Carboniferous Lisburne Group, Arctic National Wildlife Refuge, northeast Alaska. *AAPG Bull.* **72**, 257.

Weiss, L. E. 1968. Flexural slip folding of foliated model materials. In: *Kink bands and brittle deformation* (edited by Baer, A.J. & Norris, D.K.). *Geol. Surv. Pap. Can. 68*, 294-357.

Willis, B. & Willis, R. 1934. *Geologic structures.* McGraw Hill, New York.

Wiltschko, D. V. & Chapple, W. M. 1977. Flow of weak rocks in the Appalachian Plateau folds. *Bull. Am. Ass. Petrol. Geol.* **61**, 653-670.

Woodward, N. B., Boyer, S. E. & Suppe, J. 1985. *An outline of balanced cross-sections.* Univ. of Tennessee, Studies in Geology 11, 2nd edition.

Woodward, N. B., Boyer, S. E. & Suppe, J. 1989. Balanced geological cross-sections: An essential technique in geological research and exploration. *American Geophysical Union Short Course in Geology* 6.

Ziegler, J. A., 1989. A detailed structural analysis across a regional unconformity, forks of the Canning River, Franklin Mountains, northeastern Brooks Range, Alaska. Unpublished M.S. thesis, University of Alaska, Fairbanks.

Reproduced with permission of the copyright owner. Further reproduction prohibited without permission.

PLEASE NOTE

The diskette is not included in this material. It is, however, available for consulation at the author's graduate school library.

University Microfilms International

Reproduced with permission of the copyright owner. Further reproduction prohibited without permission.

PLEASE NOTE:

Oversize maps and charts are filmed in sections in the following manner:

LEFT TO RIGHT, TOP TO BOTTOM, WITH SMALL OVERLAPS

The following map or chart has been refilmed in its entirety at the end of this dissertation (not available on microfiche). A xerographic reproduction has been provided for paper copies and is inserted into the inside of the back cover.

Black and white photographic prints (17" x 23") are available for an additional charge.

UMI

Reproduced with permission of the copyright owner. Further reproduction prohibited without permission.

Reproduced with permission of the copyright owner. Further reproduction prohibited without permission.

PLATE A2.1 Geologic

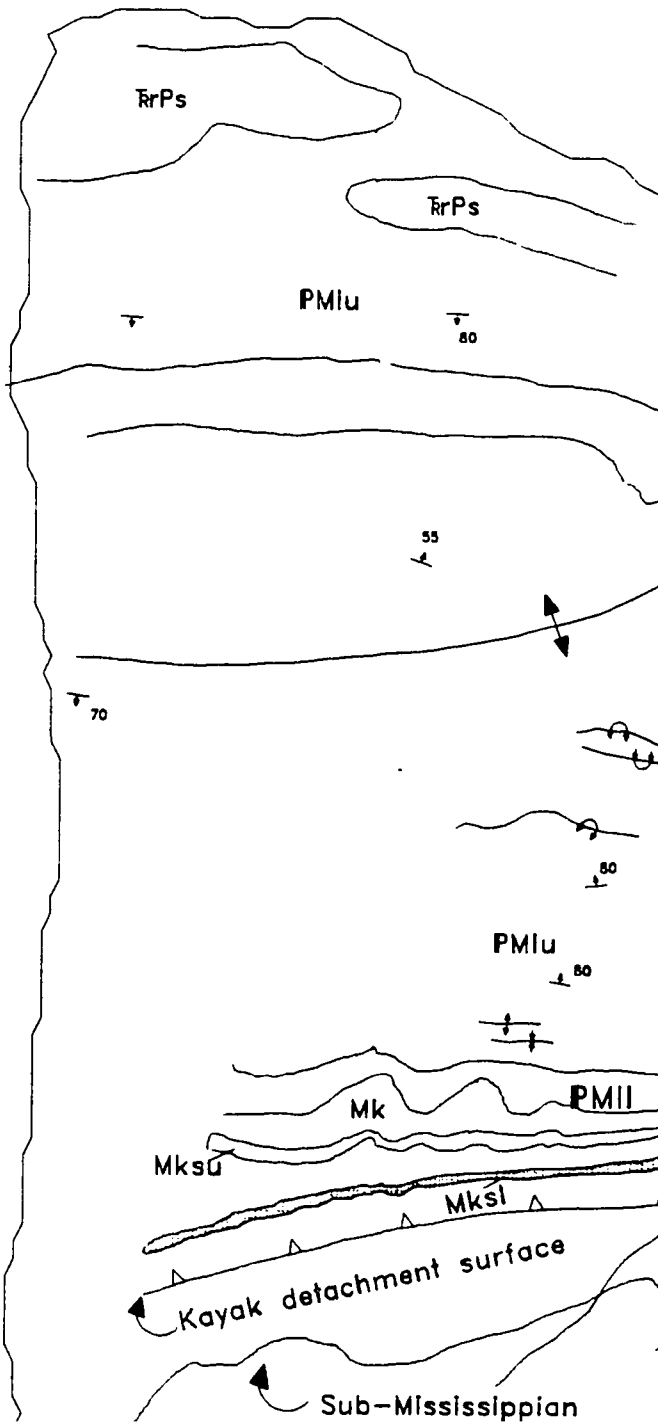

Reproduced with permission of the copyright owner. Further reproduction prohibited without permission.

Geologic map of the headwaters area of Straight Creek

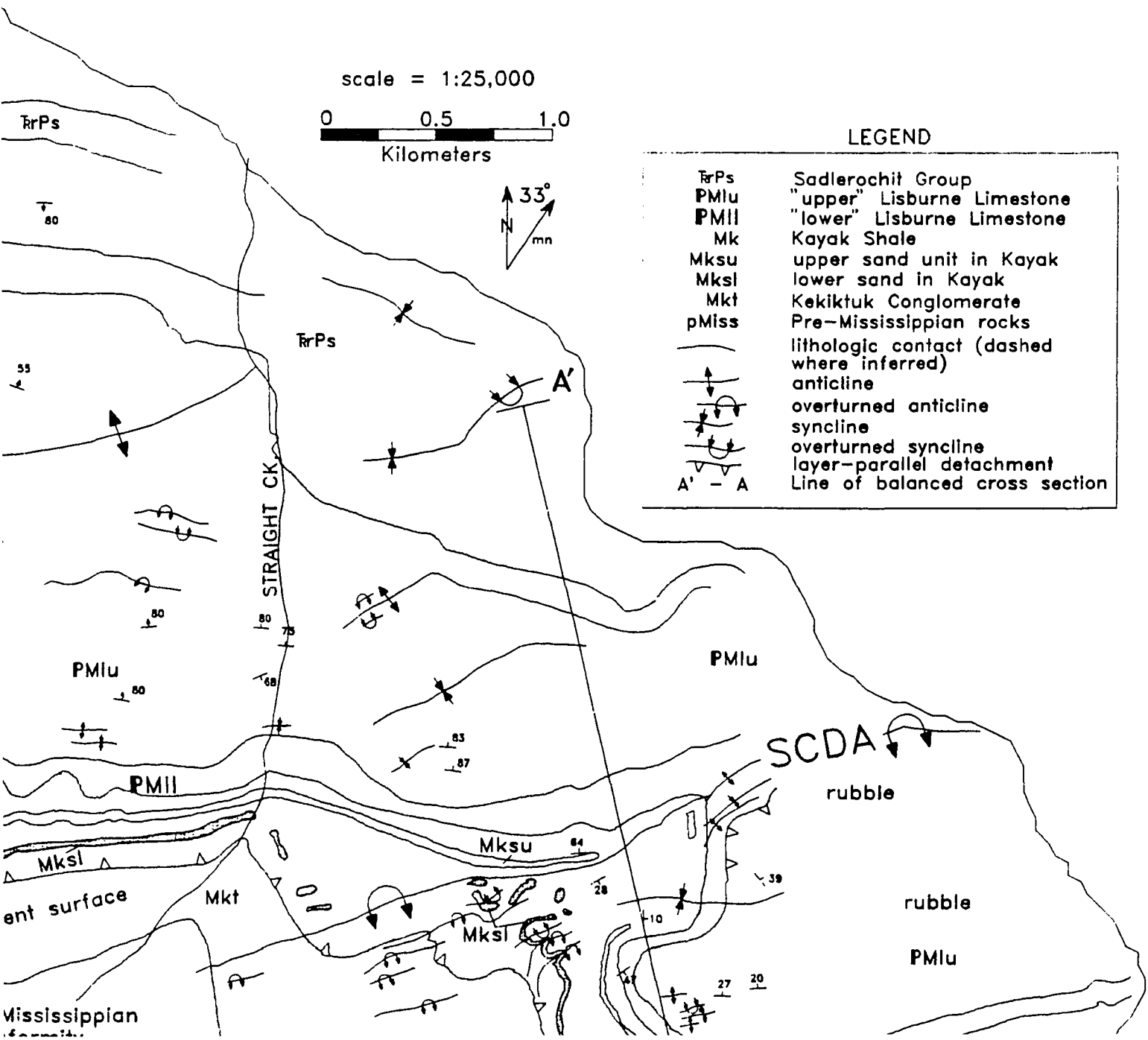

Reproduced with permission of the copyright owner. Further reproduction prohibited without permission.

ht Creek

Limestone
Limestone

in Kayak
ayak
nerate
rocks
(dashed

ne

ne
tachment
cross section

Reproduced with permission of the copyright owner. Further reproduction prohibited without permission.

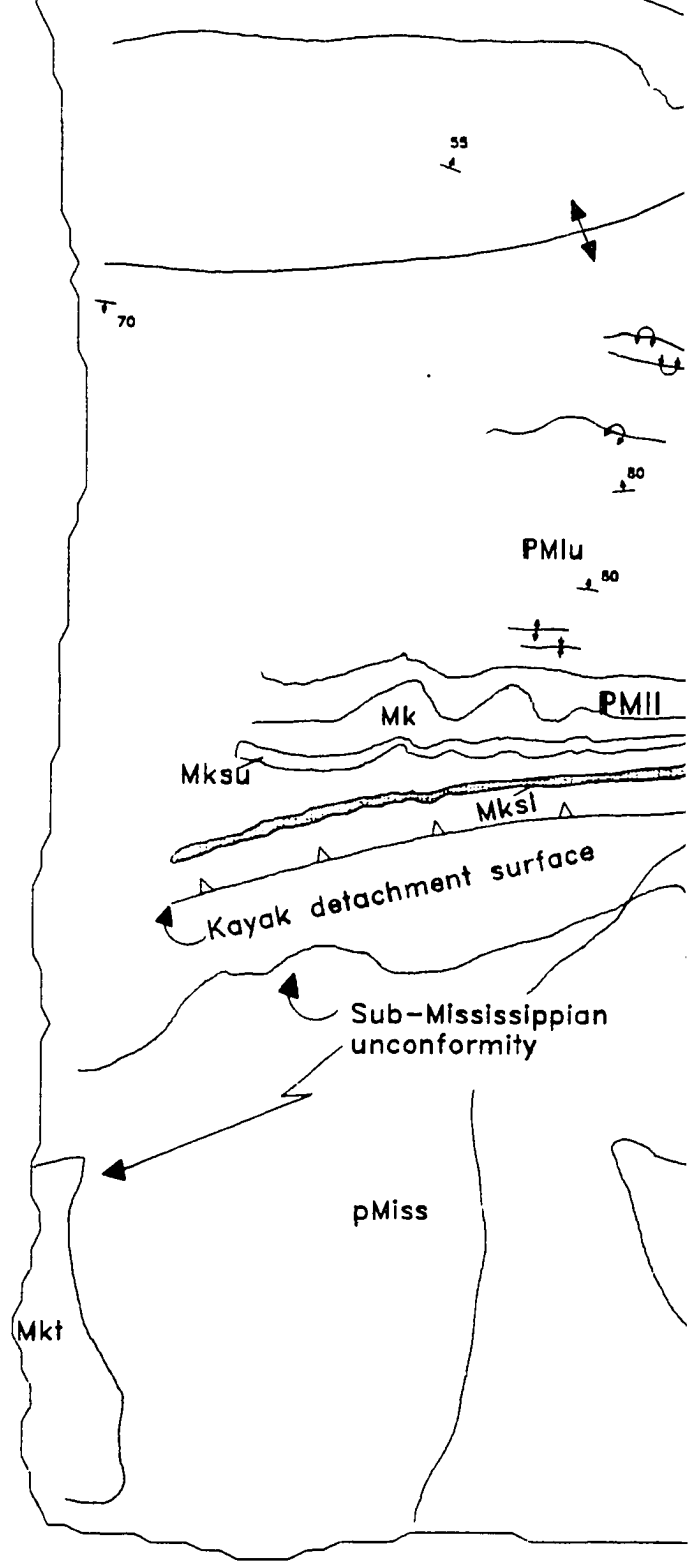

Reproduced with permission of the copyright owner. Further reproduction prohibited without permission.

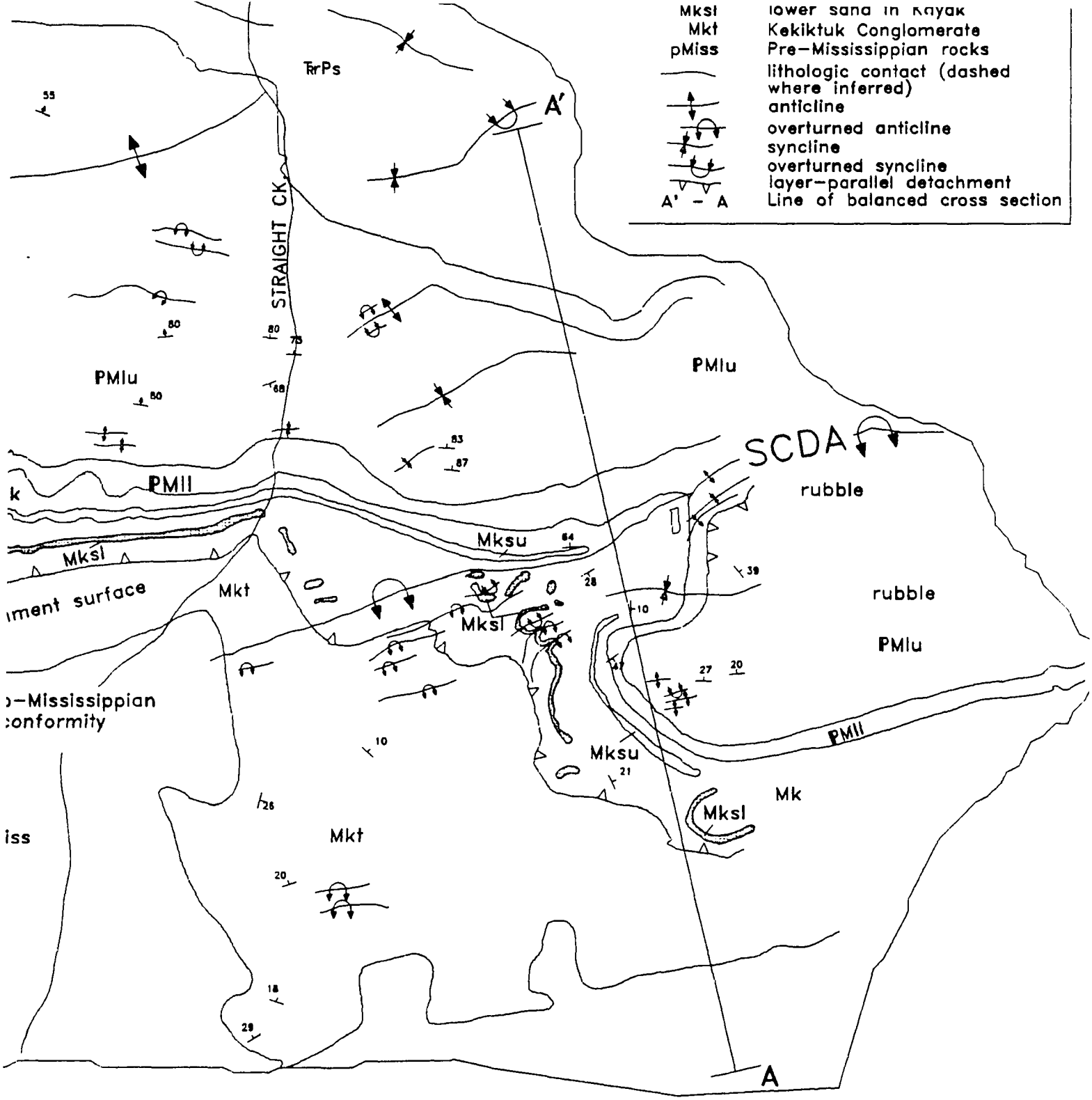

See Plate A2.2 for cro
See figure 1.6 for l

Reproduced with permission of the copyright owner. Further reproduction prohibited without permission.

yak
erate
rocks
(dashed

ıe

ıe
achment
cross section

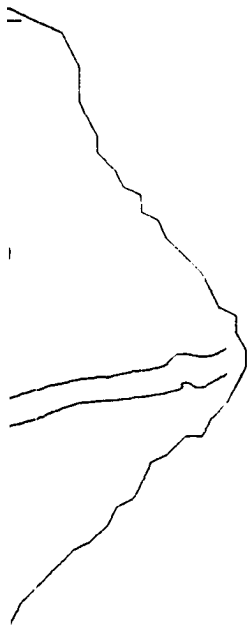

ıte A2.2 for cross section.
figure 1.6 for location.

Reproduced with permission of the copyright owner. Further reproduction prohibited without permission.

PLEASE NOTE:

Oversize maps and charts are filmed in sections in the following manner:

LEFT TO RIGHT, TOP TO BOTTOM, WITH SMALL OVERLAPS

The following map or chart has been refilmed in its entirety at the end of this dissertation (not available on microfiche). A xerographic reproduction has been provided for paper copies and is inserted into the inside of the back cover.

Black and white photographic prints (17" x 23") are available for an additional charge.

UMI

Reproduced with permission of the copyright owner. Further reproduction prohibited without permission.

PLATE A2.2 – Balanced cross

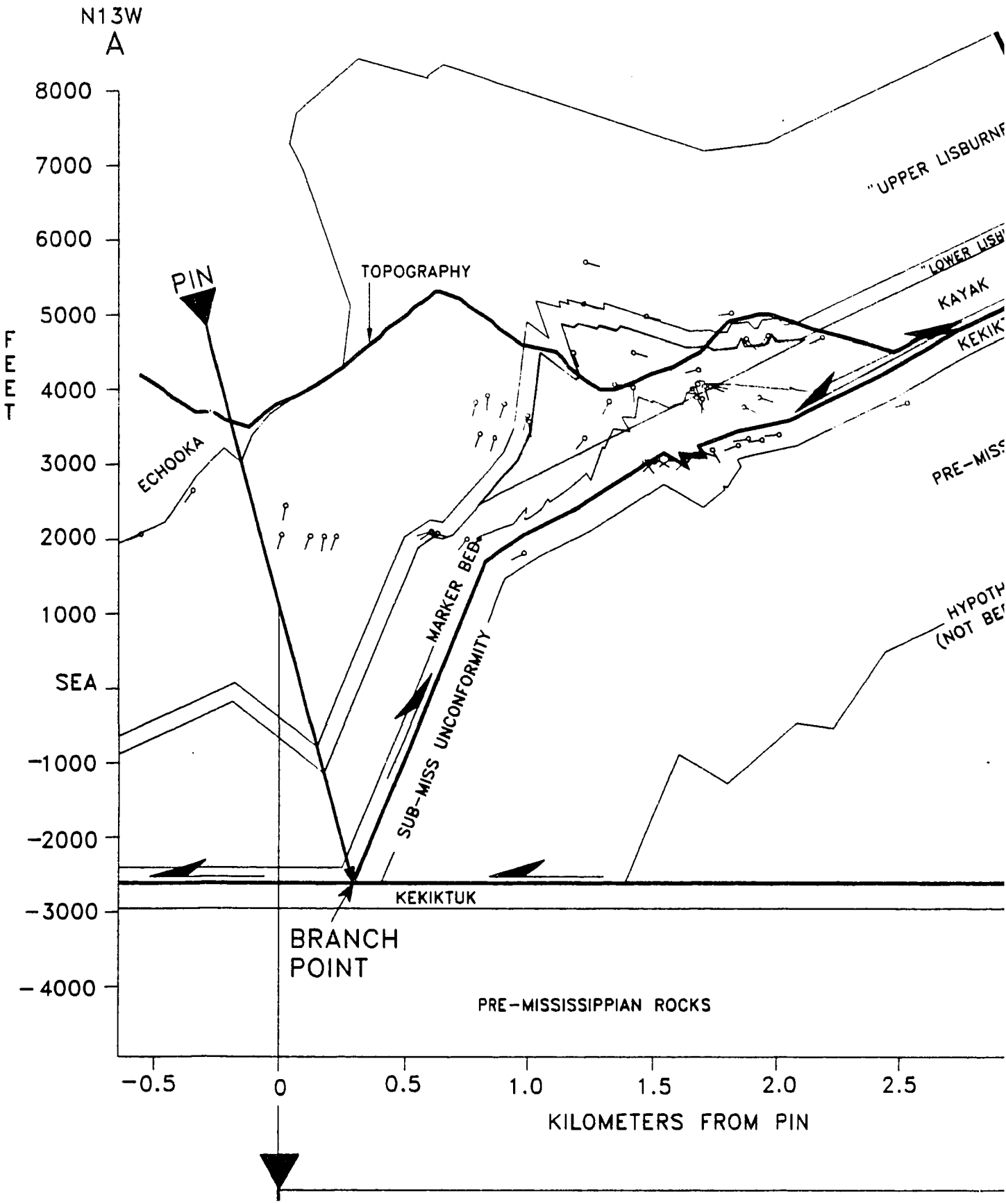

Reproduced with permission of the copyright owner. Further reproduction prohibited without permission.

cross section across the Straight C

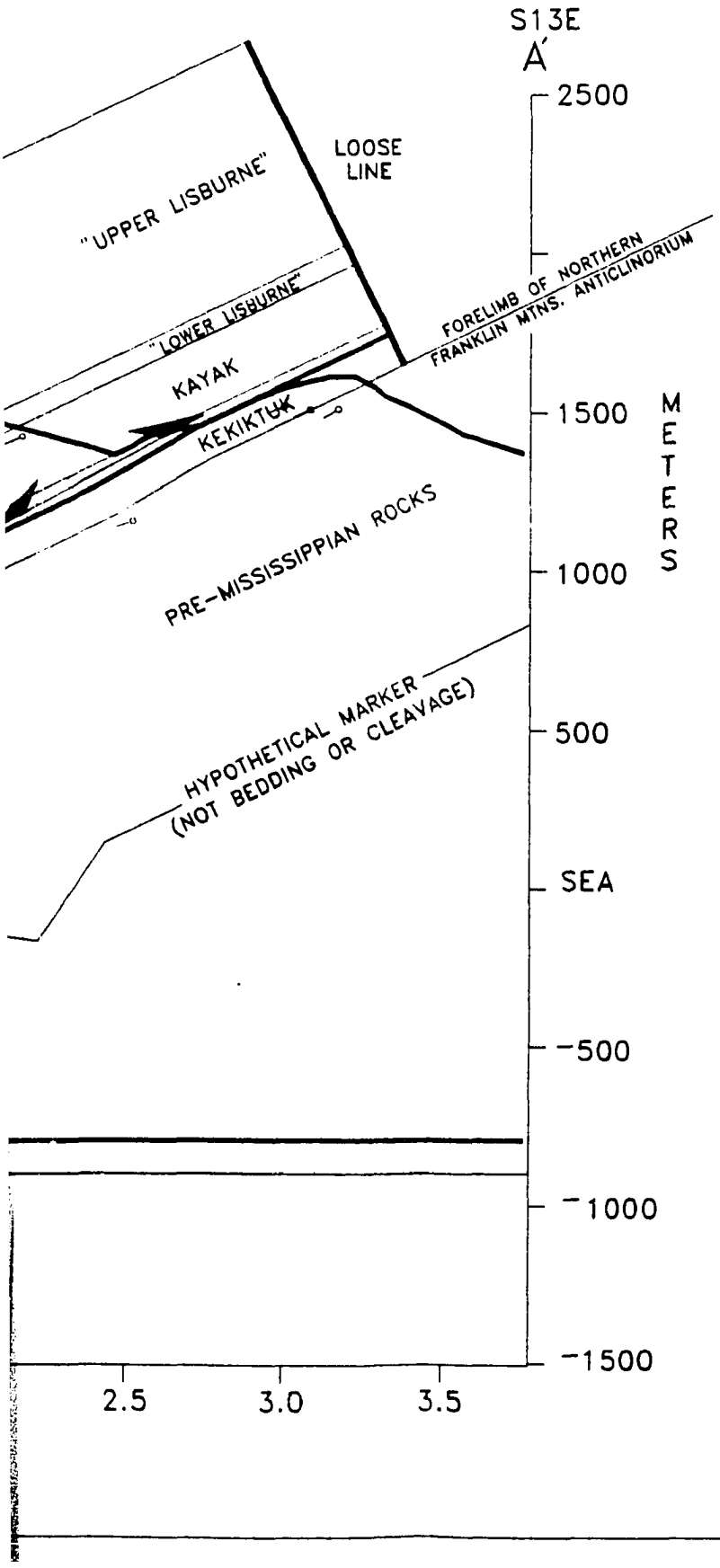

MEASUREMENTS RELATIVE T(

PRE-DEFORMATIONAL LENGTH OF KAYAK/LISBURNE CONTACT

POST-DEFORMATIONAL LENGTH OF KAYAK/LISBURNE CONTACT

SHORTENING OF KAYAK/ LISBURNE CONTACT

SHORTENING OF KAYAK/ LISBURNE CONTACT DUE TO TILTING ALONE

SHORTENING OF KAYAK/ LISBURNE CONTACT NOT DUE TO TILTING

TOTAL SHORTENING OF KEKIKT (IN HANGINGWALL)

SHORTENING OF KEKIKTUK NOT FROM TILTING (IN HANGINGWALL)

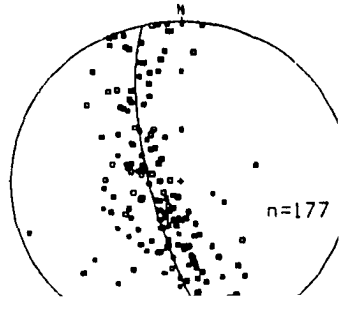

Reproduced with permission of the copyright owner. Further reproduction prohibited without permission.

aight Creek detachment anticline

TS RELATIVE TO REGIONAL DATUM

ONAL LENGTH URNE CONTACT	~ 4760 m
TIONAL LENGTH URNE CONTACT	~ 3047 m
KAYAK/ ACT	~ 1713 m ~ 36 %
KAYAK/ ACT DUE TO	~ 778 m
KAYAK/ ACT NOT DUE	~ 935 m ~ 20 %
ING OF KEKIKTUK LL)	~ 1281 m ~ 30 %
KEKIKTUK ING LL)	~ 404 m ~ 10 %

MEASUREMENTS RELATIVE TO DETACHI

DETACHMENT DEPTH	~ 269
WAVELENGTH	~ 839
HEIGHT	~ 507
BACKLIMB DIP (α)	~ 45°
INTERLIMB ANGLE (γ)	~ 78°
SHORTENING OF KAYAK/ LISBURNE CONTACT IN ANTICLINE	~ 621
STRUCTURAL THICKENING IN KAYAK SHALE	~ 396 ~ 150%
DIP OF AXIAL SURFACE	~ 58° S

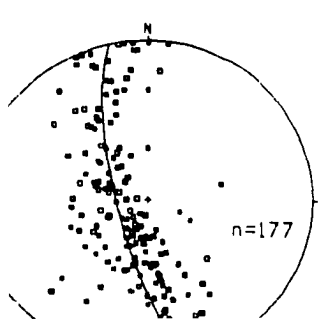

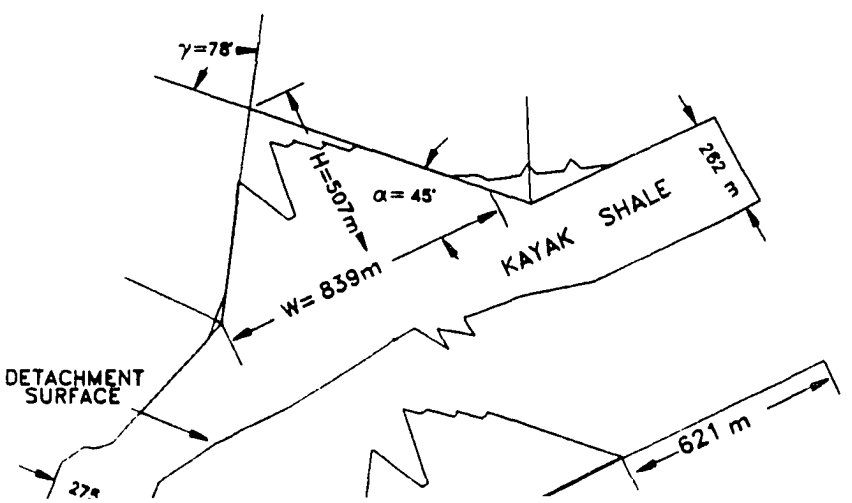

Reproduced with permission of the copyright owner. Further reproduction prohibited without permission.

Creek detachment anticline

TO REGIONAL DATUM

H CT	~ 4760 m
TH CT	~ 3047 m
	~ 1713 m
	~ 36 %
	~ 778 m
E	~ 935 m
	~ 20 %
IKTUK	~ 1281 m
	~ 30 %
	~ 404 m
	~ 10 %

=177

MEASUREMENTS RELATIVE TO DETACHMENT

DETACHMENT DEPTH	~ 269 m
WAVELENGTH	~ 839 m
HEIGHT	~ 507 m
BACKLIMB DIP (α)	~ 45°
INTERLIMB ANGLE (γ)	~ 78°
SHORTENING OF KAYAK/ LISBURNE CONTACT IN ANTICLINE	~ 621 m
STRUCTURAL THICKENING IN KAYAK SHALE	~ 396 m ~ 150%
DIP OF AXIAL SURFACE	~ 58° S

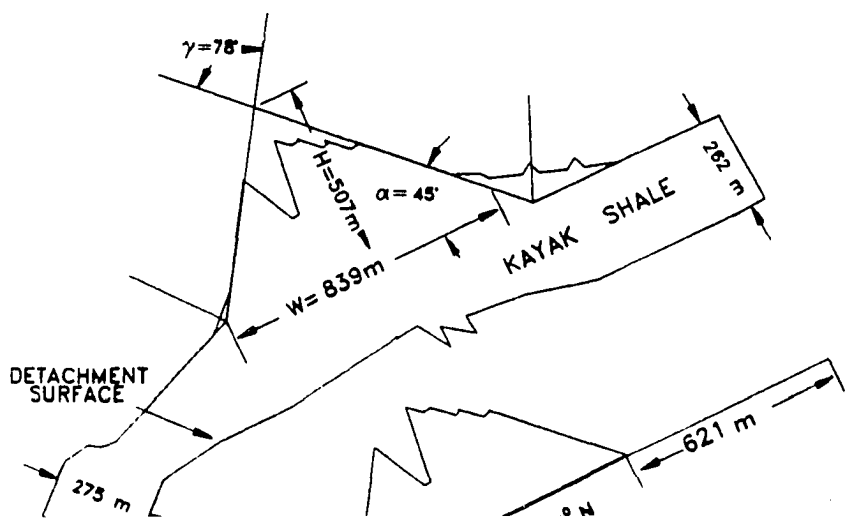

Reproduced with permission of the copyright owner. Further reproduction prohibited without permission.

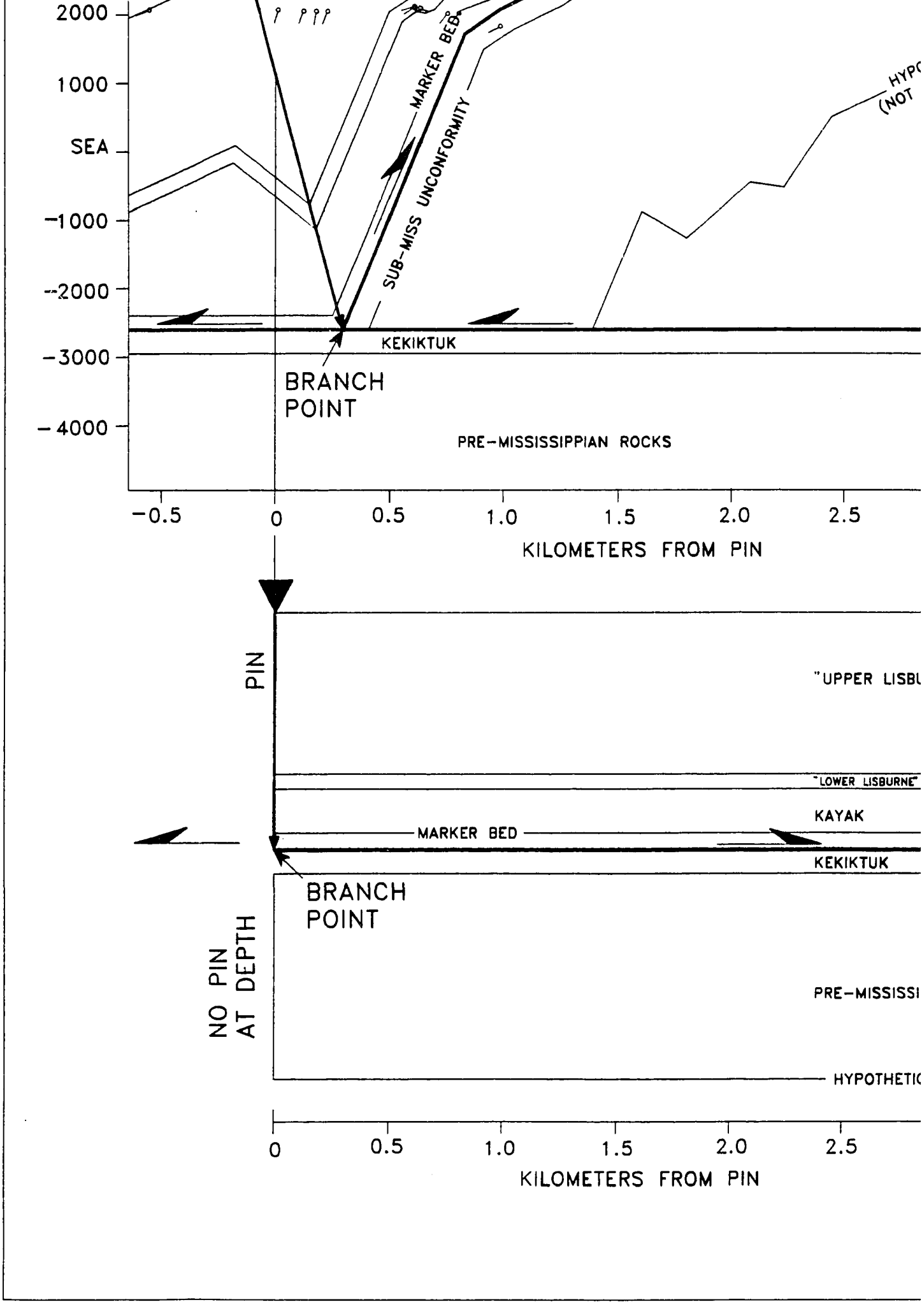

Reproduced with permission of the copyright owner. Further reproduction prohibited without permission.

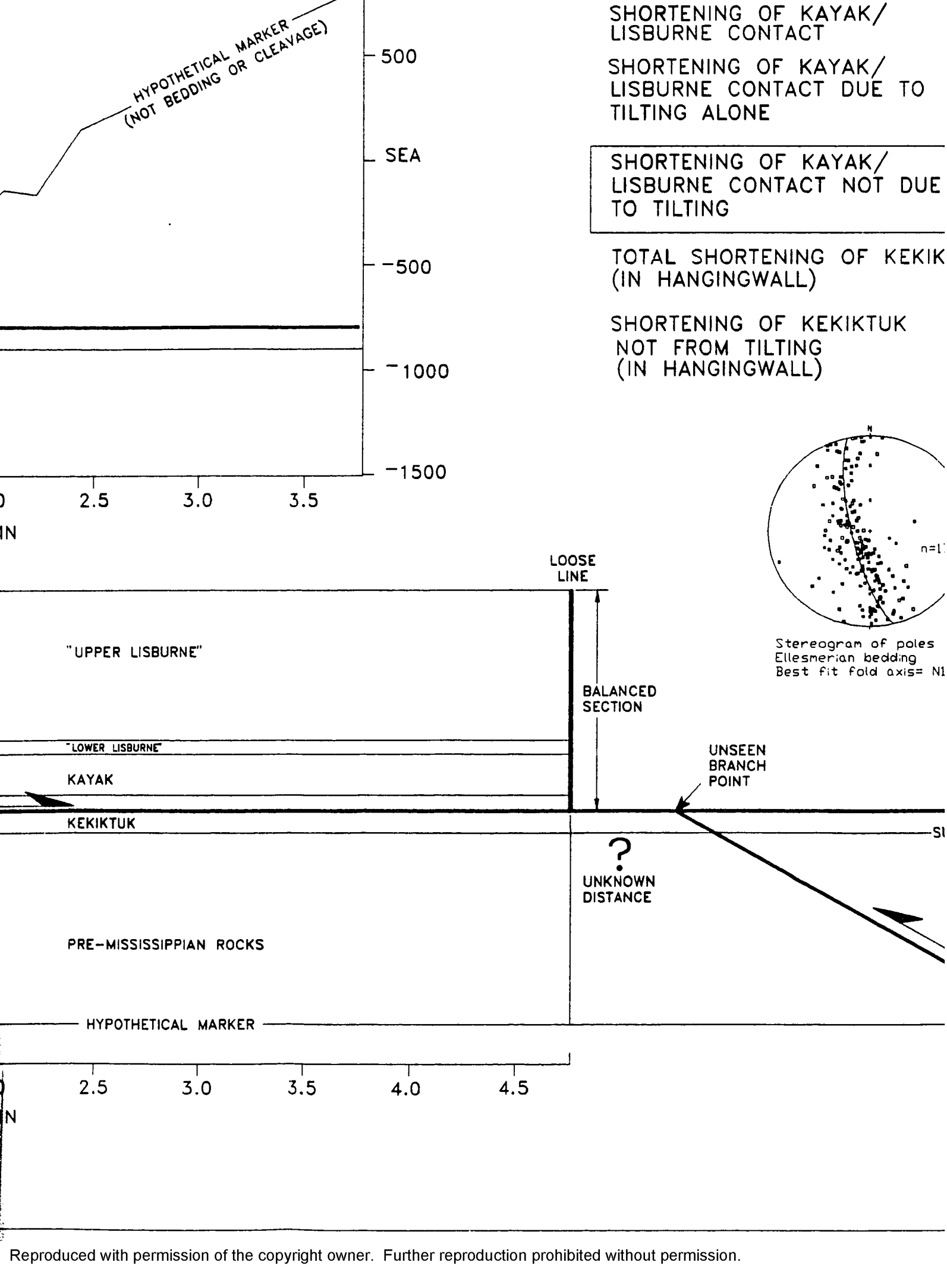

Reproduced with permission of the copyright owner. Further reproduction prohibited without permission.

F KAYAK/ TACT	~ 1713 m
	~ 36 %
F KAYAK/ TACT DUE TO	~ 778 m
)F KAYAK/ ITACT NOT DUE	~ 935 m
	~ 20 %
NING OF KEKIKTUK ALL)	~ 1281 m
	~ 30 %
)F KEKIKTUK LTING VALL)	~ 404 m
	~ 10 %

INTERLIMB ANGLE (γ)	~ 78°
SHORTENING OF KAYAK/ LISBURNE CONTACT IN ANTICLINE	~ 621 m
STRUCTURAL THICKENING IN KAYAK SHALE	~ 396 m
	~ 150%
DIP OF AXIAL SURFACE	~ 58° S

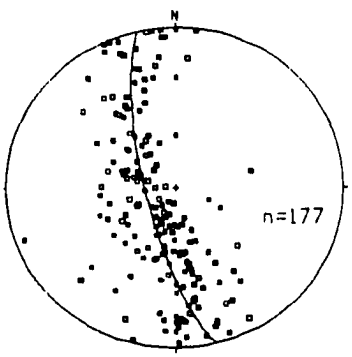

Stereogram of poles to Ellesmerian bedding
Best fit fold axis= N13°W, 15°NE

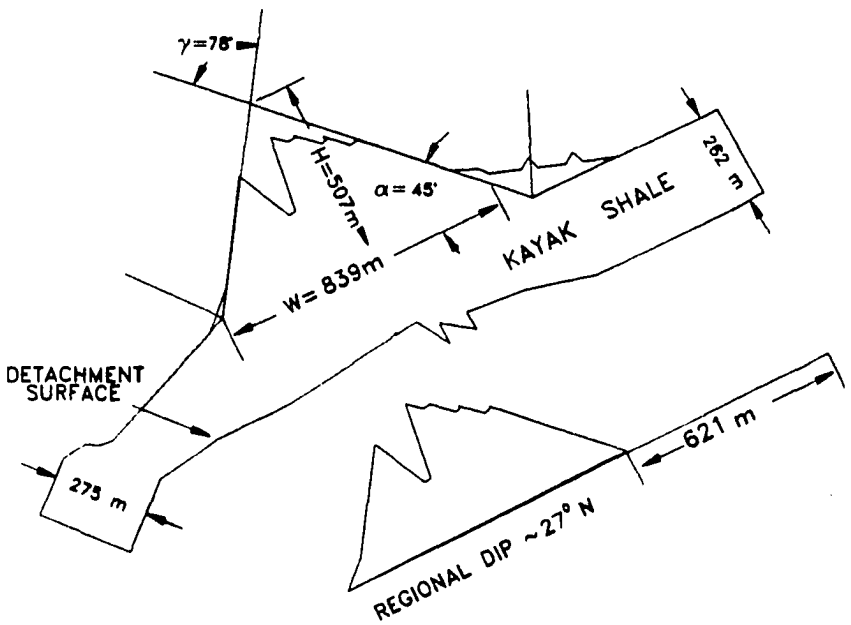

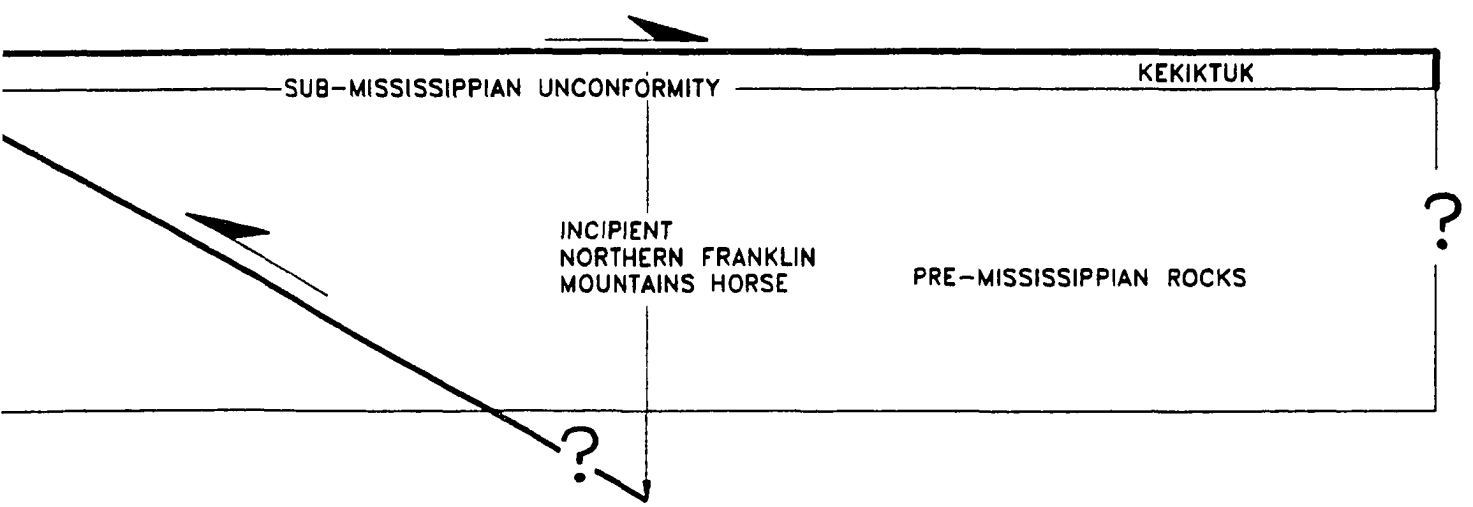

See Plate A2.1 for map.

Reproduced with permission of the copyright owner. Further reproduction prohibited without permission.

	~ 1713 m ~ 36 %
TO	~ 778 m

DUE	~ 935 m ~ 20 %
EKIKTUK	~ 1281 m ~ 30 %
	~ 404 m ~ 10 %

INTERLIMB ANGLE (γ)	~ 78°
SHORTENING OF KAYAK/ LISBURNE CONTACT IN ANTICLINE	~ 621 m
STRUCTURAL THICKENING IN KAYAK SHALE	~ 396 m ~ 150%
DIP OF AXIAL SURFACE	~ 58° S

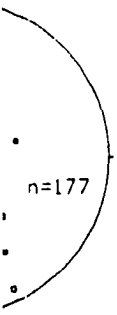

oles to
g
s= N13°W, 15°NE

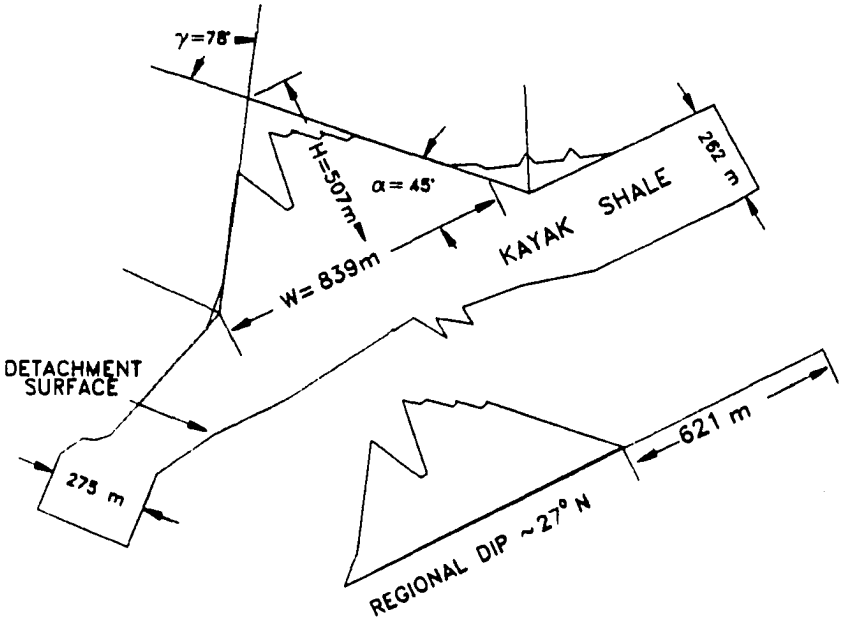

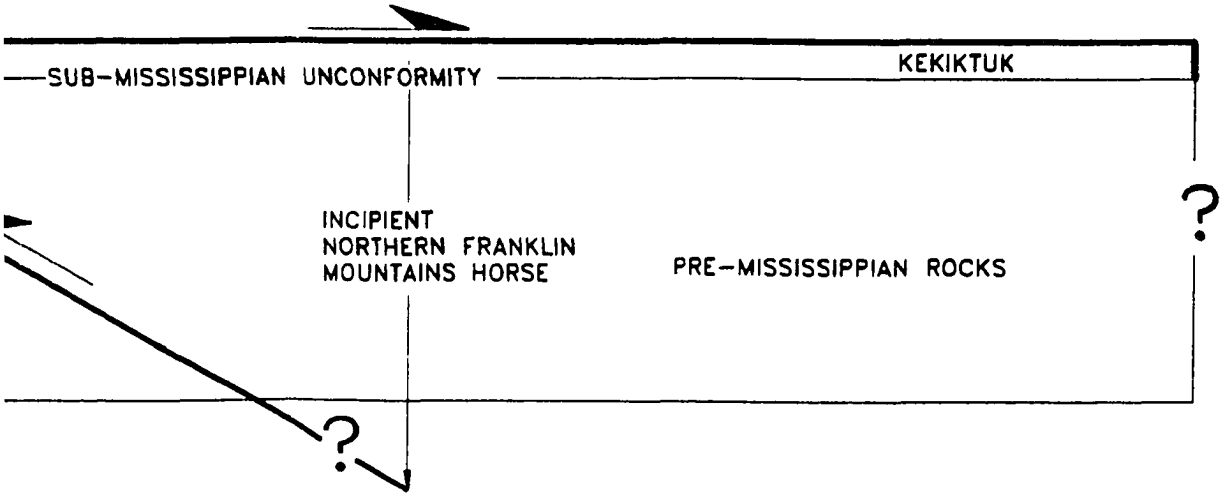

See Plate A2.1 for map.

Reproduced with permission of the copyright owner. Further reproduction prohibited without permission.

PLEASE NOTE:

Oversize maps and charts are filmed in sections in the following manner:

LEFT TO RIGHT, TOP TO BOTTOM, WITH SMALL OVERLAPS

The following map or chart has been refilmed in its entirety at the end of this dissertation (not available on microfiche). A xerographic reproduction has been provided for paper copies and is inserted into the inside of the back cover.

Black and white photographic prints (17" x 23") are available for an additional charge.

UMI

Reproduced with permission of the copyright owner. Further reproduction prohibited without permission.

PLATE A3.1 — Geo

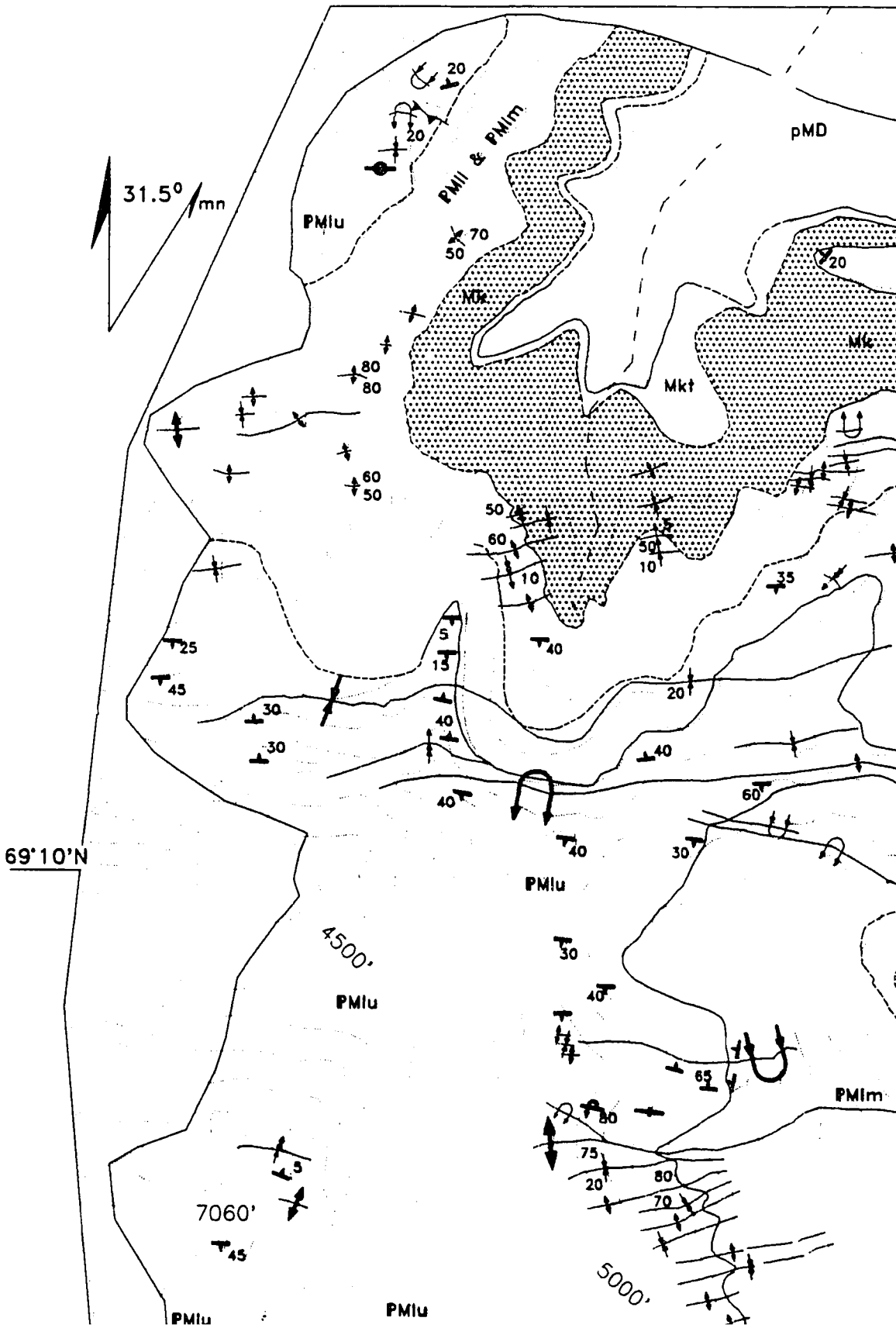

Reproduced with permission of the copyright owner. Further reproduction prohibited without permission.

Geologic map of the Salisbu

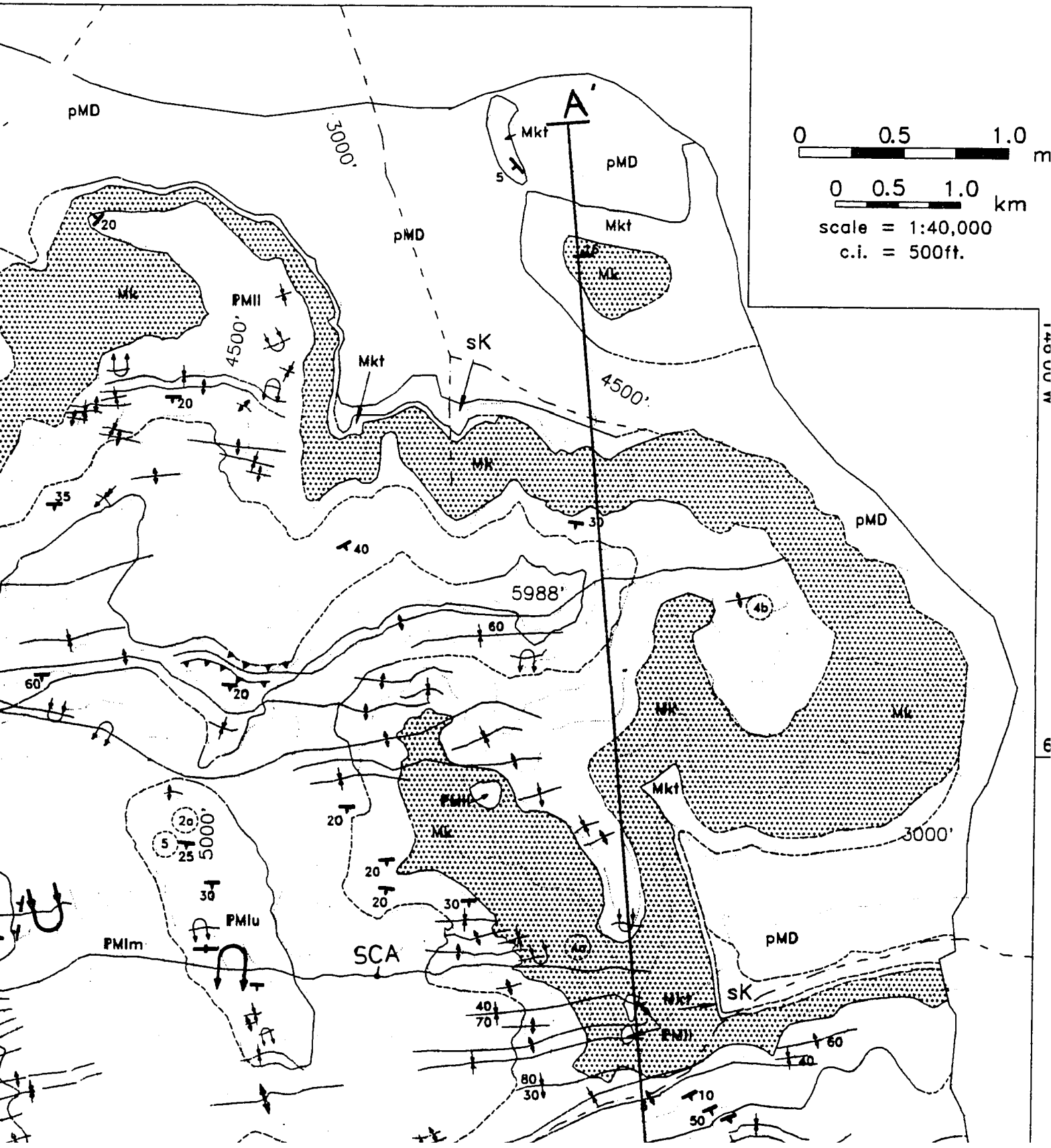

Reproduced with permission of the copyright owner. Further reproduction prohibited without permission.

lisbury Creek area

5 1.0 miles

1.0 km

1:40,000

500ft.

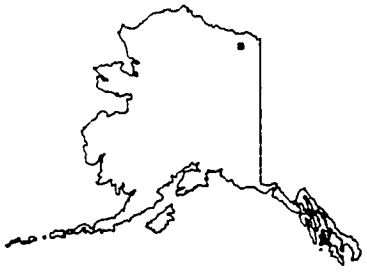

Mt. Michelson A–4

146°00'W

69°10'N

3000'

STRUCTURAL SYMBOLS

- strike of vertical bedding
- horizontal bedding
- 31 strike & dip of bedding
- 45 estimated strike & dip of bedding
- 78 strike & dip of overturned bedding
- 80 estimated strike & dip of overturned bedding
- axial trace of syncline
- axial trace of anticline
- axial trace of fold with beds dipping in the same direction (double arrow on steep limb)
- axial trace of overturned syncline
- axial trace of overturned anticline
- 56 strike & dip of axial–planar cleavage
- trace of thrust fault
- trace of inferred thrust fault
- lithologic contact
- estimated lithologic contact
- (2a) photo locality – see Appendix 3

Reproduced with permission of the copyright owner. Further reproduction prohibited without permission.

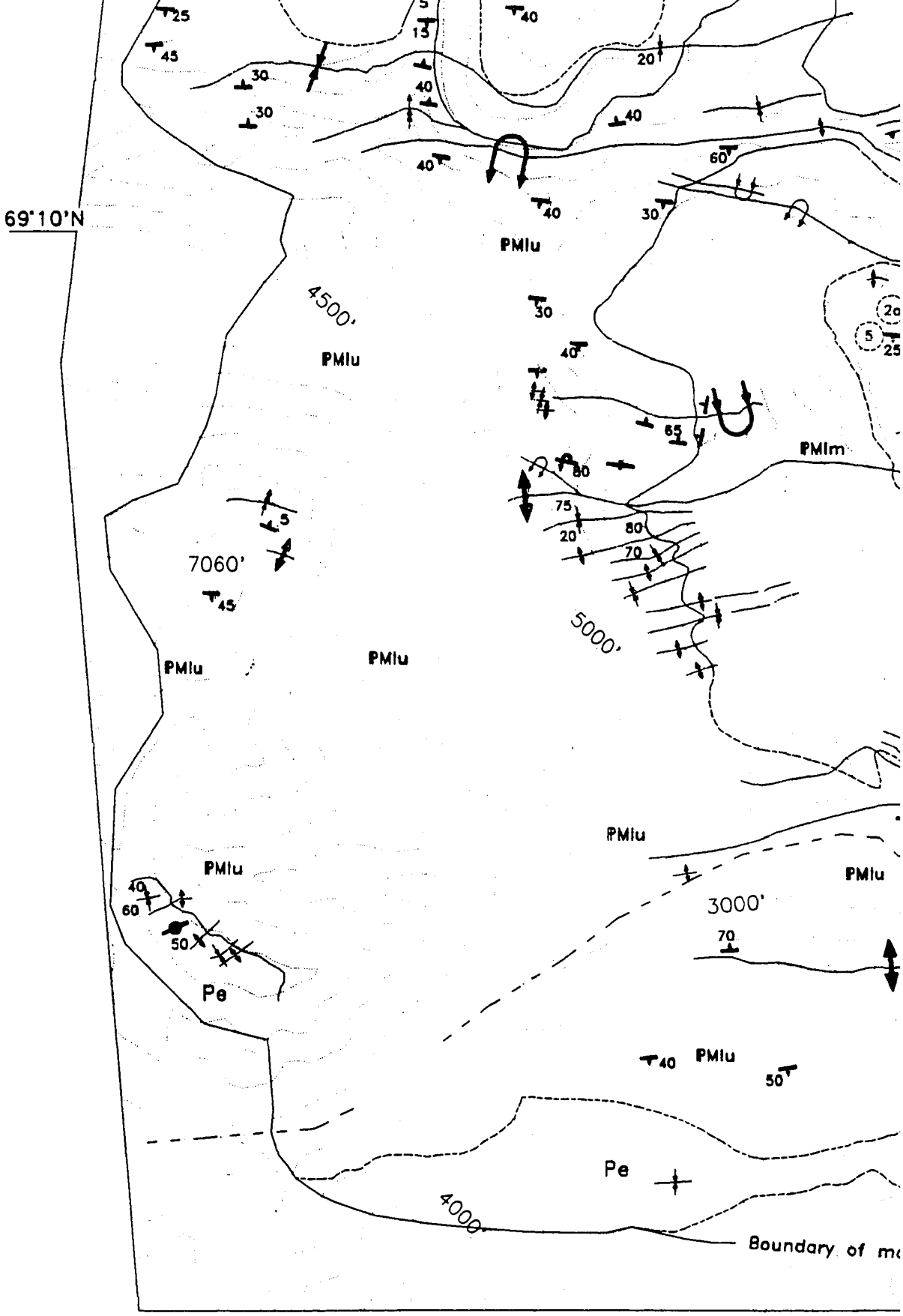

Reproduced with permission of the copyright owner. Further reproduction prohibited without permission.

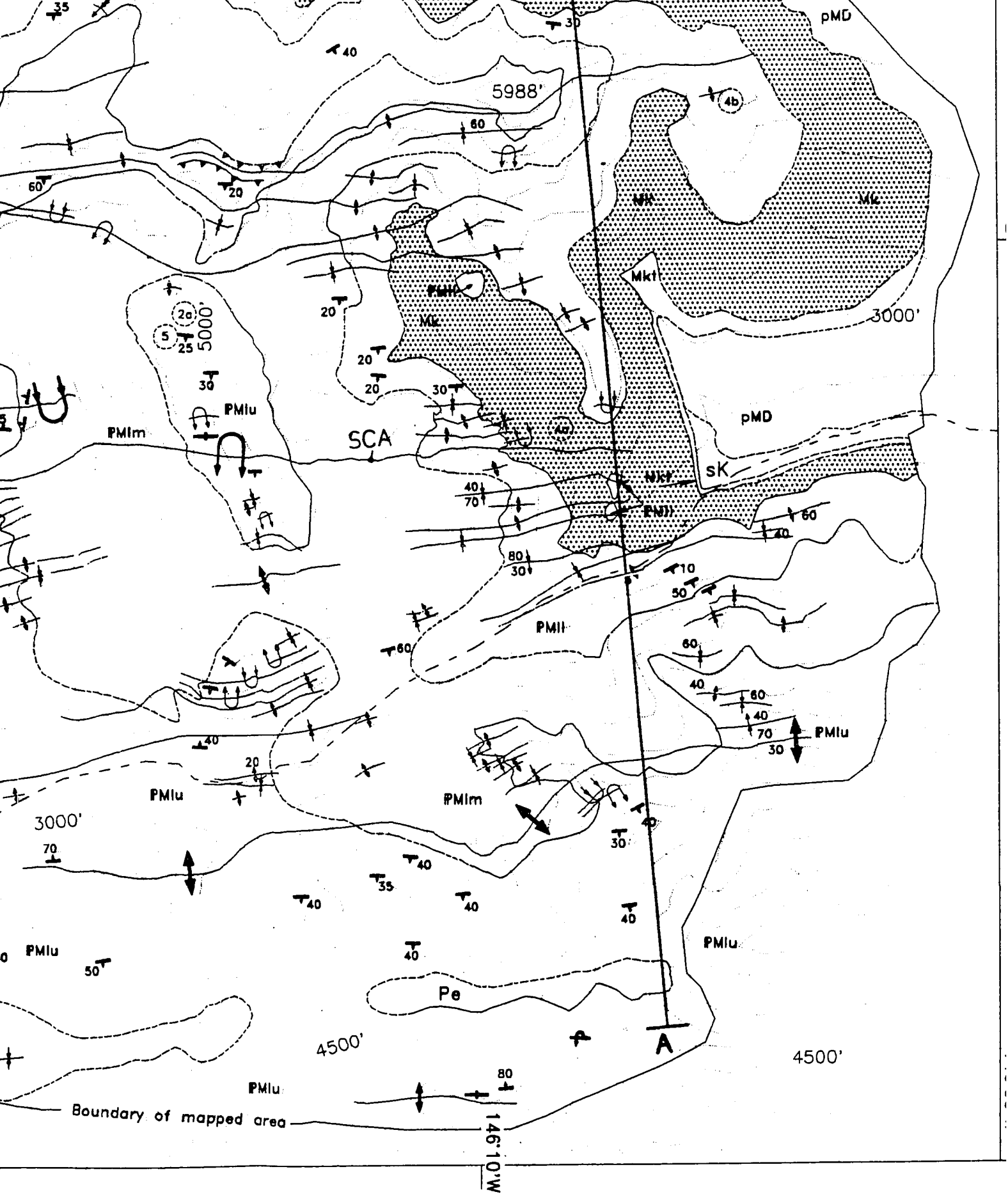

Reproduced with permission of the copyright owner. Further reproduction prohibited without permission.

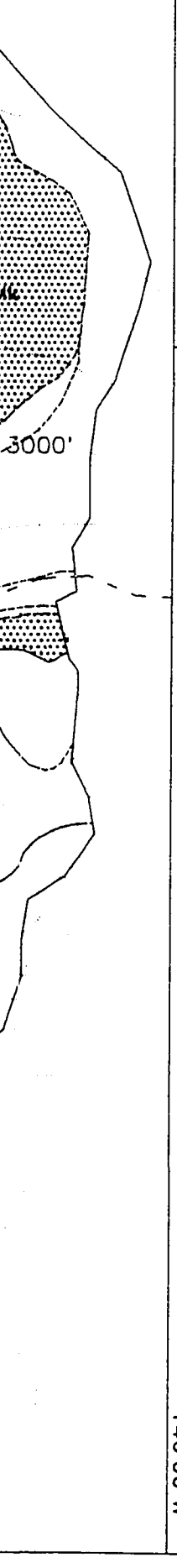

69°10'N

146°00'W

69°06'N

31 strike & dip of bedding

45 estimated strike & dip of bedding

78 strike & dip of overturned bedding

80 estimated strike & dip of overturned bedding

axial trace of syncline

axial trace of anticline

axial trace of fold with beds dipping in the same direction (double arrow on steep limb)

axial trace of overturned syncline

axial trace of overturned anticline

56 strike & dip of axial-planar cleavage

trace of thrust fault

trace of inferred thrust fault

lithologic contact

estimated lithologic contact

(2a) photo locality – see Appendix 3

STRATIGRAPHY

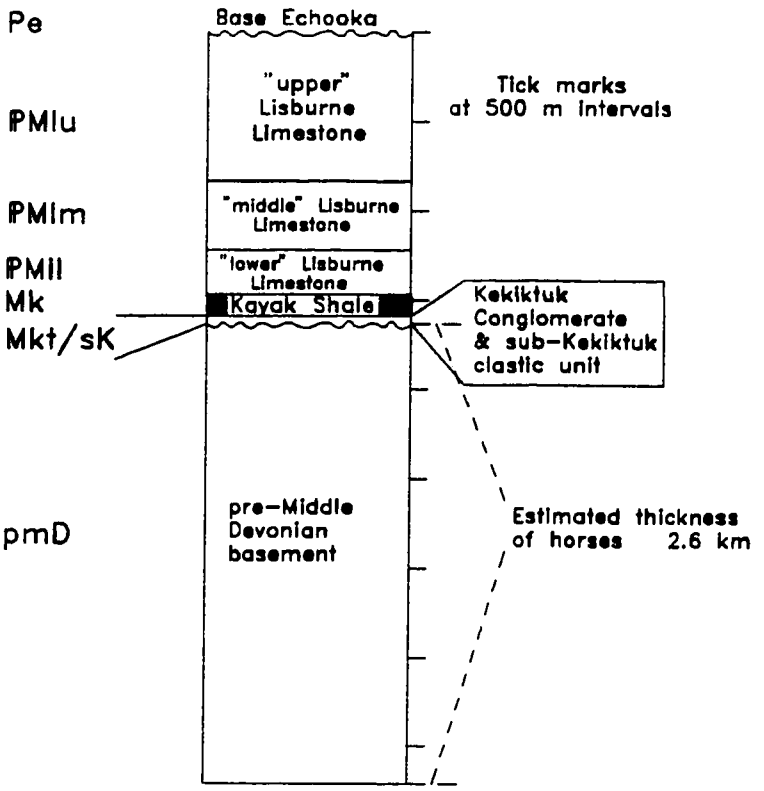

See Plate A3.2 for cross section.
See figure 1.6 for location.

Reproduced with permission of the copyright owner. Further reproduction prohibited without permission.

PLEASE NOTE:

Oversize maps and charts are filmed in sections in the following manner:

LEFT TO RIGHT, TOP TO BOTTOM, WITH SMALL OVERLAPS

The following map or chart has been refilmed in its entirety at the end of this dissertation (not available on microfiche). A xerographic reproduction has been provided for paper copies and is inserted into the inside of the back cover.

Black and white photographic prints (17" x 23") are available for an additional charge.

UMI

Reproduced with permission of the copyright owner. Further reproduction prohibited without permission.

PLATE A3.2 – Balanced cross

Stratigraphy

(scale = 1.5X cross section)

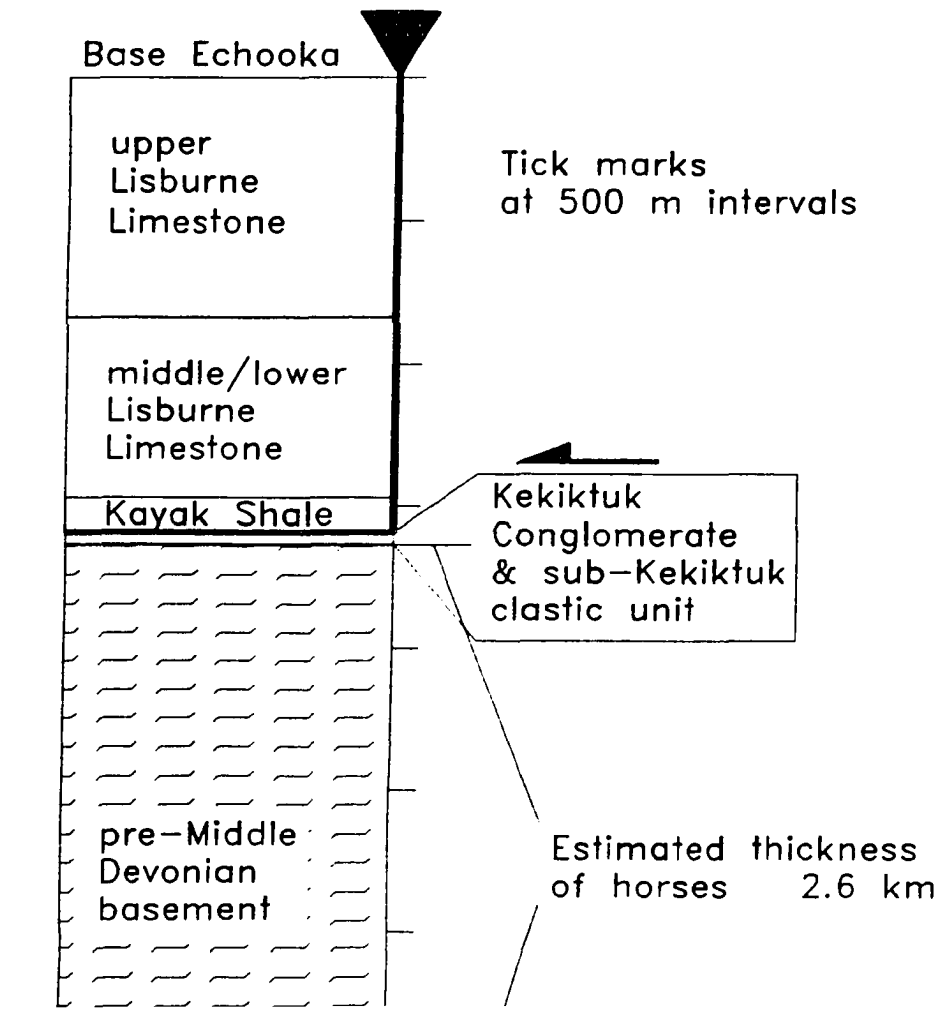

S

Observed Kekiktuk

Middle of upper Lisl

Estimated displacem
Northern Franklin M

Depth of floor thrus

Reproduced with permission of the copyright owner. Further reproduction prohibited without permission.

cross section across the crest and backl

Thomas X. Homza

Tectonics and Sedimentation Research Group
Department of Geology and Geophysics
&
Geophysical Institute
University of Alaska Fairbanks

1994

scale = 1:40,000

Shortening

d Kekiktuk	128m
of upper Lisburne	2.9km
ed displacement of n Franklin Mountains horse	19.3km
f floor thrust	3.9km subsea

notes:

1) Pin & loc
extend only
Kayak Shale
arbitrarily le
of the North
for the ease
thrust fault
section is cc
required to
lying fold is
fault since e
faults occur
(Ziegler 198

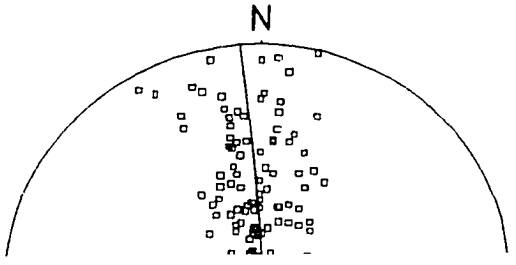

Reproduced with permission of the copyright owner. Further reproduction prohibited without permission.

d backlimb of the western end of the nc

DEFORMED

plane of section
N05W,88NE

A
S05E

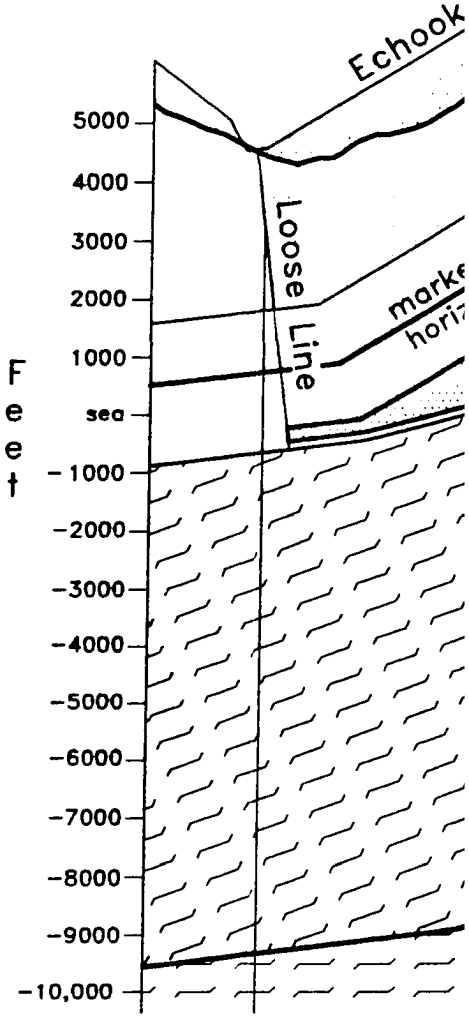

1) Pin & loose lines in the roof sequence extend only as deep as the base of the Kayak Shale. 2) The roof sequence was arbitrarily left fixed relative to the footwall of the Northern Franklin Mountains horse for the ease of reconstruction. 3) The thrust fault in the southern part of the section is conjectural. However, shortening required to accommodate the overlying lying fold is likely to be taken up on a thrust fault since eastward, along strike, thrust faults occur in similar structural positions (Ziegler, 1989).

Reproduced with permission of the copyright owner. Further reproduction prohibited without permission.

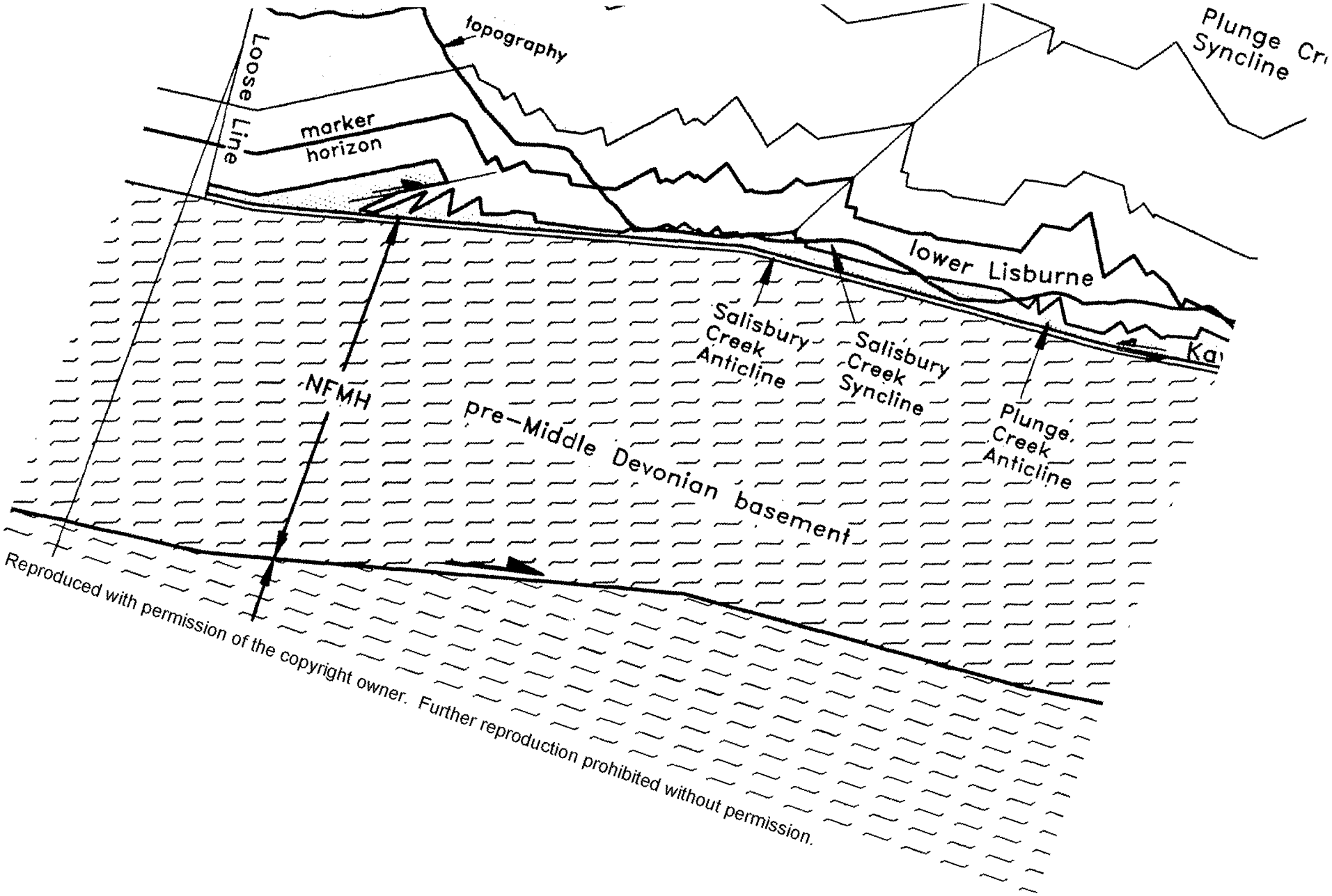

Reproduced with permission of the copyright owner. Further reproduction prohibited without permission.

Mountains anticlinorium

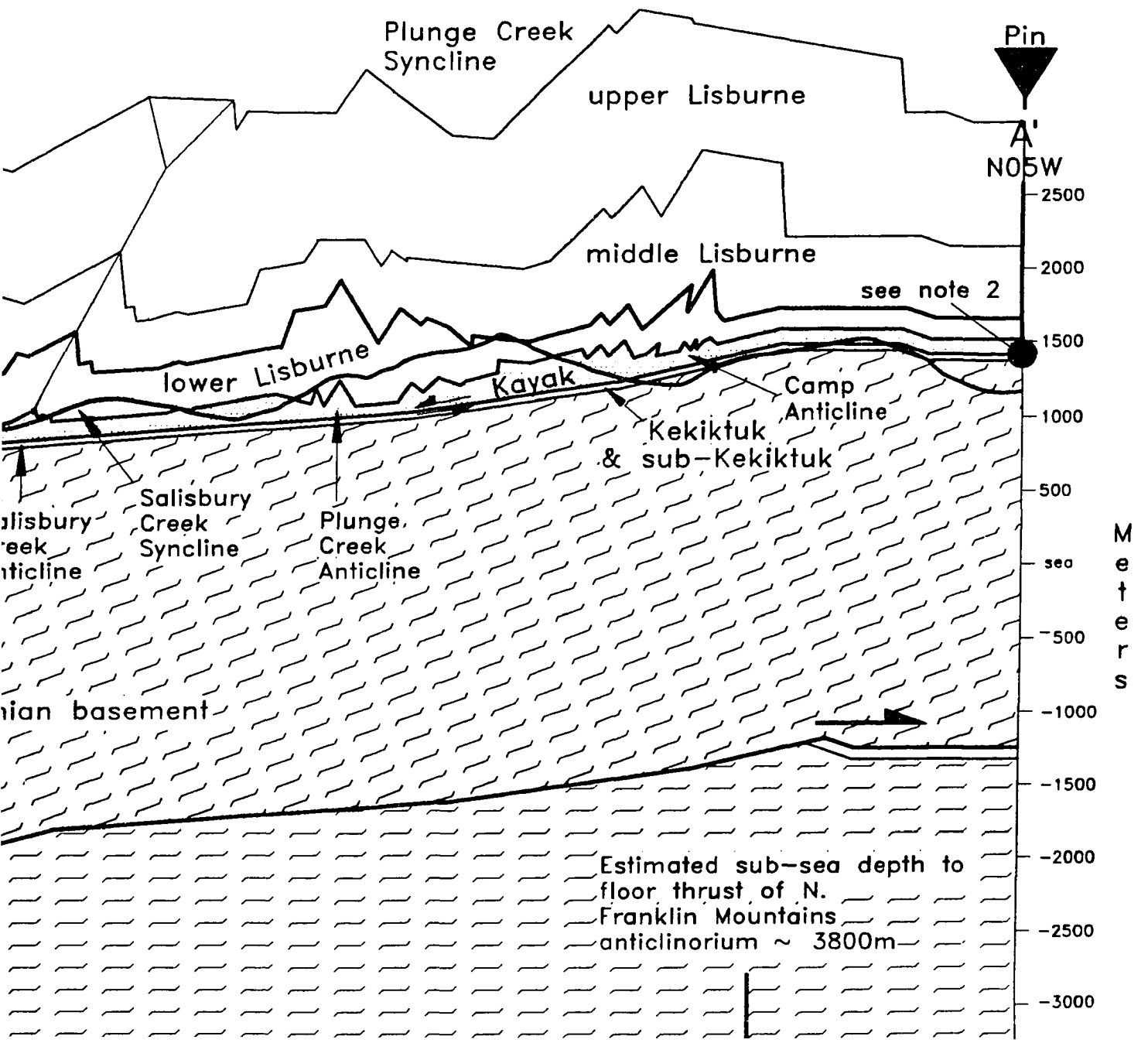

Reproduced with permission of the copyright owner. Further reproduction prohibited without permission.

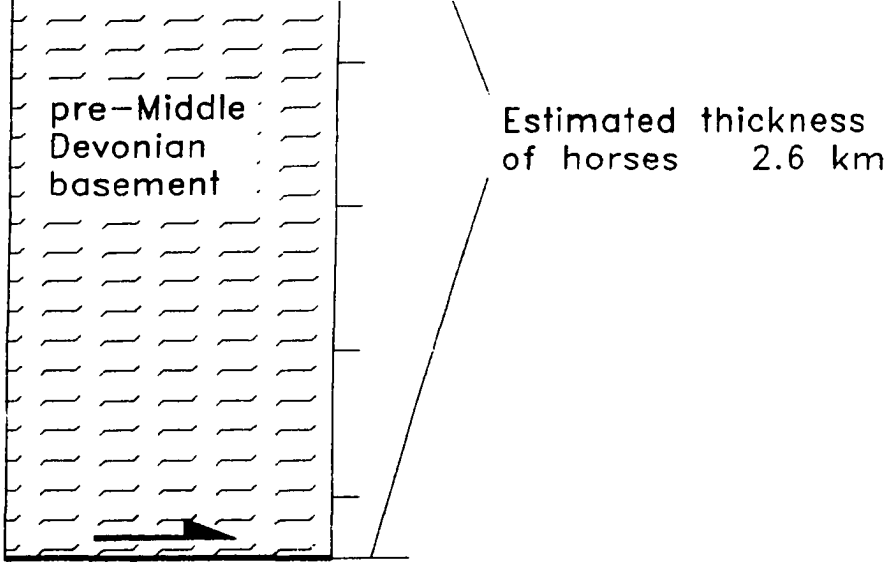

Ste

RESTORED SECTION

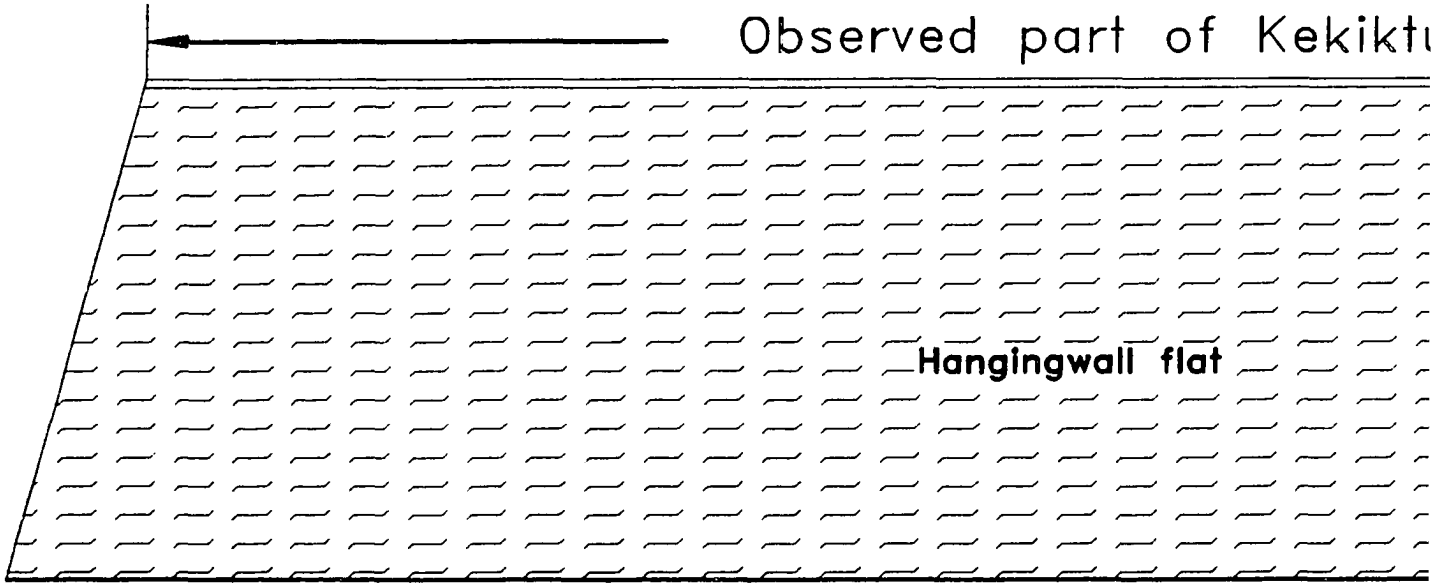

Reproduced with permission of the copyright owner. Further reproduction prohibited without permission.

section is c
required to
lying fold is
fault since
faults occur
(Ziegler, 19

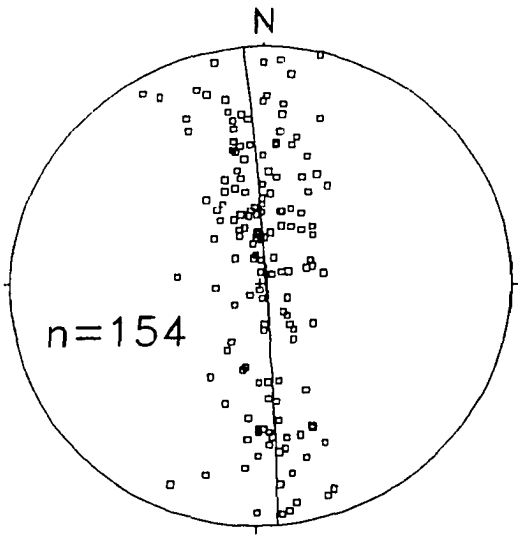

Stereogram of poles to Ellesmerian bedding
Best-fit fold axis N85°E,2°NE

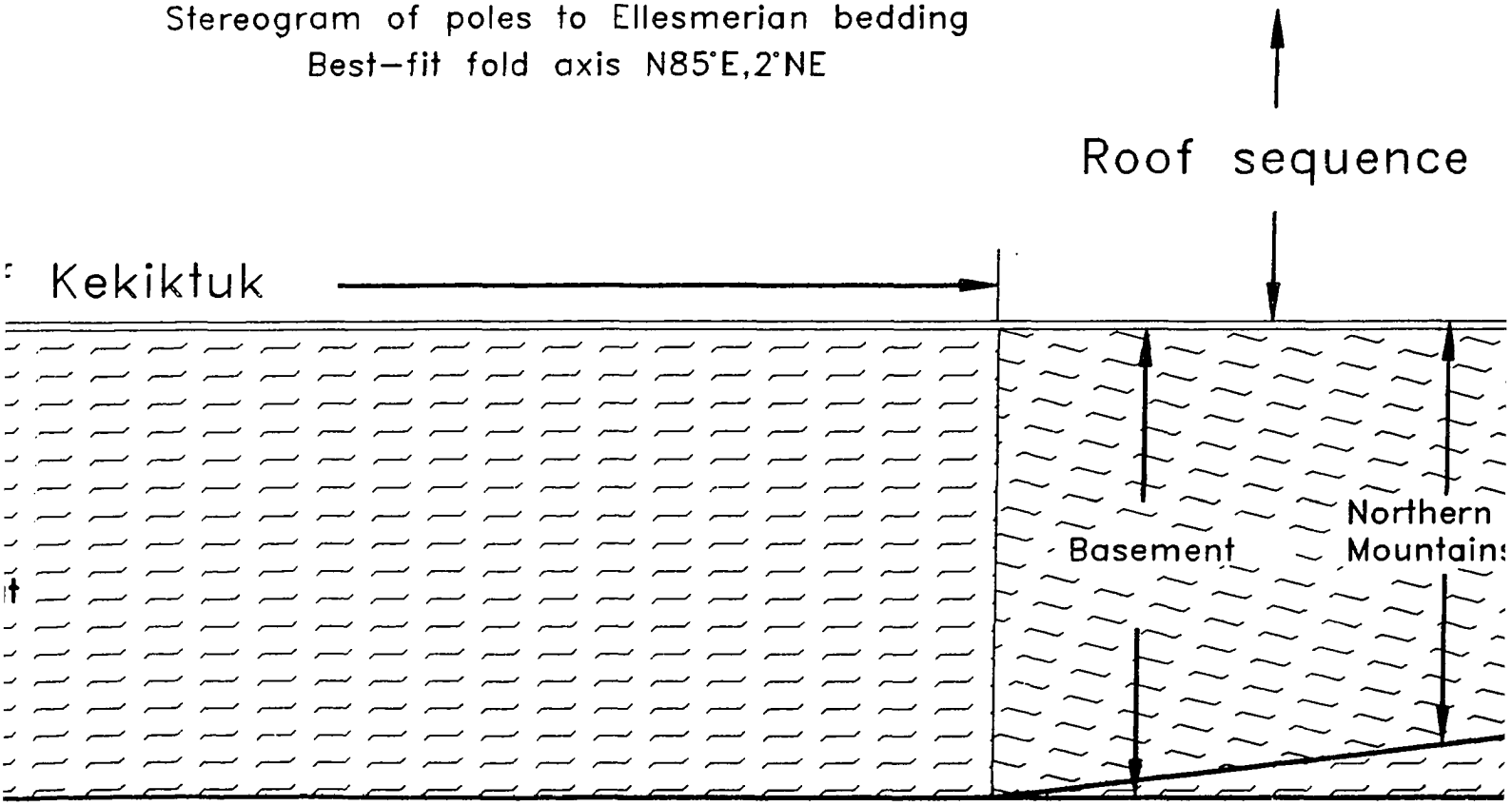

Reproduced with permission of the copyright owner. Further reproduction prohibited without permission.

section is conjectural. However, shortening required to accommodate the overlying lying fold is likely to be taken up on a thrust fault since eastward, along strike, thrust faults occur in similar structural positions (Ziegler, 1989).

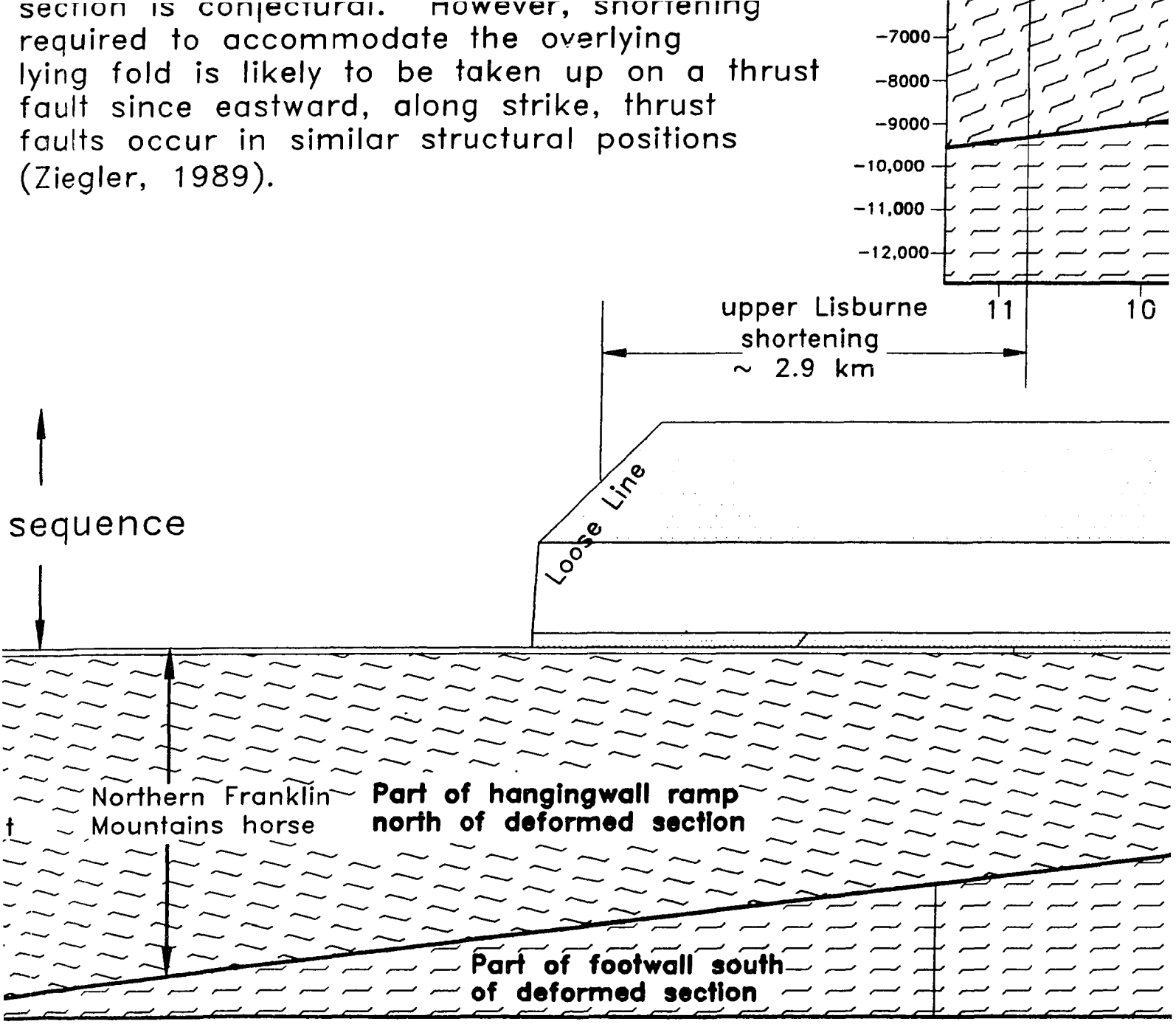

Reproduced with permission of the copyright owner. Further reproduction prohibited without permission.

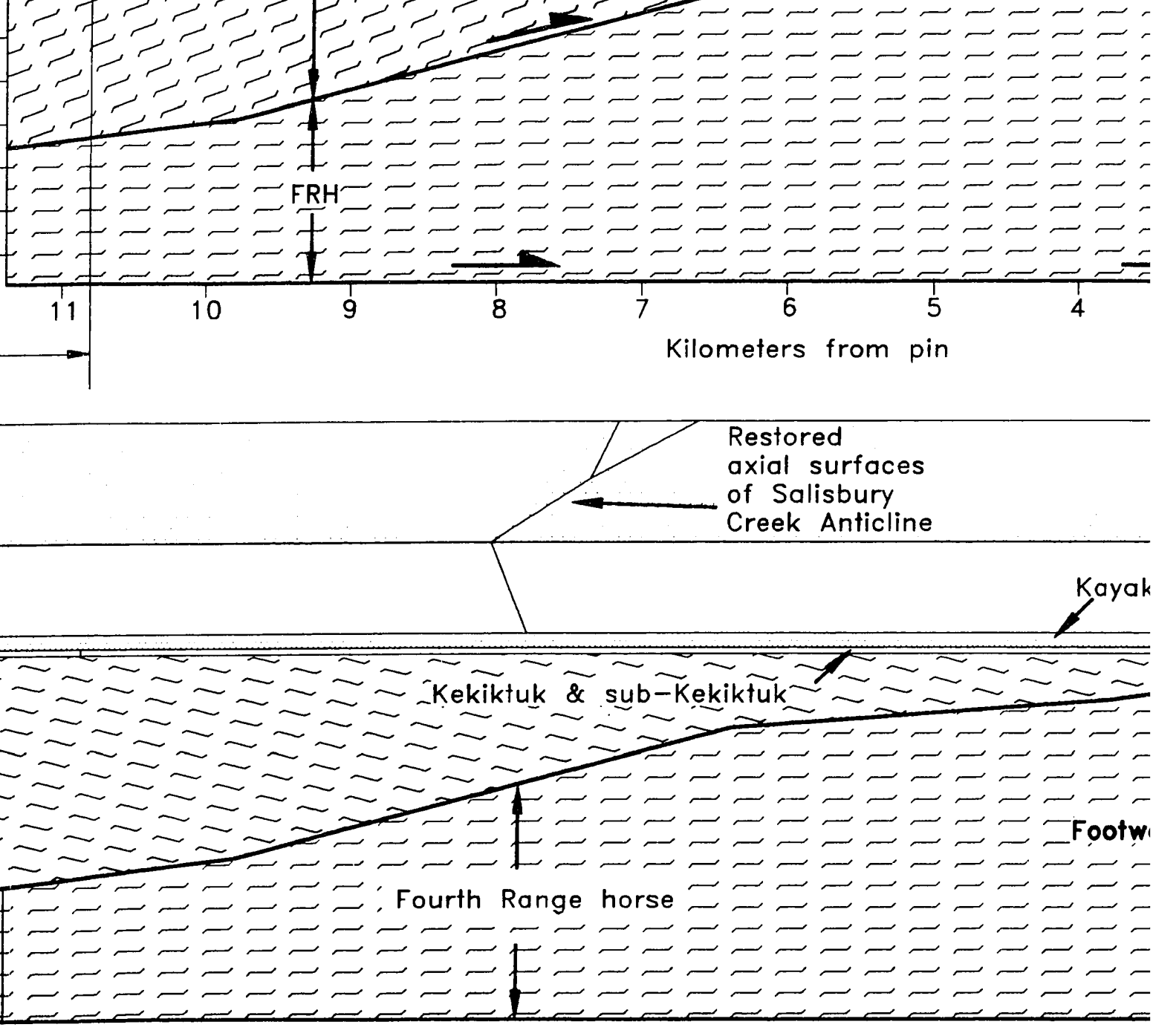

Reproduced with permission of the copyright owner. Further reproduction prohibited without permission.

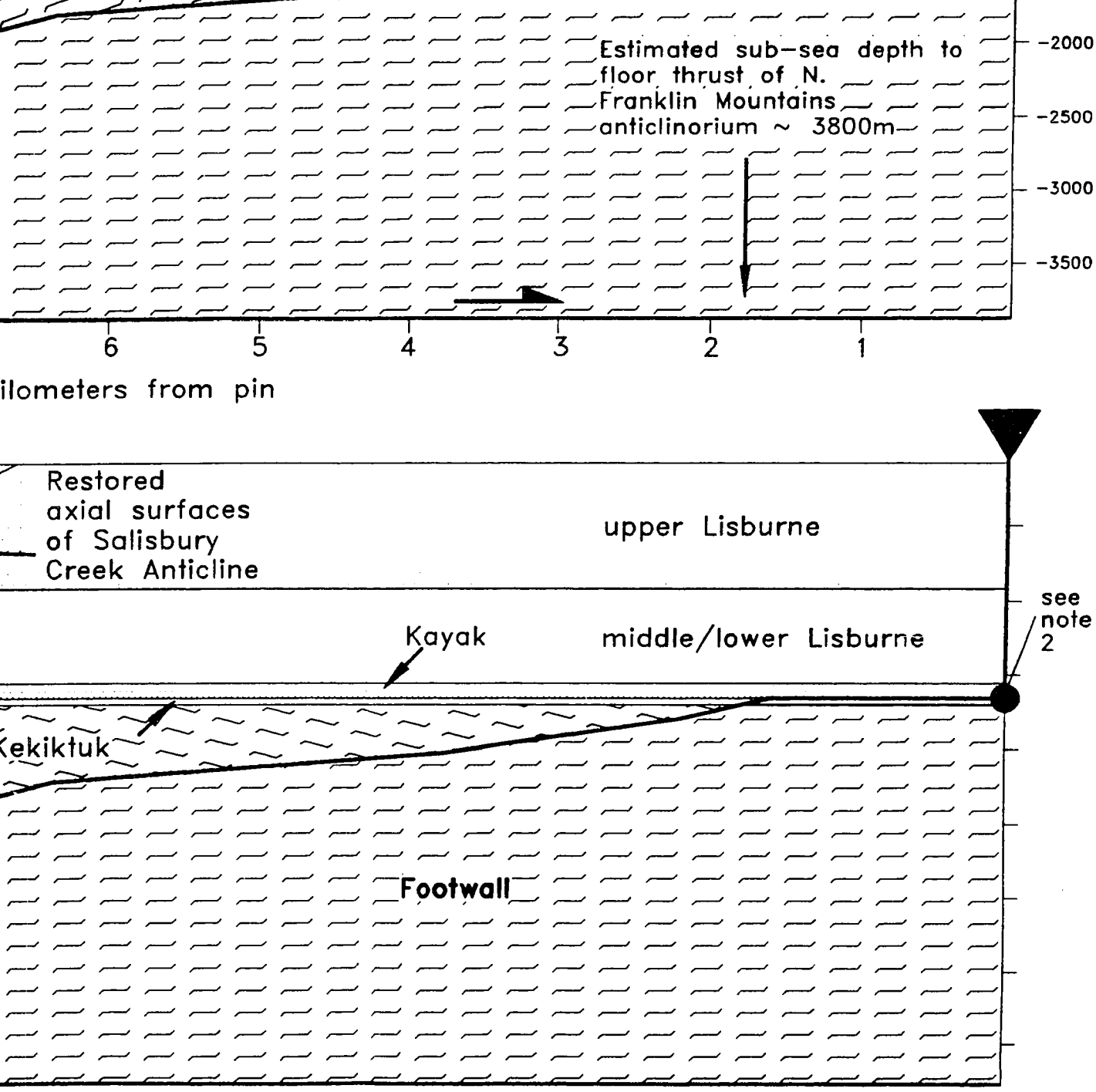

See Plate A3.1 for map.

Reproduced with permission of the copyright owner. Further reproduction prohibited without permission.

PLEASE NOTE:

Oversize maps and charts are filmed in sections in the following manner:

LEFT TO RIGHT, TOP TO BOTTOM, WITH SMALL OVERLAPS

The following map or chart has been refilmed in its entirety at the end of this dissertation (not available on microfiche). A xerographic reproduction has been provided for paper copies and is inserted into the inside of the back cover.

Black and white photographic prints (17" x 23") are available for an additional charge.

UMI

Reproduced with permission of the copyright owner. Further reproduction prohibited without permission.

PLATE A3.

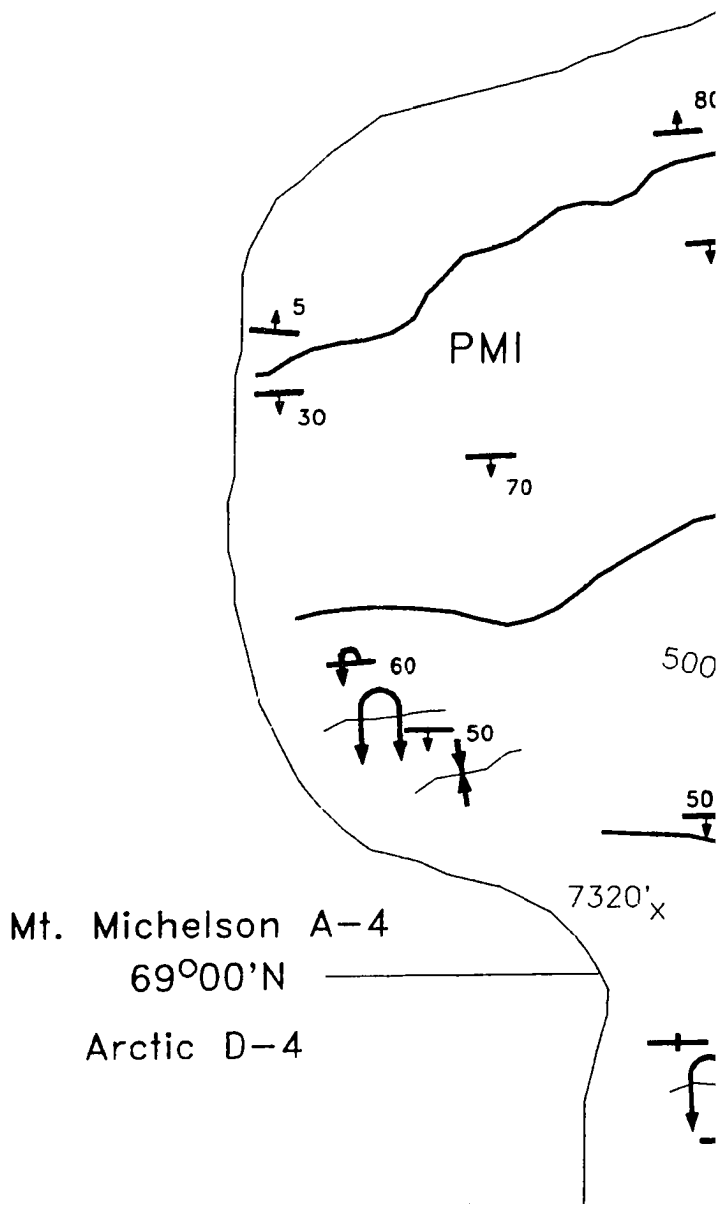

Reproduced with permission of the copyright owner. Further reproduction prohibited without permission.

ATE A3.3 – Geologic map of the wes

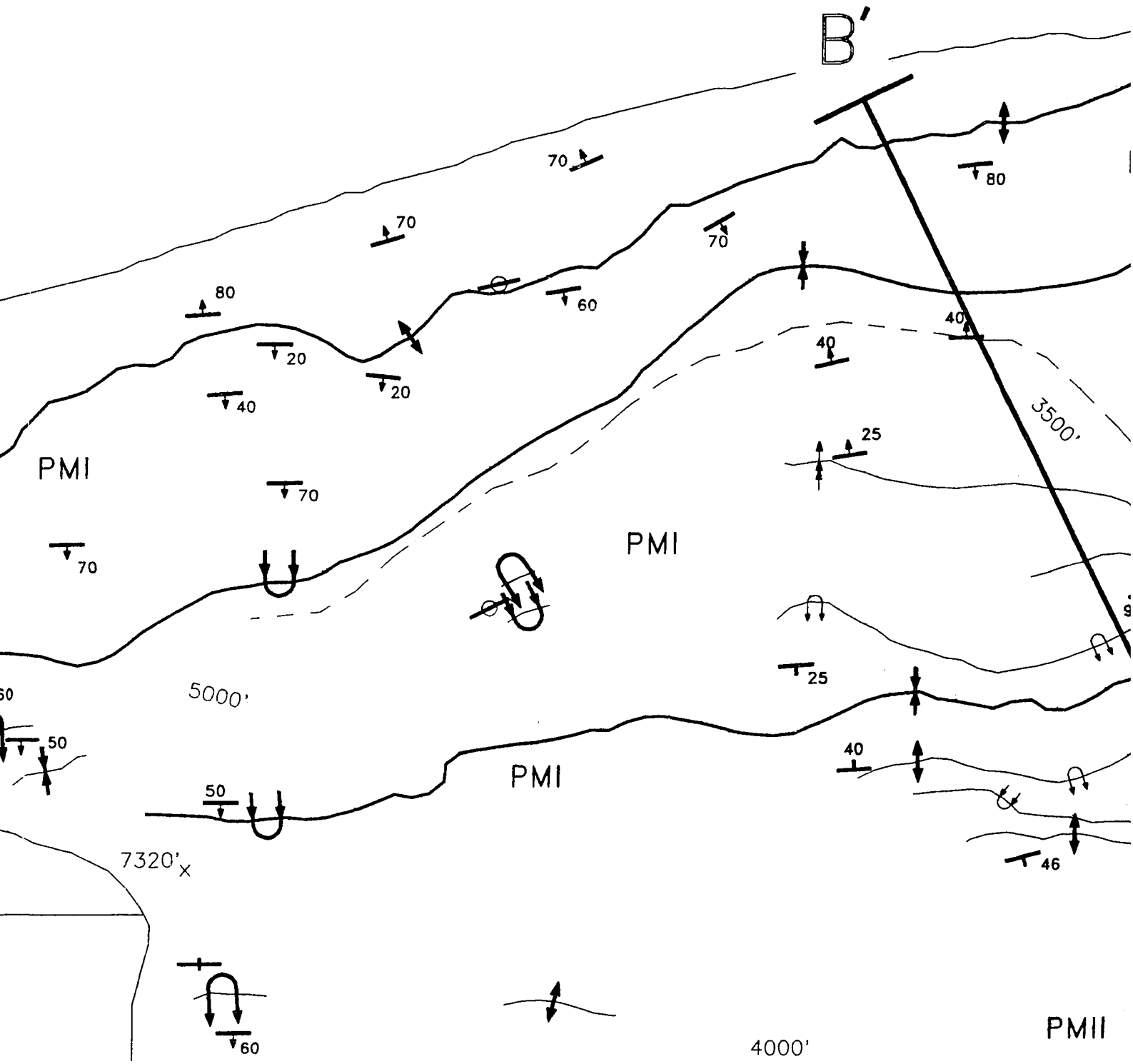

Reproduced with permission of the copyright owner. Further reproduction prohibited without permission.

the western end of the southern Fra

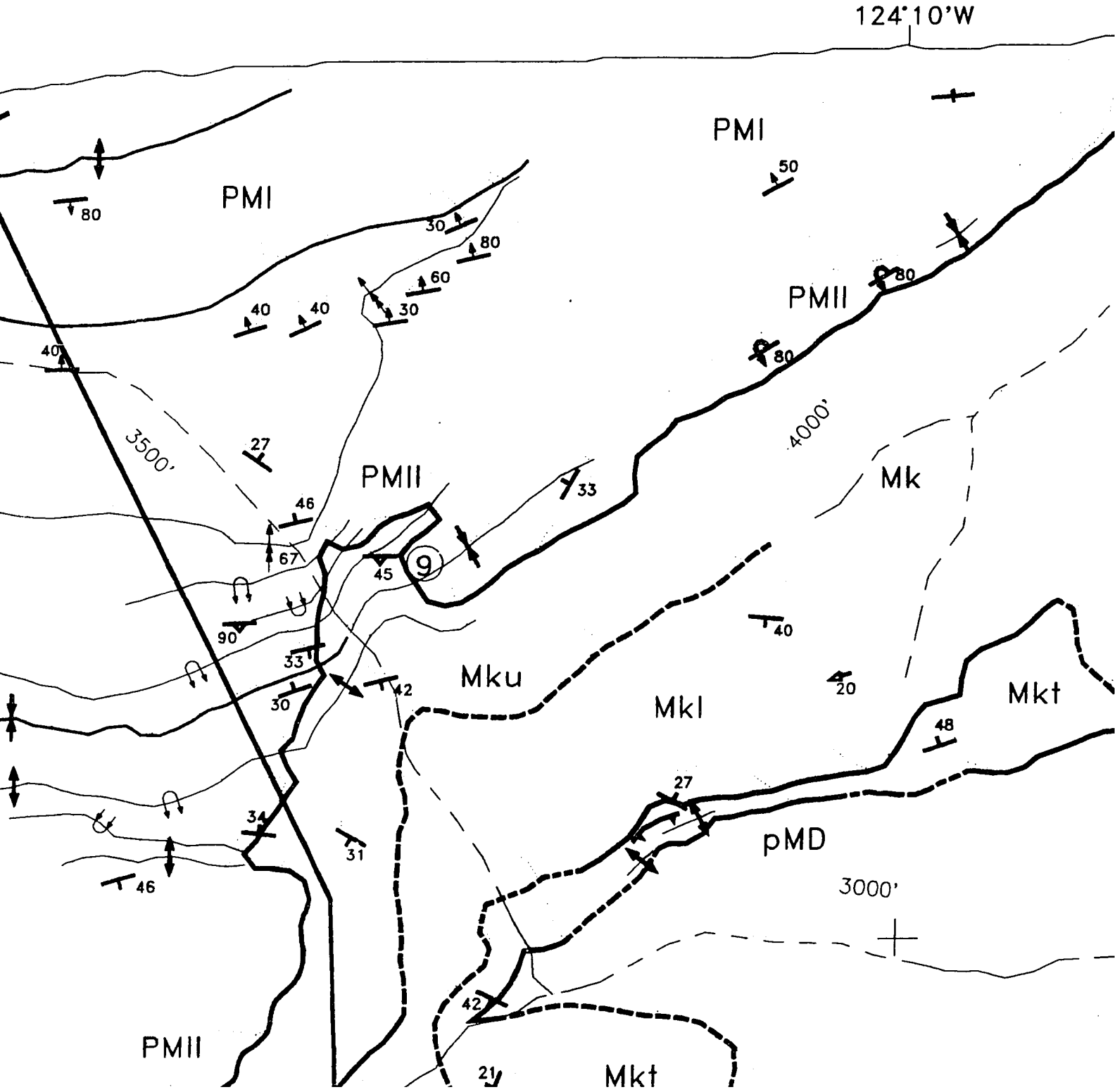

Reproduced with permission of the copyright owner. Further reproduction prohibited without permission.

ern Franklin Mountains anticlinorium

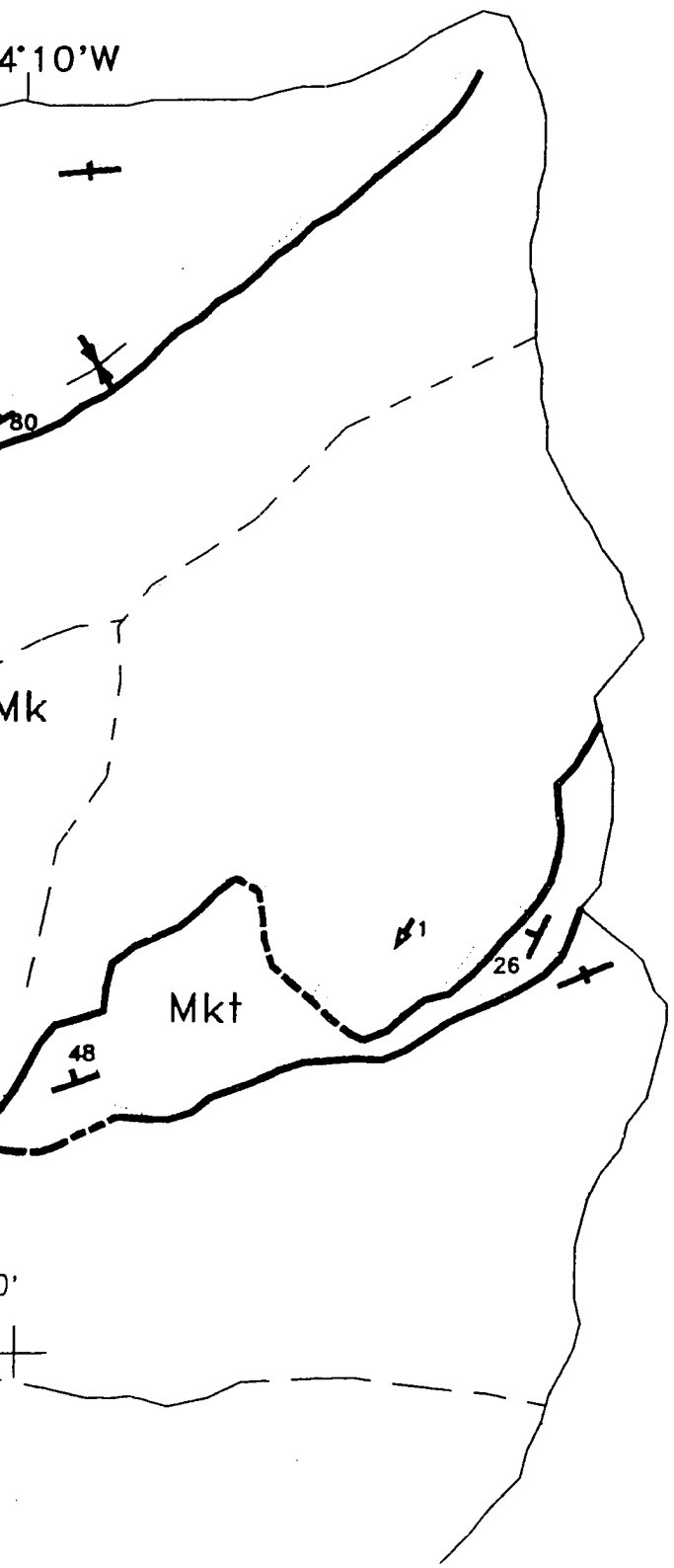

STRUCTURAL SYMBOLS

- strike of vertical bedding
- horizontal bedding
- 31 strike & dip of bedding
- 45 estimated strike & dip of bedding
- 76 strike & dip of overturned bedding
- 80 estimated strike & dip of overturned bedding
- axial trace of syncline
- axial trace of anticline
- 60 / 20 axial trace of fold with beds dippin same direction (double arrows on s
- axial trace of overturned syncline
- axial trace of overturned anticline
- 56 strike & dip of axial planar cleavag
- trace of thrust fault
- trace of inferred thrust fault
- 4 trend & plunge of fold axis
- lithologic contact

Reproduced with permission of the copyright owner. Further reproduction prohibited without permission.

nticlinorium

RAL SYMBOLS

:e of vertical bedding

zontal bedding

:e & dip of bedding

nated strike & dip of bedding

:e & dip of overturned bedding

nated strike & dip
overturned bedding

l trace of syncline

l trace of anticline

l trace of fold with beds dipping in the
e direction (double arrows on steep limb)

l trace of overturned syncline

l trace of overturned anticline

e & dip of axial planar cleavage

e of thrust fault

e of inferred thrust fault

d & plunge of fold axis

loaic contact

Reproduced with permission of the copyright owner. Further reproduction prohibited without permission.

Mt. Michelson A–4

69°00'N

Arctic D–4

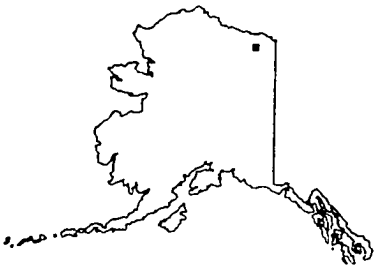

Mt. Michelson A–4, Arctic

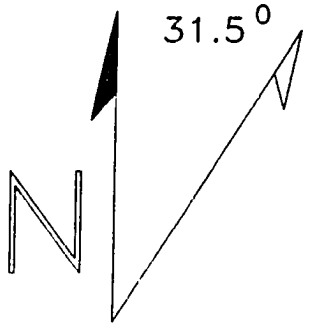

Reproduced with permission of the copyright owner. Further reproduction prohibited without permission.

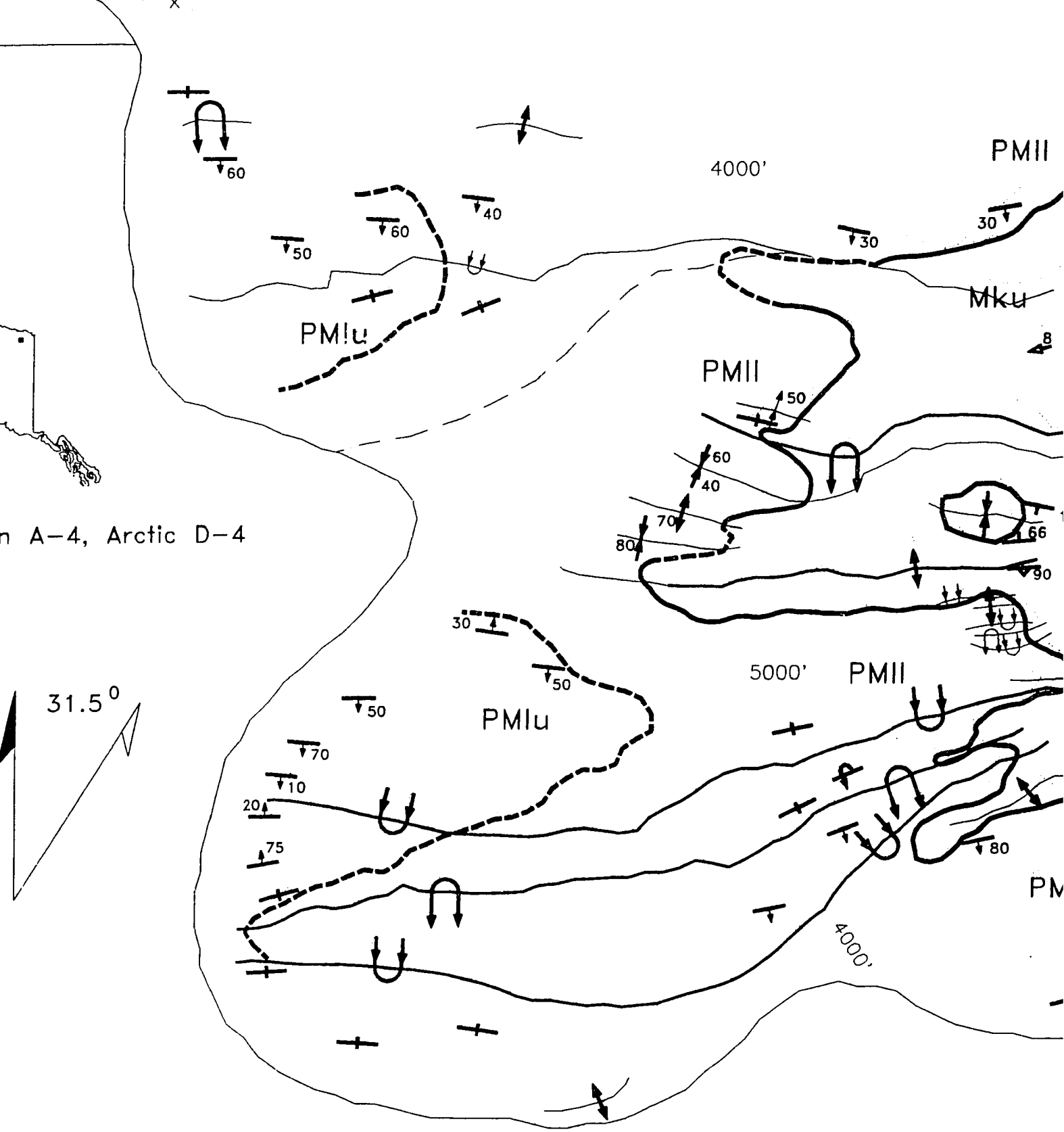

Reproduced with permission of the copyright owner. Further reproduction prohibited without permission.

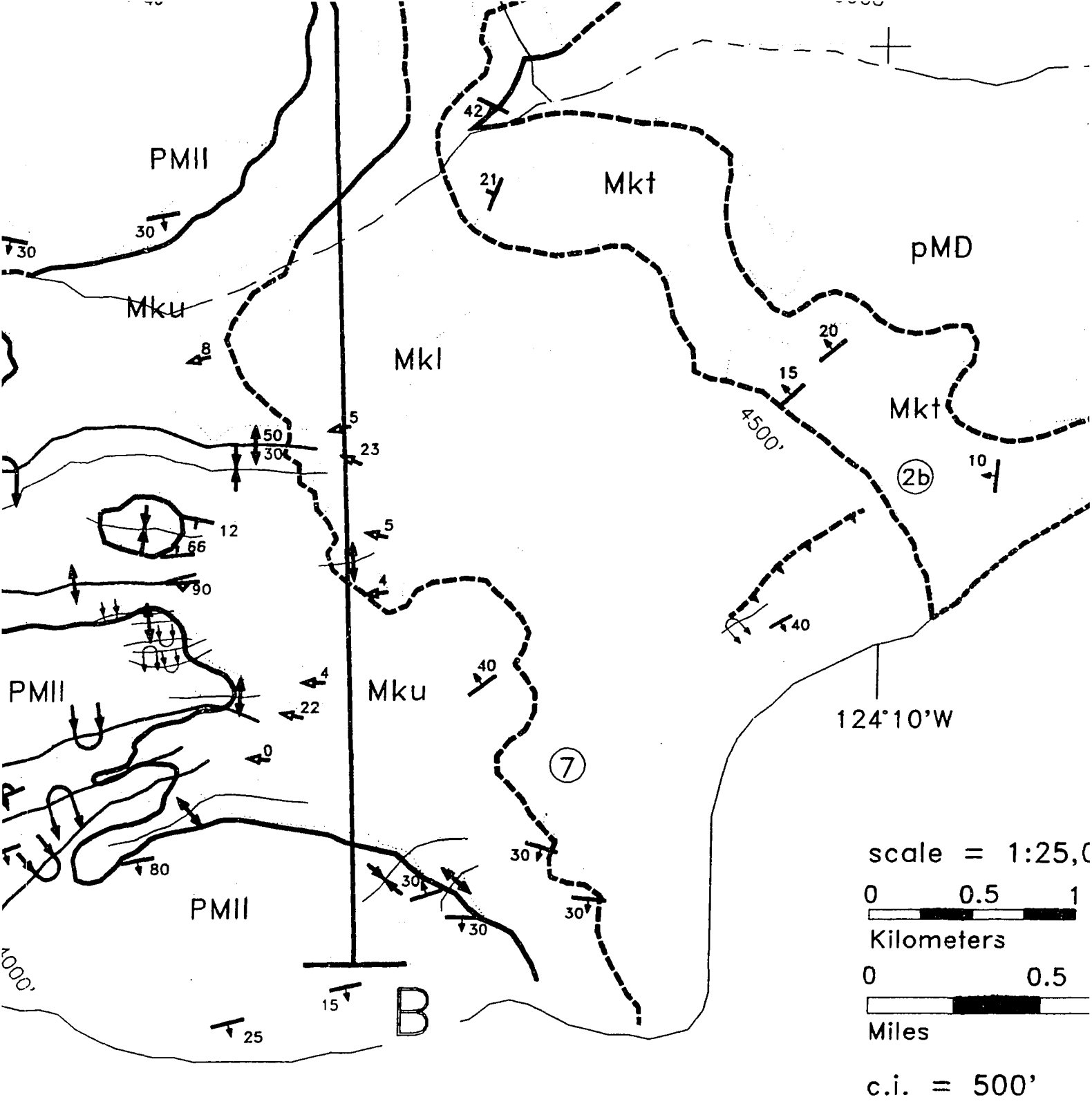

Reproduced with permission of the copyright owner. Further reproduction prohibited without permission.

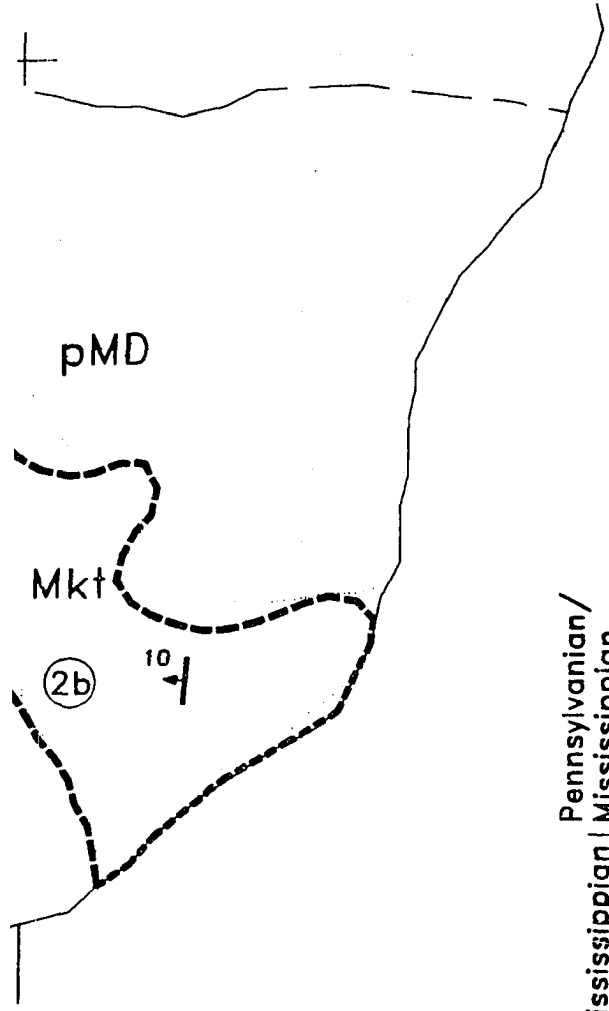

trace of inferred thrust fault

4 trend & plunge of fold axis

lithologic contact

inferred lithologic contact

STRATIGRAPHY

Pennsylvanian/ Mississippian	PMl	Lisburne Group (undivided)
	PMlu	"upper" Lisburne
	PMll	"lower" Lisburne
Mississippian	Mk	Kayak Shale (undivided)
	Mku	"upper" Kayak
	Mkl	"lower" Kayak
	Mkt	Kekiktuk Conglomerate
pre-Middle Devonian	pMD	pre-Middle Devonian rocks (undivided)

scale = 1:25,000

0 0.5 1

Kilometers

0 0.5 1

Miles

c.i. = 500'

⑦ Photo locality – see text

See Plate A3.4 for cr
See figure 1.6 for

Reproduced with permission of the copyright owner. Further reproduction prohibited without permission.

e of thrust fault

e of inferred thrust fault

l & plunge of fold axis

logic contact

red lithologic contact

PHY

e Group (undivided)

Lisburne

Lisburne

Shale (undivided)

Kayak

Kayak

: Conglomerate

dle Devonian rocks
ed)

ocality – see text

See Plate A3.4 for cross section.
See figure 1.6 for location.

Reproduced with permission of the copyright owner. Further reproduction prohibited without permission.

PLATE A3.4 Geologic cross section of the we

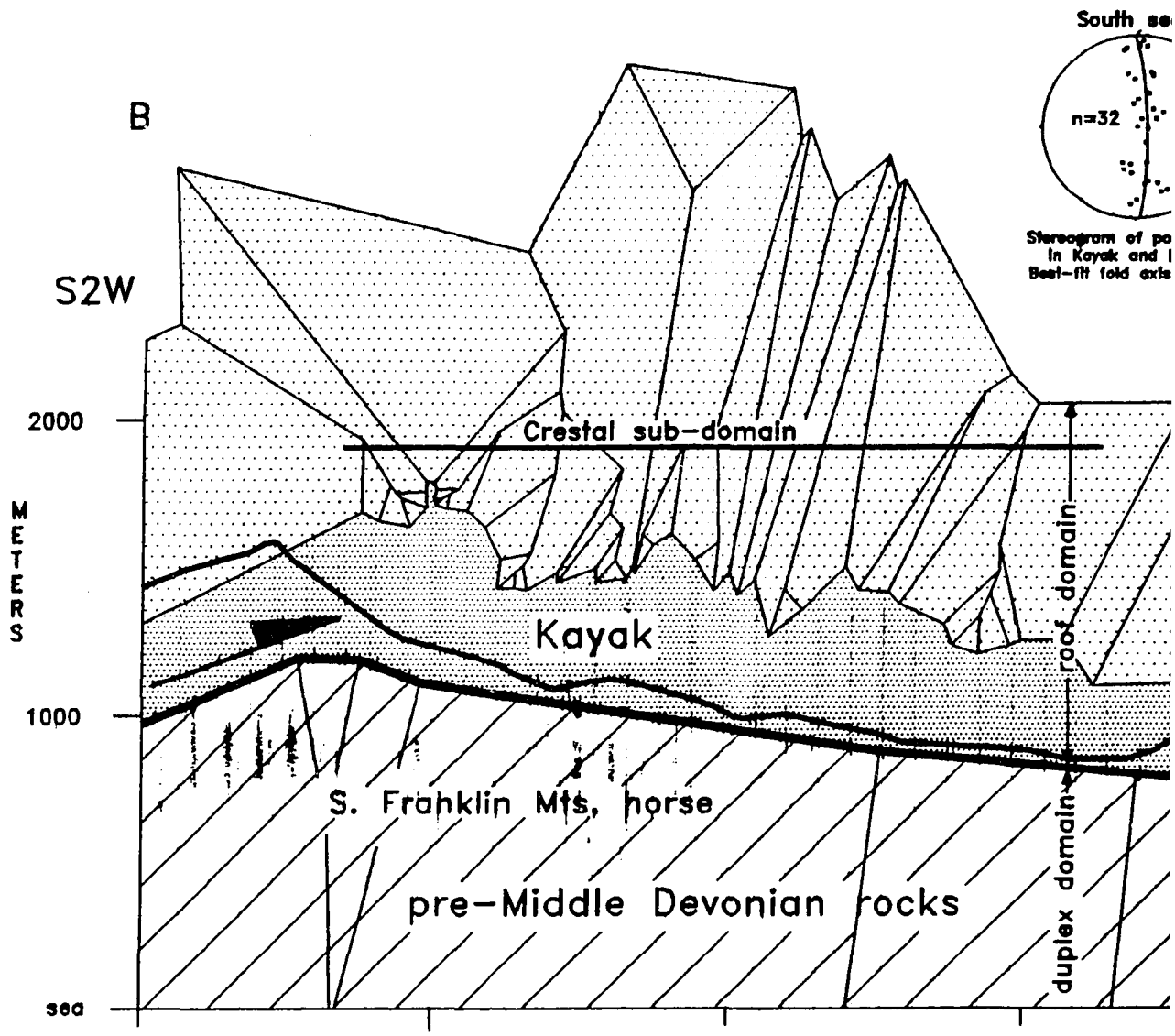

Reproduced with permission of the copyright owner. Further reproduction prohibited without permission.

Reproduced with permission of the copyright owner. Further reproduction prohibited without permission.

of the western end of the southern Franklin Mountains anticli

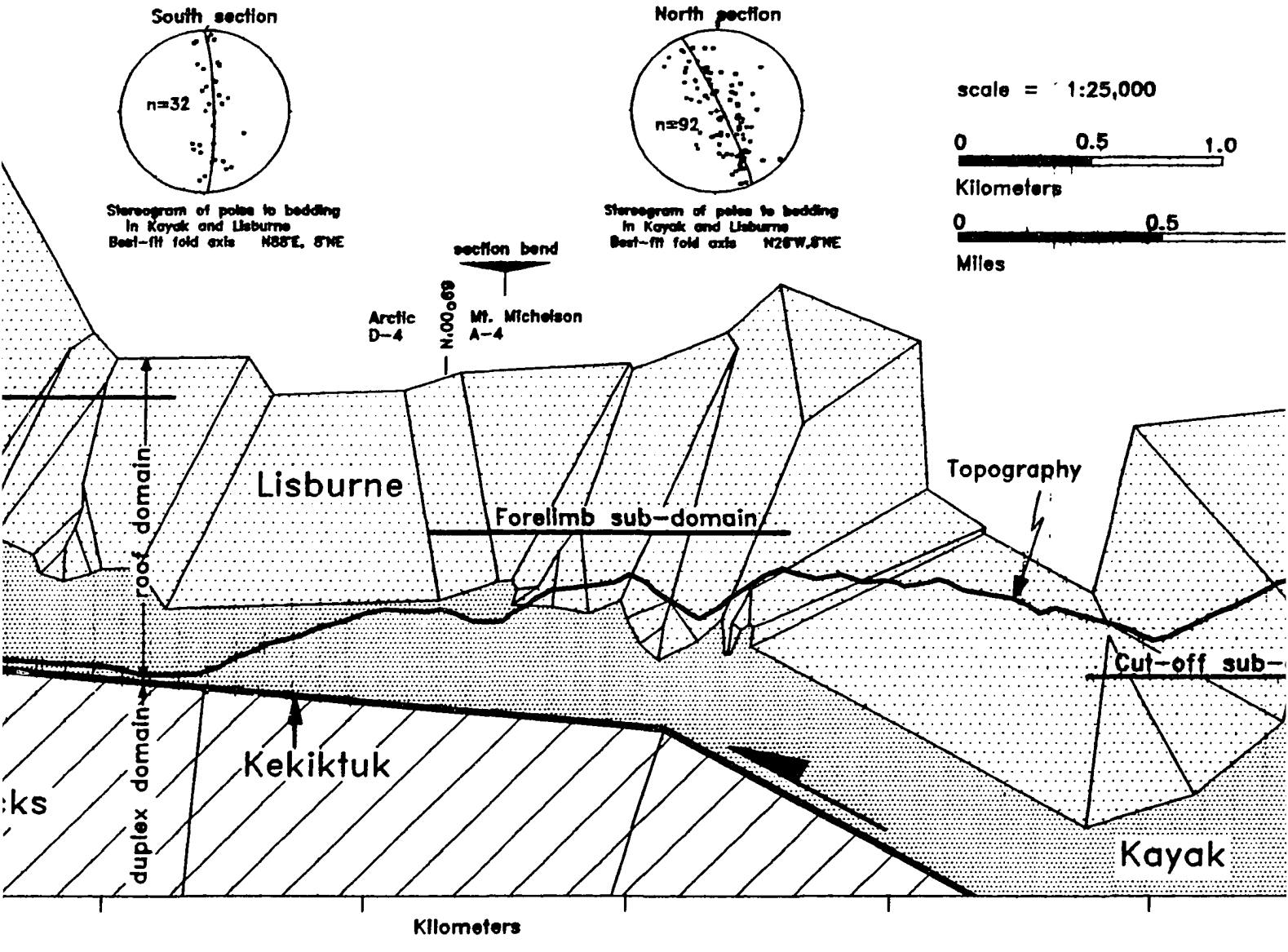

See P

Reproduced with permission of the copyright owner. Further reproduction prohibited without permission.

Reproduced with permission of the copyright owner. Further reproduction prohibited without permission.

ıd of the southern Franklin Mountains anticlinorium

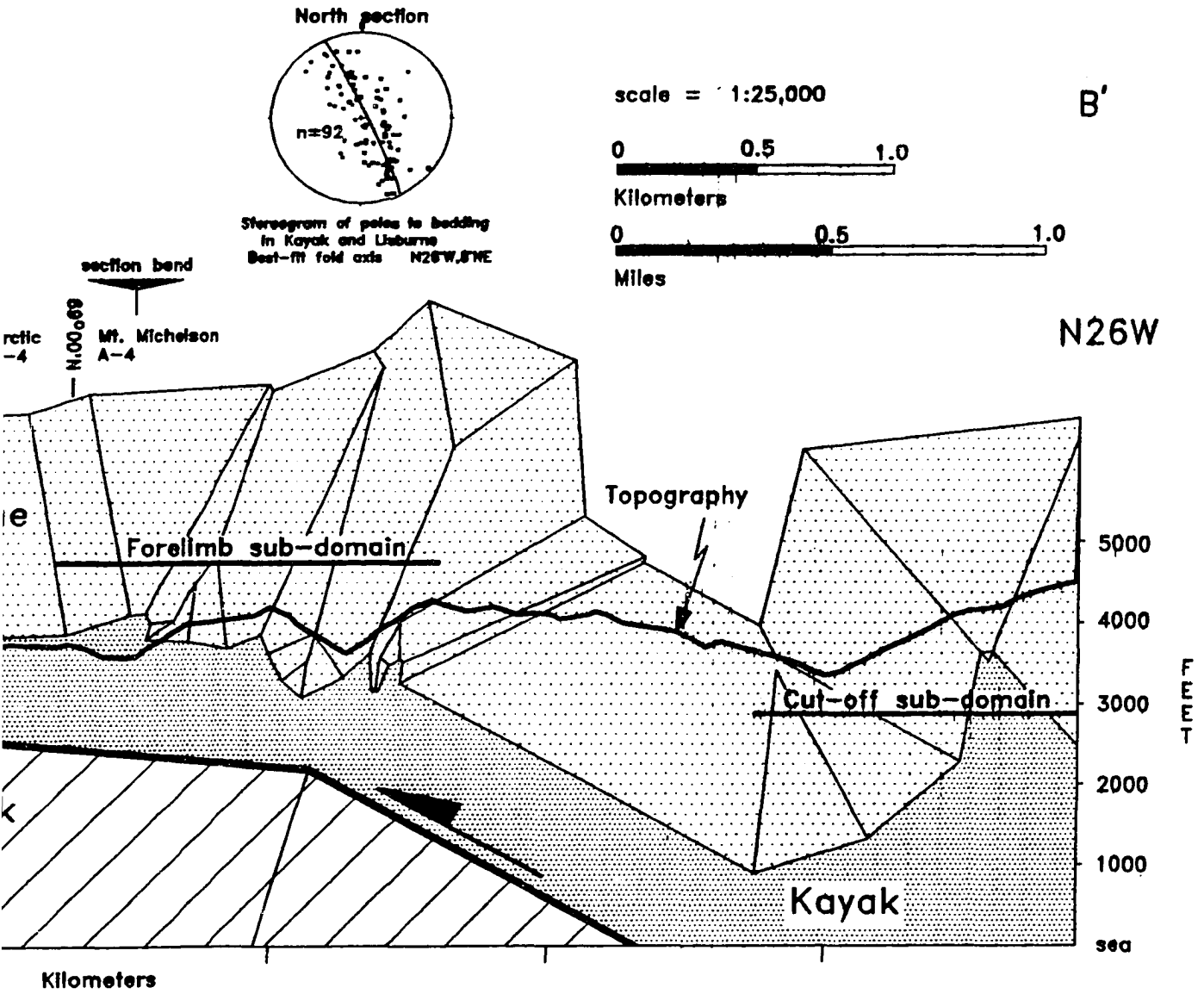

See Plate A3.3 for map.

Reproduced with permission of the copyright owner. Further reproduction prohibited without permission.

Reproduced with permission of the copyright owner. Further reproduction prohibited without permission.

PLEASE NOTE:

Oversize maps and charts are filmed in sections in the following manner:

LEFT TO RIGHT, TOP TO BOTTOM, WITH SMALL OVERLAPS

The following map or chart has been refilmed in its entirety at the end of this dissertation (not available on microfiche). A xerographic reproduction has been provided for paper copies and is inserted into the inside of the back cover.

Black and white photographic prints (17" x 23") are available for an additional charge.

UMI

Reproduced with permission of the copyright owner. Further reproduction prohibited without permission.

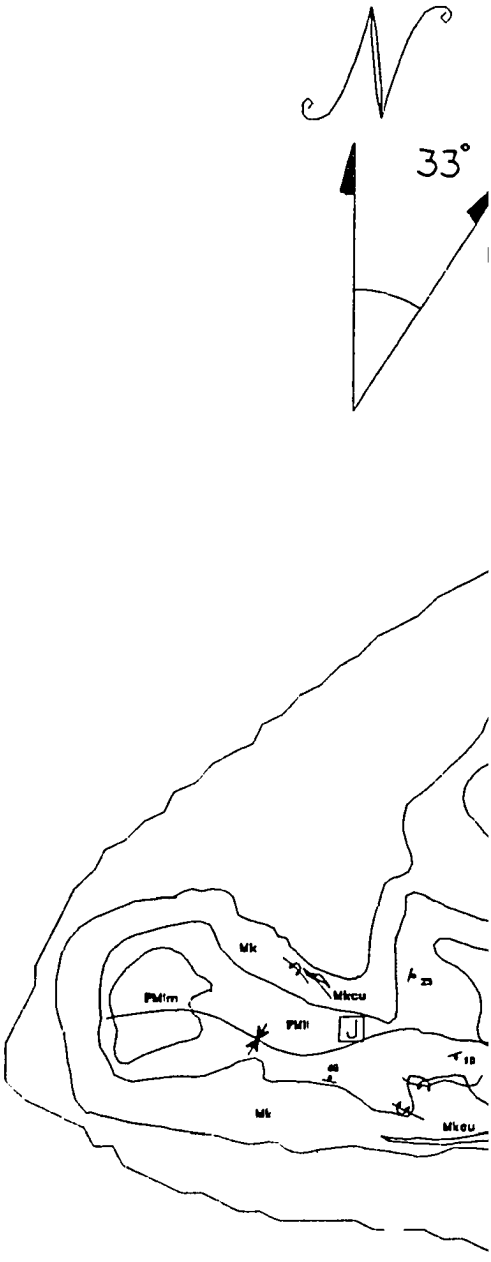

Reproduced with permission of the copyright owner. Further reproduction prohibited without permission.

Reproduced with permission of the copyright owner. Further reproduction prohibited without permission.

PLATE A4.1 Geologic map of

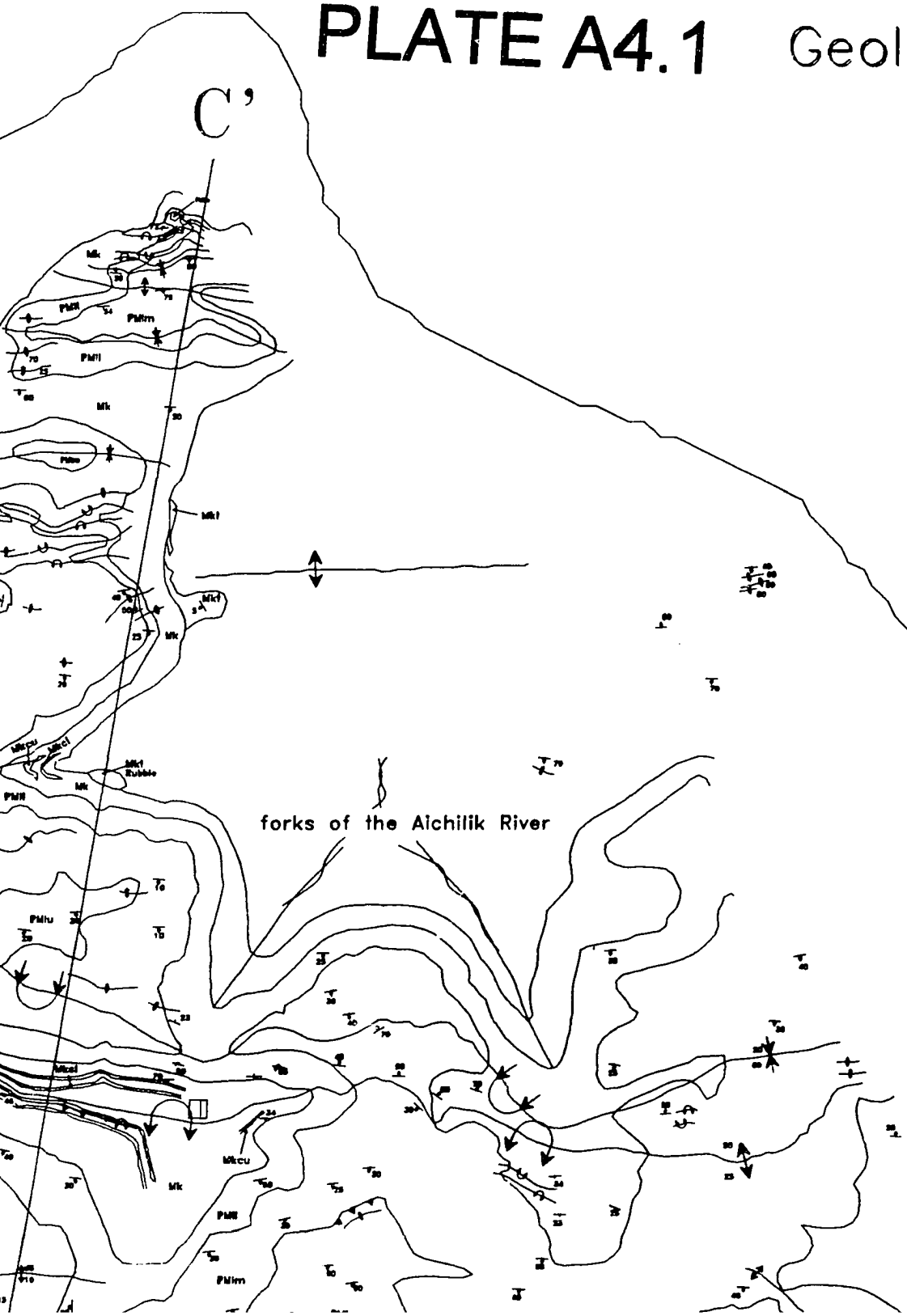

This plate is c
during the sur
thesis – Homz
completed dur
(part of a Phl
See Homza (1

Reproduced with permission of the copyright owner. Further reproduction prohibited without permission.

map of the Aichilik Forks area

This plate is a compilation of mapping completed during the summer of 1990 (part of a Master's thesis – Homza (1992a)) and mapping completed during the summer of 1992 (part of a PhD thesis – present report)

See Homza (1992a) for cross sections A & B

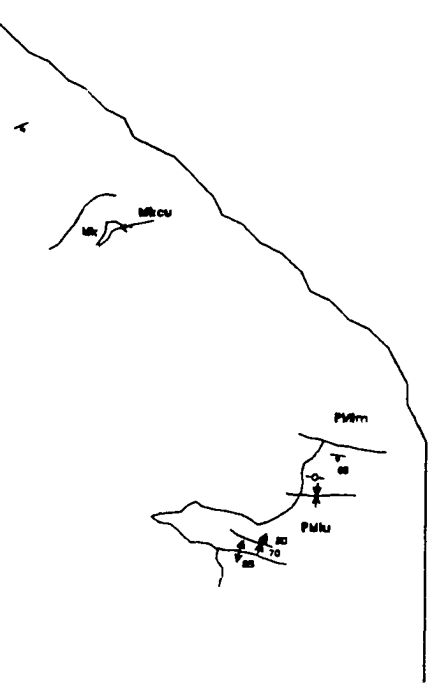

LEGEND

STRATIGRAPHY

Age	Symbol	Unit Name	Detachment Layers
Cretaceous / Jurassic	KJk	Kingak Shale	
	TrS	Shublik Fm.	
Triassic	TrPsi	undivided Ivishak Fm.	
	TrPsid	Ivishak "d" member	
	TrPsic	Ivishak "c" member	
	TrPsib	Ivishak "b" member	
	TrPsia	Ivishak "a" member	
Permian Penn	Pe	Echooka Fm.	
	PMlu	upper Lisburne Limestone	
Miss	PMlm	middle Lisburne Limestone	
	PMll	lower Lisburne Limestone	
	Mk	Kayak Shale	
	Mkcu	(upper carb. unit)	
	Mkcl	(lower carb. unit)	
	Mes	"Endicott Siltstone"	
pMu pre-Miss ?	Mkt	Kekiktuk Conglomerate	
	O€cp	pre-Mississippian Cherts and Phyllites	? ?

MAP SYMBOLS

- Strike & Dip of Bedding
- Estimated Strike & Dip of Bedding
- Strike & Dip of overturned Bedding
- Estimated Strike & Dip of Overturned Bedding
- Axial Trace of Anticline
- Thrust Fault
- Layer Parallel Detachment
- Inferred Thrust Fault
- Trace of Fold Axial Surface

Reproduced with permission of the copyright owner. Further reproduction prohibited without permission.

area

END

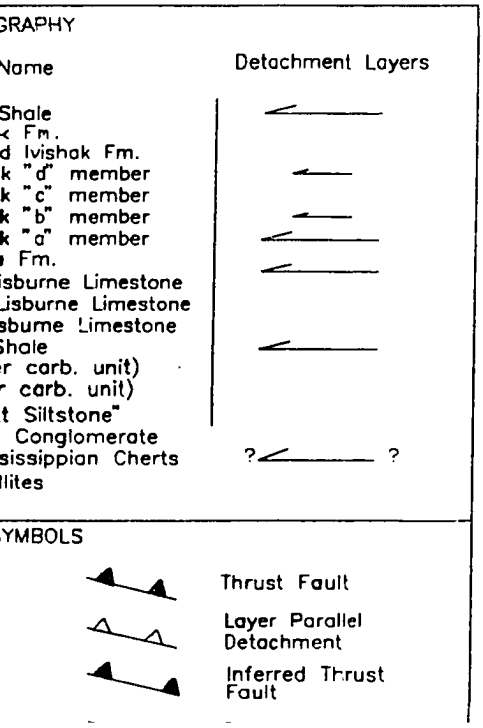

Reproduced with permission of the copyright owner. Further reproduction prohibited without permission.

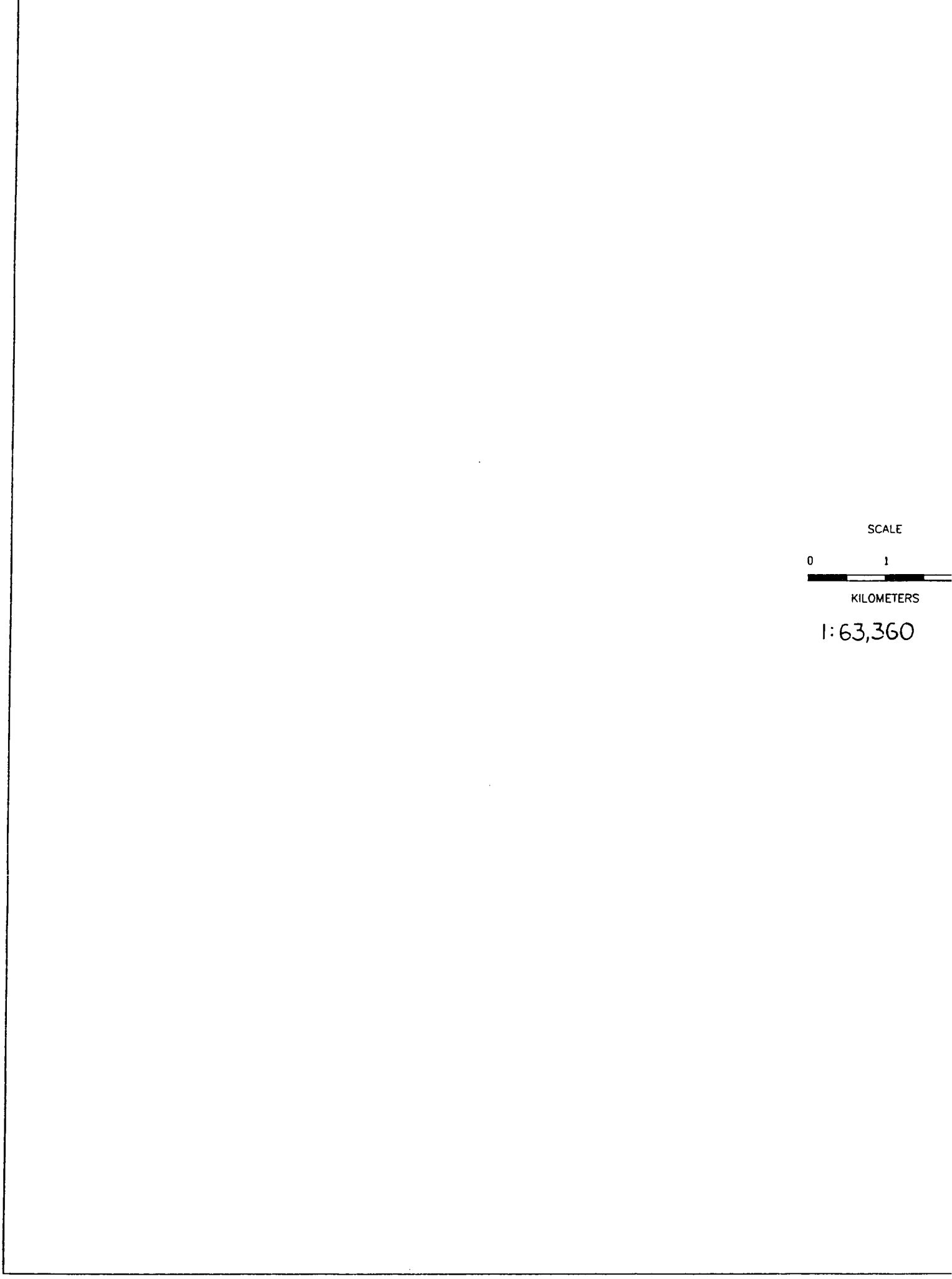

Reproduced with permission of the copyright owner. Further reproduction prohibited without permission.

SCALE

0 1 2

KILOMETERS

1:63,360

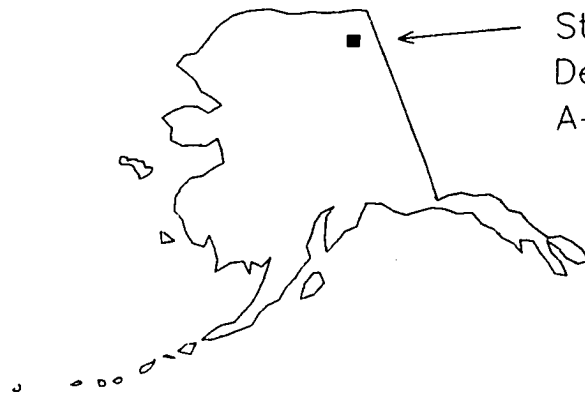

Study Area : Parts of Demarcation Point A–3 A–4 and A–5 Quadrangles

Reproduced with permission of the copyright owner. Further reproduction prohibited without permission.

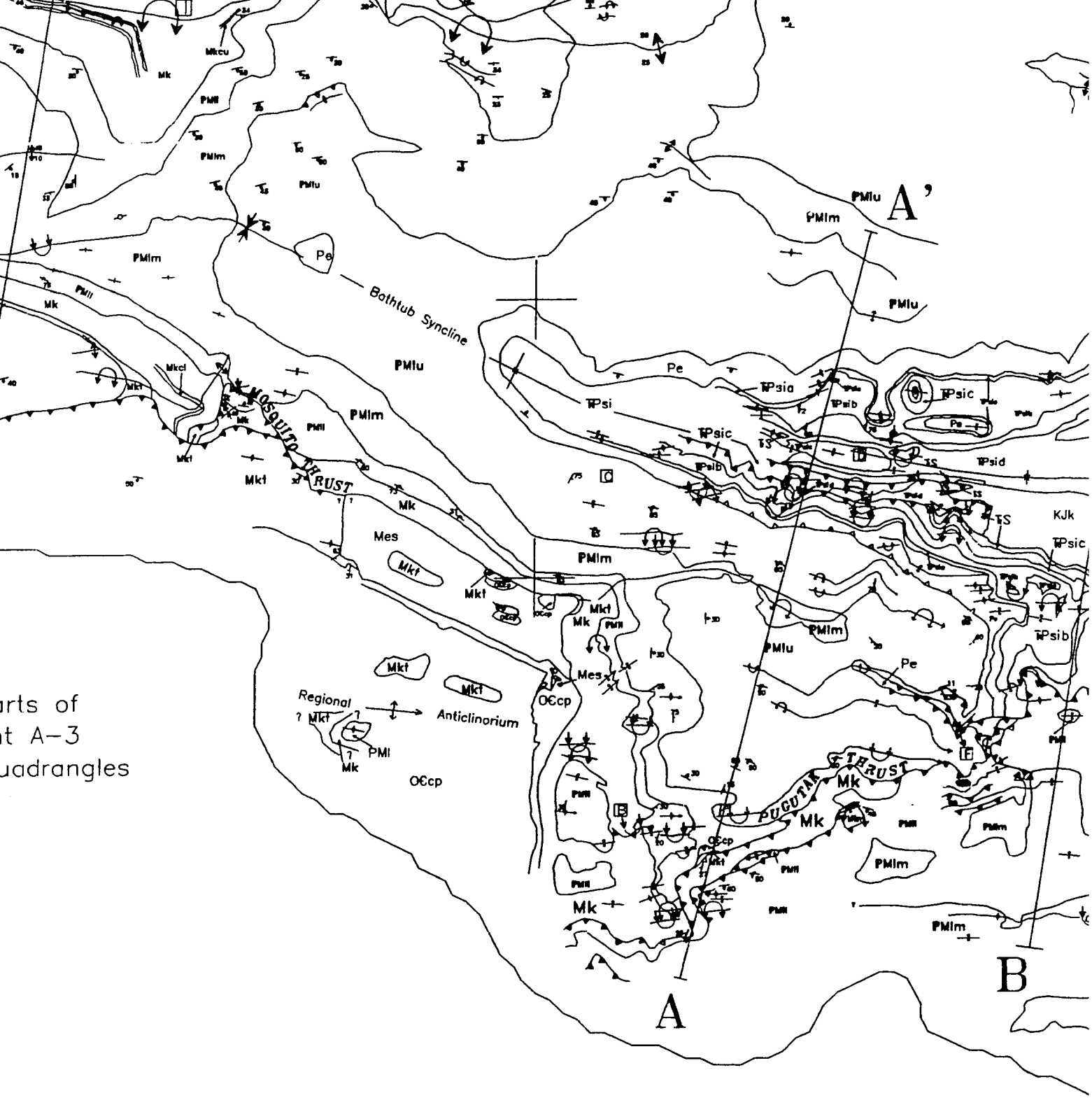

arts of
t A–3
uadrangles

Reproduced with permission of the copyright owner. Further reproduction prohibited without permission.

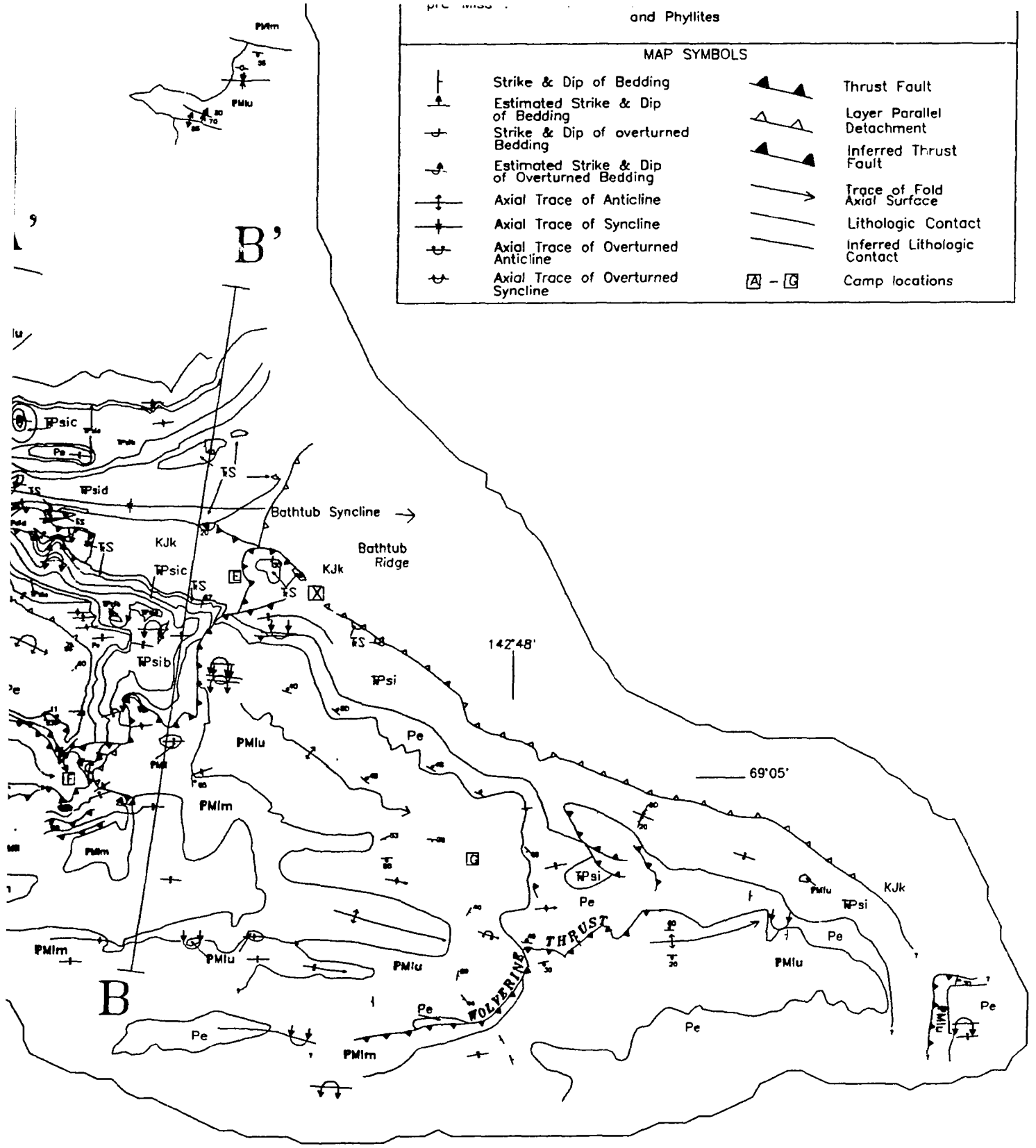

See Plate A4.2 for cross sec
See figure 1.6 for location

Reproduced with permission of the copyright owner. Further reproduction prohibited without permission.

SYMBOLS

- Thrust Fault
- Layer Parallel Detachment
- Inferred Thrust Fault
- Trace of Fold Axial Surface
- Lithologic Contact
- Inferred Lithologic Contact
- A – C Camp locations

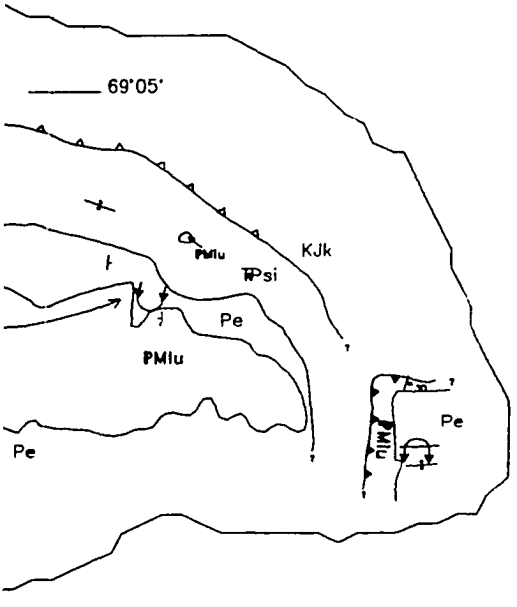

See Plate A4.2 for cross section.
See figure 1.6 for location.

Reproduced with permission of the copyright owner. Further reproduction prohibited without permission.

PLEASE NOTE:

Oversize maps and charts are filmed in sections in the following manner:

LEFT TO RIGHT, TOP TO BOTTOM, WITH SMALL OVERLAPS

The following map or chart has been refilmed in its entirety at the end of this dissertation (not available on microfiche). A xerographic reproduction has been provided for paper copies and is inserted into the inside of the back cover.

Black and white photographic prints (17" x 23") are available for an additional charge.

UMI

Reproduced with permission of the copyright owner. Further reproduction prohibited without permission.

PLATE A4.2 – Balanced cross section of the Aichilik F

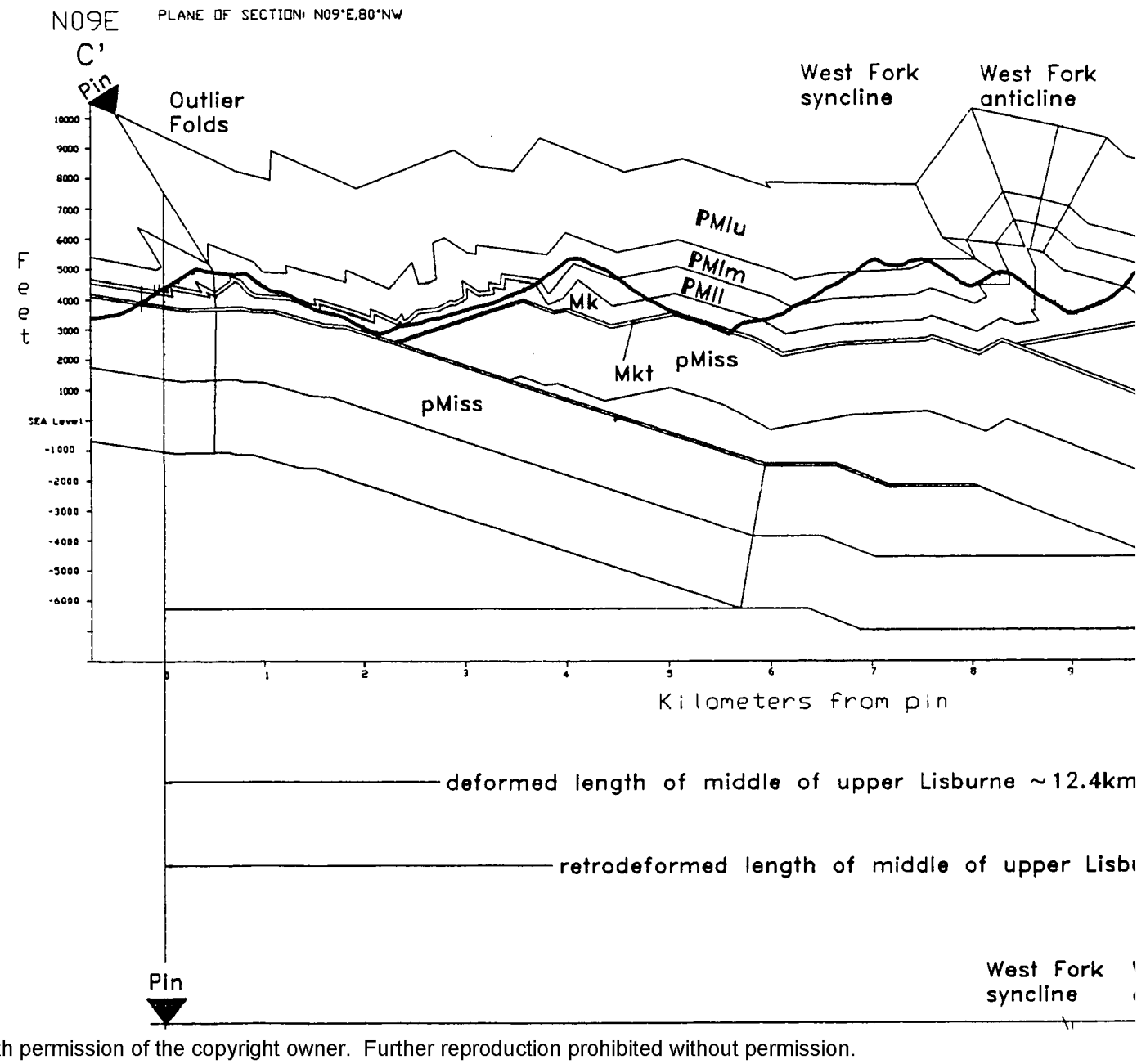

Reproduced with permission of the copyright owner. Further reproduction prohibited without permission.

ne Aichilik Forks area

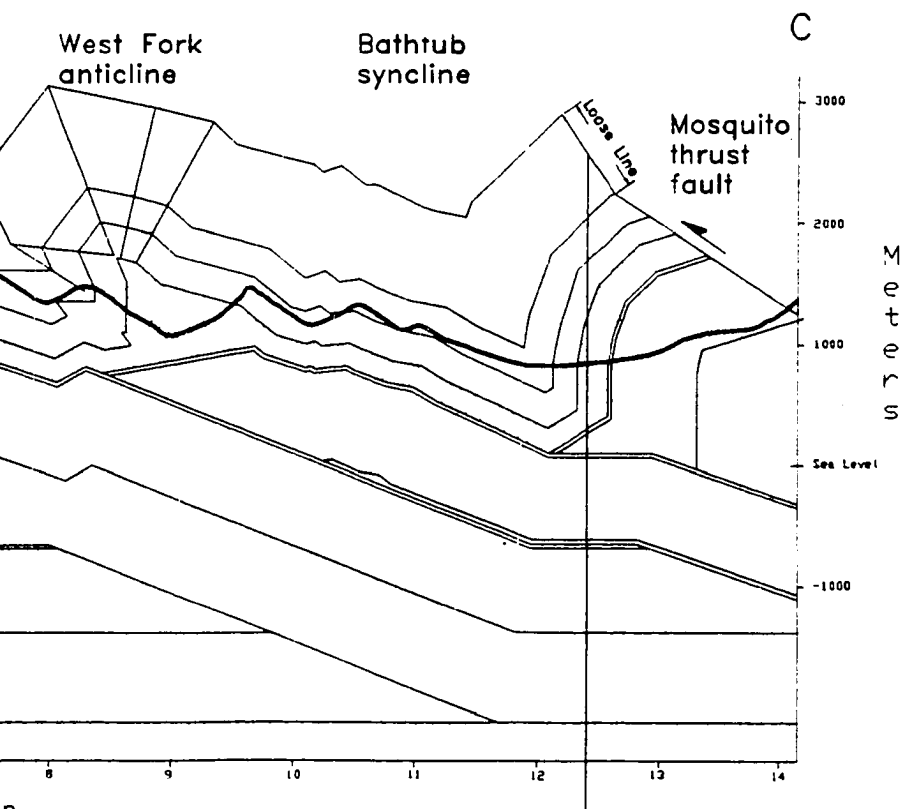

Tho

Tectonics
Departme
Geophy
A

Note: The pin only penetrates rocks above the Kayak detachment and the original relative position of rocks across this detachment is unknown. No displacement of the pin with respect to rocks beneath the detachment is arbitrarily assumed for the purposes of reconstruction, but either forward or hindward displacement of the pin above the detachment is geometrically and kinematically possible.

n

shortening of middle of upper Lisburne ~2.9km

isburne ~12.4km

e of upper Lisburne ~15.2km

Kayak Sh

Units not balanced

Units not cross-se

West Fork syncline

West Fork anticline

Mosquito

Reproduced with permission of the copyright owner. Further reproduction prohibited without permission.

Thomas X. Homza
1993

Tectonics and Sedimentation Research Group
Department of Geology & Geophysics and
Geophysical Institute, University of
Alaska Fairbanks

nt
tion
t
of

trarily

nt
t
al.y possible.

Kayak Shale

Units not balanced

Units not on cross-section

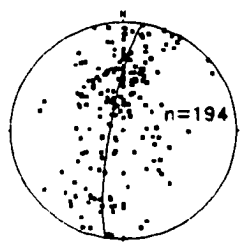

Stereogram of poles to bedding in Kayak and Lisburne

Best fit fold axis S81°E, 10°SE

0 0.5 1.0

Reproduced with permission of the copyright owner. Further reproduction prohibited without permission.

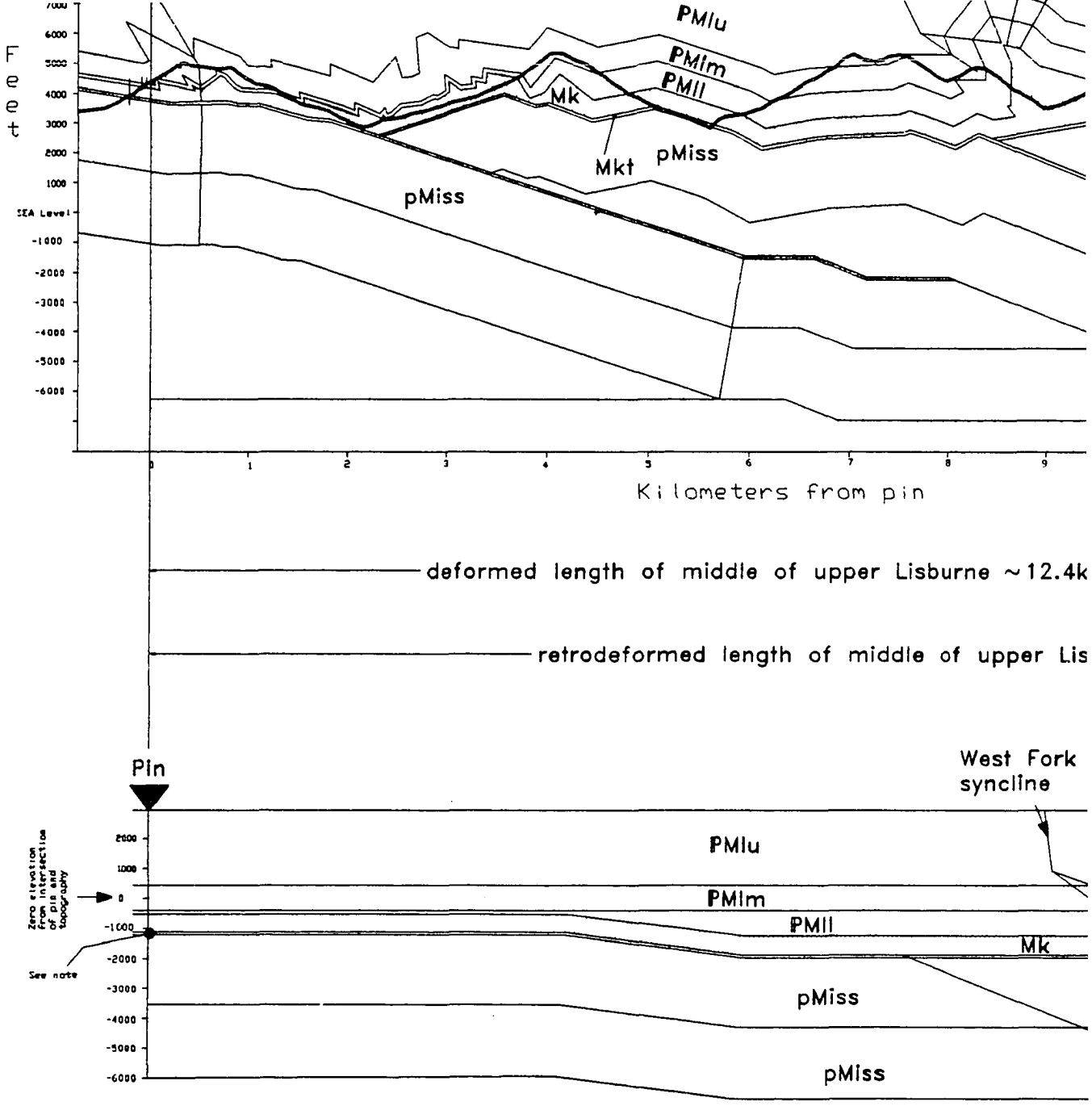

Reproduced with permission of the copyright owner. Further reproduction prohibited without permission.

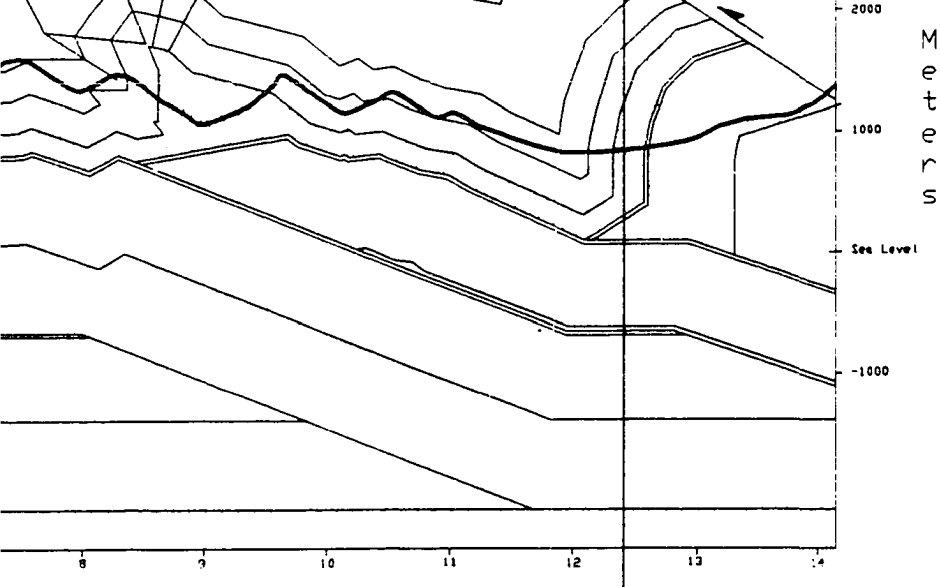

Tectonics
Departm
Geoph

Note: The pin only penetrates rocks above the Kayak detachment and the original relative position of rocks across this detachment is unknown. No displacement of the pin with respect to rocks beneath the detachment is arbitrarily assumed for the purposes of reconstruction, but either forward or hindward displacement of the pin above the detachment is geometrically and kinematically possible.

pin

shortening of middle of upper Lisburne ~2.9km

Lisburne ~12.4km

ddle of upper Lisburne ~15.2km

Kayak

Units n balance

Units n cross-s

West Fork syncline

West Fork anticline

Mosquito thrust fault

0 0.5 1.0
KILOMETERS

1:63,360

Mk

Mkt

s

Reproduced with permission of the copyright owner. Further reproduction prohibited without permission.

1993

Tectonics and Sedimentation Research Group
Department of Geology & Geophysics and
Geophysical Institute, University of
Alaska Fairbanks

on

arily

ly possible.

Kayak Shale

Units not balanced

Units not on cross-section

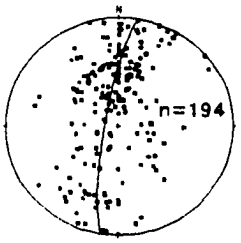

Stereogram of poles to bedding in Kayak and Lisburne

Best fit fold axis S81°E, 10°SE

0 0.5 1.0
KILOMETERS

1:63,360

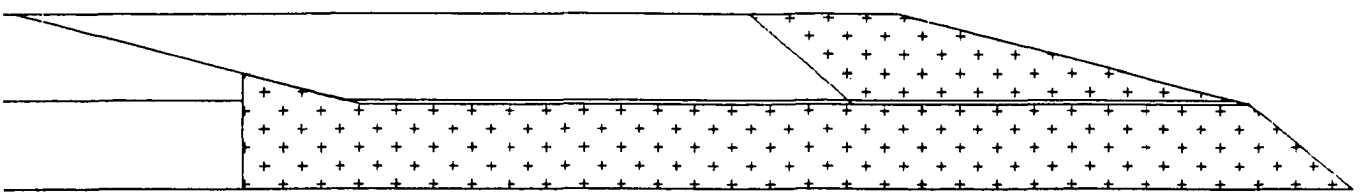

See Plate A4.1 for map.

Reproduced with permission of the copyright owner. Further reproduction prohibited without permission.

PLEASE NOTE:

Oversize maps and charts are filmed in sections in the following manner:

LEFT TO RIGHT, TOP TO BOTTOM, WITH SMALL OVERLAPS

The following map or chart has been refilmed in its entirety at the end of this dissertation (not available on microfiche). A xerographic reproduction has been provided for paper copies and is inserted into the inside of the back cover.

Black and white photographic prints (17" x 23") are available for an additional charge.

UMI

Reproduced with permission of the copyright owner. Further reproduction prohibited without permission.

PLATE A5.1

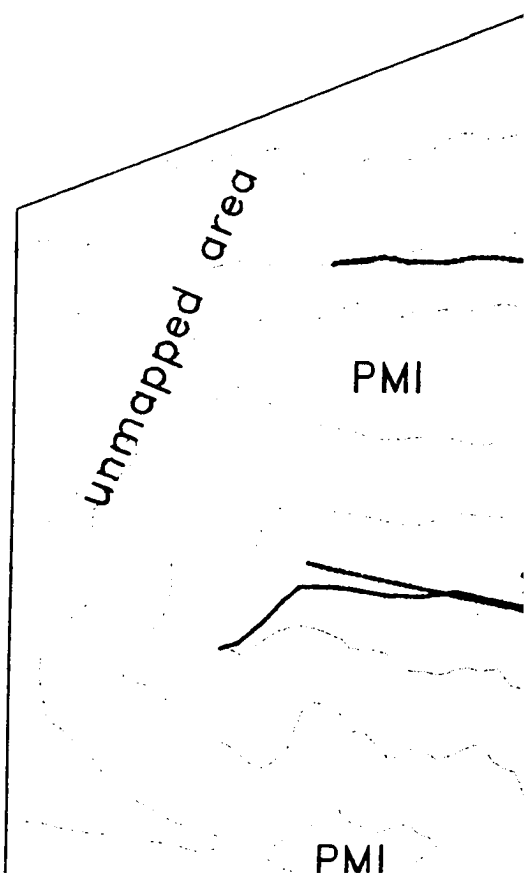

Reproduced with permission of the copyright owner. Further reproduction prohibited without permission.

E A5.1 – Geologic map of the Ellesmeri

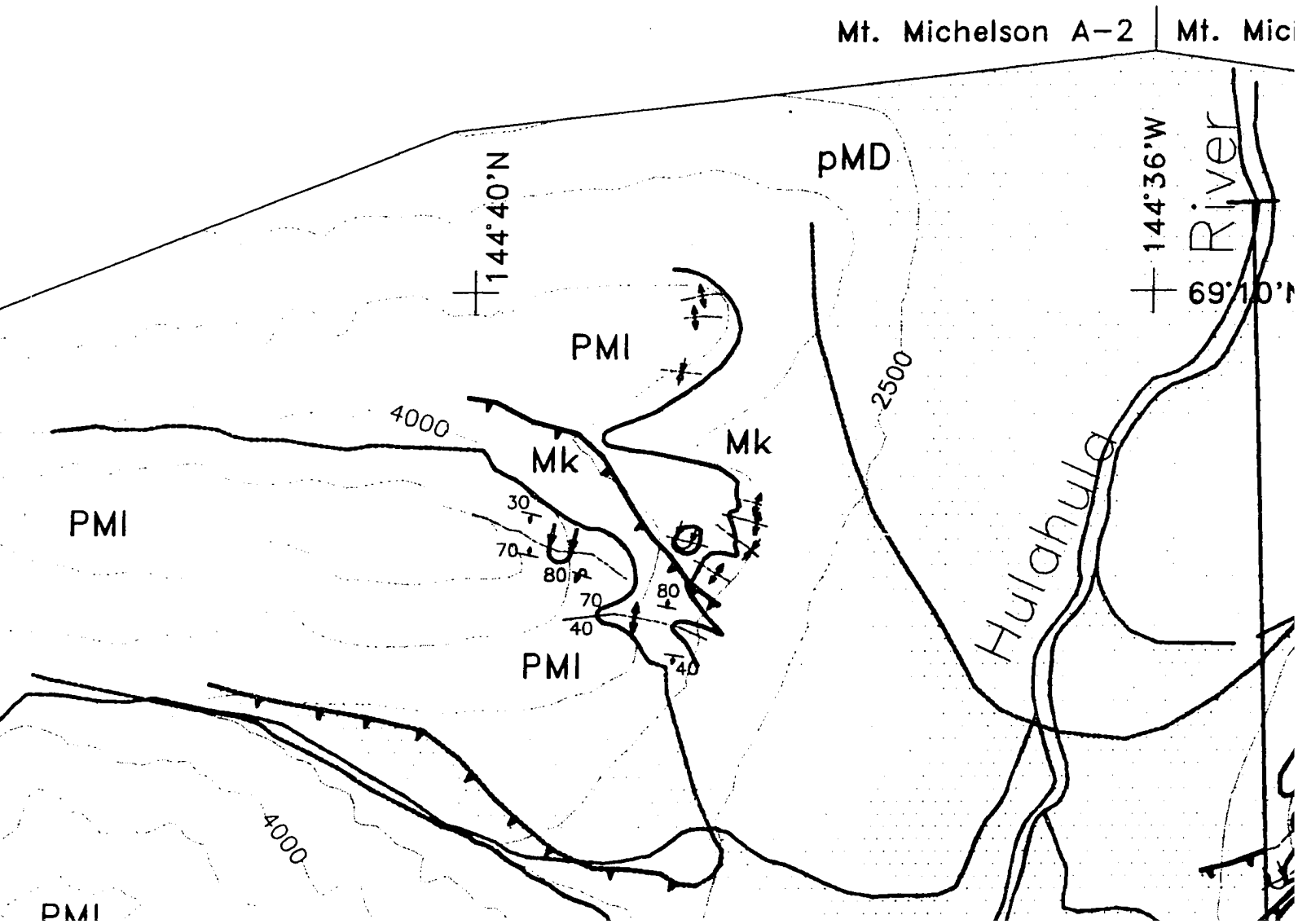

Reproduced with permission of the copyright owner. Further reproduction prohibited without permission.

esmerian sequence inlier on the Hulahul

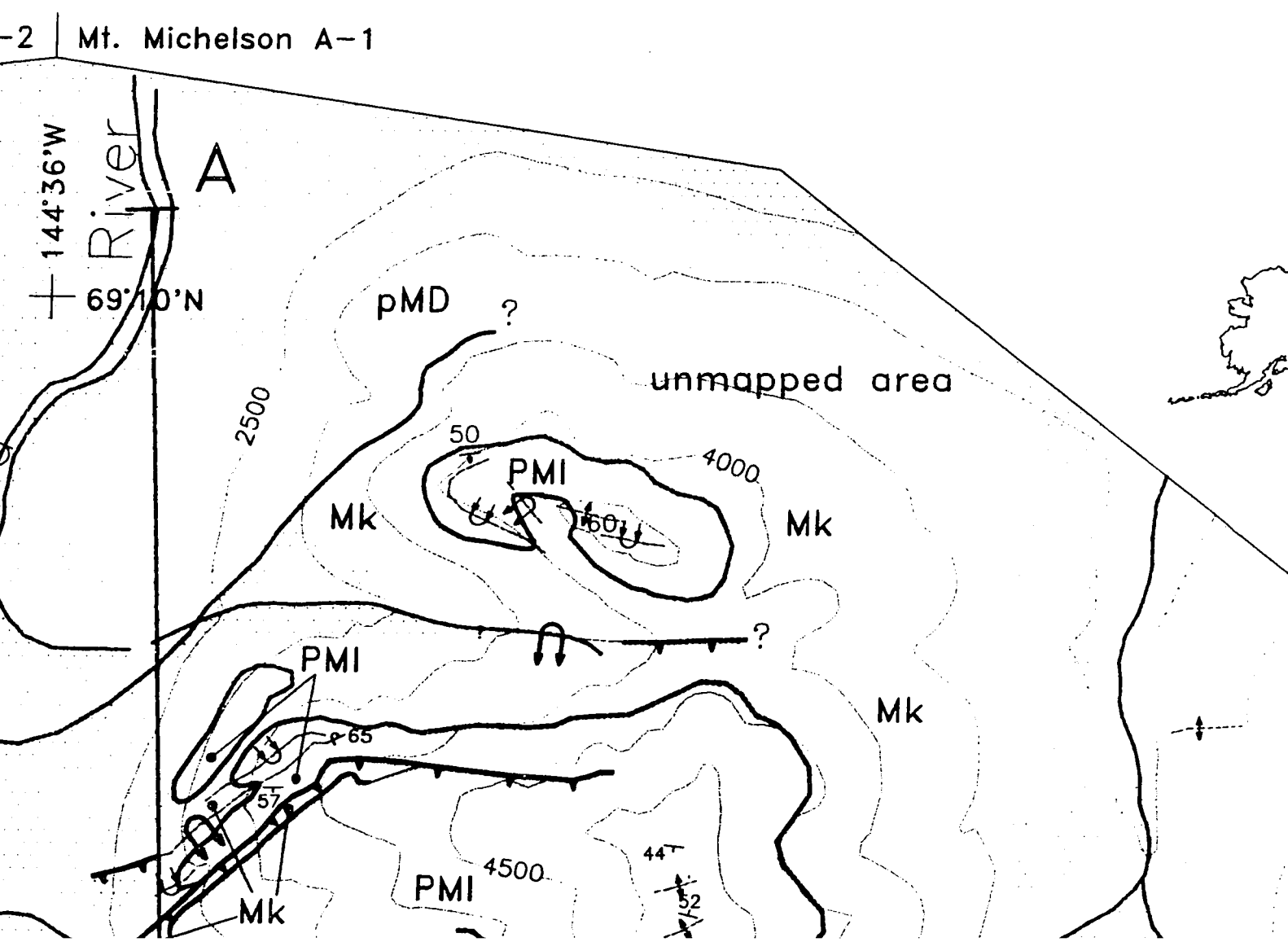

Reproduced with permission of the copyright owner. Further reproduction prohibited without permission.

ulahula River

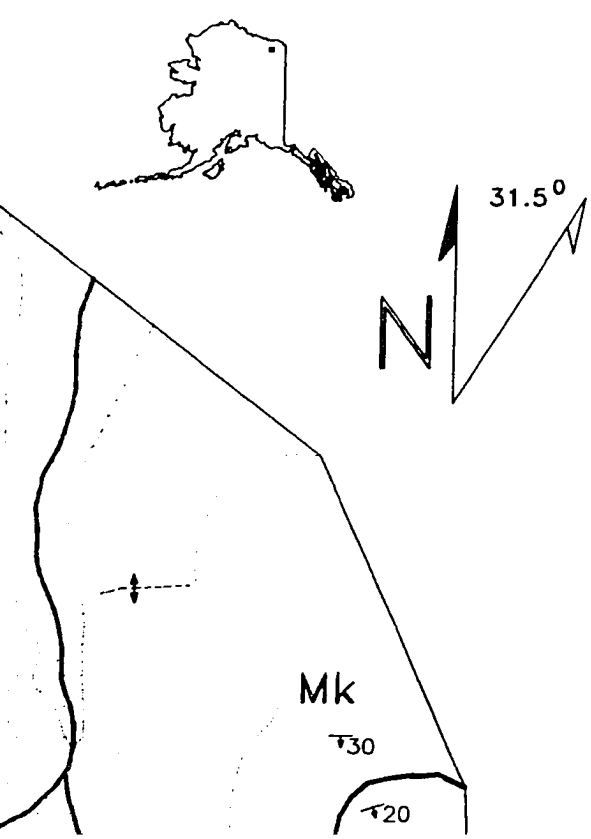

STRUCTURAL SYMBOLS

- vertical bedding
- horizontal bedding
- 20 — strike & dip of bedding
- 52 — estimated strike & dip of bedding
- 30 — strike & dip of overturned bedding
- 85 — estimated strike & dip of overturned bedding
- axial trace of syncline
- axial trace of anticline
- axial trace of overturned syncline
- axial trace of overturned anticline
- trace of thrust fault
- trace of inferred thrust fault

Reproduced with permission of the copyright owner. Further reproduction prohibited without permission.

TURAL SYMBOLS

vertical bedding

horizontal bedding

strike & dip of bedding

estimated strike & dip of bedding

strike & dip of overturned bedding

estimated strike & dip
of overturned bedding

axial trace of syncline

axial trace of anticline

axial trace of overturned syncline

axial trace of overturned anticline

trace of thrust fault

trace of inferred thrust fault

Reproduced with permission of the copyright owner. Further reproduction prohibited without permission.

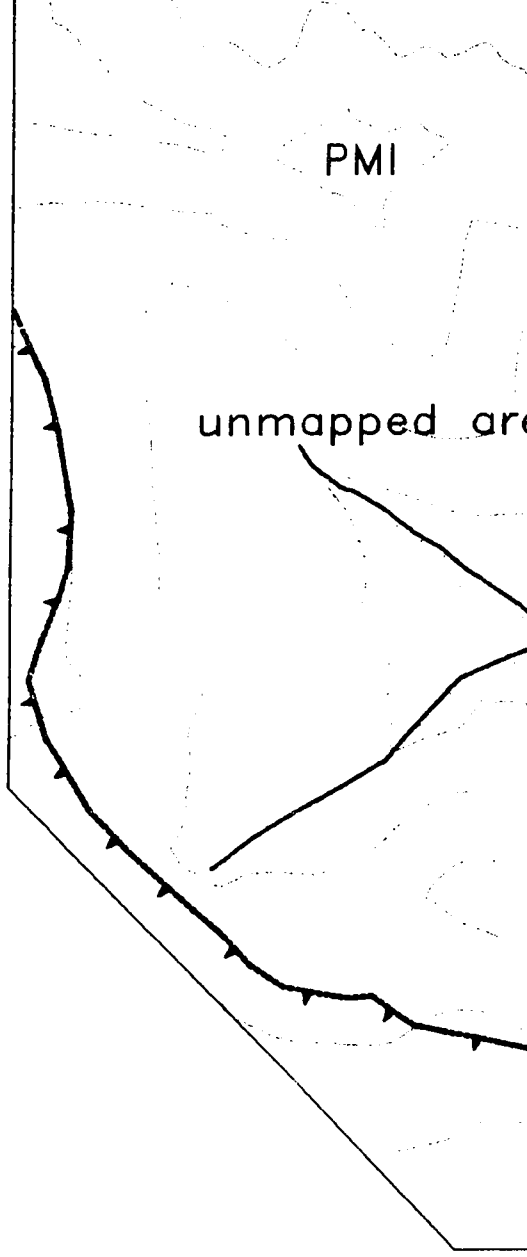

Reproduced with permission of the copyright owner. Further reproduction prohibited without permission.

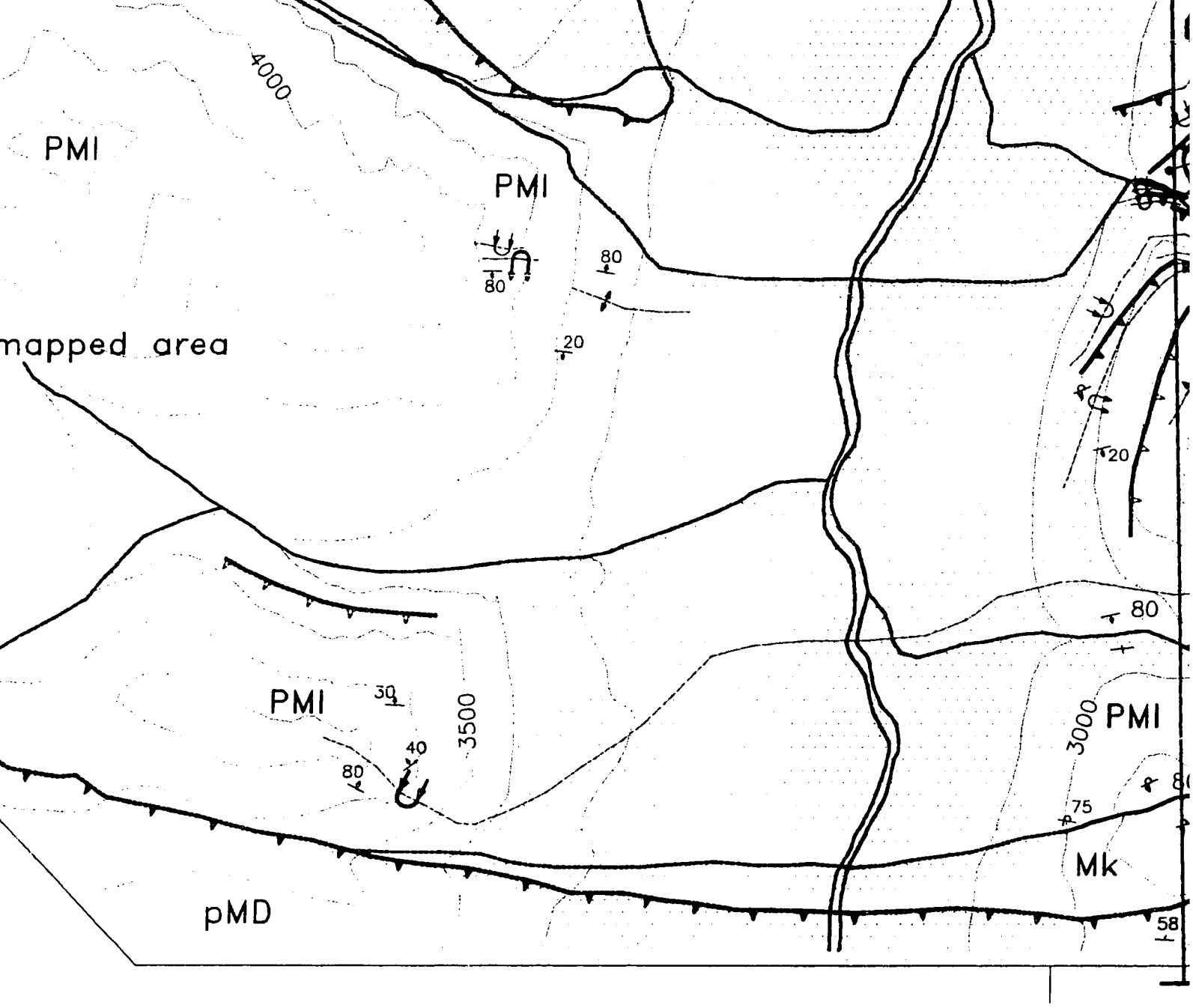

Reproduced with permission of the copyright owner. Further reproduction prohibited without permission.

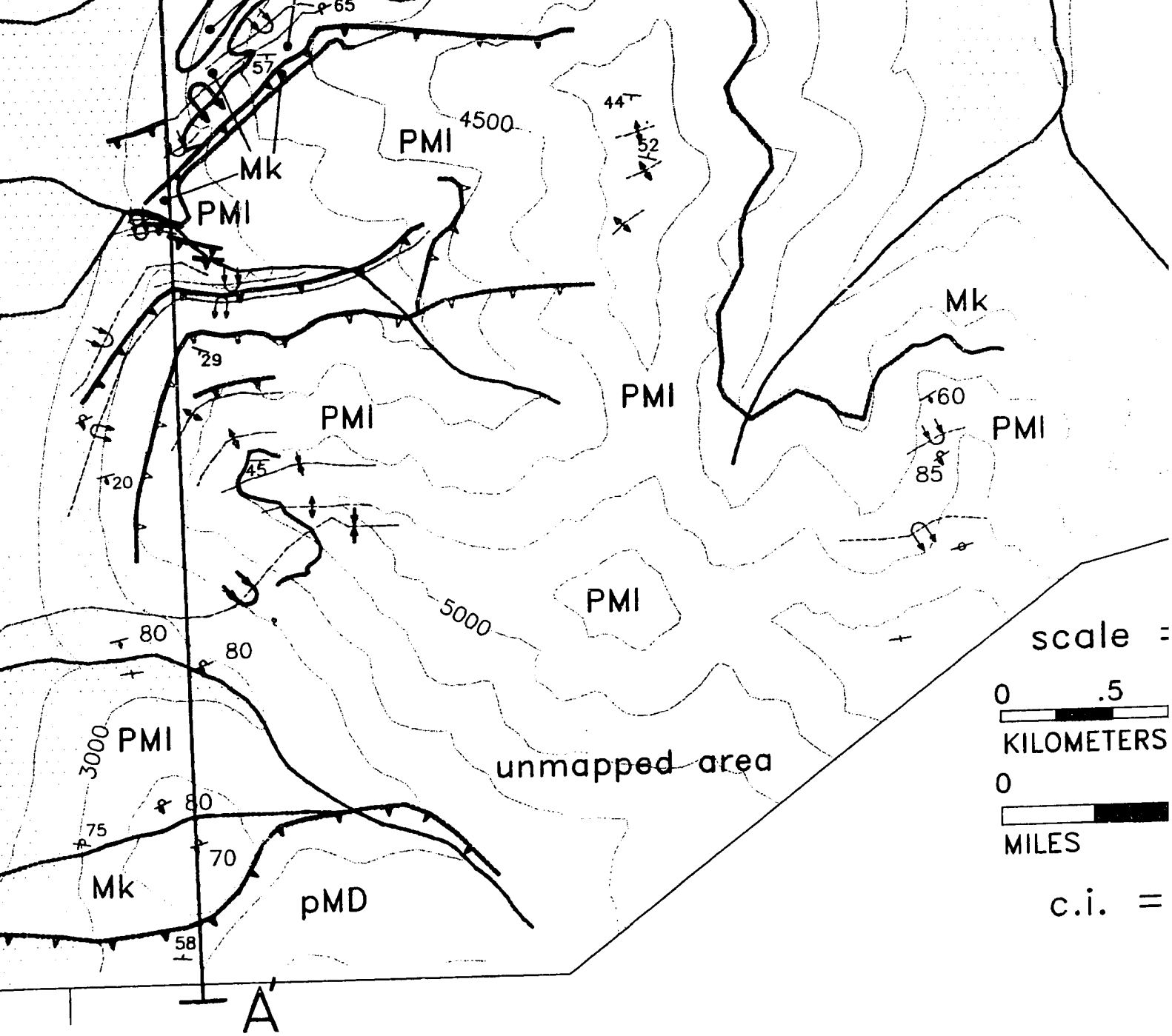

Reproduced with permission of the copyright owner. Further reproduction prohibited without permission.

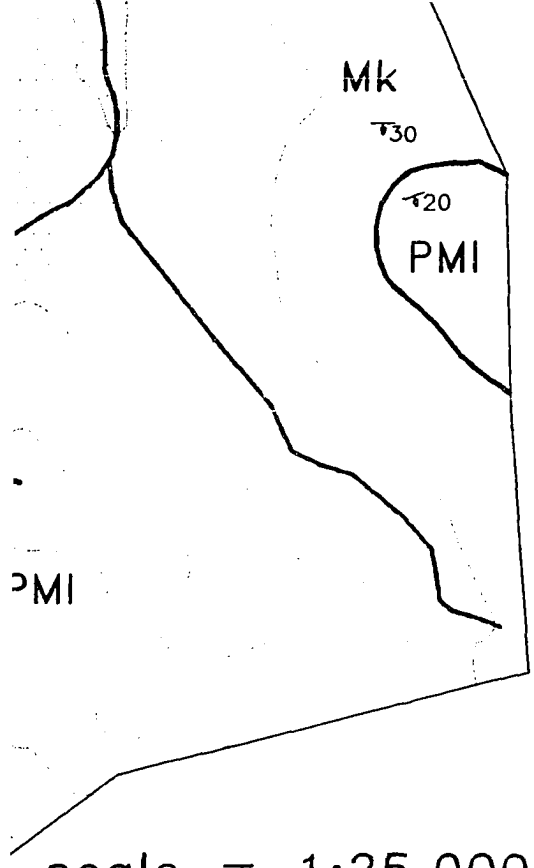

scale = 1:25,000

.5 1

KILOMETERS

.5 1

MILES

c.i. = 500'

axial trace of overturned anticline

trace of thrust fault

trace of inferred thrust fault

trace of layer-parallel fault

lithologic contact

inferred lithologic contact

STRATIGRAPHY

	Q	Quaternary deposits
Pennsylvanian/ Mississippian	PMI	Lisburne Group (undivided)
Mississippian	Mk	Kayak Shale (undivided)
pre-Middle Devonian	pMD	pre-Middle Devonian rocks (undivided)

See Plate A5.2 for cross section.
See figure 1.6 for location.

Reproduced with permission of the copyright owner. Further reproduction prohibited without permission.

axial trace of overturned syncline

axial trace of overturned anticline

trace of thrust fault

trace of inferred thrust fault

trace of layer-parallel fault

lithologic contact

inferred lithologic contact

STRATIGRAPHY

Quaternary deposits

Lisburne Group (undivided)

Kayak Shale (undivided)

D pre-Middle Devonian rocks (undivided)

See Plate A5.2 for cross section.
See figure 1.6 for location.

Reproduced with permission of the copyright owner. Further reproduction prohibited without permission.

PLATE A5.2 · Geologic cross section of the Ellesmerian se

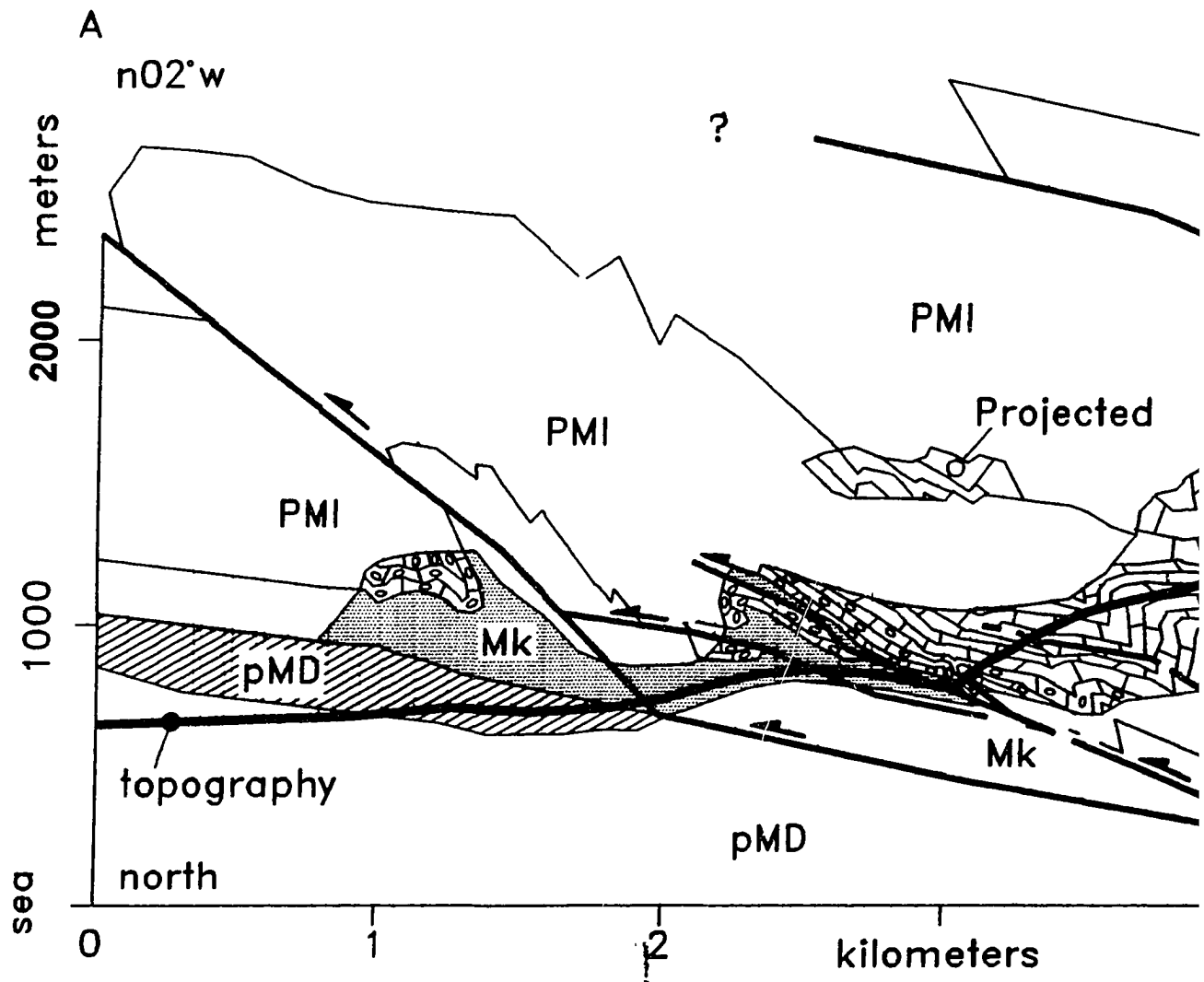

Reproduced with permission of the copyright owner. Further reproduction prohibited without permission.

Reproduced with permission of the copyright owner. Further reproduction prohibited without permission.

ion of the Ellesmerian sequence inlier on the Hulahula River

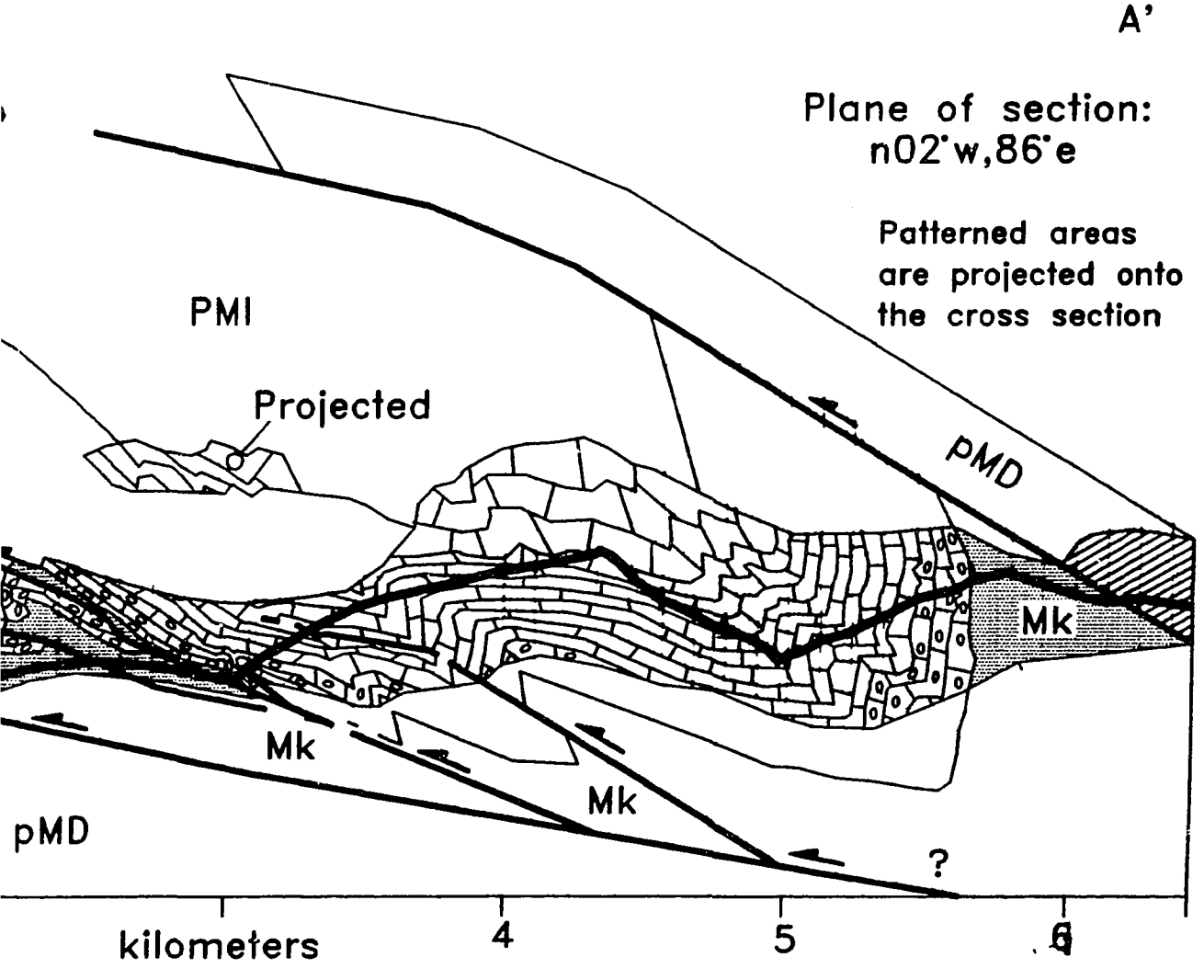

See Plate A5.1 for map.

Reproduced with permission of the copyright owner. Further reproduction prohibited without permission.